Role of reactive oxygen species in modulating carbohydrate metabolism in acute myeloid leukaemia

by

Andrew J Robinson

2017

A thesis presented to Cardiff University in partial fulfilment of the requirement for the degree of Doctor of Philosophy

Department of Haematology,

School of Medicine,

Cardiff University.

Supervisors: Dr. Alex Tonks and Professor R Darley

Declaration and statements

DECLARATION

This work has not been submitted in substance for any other degree or award at this or any other university or place of learning, nor is being submitted concurrently in candidature for any degree or other award.

Signed..... (candidate) Date.....

STATEMENT 1

This thesis is being submitted in partial fulfilment of the requirements for the degree of Doctor of Philosophy (PhD).

Signed..... (candidate) Date.....

STATEMENT 2

This thesis is the result of my own independent work/investigation, except where otherwise stated, and the thesis has not been edited by a third party beyond what is permitted by Cardiff University's Policy on the Use of Third Party Editors by Research Degree Students. Other sources are acknowledged by explicit references. The views expressed are my own.

Signed..... (candidate) Date.....

STATEMENT 3

I hereby give consent for my thesis, if accepted, to be available online in the University's Open Access repository and for inter-library loan, and for the title and summary to be made available to outside organisations.

Signed..... (candidate) Date.....

STATEMENT 4: PREVIOUSLY APPROVED BAR ON ACCESS

I hereby give consent for my thesis, if accepted, to be available online in the University's Open Access repository and for inter-library loans after expiry of a bar on access previously approved by the Academic Standards & Quality Committee.

Signed..... (candidate) Date.....

Acknowledgements

I would like to express my sincerest thanks to my supervisors Dr. Alex Tonks and Prof. Richard Darley. Their knowledge, guidance and inexhaustible patience, alongside their unswerving support and encouragement have been essential in completing this study.

I would also like to thank Dr's Paul Hole, Nader Omidvar and Chinmay Munje, for their generous assistance in providing knowledge around particular aspects of this project.

Grateful thanks also to Sara Davies and Sarah Baker for their technical assistance, for 'showing me the laboratory ropes' and for making me feel welcome.

I wish also to acknowledge the contribution of Prof. Awen Gallimore, who convinced me I still had what it takes to engage in academic research.

In addition, a huge thank-you to my family and friends, for their laughter (both with and at me), their endless encouragement and their belief in my ability.

Finally, it would be remiss of me not to expressly acknowledge the I.T. expertise provided by Dr. Alex Tonks, without which this document may well have been presented on Vellum.

Ultimately, none of this work would have been possible without the generosity of Tenovus Cancer Care who funded this research, and in particular the volunteers who tirelessly collect, in the pursuit of curing cancer. My thanks to them all.

This work is dedicated to my wife Katie and my children, Seren and Carys.

I wish to thank them from the bottom of my heart.

Ever tried. Ever failed. No matter. Try again. Fail again. Fail better.

- Samuel Beckett

Publications and presentations

Abstracts

Hopkins, G.L., Robinson A.J., Hole, P. S., Darley, R. L., & Tonks, A. Analysis of ROS responsive genes in mutant RAS expressing hematopoietic progenitors identifies the glycolytic pathway as a major target promoting both proliferation and survival.

American Society of Haematology Annual Meeting, December 2014. (Accompanied by poster presentation).

Oral presentations

Robinson, A.J., Kreuser, S., Davies, S., Darley, R., & Tonks, A. Reactive oxygen species increases glycolysis in acute myeloid leukaemia via overexpression of PFKFB3.

17th International Conference on Oxidative Stress Reduction, Redox Homeostasis and Antioxidants, June 2016.

Abstract

Reactive oxygen species (ROS) are known to play a significant role in cellular signalling pathways, associated with growth, differentiation and survival and in many cancers, elevated ROS levels have been linked with aberrant signalling. Previously, we showed that human haematopoietic progenitor cells expressing mutant RAS (a common abnormality in AML) had elevated NOX2 derived ROS which led to increased cell proliferation. However, it is currently unknown how ROS mediates these effects. Previous preliminary data suggests significant ROS attributable gene changes are associated with glycolysis, a feature also common in solid tumours. Using human haematopoietic progenitor cells, it is reported here for the first time that, elevated ROS leads to changes in extracellular lactate production and increases in glucose uptake. Furthermore, modulation of ROS levels in AML cell lines also generate results consistent with a ROS induced model of increased glycolysis. Gene expression profiling identified ROS related changes in specific glycolytic enzymes, whilst immunoblotting verified ROS dependent increases in protein expression of a key regulatory glycolytic enzyme, 6-phosphofructo-2-kinase/fructose-2,6-bisphosphatase 3 (PFKFB3), in both human cells and AML cell lines. Metabolomic analysis using mass spectrometry, was performed on AML cell lines in which ROS levels were manipulated and AML patient samples were characterised according to ROS production. This revealed changes in concentrations of metabolites associated with glycolysis and metabolic pathways important in ROS regulation. Modulation of PFKFB3 expression generated changes in glucose uptake consistent with ROS mediated changes in this enzyme. In summary, this study establishes for the first time that increased ROS production in AML models leads to increased glycolysis and metabolic reprogramming as a consequence of modulation of PFKFB3 expression by ROS.

List of Abbreviations

1,3-BPG	1,3-bisphosphoglycerate
2-NBDG	2-(N-(7-nitrobenz-2-oxa-1,3-diazol-4-yl) amino)-2-D-deoxyglucose
2-PG	2-phosphoglcyerate
3-PG	3-phosphoglycerate
3PO	3-(3-pyridinyl)-1-(4-pyridinyl)-2-propen-1-one
6-PG	6-phosphogluconolactone
6-PGD	6-phosphogluconate dehydrogenase
7-AAD	7-aminoactinomycin D
ADP	adenosine diphosphate
ALDO	aldolase
ALL	acute lymphocytic leukaemia
AKT	protein kinase B
AML	acute myeloid leukaemia
AMPK	5’ adenosine monophosphate-activated protein kinase
ARA-C	Cytarabine
ATP	adenosine triphosphate
BM	bone marrow
BSA	bovine serum albumin fraction V
CD	cluster of differentiation
CLL	chronic lymphocytic leukaemia
CML	chronic myeloid leukaemia
DHAP	dihydroxyacetone phosphate
DMEM	Dulbecco Modified Eagle Medium
DPI	diphenyleneiodonium
ENO	enolase
ERK	extracellular signal-regulated proteins
ETC	electron transport chain
F-6-P	fructose-6-phosphate
F-1,6-BP	fructose-1,6-bisphosphate
F-2,6-BP	fructose-2,6-bisphosphate
FACS	fluorescence activated cell sorting

FBS	foetal bovine serum
G-3-P	glyceraldehyde-3-phosphate
G-6-P	glucose-6-phosphate
G-6-PD	glucose-6-phosphate dehydrogenase
GAP	GTPase activating proteins
GAPDH	glyceraldehyde-3-phosphate dehydrogenase
G-CSF	granulocyte-colony stimulating factor
GDP	guanosine diphosphate
GEF	guanine nucleotide exchange factor
GFP	green fluorescent protein
GLUT	glucose transporter
GM-CSF	granulocyte macrophage-colony stimulating factor
GOX	glucose oxidase
GPX	glutathione peroxidase
GSH	glutathione
GSR	glutathione reductase
GSSG	glutathione disulphide
GTP	guanosine triphosphate
GTPase	guanosine triphosphatase
H_2O_2	hydrogen peroxide
HIF-1α	hypoxia inducible factor-1 alpha
HK	hexokinase
HOCl	hypochlorous acid
HPC	haematopoietic progenitor cells
HSC	haematopoietic stem cells
IL-3	interleukin-3
IL-6	interleukin-6
IMDM	Iscove's Modified Dulbecco's Medium
LDH	lactate dehydrogenase
LSC	leukaemia stem cells
MAPK	mitogen activated protein kinase
MCT	monocarboxylate transporter
MEK	meiosis specific serine/threonine-protein kinase

mTOR	mammalian target of rapamycin
NADPH	nicotinamide adenine dinucleotide phosphate
NF-κB	nuclear factor kappa-light-chain-enhancer of activated B-cells
NOX	NADPH oxidase
Nrf2	nuclear-related factor 2
O_2	diatomic oxygen
$O_2^{\bullet-}$	superoxide
$OH^{\bullet}$	hydroxyl radical
PBS	phosphate buffered saline
PEP	phosphoenolpyruvate
PFK	phosphofructokinase
PFK158	1-(pyridine-4-yl)-3-(7-(trifluoromethyl)-quinolin-2-yl)-prop-2-en-1-one
PFKFB3	6-phosphofructo-2-kinase/fructose-2,6-bisphosphatase 3
PGAM	phosphoglycerate mutase
PGI	phosphoglucose isomerase
PGK	phosphoglycerate kinase
PHGDH	phosphoglycerate dehydrogenase
PI3K	phosphatidylinositol 3-kinase
PKM2	pruvate kinase muscle 2
PPP	pentose phosphate pathway
Prx	peroxiredoxin
PTEN	phosphatase and tensin homolog
PTP	protein tyrosine phosphatase
R-5-P	ribose-5-phosphate
RAS	rat sarcoma
ROS	reactive oxygen species
RPMI	Roswell Park Memorial Institute 1640 medium
Ru-5-P	ribulose-5-phosphate
SCF	stem cell factor
SOD	superoxide dismutase

SSP	serine synthesis pathway
TIGAR	TP53-induced glycolysis and apoptosis regulator
TPI	triose phosphate isomerase
Trx	thioredoxin
TrxR	thioredoxin reductase
VAS-2870	3-Benzyl-7-(2-benzoxazolyl) thio-1,2,3-triazolo (4,5-d) pyrimidine
X-5-P	xyulose-5-phosphate

Table of figures

Summary of Tables

Table of contents

1 General Introduction

The average adult human contains five litres of blood, which consists of plasma and a heterogeneous mix of different cell types. Cells constitute approximately 46% of total blood volume, with plasma, composed of water, proteins, glucose, minerals and clotting factors, making up the rest (reviewed in Kumar, 2015). Haematopoietic cells are commonly divided into three major subgroups, comprising of those derived from the erythroid, lymphoid and myeloid lineage. The erythroid cells are composed of erythrocytes which bind oxygen via haemoglobin for transport around the body and thrombocytes which are involved in haemostasis. Cells derived from the lymphoid lineage are leukocytes and consist of lymphocytes (T-cells and B-cells) which are highly specialised cells involved in adaptive immunity, and natural killer cells, which whilst classically considered to be cells involved in innate immunity, also exhibit features of the adaptive system. The third subgroup comprise of those derived from the myeloid lineage; they are involved in innate immunity and can themselves be further divided into monocytes and granulocytes. Monocytes ultimately differentiate into macrophages which are phagocytes, and dendritic cells which process and present antigens to T-cells. Granulocytes are distinguished by the presence of granules in the cytoplasm and consist of three types of cell, neutrophils which are phagocytes, basophils which secrete histamine and eosinophils which destroy parasites and affect allergic responses.

The average lifespan of mature haematopoietic cells varies; in adult humans erythrocytes circulate for around 100-120 days before being engulfed by macrophages, whereas neutrophils are relatively short-lived, with a circulatory half-life of between 6-90 hours (Tak *et al.*, 2013). Consequently, to maintain haematopoietic cells at stable levels, new blood cells must be constantly generated. This process of haematopoiesis occurs, in adult humans, primarily in the bone marrow (BM), from haematopoietic stem cells (HSC) which are self-renewing and have the capacity to differentiate into any blood cell, at the rate of $1x10^{12}$ cells per day (reviewed in Doulatov *et al.*, 2012).

Leukaemia is a cancer of the blood which develops, typically in the bone marrow due to disruption of the haematopoietic process. In acute myeloid leukaemia (AML) (1.2.1) this can be characterised as a failure in proper differentiation and the accumulation of immature myeloid progenitor cells, occurring due to successive genetic alterations to

critical genes involved in cell survival, differentiation and growth. Approximately 55% of AML patients present with cytogenetic abnormalities, whilst the rest have a normal karyotype. Of these, FMS-like tyrosine kinase receptor 3 (FLT-3) internal tandem duplications (approx. 30%) or somatic mutations to genes like nucleophosmin-1 (NPM-1) (50-60%) or rat sarcoma (RAS) (15-30%) (Estey and Dohner, 2006), are most frequently observed.

Reactive oxygen species (ROS) are small molecules, that react readily with a large number of molecules, due to the presence of an unpaired electron, or their ready conversion into free radicals (1.3.1). Initially ROS were identified for their destructive function, as part of a cellular immune response (1.3.3.1), but more recently their role in cell signalling has gained prominence (1.3.3.2). There are multiple cellular sources of ROS (1.3.2). Their reactivity means they are highly regulated, with dysregulated ROS production, signalling, and regulation, and its role in cancer (1.3.3.4) a much studied area (reviewed in Galadari *et al.*, 2017).

Metabolism (1.4) is a highly integrated network of chemical reactions, that in animals are used by cells to either break down biomolecules and generate energy, or to build the substrates into more complex molecules, a process with a net energy loss. There are four main classes of biomolecules, proteins, nucleic acids, lipids, as well as carbohydrates such as glucose. Glucose is central to metabolism, as it is the primary fuel in the generation of energy, both in the form of adenosine triphosphate (ATP) which is a product of the glycolytic pathway (1.4.3) and in supplying intermediates for oxidative phosphorylation. Oxidative phosphorylation is much more efficient than glycolysis in ATP generation and is the primary energy source in normal cells, however it requires oxygen to proceed so under low oxygen conditions (hypoxia), cells produce energy anaerobically via the glycolytic pathway alone. The German scientist Otto Warburg was the first to notice that in many cancer cells glycolysis is enhanced (Warburg, 1956), even in the presence of sufficient oxygen for oxidative phosphorylation to proceed (1.4.1), whilst the reasons for this are an ongoing area of active research (reviewed in Liberti and Locasale, 2016).

This study then aims to investigate the role that ROS has on metabolic (primarily glycolytic) function, from an AML perspective.

1.1 Haematopoiesis

In order to maintain haemostasis, new blood cells must be constantly generated to replace those lost through injury, disease or age. Haematopoiesis, the process by which HSC differentiate into mature blood cells, occurs via a series of stages known as lineage commitment (reviewed in Cvejic, 2016) (1.1.2) and is tightly regulated by the BM environment (or stem cell niche; reviewed in Ho *et al.*, 2015) (1.1.1), signal transduction pathways (reviewed in Luis *et al.*, 2012), cytokines (reviewed in Tarasova *et al.*, 2011, Metcalf, 2008, Robb, 2007) (1.1.3), transcription factors (reviewed in Wolff and Humeniuk, 2013, Rosenbauer and Tenen, 2007) (1.1.4), epigenetics, (reviewed in Alvarez-Errico *et al.*, 2015) and metabolic pathways (reviewed in Oburoglu *et al.*, 2016) (1.4). HSC are rare, constituting only 0.001% of peripheral blood (PB) and 0.05% of BM cells, but are responsible for producing a lifetime supply of blood cells (reviewed in Mendelson and Frenette, 2014). In order to achieve this, they undergo a process of self-renewal, either symmetric renewal, which generates two undifferentiated stem cells or two differentiated cells, or asymmetric renewal resulting in one stem cell and one differentiated cell. As above, this process is regulated by both intrinsic and extrinsic factors (reviewed in Zon, 2008) (1.1.1).

Blood is mesodermally derived tissue. Ontogenetically, blood is derived initially from the embryonic stem cells (ES) of the epiblast. The cytokine bone morphogenetic protein 4 (BMP4), is a critical signalling molecule in the differentiation of these early ES towards a haematopoietic fate. Haemogenic endothelium cells (HE) then develop in the mesoderm which requires the transcription factor Scl, with primitive HSC first emerging in the aorta-gonad-mesonephros (AGM) and yolk sac 4 weeks post conception in humans (reviewed in Wang and Wagers, 2011). The process of HE to primitive HSC is known as endothelial-to-haematopoietic transition and is under the control of the transcription factor runt-related transcription factor 1 (RUNX1) (Landry *et al.*, 2008). These primitive HSC, or erythroid-myeloid progenitors (EMP) have the capacity to develop into erythrocytes, macrophages and megakaryocytes, but not lymphocytes and do not have the capacity to self-renew. In humans, 5 weeks post conception, HSC then migrate from the AGM to the foetal liver and placenta. Whilst the factors responsible for this migration are still not fully established, both the chemokine CXCL12 (Sugiyama *et al.*, 2006) and the cytokine stem-cell factor (SCF) (Barker, 1994) are known to be critical for this process. Several signalling pathways including

NOTCH, BMP4, Hedgehog, TIE2-angioprotein and vascular endothelial growth factor (VEGF), are then responsible for establishing HSC in the BM, around 12 weeks post conception (reviewed in Kim *et al.*, 2014). Postnatally, HSC mainly reside in the BM, where, with the exception of T-cells which develop latterly in the thymus, adult haematopoiesis occurs.

1.1.1 Human haematopoietic stem cells

To qualify as a HSC, a cell must be able to durably self-renew whilst also being multipotent, i.e. capable of differentiating into all types of blood cell. This differentiation is generally considered to occur via several intermediate progenitor cells, ultimately terminating in the specific mature blood cell through a process termed fate restriction or lineage commitment. These stages of lineage commitment can be observed by changes in the expression of proteins on the cell surface of the differentiating cell. Civin *et al.*, 1984 were the first to report a cell surface marker for primitive haematopoietic cells. Using a monoclonal antibody (anti-My-10, raised against the morphologically primitive leukaemic cell line, KG-1a) they identified a small population (1-2%) of undifferentiated haematopoietic BM cells which were not observed in PB, but were also present on greater than 30% of blasts obtained from some patients with AML. This cell surface protein, CD34, is now routinely used in the laboratory to separate HSC and haematopoietic progenitor cells (HPC) from differentiated haematopoietic cells. Subsequent work identified CD90 (or Thy1) as a marker to separate HSC from more differentiated progenitor cells (Baum *et al.*, 1992), whilst more recently CD49f $^{+}$ cells (Notta *et al.*, 2011) have been shown to correlate with properties of long term HSC (LT-HSC) as distinct from CD49f $^{-}$ short term HSC (ST-HSC) (reviewed in Doulatov *et al.*, 2012).

The difference between LT-HSC and ST-HSC is defined by their relative abilities to sustain long term blood production of all lineages in lethally irradiated mice that have received a BM engraftment. LT-HSC have traditionally been seen as those capable of self-renewal and blood production in these mice for a period greater than 12 weeks, whilst ST-HSC only sustain blood production for a shorter period (2-3 weeks for myeloid cells and 4-6 weeks for lymphoid progeny) (reviewed in Doulatov *et al.*, 2012). Work by Benveniste *et al.*, 2010 identified a population of HSC termed intermediate HSC (IT-HSC) that maintain reconstitution potential in engrafted mice for 16-44 weeks. Other studies examining reconstitution kinetics have also identified subpopulations of

HSC with some clones preferentially generating cells of a lymphoid lineage (Ly-bi HSC), some a myeloid lineage (My-bi HSC) and others a more balanced lineage commitment (Bala-HSC) (Muller-Sieburg *et al.*, 2002). Recently a review by Ema *et al.*, 2014 has noted that HSC defined as My-bi predominantly overlap with LT-HSC and Ly-bi with ST-HSC. The exact process of HSC self-renewal, lineage commitment (1.1.2) and cell fate determination (1.1.3 & 1.1.4) is still a matter of contention, however it is in part at least determined by the stem-cell niche.

1.1.1.1 The haematopoietic stem cell niche

The hypothetical idea of a stem cell niche, as an anatomically defined site in which stem cell differentiation is inhibited, was first proposed by (Schofield, 1978). However it was not until 1998 that his hypothesis was experimentally validated in ovary tissue of *Drosphilia* (Xie and Spradling, 1998), whilst definitive identification of the mammalian HSC niche did not occur until 2003 (Zhang *et al.*, 2003, Calvi *et al.*, 2003). Using different mechanisms, these independent murine studies generated increased levels of osteoblasts in the BM and both observed concomitant increases in levels of HSC. Furthermore, Zhang *et al*. 2003 demonstrated that the cell adhesion protein N-cadherin was a point of contact between osteoblasts and HSC, whilst Calvi *et al*, 2003 demonstrated that the Notch ligand, Jagged 1, was the protein responsible for this increase. Current understanding of the HSC niche microenvironment now encompasses not only these, but several other cell signalling molecules and cytokines, as well as many non-proteinaceous factors.

The HSC niche can be physiologically divided into the endosteal niche and perivascular niche. These niches are populated by several cells that, in addition to HSC, have been shown to be important in their maintenance, and include mesenchymal stem cells (MSC), CXCL12-abundant reticular (CAR) cells, endosteal cells, osteoblasts, adipocytes, chondrocytes, osteoclasts, immune cells and neuronal cells (reviewed in Ho *et al.*, 2015, Reagan and Rosen, 2016). Until recently, the role of osteoblasts (which reside in the endosteal niche) appeared to be particularly crucial. In addition to expression of N-cadherin and Jagged 1, osteoblasts have also been shown to express anigiopoietin-1, thrombopoietin (TPO), osteopontin and WNT and to secrete granulocyte colony-stimulating factor (G-CSF), granulocyte macrophage CSF (GM-CSF), interleukin-6 (IL-6) (reviewed inWang and Wagers, 2011) and c-x-c motif chemokine 12 (CXCL12) (Ponomaryov *et al.*, 2000), all of which have been shown to

be important in the maintenance or physiological function of the niche. In particular osteoblast secretion of CSXCL12 was thought to be crucial in HSC homing and engraftment (Ponomaryov *et al.*, 2000), whilst expression of angiopoietin on the osteoblast cell surface was shown to interact with tyrosine kinase receptor Tie2, a ligand expressed on the LT-HSC subpopulation of HSC (Arai *et al.*, 2004). However, the importance of osteoblasts in HSC maintenance has recently been questioned (reviewed in Crane *et al.*, 2017). Improved HSC purification resulting from the identification of signalling lymphocyte activation molecule family markers have shown that quiescent HSC primarily reside near sinusoidal blood vessels of the perivascular niche. Furthermore, whilst loss of osteoblasts from the stem cell niche resulted in the depletion of early lymphoid progenitors, loss of HSC's was severely delayed, occurring only once the BM was pancytopenic. Additionally, SCF has been shown to be crucial for HSC maintenance and has been shown to be primarily expressed by perivascular cells, whilst SCF deletion from osteoblasts in murine models showed no effect of HSC function (Ding *et al.*, 2012). In contrast CAR cells found in the perivascular region of the BM are the major source of BM SCF and they additionally express CXCL12 at levels three orders of magnitude higher than that of osteoblasts (Ding and Morrison, 2013). CXCL12 is required, as HSC express CXC-chemokine receptor 4 (CXCR4) and CXCL12-CXCR4 signalling regulates HSC proliferation and quiescence (Nie *et al.*, 2008). Megakaryocytes and non-myelinating Schwann cells are also important in maintaining HSC quiescence through activation of transforming growth factor beta (TGFβ), whilst depletion of macrophages has also been shown to reduce CXCL12 expression and increased HSC proliferation (reviewed in Crane *et al.*, 2017). Additionally adipocytes also positively regulate HSC survival through expression of CXCL12 (Mattiucci *et al.*, 2018), whilst immune cells such as osteomacs and myeloid-derived suppressor cells protect HSC from cytotoxic lymphocytes and maintain HSC homeostasis (reviewed in Reagan and Rosen, 2016).

Physiochemical factors also are important in HSC niche regulation. Mechanical support by the extracellular matrix can be important in stem cell differentiation, shear stress is a factor in the upregulation of the haematopoietic transcription factor RUNX1 in embryogenesis and calcium ion concentration of the HSC niche is crucial in the chemoattraction and engraftment of LT-HSC (reviewed in Wang and Wagers, 2011). Furthermore, oxygen levels vary with the HSC niche, with low hypoxic regions

reported in areas that correlate with higher levels of quiescent LT-HSC (Parmar *et al.*, 2007, Winkler *et al.*, 2010), which include the perisinusoidal region of the BM (Spencer *et al.*, 2014). It has been demonstrated that LT-HSC manage the hypoxic environment through the upregulation/stabilisation of hypoxia inducible factor alpha (HIF-1α) (Takubo *et al.*, 2010), a master regulator of hypoxia (1.4.2.1), and through a concomitant increase in glycolytic function and decrease in mitochondrial activity (Simsek *et al.*, 2010). Mitochondrial oxidative phosphorylation, generates ROS (1.3.2.1). Changes in the intracellular levels of ROS have been shown to impact on HSC quiescence, with higher levels leading to increased HSC differentiation and proliferation (reviewed in Ludin *et al.*, 2014) potentially mediated via hyperactivation of 5' adenosine monophosphate-activated protein kinase (AMPK) (Liu *et al.*, 2015). Interestingly AMPK activation has been shown to stimulate increased glycolysis via the upregulation and phosphorylation (Ser 461) of 6-phosphofructo-2-kinase/fructose-2,6-bisphosphatase 3 (PFKFB3) (Domenech *et al.*, 2015, Esteban-Martinez *et al.*, 2015, Mendoza *et al.*, 2012) (1.5.1.1).

Clearly, the microenvironment of the HSC niche is tightly controlled and subject to numerous positive and negative feedback mechanisms, that are important in maintaining the quiescence and long-term viability of HSC, whilst ensuring appropriate levels of HSC lineage specific differentiation occur, in order to retain suitable levels of mature blood cells in the PB. The mechanisms by which this process of differentiation occurs will be introduced below.

1.1.2 The myeloid model of haematopoiesis

Adult human haematopoiesis has traditionally been described as a process in which HSC gradually differentiate in a stepwise manner into different mature blood cells, via a series of intermediate progenitor cells. As differentiation occurs cells lose the capacity to self-renew and progenitor cells emerge that are increasingly committed to a given branch of haematopoietic lineage in a process known as cell fate determination. Fate decisions occur as a consequence of changes in the regulation of lineage specific gene expression, that stem from changes in the cellular microenvironment as a result of cell-cell interactions, changes in physiochemical factors (1.1.1.1) and the relative concentrations of certain cytokines (1.1.3) (Rieger and Schroeder, 2012).

The compartmentalisation of HSC, their progenitors and terminally differentiated blood cells, into different stages of differentiation, has traditionally been done on the basis of the expression of different cell surface proteins (Figure 1-1) (reviewed in Doulatov *et al.*, 2012). These can be isolated by fluorescence activated cell sorting (FACS) and their differentiation potential determined by colony-forming cell assays or xenograft models. Initial work in mice led to the identification of common myeloid progenitors (CMP) (Akashi *et al.*, 2000) and common lymphoid progenitors (CLP) (Kondo *et al.*, 1997), which gave rise to a hierarchical model of haematopoiesis being developed. This model pictured haematopoiesis as a developmental tree with HSC representing the trunk and differentiation occurring via intermediate progenitor cells, through serial bifurcation, until unipotent mature blood cells were generated (Figure 1-1). This positioning of CMP and CLP at the earliest lineage committed step of the hierarchical tree has proved problematic, leading to a number of alternative models being proposed (reviewed in Kawamoto and Katsura, 2009). In particular, the failure to detect CLP that did not also have myeloid potential led (Kawamoto *et al.*, 2010) to propose the 'myeloid-based model' of haematopoiesis. This model suggests that initial HSC differentiation, leads to the formation of common erythroid progenitors and common lymphoid progenitors, both of which retain myeloid differential potential. This myeloid potential is retained throughout subsequent bifurcations and only lost upon terminal differentiation into specialised mature blood cells. However, more recently, evidence has emerged that megakaryocytes can be generated from multiple pathways, including a subset of HSC (reviewed in Woolthuis and Park, 2016), which would place this lineage committed step at the apex of the hierarchical tree.

The recent emergence of single cell technologies such as fluorescent in situ hybridisation, high-throughput single-cell quantitative PCR, single cell mass spectrometry and mass cytometry (Ye *et al.*, 2017), have led to further re-analysis of these models of haematopoietic differentiation. Discrete progenitor cell populations, as determined by cell surface markers, have actually been shown to consist of heterogenous populations with different differential fates (reviewed in Cvejic, 2016). Single cell transcriptome analysis recently indicated that association of LT-HSC with von-Willebrand factor, primed these cells for megakaryocyte-erythroid differentiation, lending support to the idea that these progenitor cells branch first from the hierarchical differentiation tree (Sanjuan-Pla *et al.*, 2013). More recently, a study by Velten *et al.*,

2017, further challenged the idea of a hierarchical model governing haematopoiesis. Using a combination of single cell technologies and xenotransplantation as functional validation, they proposed that early haematopoiesis consists of, a cellular continuum of low-primed undifferentiated (CLOUD) haematopoietic stem progenitor cells (HSPC), with simultaneous lineage gene expression for multiple directions. This study suggested that early discrete stable progenitors do not exist, with any lineage determination occurring further downstream than originally presumed.

Whilst these studies have generated further debate regarding the order of progression and delineation of haematopoietic differentiation, they have also provided additional insight into a much debated issue within the field of haematopoiesis, how HSC differentiation is determined (1.1.3).

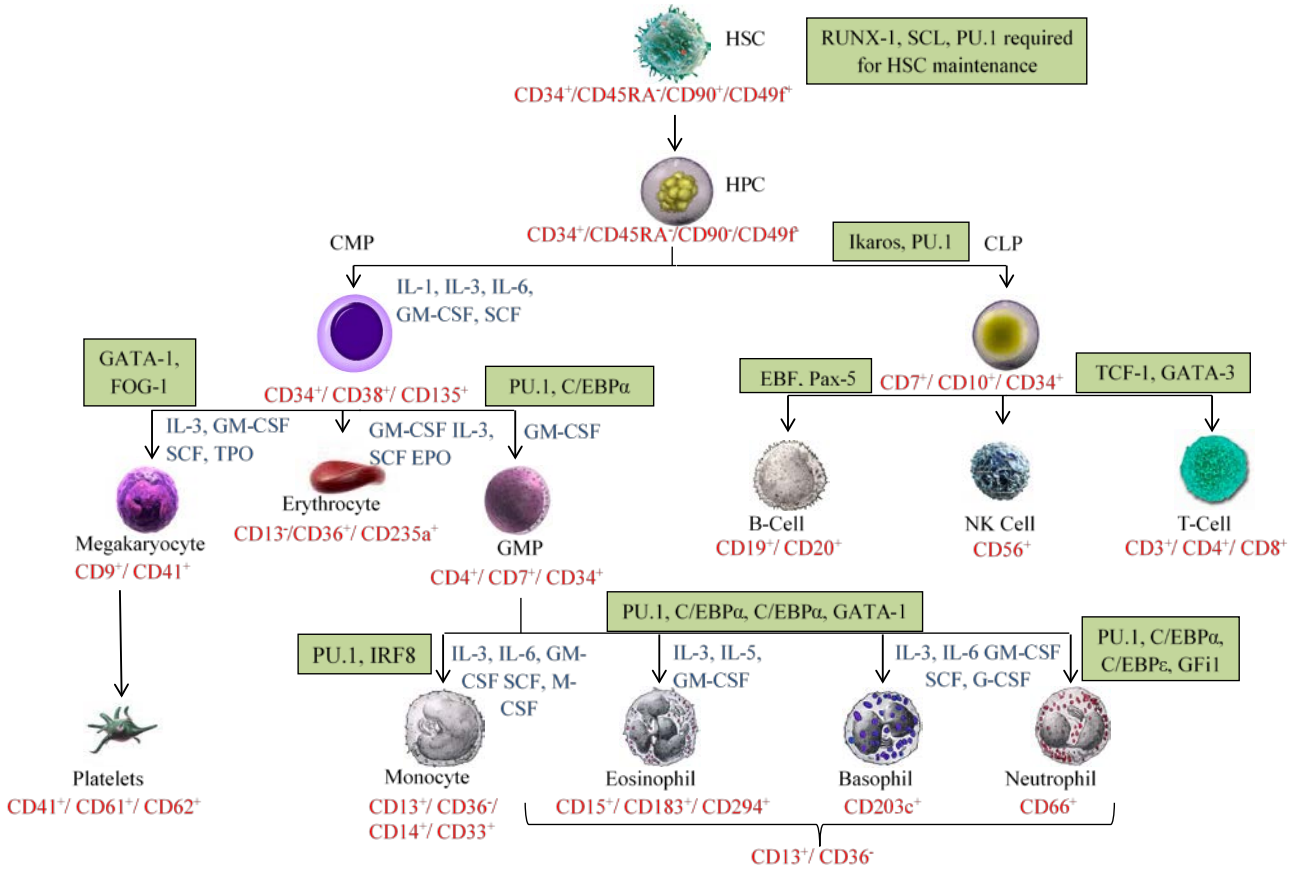

Figure 1-1. Human haematopoiesis. Schematic diagram showing classical model of haematopoietic lineage commitment, with phenotypical cell surface markers (red), transcription factors determining differentiation (green box) and growth factors involved in myelopoiesis (blue). Haematopoietic stem cell (HSC), cluster of differentiation (CD), haematopoietic progenitor cell (HPC), common myeloid progenitor (CMP), common lymphoid progenitor (CLP),.interleukin (IL), granulocyte macrophage (GM) colony-stimulating-factor (CSF), stem cell factor (SCF), thrombopoietin (TPO), erythropoietin (EPO), granulocyte myeloid progenitor (GMP), runt-related transcription factor 1 (RUNX1), transcription factor stem cell leukaemia (SCL), ccaat enhancer binding proteins (C/EBP**),** friend of GATA protein 1 (FOG-1).

1.1.3 Cytokines

Cytokines are small soluble proteins that can be secreted or remain membrane bound and are produced by a wide variety of cells either within the HSC niche or for transportation through the bloodstream. There are currently over 60 that are identified as being involved in haematopoiesis (reviewed in Tarasova *et al.*, 2011) and include, interleukins, colony-stimulating factors, interferons, erythropoietin and TPO. They signal via two major classes of receptors, tyrosine kinase receptors such as c-KIT and FLT3, or those belonging to the cytokine receptor superfamily, such as type I and type II cytokine receptors (reviewed in Endele *et al.*, 2014). Type I and type II cytokine receptors share similar structural features and are composed of homodimeric or heterodimeric extracellular receptor chains and Box1/Box2 intracellular regions for binding of signalling molecules. Type 1 cytokine receptors have a tryptothan-serine-x-tryptophan-serine motif in the extracellular portion of the chain, which is not present in type II cytokine receptors. Binding of a cytokine to a cytokine receptor, induces conformational changes leading to the activation of Janus Kinases (JAKs) bound to the Box1/Box2 domains, phosphorylation of tyrosine's of the cytoplasmic portion of the chain, which leads to the generation of docking sites for Src homology 2 (SH2) domains of signal transducer proteins, which can translocate to the nucleus and activate transcription (1.1.4) (reviewed in Robb, 2007).

The process by which basal and emergency haematopoiesis occurs, is mediated mainly by cytokines. They interact with cellular membrane cytokine receptors, initiating cell signalling pathways that ultimately lead to lineage characteristic gene expression which governs differential fate. Individual cytokines can be lineage specific or regulate multiple cells, with some cells such as HSC and megakaryocyte progenitors requiring simultaneous action of multiple cytokines. Furthermore, different cytokine receptors may activate similar signalling pathways but generate different lineage commitment (reviewed in Metcalf, 2008). Other factors such as signalling molecule availability, epigenetics and even the nature of signalling dynamics activation (Marshall, 1995), have been shown to be significant in lineage determination.

Whilst individual cytokines cannot on their own be prescriptive for a defined differentiation outcome of any given cell, many studies have demonstrated that the action of certain combinations of cytokines on given cells, promote particular patterns

of cell survival and differentiation (Figure 1-1) (reviewed in Robb, 2007). However, whether cytokines determine cell fate, or whether they facilitate cell fate has long been disputed. Two models governing the determination of cell fate have been proposed, a deterministic model and a stochastic model. The deterministic model, proposes that all HSC have an equal capacity to differentiate down any haematopoietic lineage and that cell fate is determined by cell surface interactions between the HSC and cytokines, which then generate intracellular signals that drive changes in gene expression. The stochastic model in contrast argues that different HSC (and early progenitors) are primed for different lineage commitment, through the expression of different transcription factors, and that the presence or absence of particular cytokines simply generate a permissive or suppressive environment for their proliferation and survival, dependent on their pre-defined lineage preference (reviewed in Enver *et al.*, 1998). Evidence supporting the deterministic model initially came from the observation that when GM-colony forming cells were treated with either GM-CSF or macrophage-CSF (M-CSF), then granulocytes or macrophages were cultured, and that clones of these cells still gave rise to different lineages dependent on the cytokine environment (Metcalf and Burgess, 1982). Another study demonstrated that CLP treated with IL-2 was able to divert these cells from a lymphoid fate to develop granulocytes and monocytes (Kondo *et al.*, 2000). More recently, using single cell time-lapse bioimaging, murine granulocyte-macrophage progenitors were tracked in culture conditions containing either M-CSF or GM-CSF. The authors reported that, almost exclusively, culturing with M-CSF or GM-CSF led to monocytic or neutrophilic development respectively (Rieger *et al.*, 2009). Nonetheless, the majority of evidence supports the idea of a stochastic, or permissive model, of haematopoiesis. Mice engineered to be deficient in cytokines or cytokine receptors were still able to generate cells of associated lineage (reviewed in Robb, 2007), whilst overexpression of apoptotic regulator bcl-2 into the IL-3 dependent, multipotent haematopoietic cell line, FDCP mix, allowed multi-lineage differentiation in the absence of cytokines (Fairbairn *et al.*, 1993). Furthermore, analysis of EML cells, another multipotent haematopoietic mouse cell line, showed metastable transcriptome states within individual cells, that pre-determined lineage commitment (Chang *et al.*, 2008). Recently, studies employing single cell analysis have also lent support to the idea of a stochastic rather than deterministic model of cell fate determination (reviewed in Cvejic, 2016). It appears then that whilst cytokines allow proliferation and survival of progenitor cells, lineage decisions are more likely determined by transcription factors.

1.1.4 Transcription factors

Transcription factors are nuclear proteins that drive the expression of target genes. Whilst debate remains as to the precise mechanism by which, and at what stage, different haematopoietic lineages differentiate from each other (1.1.2), different transcription factors have been shown to drive phenotypically distinct haematopoietic cells to different lineage fates. Furthermore, whilst there is not yet definitive evidence that cytokines do not drive haematopoietic cell fate, deletion of genes encoding key haematopoietic transcription factors in mice typically generate graver phenotypes than deletions involving cytokines or cytokine receptors (reviewed in Rosenbauer and Tenen, 2007). Activation of signal transduction pathways lead to nuclear localisation of transcription factors, for example via association with carrier proteins containing nuclear localisation sequences or their release from cytosolic anchor proteins (reviewed in Cyert, 2001). In haematopoiesis, cytokine activation of JAK generates SH2 domains (1.1.3), resulting in the docking of signal transducer and activator of transcription (STAT) transcription factors and its subsequent phosphorylation. Dimerisation of STAT's then allows nuclear translocation and inducement of haematopoietic STAT target genes, important in differentiation, proliferation and survival (reviewed in Dorritie *et al.*, 2014). Other signalling pathways important in haematopoiesis include the Wnt signalling pathway (reviewed in Undi *et al.*, 2016), the NOTCH pathway (reviewed in Suresh and Irvine, 2015), the transforming growth factor beta (TGF-β) pathway (reviewed in Blank and Karlsson, 2015), and the phosphatidylinositol 3-kinase (PI3K) pathway (reviewed in Martelli *et al.*, 2010), and dysregulation of these pathways are important factors in haematological malignancy (1.2.1 and 1.2.2.2).

The role of transcription factors in haematopoiesis involves the interplay of a number of transcription factors which may be mutually antagonistic or synergistic to each other and whose expression levels are controlled by *cis*-regulatory elements and regulated by post-transcriptional modifications. Transcription factors important in myelopoiesis and megakaryopoiesis/erythropoiesis include RUNX1, transcription factor stem cell leukaemia (SCL), PU.1, GATA-(1&2), ccaat enhancer binding proteins (C/EBP) (α,β&ε), growth factor independent 1 (GFi1), interferon regulatory factor 8 (IRF8), erythroid Krüeppel-like factor (EKLF) and friend of GATA protein 1 (FOG-1), whilst in lymphopoiesis, Ikaros, transcription factor 1 (TCF-1), GATA-3, early B-cell factor (EBF), and paired box protein-5 (PAX-5) are all important in early lymphocyte

development (Figure 1-1) (reviewed in Wolff and Humeniuk, 2013). For example, conditional deletion of RUNX1 in mice using a Cre-loxP recombination system resulted in defective T-cell, B-cell and megakaryocyte maturation (Ichikawa *et al.*, 2004), whilst conditional deletion of SCL also resulted in the loss of megakaryocyte and erythroid differentiation (Mikkola *et al.*, 2003). The transcription factor PU.1, is downstream from RUNX1 and is considered the master regulator of myelopoiesis (reviewed in Imperato *et al.*, 2015). Conditional deletion of PU.1 in mice resulted in loss of HSC self-renewal, a block in generation of CMP and CLP, and disruption of granulocyte myeloid progenitor (GMP) differentiation (Iwasaki *et al.*, 2005). Levels of PU.1 expression are also important in determining cell fate. Downregulation of PU.1 is required for megakaryopoiesis/erythropoiesis and T-cell development, high levels of expression in GMP support macrophage development, whilst low (but not zero) expression levels are required for neutrophil production (reviewed in Rosenbauer and Tenen, 2007). Macrophage/neutrophil determination is note solely regulated by PU.1 however, increased levels of C/EBPα upregulates expression of GFi1, which inhibits PU.1 expression and drives neutrophilic differentiation (Laslo *et al.*, 2006), whilst synergistic expression of IRF8 and PU.1 is required for macrophage development (Tamura *et al.*, 2000). Expression levels of PU.1 and GATA-1 offer a further example of antagonistic transcription factor regulation in haematopoiesis. GATA-1 is considered to be the master regulator in erythropoiesis and activation of this transcription factor in murine GMP resulted in redirection of these cells to an erythroid fate (Heyworth *et al.*, 2002). Conversely, activation of PU.1 in avian megakaryocyte-erythroid progenitors (MEP) resulted in commitment to the myeloid lineage (Nerlov and Graf, 1998). Given the importance and array of transcription factors in haematopoiesis, it is perhaps then not surprising that their dysregulation or mutation is a major factor in AML (1.2.1).

1.2 Leukaemogenesis

Leukaemia is characterised by the accumulation of immature white blood cells (blasts) in the BM. There are four main types of leukaemia, chronic lymphocytic leukaemia (CLL), chronic myeloid leukaemia (CML), acute lymphocytic leukaemia (ALL) and AML. The acute form of the diseases is characterised by a rapid increase in immature blasts, whilst the chronic forms are typified by a slower build up in abnormal haematopoietic cells. In the UK, leukaemia was the 12th most common cancer between 1987 and 2006 and accounted for 2.5% of all cancers. Mortality rate is 4,300 people per

year with 7,000 new cases diagnosed annually, with children under the age of 10 constituting 4.5% of these cases (Bhayat *et al.*, 2009). In the U.S.A., leukaemia accounted for 4% of new cancers reported in 2016 and 4% of cancer mortalities. Five-year survival rate has improved from 34% in the mid 1970's to 62% between 2005 and 2011. In children (0-14 years) leukaemia accounts for 30% of all childhood cancers, with ALL being the most common. The five-year survival rate in children with ALL is currently 91%, whereas in children with AML this is reduced to 67%. In contrast, AML was the most commonly diagnosed form of leukaemia in adults in the U.S.A in 2016, accounting for 37% of new cases and 59% of the leukaemic mortality rate, whilst CLL accounted for 35% of new cases and 26% of mortalities, CML 15% of new cases and 6% of mortalities and ALL 12% of new cases and 8% of mortalities (Siegel *et al.*, 2016).

1.2.1 Acute Myeloid Leukaemia

AML is a heterogenous disease, resulting in a block in haematopoietic myeloid differentiation as a result of one or more genetic insults including chromosomal abnormalities, mutations of genes involved in signalling pathways or transcription and genetic effects such as methylation and histone modification (Table 1).

Originally, AML was classified according to the French-American-British (FAB) disease classification system (Bennett *et al.*, 1976), which has now been superseded by the World Health Organisation (WHO) classification system (4^{th} edition) which incorporates genetic information alongside the traditional morphological, cytochemical, immunophenotypic and clinical information (Swerdlow *et al.*, 2016). The WHO system uses consensus classification to define clinically distinct diseases entities and incorporates provisional entries, such as AML with mutated NPM1, for data that is yet to be fully established. For a diagnosis of AML PB or BM must contain greater than 20% myeloid blasts with the exception of AML with t(8;21)(q22;q22), AML with inversion (16)(p13.lq22) or t(16;16)(p13.1;q22) and acute promyelocytic leukaemia (APL) with t(15;17)(q22;q12) where the genetic abnormality is sufficient on its own. Percentage blast counts are derived from 200-cell leukocyte differential counts of PB smears and 500-cell differential counts of all nucleated BM cell smears. Multi-parameter flow cytometry is used to determine blast lineage, cytogenic analysis of BM cells is used to establish baseline karyotypes and real-time polymerase chain reaction or fluorescence in situ hybridisation allows for detection of specific gene mutation, such as

RAS, which are increasingly useful in determining prognosis outcome (Vardiman *et al.*, 2009). Recently, the WHO classification (4th edition) was updated to incorporate the prognostic significance of a number of these genetic mutations, such as FLT-3, C/EBPα and NPM1 (Arber *et al.*, 2016). These factors led to a recent refinement of European Leukemia Net risk stratification for AML, which is now based on three risk groups favourable, intermediate and adverse (Bullinger *et al.*, 2017).

AML patients typically present with anaemia, fatigue, shortness of breath, difficulties clearing infections, dizziness, bruising and excessive bleeding. Predisposing factors include genetics, smoking, alcohol use, obesity and exposure to radiation or alkylating agents. The median age of diagnosis is 75 in the UK, 67 in the U.S.A. and 72 in Sweden. In the UK remission rates in patients under 60 have improved to nearly 80%, whilst overall survival is between 40-45%. In the over 60's, between 1980 and 2000 remission rates improved to 65%, but overall survival after 5 years remained at around 12% (Newland, 2002). In Sweden, the adult five year survival rate for the under 70's improved from less than 10% in the 1970's to between 28-64% between 2006-2011, however, in the over 70's five year survival has remained below 10% (Bower *et al.*, 2016). In patients fit enough to tolerate chemotherapy, the standard treatment for AML since 1973 has been a seven-day continuous intravenous infusion of cytarabine (Ara-C) (100-200 mg/m^2) and 3 daily doses of daunorubicin (45-90 mg/m^2), sometimes followed by allogeneic or autologous stem cell transplantation. Recent attempts to improve treatment outcomes have involved higher doses of Ara-C (>1000 mg/m^2) alongside nucleoside analogues such as fludarabine, cladribine and clofarabine, which in the case of fludarabine showed a 20% improvement in 8 year overall survival (OS) compared to standard regimen chemotherapy (reviewed in Tamamyan *et al.*, 2017). Recently a phase III clinical trial involving CPX 351, a drug which packages Ara-C and daunorubicin into liposomes reported improved OS (9.6 vs 6 months) in high risk secondary AML patients (Medeiros *et al.*, 2016).

Table 1. Common abnormalities in AML. Class and frequency of gene mutations involved in AML (reviewed in Naoe and Kiyoi, 2013). * denotes most common mutation; N-RAS position 12 glycine to aspartic acid (G12D) 9-14%; K-RAS position 12 glycine to valine (G12C) 5-17%; H-RAS position 12 glycine to valine (G12V) not detected in AML.

Group	Gene	Mutational Frequency
Class 1 (Signal Transduction)	FLT-3	25-45%
	c-KIT	6-10%
	PTPNII	2-5%
	RAS*	15-30%
	CBL	2-3%
	JAK	2-3%
Class 2 (Transcriptional)	RUNX1	6-11%
	C/EBPα	4-9%
	NPM1	25-35%
	GATA2	3-5%
	RUNX1-ETO	10-15%
	CBFβ	3-8%
	PML-RARA	5-10%
	MLL	5-9%
Class 3 (Epigenetic)	TET2	8-27%
	IDH1	6-9%
	IDH2	9-12%
	DNMT3A	18-23%
	TP53	7-12%
	WT1	10-13%
	ASXL1	3-11%
	BCOR	5%
	BCOR1	6%
miRNA	miR15, miR16 miR17-92, miR125, miR155, miR196	

Historically it has been difficult to determine the initiating events in AML, but more recently clonal evolution studies and information from the cancer genome project have suggested that mutations of genes involved in epigenetic regulation occur in self-renewing HSC and precede leukaemia initiating events such as chromosomal translocations and the driver mutations involved in cell signalling molecules (Jan *et al.*, 2012, Welch *et al.*, 2012, Bullinger *et al.*, 2017). Population studies have shown that pre-leukaemic mutations, for example of DNA (cytosine-5)-methyltransferase 3A (DNMT3A) (an enzyme that catalyses the transfer of methyl groups to DNA), can be detected in HSC of AML patients with CR and have a multilineage repopulation advantage over HSC not carrying the mutation (Shlush *et al.*, 2014). The evidence that class III mutations occurring in HSC prior to initiating events, fits with the concept of leukaemia stem cells (LSC), first proposed in 1994, when severe combined immune deficient (SCID) mice were transplanted with PB from AML patients and it was found that only $CD34^+$ $CD38^-$ haematopoietic cells (a phenotype indicative of HSC or HPC status) engrafted and that the resulting leukaemia had a immunophenotype identical to the donor cells (Lapidot *et al.*, 1994). Subsequently it has been shown that analogous with HSC, LSC reside in the BM and have the capacity for both self-renewal and multi-lineage differentiation. Additionally they can exhibit characteristics that allow evasion of the cytotoxic effects of chemotherapy and immuno-surveillance and their frequency in patients at diagnosis has been correlated with increased residual disease and the likelihood of relapse (reviewed in Lane and Gilliland, 2010)).

Additionally, signalling pathways such as Wnt/β-catenin, Hedgehog, JAK/STAT and PI3K/AKT, which play important roles in maintaining LSC self-renewal and differentiation have also been targeted. Activation of Wnt/β-catenin results in inhibition of glycogen synthase kinase 3β (GSK-3β) (involved in proteasomal degradation β-catenin), which promotes translocation of β-catenin to the nucleus where it activates a number of genes associated with proliferation, including c-MYC, cyclin D1 and c-JUN. Currently an inhibitor of β-catenin, CWP232291, is undergoing phase I clinical trials in relapsed or refractory (R/R) AML patients (Cortes *et al.*, 2015). GSK-3 is also involved in the regulation of the PI3K/AKT pathway, the RAS/RAF/MEK/ERK pathway, the Hedgehog pathway and the NOTCH signalling pathway and as such, has generated particular interest as a target in leukaemia. To date over fifty inhibitors of GSK-3 have been developed, however while some *in vitro* studies have shown inhibition of growth

in leukaemic cell lines, other studies in breast cancer and medulloblastoma have reported GSK-3 overexpression induces apoptosis, and their potential benefit remains unclear (reviewed in McCubrey *et al.*, 2014). Inhibitors of the PI3K/AKT (which activates mammalian target of rapamycin (mTOR) important in cellular proliferation) such as CAL-101, perifosine and MK-2206 have also been developed and are currently in phase I/II clinical trials (reviewed in Wang *et al.*, 2017).

Recent advances in microarray and next generation sequencing have led to improved understanding of AML heterogeneity and the possibility of tailored treatments based on genome sequencing. In conjunction with this, several clinical trials are currently taking place examining the efficacy of drugs specifically targeted at specific AML phenotypes. Epigenetic modifiers such as DNMT3A which catalyses the methylation of DNA are commonly mutated in AML (Table 1). Trials involving guadecitabine, a second generation hypermethylating agent which inhibits DNMT3A activity showed promise in R/R AML patients and is currently undergoing phase III clinical trials. Isocitrate dehydrogenase (IDH) an enzyme of the citric acid cycle that catalyses the D-isocitrate to α-ketoglutarate reaction is also frequently mutated in AML, generating high levels of 2-hydroxyglutarate which competitively inhibit α-ketoglutarate enzymes. Treatment of R/R AML patients with the IDH inhibitors AG-120 and FT-2102 in phase I clinical trials showed CR of 18% and 9.5% respectively, whilst treatment with the IDH2 inhibitor Enasidenib also resulted in 18% CR of R/R AML patients and is currently recruiting for phase III clinical trials in R/R AML patients over 60. Other inhibitors of epigenetic modifiers such as bromodomain and extraterminal proteins and lysine specific demethylase-1 inhibitors are also currently in phase I clinical trials. In addition to inhibitors of epigenetic modifiers, signal transduction receptor such as JAK/STAT and FLT-3 are also therapeutic targets for inhibition and a number of clinical trials are underway. FLT-3 is the most frequently mutated gene in AML (Table 1) and several inhibitors have been developed such as Midostaurin, Sorafenib, Quizartinib, Gliteritinib and Crenolanib. In particular, Crenolanib has shown promise, with one study reporting an increased OS of 42 weeks in R/R AML patients which were FLT-3 inhibitor naïve, and interim analysis of a phase II clinical trial in newly diagnosed FLT-3 AML patients reporting CR of 88% at 6 months (reviewed in Saygin and Carraway, 2017). Finally, microRNA's (miRNA) which are 18-22 nucleotides in length, non-coding and regulate gene expression via the promotion of mRNA degradation or inhibition of translation,

are also known to be important both in haematopoiesis and leukaemogenesis. In particular, aberrant expression of miR125, which regulates haematopoietic differentiation, has been implicated in a number of AML subtypes (reviewed in Alemdehy and Erkeland, 2012) and their targeting using chemically modified antisense oligonucleotides offer further therapeutic targets.

1.2.2 RAS

The RAS superfamily are small guanosine triphosphatases (GTPase) proteins that are divided into five major classes, RAS, RHO, RAB, RAN and ARF, based on functional and structural data. The RHO family regulate signalling networks involved in actin organisation and cell cycle progression, the RAB and ARF families are involved in intracellular trafficking of proteins between different organelles, the RAN family transport RNA and proteins between the cytoplasm and the nucleus, whilst the RAS family are involved in signal transduction controlling gene expression regulating cellular proliferation, differentiation and survival (reviewed in Wennerberg *et al.*, 2005).

The RAS subfamily of proteins consists of 36 genes encoding 39 RAS proteins. Of particular importance from an oncology perspective are four isoforms, H-RAS, K-RAS4A, K-RAS4B and N-RAS, which are together mutated in approximately 16% of all cancers. Within the context of leukaemia, *RAS* mutations occur in approximately 15% of haematological malignancies, with *K-RAS* accounting for 5%, *N-RAS* 10% and *H-RAS* less than 1% (Prior *et al.*, 2012).

RAS proteins are functionally analogous to G-proteins and act as molecular switches inside cells. X-ray crystallographic structures have been determined and consist of a hydrophobic core of six stranded β-sheets and five α-helices connected by ten loops (Pai *et al.*, 1989). They function as molecular switches that activate a variety of signal transduction pathways in apoptosis, survival, differentiation, and proliferation.

1.2.2.1 The GTPase cycle and RAS

RAS proteins are synthesised in the cytosol and require post-translational modifications to translocate to the plasma membrane, which is crucial for their function in cell signalling. Initially, the hypervariable C-terminal region, containing a CAAX motif (where ‘C’ is cysteine, ‘A’ are aliphatic amino acids and X is any amino acid) is farnesylated at the cysteine residue, followed by cleavage of the AAX sequence, prior to carboxymethylation of the cysteine residue by the enzyme isoprenylcysteine

carboxymethyltransferase (Casey *et al.*, 1989). In the case of K-RAS4B, this is sufficient for membrane anchorage, however K-RAS4A, N-RAS and H-RAS require the addition of two further palmitic acids to cysteine residues that are upstream of the initial farnesylation site (Hancock *et al.*, 1990).

RAS proteins bind to guanosine nucleotides, which determines their functional activation status, where RAS, bound to guanosine triphosphate (GTP) is active, and when bound to guanosine diphosphate (GDP) is inactive (Figure 1-2). They possess intrinsic GTPase activity, which involves hydrolysis of the γ-phosphate group of GTP, leaving RAS bound to GDP (RAS-GDP). However, because this intrinsic activity is relatively slow ($t_{1/2}$ = 16 mins, k_{off} = 6 x 10^{-4} s^{-1} (Hunter *et al.*, 2015)), physiological GTP hydrolysis is catalysed by GTPase activating proteins (GAP), such as p120-RAS-GAP, neurofibrimin-1 and synaptic RAS GTPase-activating protein-1 (reviewed in Bos *et al.*, 2007). In contrast, inactive RAS-GDP is activated by guanine nucleotide exchange factors (GEF), which contain domains specific to the major classes of the RAS superfamily. GEFs specific to the RAS subfamily all contain the cell division cycle-25 (CDC25) domain of which, son of sevenless (SOS) and the RAS guanyl-releasing proteins (RAS-GRP) are best characterised from a haematological perspective. SOS (and other CDC25 domain containing GEFs) bind to RAS, resulting in conformational changes that release GDP and its replacement with GTP (Boriack-Sjodin *et al.*, 1998). Whilst GEFs do not promote preferential binding of GTP to RAS (RAS-GTP), physiological levels of intracellular GTP are an order of magnitude higher than GDP, which result in increased levels of RAS-GTP and RAS activation (Figure 1-2).

The mechanisms by which these reactions occur is the result of different preferential binding to the loops which connect the α-helices and β-sheets of the RAS protein (1.2.2). In particular, loops 1, 2 and 4 provide the binding pockets for GDP and GTP, whilst loops 3 (amino acids 30-38) and 5 (amino acids 59-76), termed switch 1 and 2 respectively, generate conformational changes in loops 1,2 and 4, resulting in the preferential binding of GDP or GTP. When GTP is bound to RAS, the amino acids T35 and G60 of switch I and II respectively, form hydrogen bonds with the γ-phosphate group of GTP, resulting in the active form of RAS. To hydrolyse GTP, GAP interacts with switch II by stabilising Q61, allowing interaction with a water molecule. Additionally, a conserved arginine finger protrudes into the phosphate binding pocket,

which neutralises the negative charge on the γ-phosphate. This allows extraction of a hydrogen ion from the water molecule, generating a hydroxyl group which then cleaves the γ-phosphate, resulting in a conformational change in switches I and II and inactivating RAS. Different GEFs are structurally unrelated, but all interact with the RAS-GDP structure by sterically occluding a Mg^{2+} ion in switch I, which co-ordinates binding of GDP/GTP in the phosphate binding site. For example SOS contains an α-helix, which interacts with switch II, resulting in a conformational change that opens the phosphate binding site, and releases GDP (reviewed in Simanshu *et al.*, 2017). GEFs themselves are subsequently replaced by GTP, via a series of intermediates, specific to individual GEFs that still are not fully elucidated (reviewed in Cherfils and Zeghouf, 2013).

1.2.2.2 RAS Signalling

The RAS subfamily of signalling molecules are involved in cell survival, apoptosis, motility, differentiation and proliferation. Haematologically, activation of RAS occurs as a result of haematopoietic cytokines binding to their receptors, subsequent activation of JAKs and the generation of docking sites for SH2 domains of signal transducer proteins, such as growth factor receptor-bound protein 2 (GRB2) (1.1.3). The c-terminal of GRB2 then interacts with a proline rich domain of SOS, whilst the pleckstrin-homology domain of SOS provides anchorage to the plasma membrane via its interactions with phospholipids. This opens the RAS exchanger motif (REM) site, which is an allosteric binding site for RAS (Figure 1-2). Interestingly, binding of RAS-GDP to REM results in much lower levels of SOS activity than binding to RAS-GTP. The CDC25 domain of SOS can then interact with membrane bound RAS, resulting in the displacement of GDP for GTP and activating RAS signalling pathways (reviewed in Buday and Downward, 2008)). The GRB2-SOS complex is only active when GRB2 is in the monomer form. Phosphorylation of tyrosine residues by proteins such as c-src (itself activated by tyrosine kinase receptors) results in the dissociation of GRB2 from its inactive dimeric form (Ahmed *et al.*, 2015). Termination of RAS signalling results in GRB2 dimerisation, dissociation of the GRB2-SOS-RAS complex and the subsequent hydrolysis of RAS-GTP to RAS-GDP by GAP.

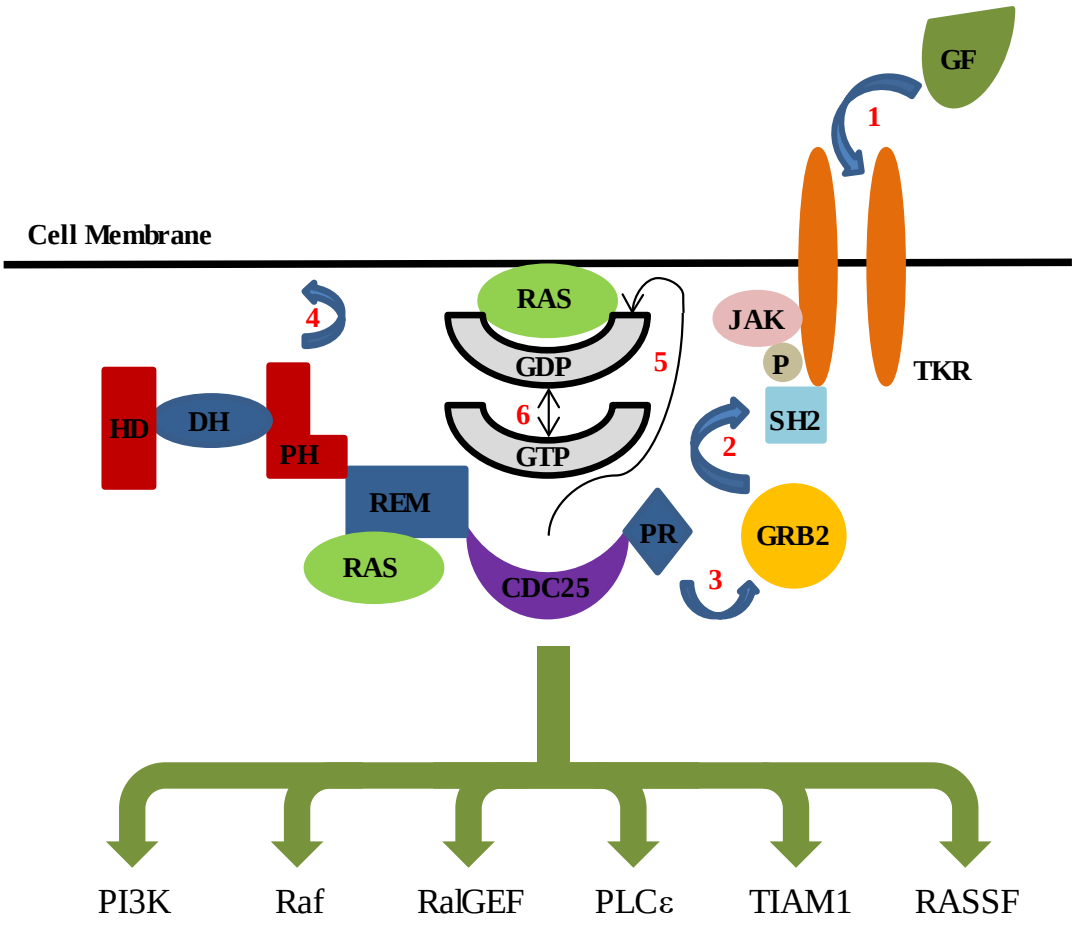

Figure 1-2. RAS signalling. Growth factor (GF) interacts with tyrosine kinase receptor (TKR) (1), resulting in activation of Janus Kinases (JAK), phosphorylation (P) of tyrosine's of the cytoplasmic portion of the TKR chain, and the generation of src homology 2 (SH2) docking site. Growth factor receptor-bound protein 2 (GRB2), is then recruited to the membrane (2) and reacts with the proline rich (PR) domain of Son of Sevenless (SOS) (3). The pleckstrin-homology domain (PH) then binds to the membrane (4) to complete docking of the SOS complex and allow binding of allosteric RAS to the RAS exchange motif (REM). The cell division cycle 25 (CDC25) domain of SOS then binds to RAS, resulting in the displacement of guanosine diphosphate (GDP) (5) and its replacement with guanosine triphosphate (GTP) (6). This results in activation of RAS effector molecules such as phosphatidylinositol 3-kinase (PI3K), rapidly accelerated fibrosarcoma (RAF), RAS related protein guanine nucleotide exchange factor (RalGEF), phospholipase C epsilon (PLCε), T-cell lymphoma invasion and metastasis 1 (TIAM1) and RAS association domain family (RASSF) and their respective signalling cascade pathways. Dbl homology domain (DH), Histone like domain (HD)

Activation of RAS results in the interaction of RAS with downstream effectors including RAS related protein GEF (RalGEF) important in endocytosis, T-cell lymphoma invasion and metastasis 1 (TIAM1) important in cell cycle progression, RAS association domain family (RASSF) important in apoptosis and cell cycle arrest, rapidly accelerated fibrosarcoma (RAF), PI3K, and phospholipase C epsilon (PLCε) (Figure 1-2). In haematopoietic cells, the RAS-RAF-MEK-ERK pathway targets genes involved in cellular proliferation and survival. Activation of RAS recruits RAFs, such as B-RAF (a serine/threonine kinase) to the cell membrane, where dimerization, changes in phosphorylation states of different domains and dissociation from its inhibitory protein occur. The RAS-GTP/B-RAF complex then phosphorylates meiosis specific serine/threonine-protein kinase (MEK) 1 and 2. MEK1/2 in turn phosphorylate extracellular signal-regulated proteins (ERK) which then activates a range of transcription factors such as c-JUN, c-FOS and c-MYC, which translocate to the nucleus where they target gene expression involved in cell growth and cell cycle progression (reviewed in McCubrey *et al.*, 2007). In particular, c-jun and c-FOS form a heterodimer which bind to a cyclin-D promoter, initiating transcription of this protein (Schutte *et al.*, 1989). Cyclin-D binds to cyclin dependent kinase (CDK) 4 and 6, which allows cellular progression through the G_1 phase of cell cycling, thus promoting proliferation (reviewed in Shaulian and Karin, 2002). The PI3K/AKT/mTOR pathway constitutes another important target of RAS signalling. RAS-GTP binds to P110α a catalytic subunit of PI3K, resulting in the translocation of PI3K to the plasma membrane. In turn PI3K phosphorylates phosphatidylinositol-4,5-biphosphate (PIP2) to produce phosphatidylinositol-3,4,5-triphosphate (PIP3), which results in translocation of protein kinase B (AKT) to the plasma membrane. Activation of AKT results in translocation to the cytosol and nucleus where it promotes cell survival through the inactivation of pro-apoptotic transcription factors such as forkhead and B-cell lymphoma 2 associated agonist of cell death (BAD) (reviewed in Vivanco and Sawyers, 2002). RAS activated PLCε signalling also constitutes an important haematopoietic pathway. PLCε binds directly to RAS-GTP, resulting in hydrolysis of PIP2, generating diacylglycerol and inositol-1,4,5-triphosphate which release Ca^{2+} and activates protein kinase C (PKC) (Song *et al.*, 2001). In turn PKC has been shown to have important functions in haematopoietic development by promoting monocytic lineage commitment of progenitor cells (Pearn *et al.*, 2007). Given the central role that RAS signalling plays in cellular proliferation, survival and growth, it is not surprising that dysregulation of its

pathways as a result of genetic mutations of its DNA, are commonly implicated in many cancers including AML.

1.2.2.3 Mutations of RAS and their effect in AML

As noted above, the three RAS isoforms implicated in haematological malignancy are N-RAS, H-RAS and K-RAS (1.2.2), which occur as the result of point mutations to amino acids at position (p) 12,13 or 61, resulting in constitutively active RAS. Mutations to p12 of N-RAS account for 51% of haematological malignancies containing an N-RAS mutation (56% of which are, N-RAS^{G12D} (glycine to aspartic acid) mutations) with mutations to p13 and p61 accounting for the other 32% and 17% respectively. In haematological malignancies involving K-RAS 70% of mutations occur at p12 (51% K-RAS^{G12D}) with 24% at p13 and 6% at p61 (Prior *et al.*, 2012).

In RAS, p12 and p13 occur in loop 1 of the GDP/GTP active binding site whilst p61 occurs in loop 5 (switch II) (1.2.2.1). Hydrolysis of RAS-GTP to RAS-GDP occurs as a result of interactions with GAPs. An important structural feature of GAPs, are an arginine finger which inserts into the active GTP/GDP binding site and is stabilised as a result of van-der-Waal forces with glycine p12. Substitution of the glycine with aspartic acid sterically hinders these van-der-Waal forces, as aspartic acid contains a side chain, leaving no room for insertion of the arginine finger (Franken *et al.*, 1993), thus preventing hydrolysis of GTP. Glutamine at p61 in switch II enhances GTP hydrolysis via an amide group on its side chain. The amide group forms a hydrogen bond with the GAP arginine finger, positioning it so that a carbonyl group can form a hydrogen bond with the nucleophilic water involved in the hydrolysis reaction. Substitution of glutamine with other amino acids prevents formation of the hydrogen bond between the carbonyl group and the nucleophilic water, inhibiting GTP hydrolysis (Gremer *et al.*, 2008).

As described above (1.2.1), initiation and progression of AML is characterised by a multistep process, (likely preceded by mutations to genes involved in epigenetic regulation of haematopoiesis (Bullinger *et al.*, 2017), which involves mutations to genes involved in haematopoietic differentiation, along with mutations to genes involved in proliferation and survival (Table 1). Whilst expression of mutational RAS in HPC has been shown to impact on haematopoietic differentiation (Darley *et al.*, 2002, Pearn *et al.*, 2007), RAS signalling in the broader context is predominantly associated with

cellular proliferation and survival (1.2.2.2) and requires co-operating mutations for transformation of cells. Early evidence for this was observed from the failure of H-RAS^{G12V} to transform normal hamster fibroblast cells (Newbold and Overell, 1983). More recently work in mice has shown that whilst transgenic mice expressing N-RAS^{D12} under the control of myeloid related protein 8 (MRP8) promoter do not develop AML like disease, crossing these mice with mice expressing BCL-2 (a regulatory protein of apoptosis frequently overexpressed in AML (Wojcik *et al.*, 2005), results in progression to human like AML disease (Omidvar *et al.*, 2007). Indeed, overexpression of RAS has been shown to cause cell senescence and quiescence through activation of the tumour suppressor proteins TP53 and $p16^{INK4A}$ (Serrano *et al.*, 1997). TP53 induces cell cycle arrest through upregulation of $p21^{Cip1}$ which inhibits CDK, and TP53 is a known mutation in AML (Table 1). Overexpression of mutant RAS has also been shown to lead to increased levels of extracellular ROS (Hole *et al.*, 2010) (1.3.3.4), which is linked with increased proliferation.

RAS mutations together with co-operating mutations can then lead to the activation of RAS signalling pathways, that collectively generate increased cellular proliferation and survival. Unsurprisingly, several efforts have been made to target this aberrant signalling. Inhibition of RAS mRNA translation using RNA interference technology, has shown promise in inhibiting growth of pancreatic, lung, colorectal and ovarian cancers in cell lines and animal models, but difficulties in delivering the drug to tumour sites and neutralisation by the immune system mean it has not yet progressed to human trials. Disruption of post-translational modifications of RAS using farnesyltransferase inhibitors (FTI), to prevent the translocation of RAS to the cell membrane have undergone phase III clinical trials, but no improvement in OS has so far been observed. Targeting of RAS downstream effector pathways such as PI3K/AKT/mTOR and RAF-MEK-ERK have also been attempted. Inhibition of PI3K with BKM120, AKT with MK2206 and mTOR with Temsirolimus and Everolimus, are all in human clinical trials. Sorafenib, which targets both C-RAF and more crucially B-RAF has been approved for use in advanced renal cell carcinomas, whilst Vemurafenib which preferentially targets mutant B-RAF, has been approved for use in patients with advanced melanoma. Inhibition of MEK using Trametinib is also being investigated in several phase III clinical trials in melanoma patients. However whilst all these drugs have shown some efficacy in improving progression free survival rates, up to now drug resistance has

been a major issue and overall survival rates have not improved (reviewed in Takashima and Faller, 2013).

1.3 Reactive Oxygen Species

Reactive oxygen species (ROS) is the collective term for several oxygen containing free radicals and other reactive molecules, such as hydrogen peroxide (H_2O_2) (1.3.1). Physiologically there are a number of sources of cellular ROS; oxidative phosphorylation in the mitochondria which generates ROS as a result of electron transport chain activity (ETC) (1.3.2.1), the nicotinamide adenine dinucleotide phosphate (NADPH) oxidase family of enzymes (NOX) (1.3.2.2), the cytochrome P450 enzymes, peroxisomes and the metabolic enzyme xanthine oxidase (XO) (1.4.2.1). Functionally, ROS is important in innate immunity (1.3.3.1), protein folding in the endoplasmic reticulum and also as a cell signalling molecule involved in cellular proliferation, survival, differentiation and gene expression (1.3.3.2). Haematopoietically, ROS has been implicated in both HSC quiescence (via signalling pathways downstream of RAS), and haematopoietic differentiation (1.3.3.3). ROS is known to be important in a number of diseases, such as atherosclerosis, rheumatoid arthritis as well as a number of cancers, including leukaemia (1.3.3.4). Consequently, ROS is of considerable interest as a therapeutic target, with both pro-oxidant and anti-oxidant cellular modulation being explored (reviewed in Hole *et al.*, 2011).

1.3.1 ROS chemistry

Physiologically, ROS are initially generated via the univalent reduction of molecular oxygen which generates superoxide ($O_2^{\bullet-}$) (Figure 1-3). Superoxide ($t_{1/2}$ = 1μs) dismutates to H_2O_2 ($t_{1/2}$ = 1ms) (Bienert *et al.*, 2006), either spontaneously or via the catalytic action of the enzyme superoxide dismutase (SOD). Alternatively, it may react with other ROS molecules, such as hypochlorous acid (HOCl) (itself formed via the catalytic reaction of peroxidase on H_2O_2) to form hydroxyl radicals ($OH^{\bullet}$) ($t_{1/2}$ = 1ns) (Sies, 1993), or nitric oxide to generate peroxynitrite, a reactive nitrogen species. H_2O_2 in the presence of Fe^{2+} ions, is catalysed to form a $OH^{\bullet}$ radical and hydroxide ion OH^-, whilst the resulting Fe^{3+} ion is reduced by $O_2^{\bullet-}$ resulting in the generation of O_2 and Fe^{2+}, in a set of reactions collectively termed Fenton chemistry. Copper ions (Cu^{2+} and Cu^+), can also catalyse these reactions, via a similar redox process, although given that the upper limit of 'free' copper is reported to be less than an atom per cell, it's physiological significance is likely limited (Rae *et al.*, 1999).

Cellular levels of 'free' iron are also severely restricted. It is transported around the cell by transferrin and stored by ferritin, which bind the iron and prevent it reacting with H_2O_2, thus leading to high levels of potentially damaging $OH^{\bullet}$ (reviewed in Ponka, 1999)). However, low levels of 'free' iron are found under normal physiological conditions and for haematopoietic cells are estimated to be in the region of 0.2-1.5μM (Epsztejn *et al.*, 1997, Ma *et al.*, 2007). Patients with β-thalassemia have frequent blood transfusions leading to iron overload, which is then free to generate ROS, which may help explain the high levels of oxidative stress encountered in these patients (Sengsuk *et al.*, 2014). Whilst ROS is necessary for a number of biological functions (1.3.3), high levels are often associated with oxidative stress, which can result in DNA damage, oxidation of proteins, enzyme inhibition and lipid peroxidation, and for this reason cellular ROS levels are tightly regulated (reviewed in Valko *et al.*, 2007).

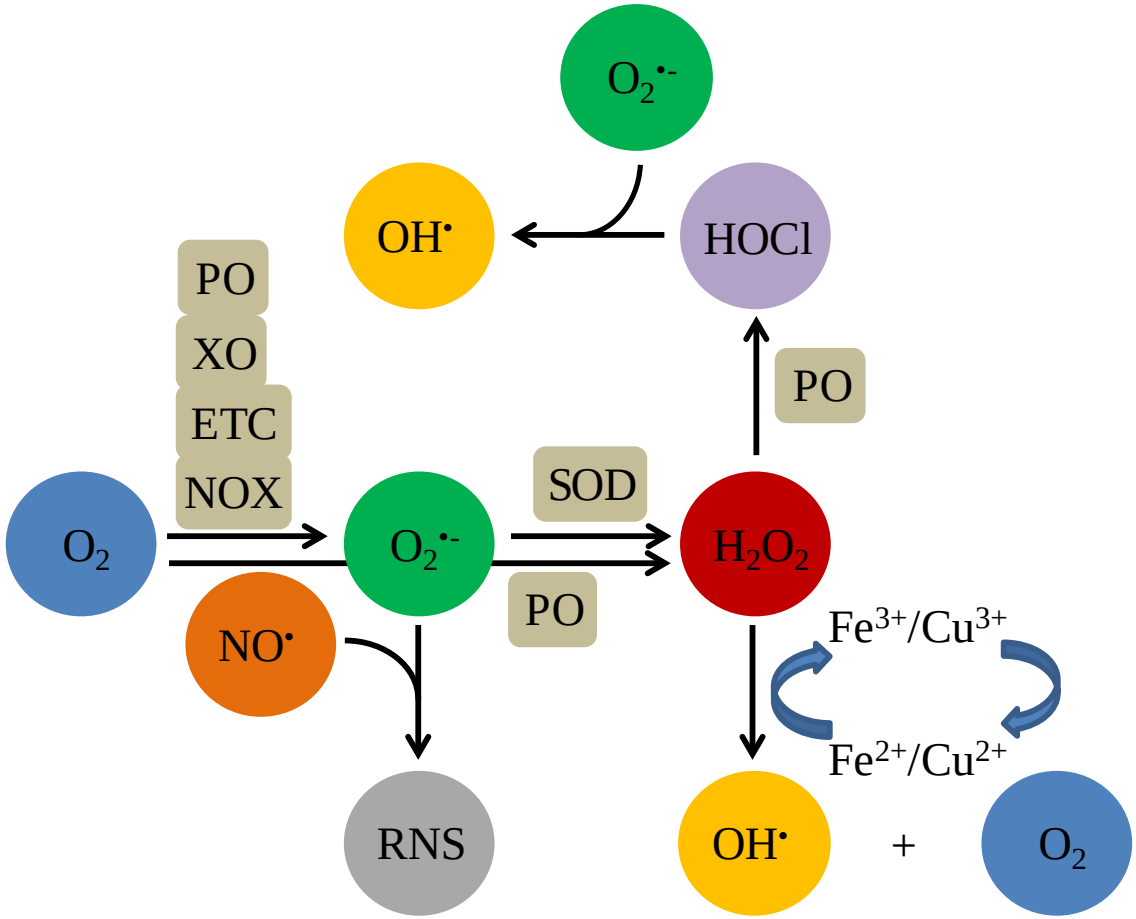

Figure 1-3. Formation of reactive oxygen species (ROS). Diatomic oxygen (O_2) is univalently reduced by peroxisomes (PO), xanthine oxidase (XO), the electron transport chain (ETC), or NADPH oxidase (NOX) to generate superoxide ($O_2^{\bullet-}$). PO may also reduce O_2 directly to form H_2O_2. $O_2^{\bullet-}$ may then dismutate to H_2O_2 either spontaneously or through the enzymatic action of superoxide dismutase (SOD). Hydroxyl radicals ($OH^{\bullet}$) may then be formed from H_2O_2 via the formation of hypochlorous radical (HOCl) in the PO, or via Fenton chemistry. Reactive nitrogen species (RNS) may also be formed through the reaction of nitric oxide radical ($NO^{\bullet}$) with $O_2^{\bullet-}$.

1.3.2 Sources of ROS production

1.3.2.1 Mitochondria as a source of ROS

One source of cellular ROS is via the mitochondrial ETC which consist of four complexes; complex I (nicotinamide adenine dinucleotide (NAD)H:ubiquinone oxidoreducatase or NADH dehydrogenase), complex II (succinate dehydrogenase (SDH) or succinate co-enzyme Q10 (CoQ) reductase), complex III (cytochrome bc_1 complex) and complex IV (cytochrome c oxidase). These complexes are located on the inner membrane of the mitochondria, with complexes I, II and IV establishing a proton gradient across this membrane, which, when protons flow back across the membrane, ATP synthase (complex V) uses to generate ATP from adenosine diphosphate (ADP), in a process collectively called oxidative phosphorylation (Gu *et al.*, 2016). The underlying mechanism behind the establishment of this gradient are a series of redox reactions involving the transfer of electrons, which drive protons into the intermembrane space generating an electrochemical gradient. Briefly, NADH, generated as a result of glycolysis (1.4.3) and the citric acid cycle (1.4.4), donates two electrons to flavin mononucleotide (FMN), which forms part of complex I. These electrons are then transferred via the iron-sulphur (Fe-S) clusters of complex I to CoQ in complex II, reducing it to $CoQH_2$ and transferring four protons across the inner membrane in the process. SDH (an enzyme that catalyses the reaction of succinate to fumarate in the citric acid cycle and reduces flavin adenine dinucleotide (FAD) to $FADH_2$ forms part of complex II. $FADH_2$ also donates its electrons to CoQ via Fe-S clusters, but does not contribute to the proton gradient as the free energy released is too small. The electrons are then transferred sequentially to cytochrome b, then c_1 of complex III and two further protons are pumped across the membrane. The final step, transfers four further protons across the membrane, as the reduced form of cytochrome c transfers the electrons to molecular oxygen, generating two water molecules. ATP synthase, a transmembrane protein of the inner mitochondrial membrane, then generates ATP from ADP as the electrochemical gradient, generated in the mitochondrial inter membrane space by the proton pump, drives protons back into the mitochondrial matrix.

Generation of ROS by the mitochondria is primarily a function of ‘electron leakage’ from the ETC, however, mitochondrial ROS may also be generated as a result of numerous enzymes including monoamine oxidase, cytochrome b5 reductase, glycerol-3-phosphate dehydrogenase, aconitase, pyruvate dehydrogenase and α-ketoglutarate

dehydrogenase (reviewed in Angelova and Abramov, 2016). Mitochondrial ROS production resulting from the ETC generates $O_2^{\bullet-}$, and is thought to occur as result of one of three mechanisms. The first mechanism is a consequence of a high NADH/NAD^+ ratio, and results from O_2 interacting with fully reduced FMN. Mitochondrial ROS generated by this mechanism has been observed due to mitochondrial mutation, physiological damage such as ischaemia or aging, and only small amounts of ROS are thought to be generated via these mechanisms in normally respiring cells (reviewed in Murphy, 2009). The second mechanism occurs when there is a high level of $CoQH_2$ in complex II, which in the presence of a high proton motive force generated by the proton pump, force electrons back into complex I in a process known as reverse electron transport (RET). Whilst RET generated ROS has also been implicated in diseases such as ischaemia, it is now also thought to be involved as a cell signalling molecule in metabolic adaptation, myeloid differentiation and response to bacterial infection (reviewed in Scialo *et al.*, 2017). The third mechanism of ROS generation by the ETC occurs at complex III and has also been implicated in ROS signalling. The formation of $O_2^{\bullet-}$ occurs at the ubiquinol oxidation centre (Q_o) site of the cytochrome bc_1 complex, in which fully oxidised CoQ supports formation of $O_2^{\bullet-}$, through the transfer of electrons from reduced haem b1 to molecular oxygen (Drose and Brandt, 2008). Generation of $O_2^{\bullet-}$ by complex I and II occurs exclusively in the mitochondrial matrix, whereas $O_2^{\bullet-}$ generated by complex III also occurs in the intermembrane space. $O_2^{\bullet-}$ generated in the mitochondrial matrix is rapidly converted to H_2O_2 by mitochondrial SOD (Mn-SOD), whereas $O_2^{\bullet-}$ generated in the intermembrane space travels through the outer mitochondrial membrane prior to conversion to H_2O_2 by cytosolic SOD (Cu/Zn-SOD).

1.3.2.2 NADPH oxidase (NOX) as a source of ROS

The NOX family of enzymes comprise of seven members, NOX1-5 and dual oxidase (DUOX) 1 and 2. They are transmembrane proteins that transfer electrons from NADPH to molecular oxygen, generating $O_2^{\bullet-}$ (or H_2O_2), which can then be converted to other forms of ROS (1.3.1). In mammals, they are distributed widely in most tissues, although high levels of expression of different isoforms, are more tissue specific. NOX1 is highly expressed in the colon, NOX2 in phagocytes, NOX3 in the inner ear, NOX4 in the kidney and blood vessels, NOX5 in lymphoid tissue and testis, and DUOX1 and 2 in the thyroid. From a haematopoietic perspective, intermediate levels of NOX1 expression are also found in osteoclasts, of NOX2 in B-cells and HSC, and of NOX4 in

osteoclasts and HSC (reviewed in Bedard and Krause, 2007). Different NOX isoforms share conserved structural features comprising of six helical transmembrane domains (TM) (with helix III and helix V containing two haem-binding histidines), and a C-terminus cytosolic domain (DH), which allows binding of FAD and NADPH (Figure 1-4). Difficulties in obtaining suitable levels of NOX proteins mean that to date relatively little crystal structure data is available. However, a recently published report (Magnani *et al.*, 2017), has elucidated the structure of the TM and DH domains (common to all NOX isoforms) of *Cylindrospermum stagnale* NOX5 in complex with FAD. In this structure, the six transmembrane helices of TM domain form a pyramidal shape with the base on the cytosolic side, a N-terminus α-helix runs parallel to the cytosolic side of the membrane and the haem groups sit in cavities formed by helices II-V, so that one is positioned near the cytosolic side of the membrane (haem 1) and the other on the outer side (haem 2). The DH domain, located on the cytosolic side, contains two pockets, one for FAD binding and one for NADPH binding. The FAD is positioned so that the flavin is in direct contact with haem 1 of the TM, to promote interdomain electron transfer. The proposed mechanism of electron transfer then involves NADPH donating its electron to FAD, which in turn donates an electron to haem 1 and then to haem 2 via Trp378 (equating to Phe 215 in human NOX2, Phe 200 in human NOX4 and Val 362 in human NOX5) of the loop between helix II and III of the TM, before reduction of molecular oxygen, via a final electron transfer step generates $O_2^{\bullet-}$ (Figure 1-4).

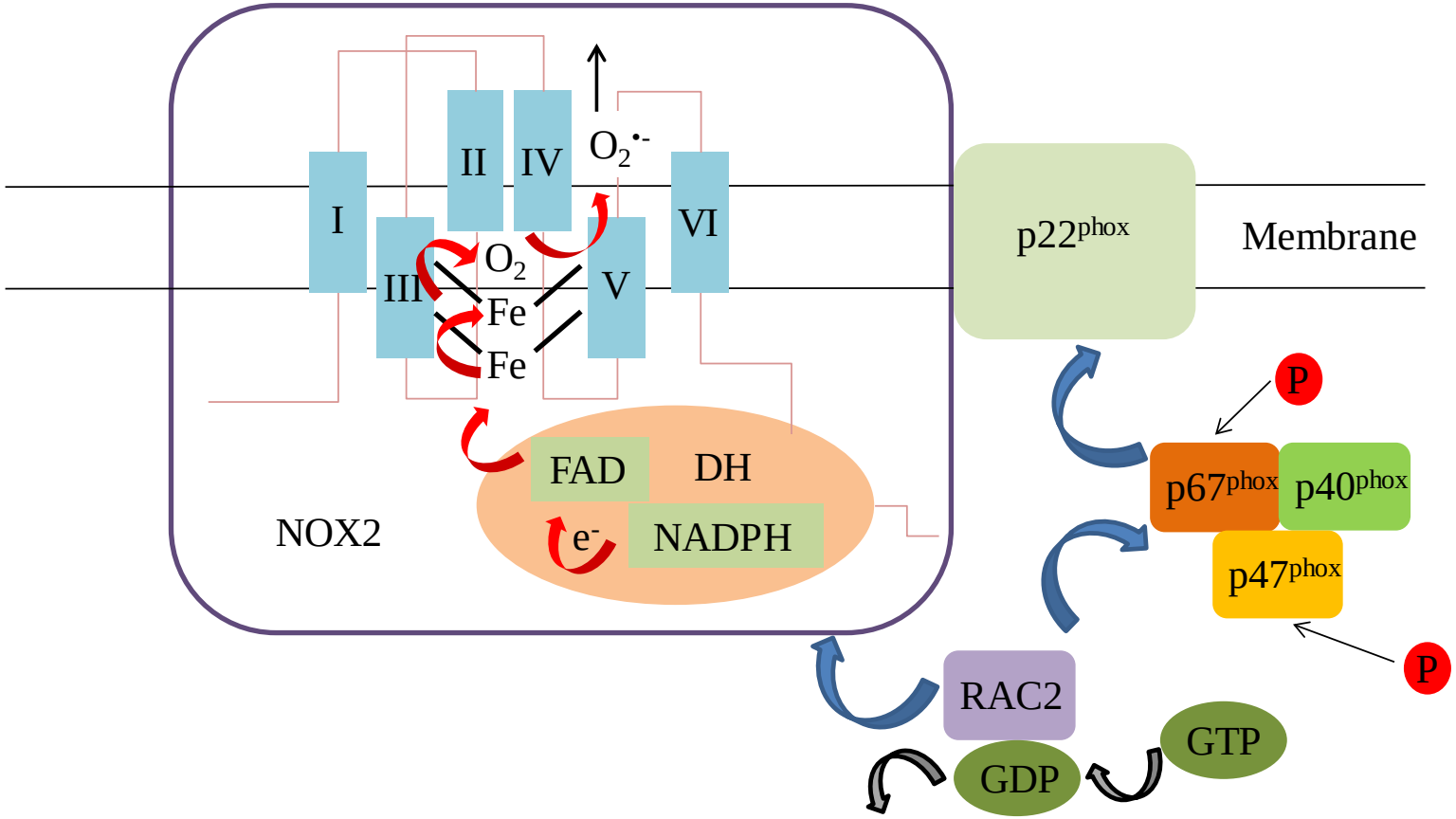

Figure 1-4. Generation of superoxide ($O_2^{\bullet-}$) by NADPH Oxidase (NOX). Schematic diagram showing the major structural features of NOX2, it's activation by phosphorylation (P) of $p67^{phox}$and $p47^{phox}$ and the assembly of the major subunits of the NOX complex, and the generation of superoxide via electron transfer from NADPH to flavin adenine dinucleotide (FAD) to haem groups to diatomic oxygen. Guanosine triphosphate (GTP), guanosine diphosphate (GDP), homology domain (DH), RAS-related C3 botulinum toxin substrate 2 (Rac2).

The NOX2 complex was the first NOX isoform to be identified and consists of six subunits, the catalytic core comprising of gp91^{phox} (NOX2) and p22^{phox}, and p40^{phox}, p47^{phox}, p67^{phox} and RAS-related C3 botulinum toxin substrate 2 (Rac2). Gp91^{phox} and p22^{phox} reside at the membrane and together form the catalytic core of NOX2 known as cytochrome b_{558}. The subunits p40^{phox}, p47^{phox} and p67^{phox} exist as a multidomain complex in the cytosol. Phagocytic stimulation, results in the phosphorylation of p47^{phox} at multiple sites by various PKC isoforms, p38^{MAPK}, p21-activated kinase and AKT. Phosphorylation of p67^{phox} by PKCδ also occurs (Zhao *et al.*, 2005) which together cause a conformational change in the complex, which allows it to interact with p22^{phox}. The complex translocates to the membrane where the conformational changes allow it to dock with cytochrome b_{558}. Simultaneously, cytosolic RHO-related RAC-2 (bound to RHO GDP dissociation inhibitor (RHOGDI) in its resting state) is activated, exchanging GDP for GTP, and it too translocates to the membrane where it interacts with gp91^{phox} and p67^{phox} and completes the activation of the enzyme complex, allowing generation of $O_2^{\bullet-}$ (Figure 1-4) (reviewed in Groemping and Rittinger, 2005). Whilst the mechanisms governing deactivation of NOX2 are not fully understood, evidence suggests that the complex is likely activated, deactivated and then reactivated in rapid cycles (reviewed in DeCoursey and Ligeti, 2005). Other NOX isoforms also require activation, but the mechanism of activation differs. NOX1-4 all associate with p22^{phox}, though this is not required in NOX5 and DUOX 1and 2, which are activated by Ca^{2+} via their long N-terminus which contains the calcium binding EF hand domain. NOX1 and NOX3 additionally require the cytosolic subunits NOX organiser 1 and NOX activator 1, which are homologs of p47^{phox} and p67^{phox} respectively, whilst activation of NOX4 does not require cytosolic subunits. NOX1 additionally requires RAC GTP, whilst its role in NOX3 and NOX4 activation is still a matter of debate (reviewed in Panday *et al.*, 2015).

1.3.2.3 Transportation of ROS across the cellular membrane

ROS is generated both intracellularly, for example in the mitochondria by the ETC, and extracellularly, for example by NOX2 (1.3.2). As described further below (1.3.2.4) the extracellular $O_2^{\bullet-}$ produced by NOX2 rapidly dismutates, either spontaneously or as a consequence of the enzymatic action of extracellular SOD (EC-SOD), to generate H_2O_2. In order for this extracellular H_2O_2 to participate in cell signalling (1.3.3.2), it is necessary for it to traverse the cell membrane. H_2O crosses the cell membrane either through natural diffusion, or active transportation via a large family of transmembrane

channel proteins, major intrinsic proteins, which can be further divided into the water permeable aquaporins (AQP) and the glycerol permeable aquaglyceroporins. This AQP facilitated transport of H_2O across the cellular membrane occurs via a hydrophilic channel which allows the passage of molecules based on size and their ability to form hydrogen bonds with the channel walls. Whilst H_2O_2 is relatively similar in size, stereochemistry and polarity to H_2O, the differences in structure and polarity mean it diffuses across the cellular membrane more slowly than H_2O, suggesting that its role as a signalling molecule requires active membrane transport (reviewed in Bienert and Chaumont, 2014). Despite these differences however, the similarities in physiochemical properties between H_2O_2 and H_2O, as well as its ability to form hydrogen bonds, does allow AQP facilitated transport, by some, but not all AQP isoforms. Using HEK293T cells treated with a H_2O_2 selective dye (peroxy yellow 1-methyl ester) and overexpressing AQP1, AQP3 or AQP8, it was shown that both AQP3 and AQP8 allow transportation of H_2O_2, whilst AQP1 does not (Miller *et al.*, 2010). In the same study, further confirmation of the role of AQP3 in H_2O_2 transport was performed in the human colon adenocarcinoma cell line, HT29, which express AQP3. Knock-down of AQP3 using shRNA, prevented H_2O_2 uptake as measured by the H_2O_2 fluorescent sensor HyPer. Further, treatment of the HT29 cells with epidermal growth factor, activated extracellular NOX production, correlating with an increase in AKT phosphorylation, which was not observed in the AQP3 knock-down cells, suggesting a role for extracellular NOX generated ROS in cell signalling. In another study, treatment of the HeLa cell line (expressing HyPer) with exogenous H_2O_2, showed decreased fluorescence when the cells were treated with the AQP inhibitor HgCl, whilst knock-down of AQP8 resulted in no change in HyPer fluorescence in these cells upon treatment with extracellular H_2O_2 (Bertolotti *et al.*, 2013). In the AML cell line B1647, cells pre-treated with the AQP inhibitor silver nitrate, then treated with exogenous H_2O_2 showed decreased intracellular H_2O_2 levels as measured by 2,7-dichlorodihydrofluorescin diacetate (DCFH-DA). Overexpression of AQP3 and AQP8 but not AQP1 in these cells led to increased intracellular H_2O_2, whilst knockdown of AQP3 and AQP8 with siRNA led to a decrease in intracellular H_2O_2 levels in cells treated with 100μM H_2O_2 and a decrease in H_2O_2 basal levels in the case of AQP8 knock-down cells. Interestingly, changes in intracellular H_2O_2 levels as a result of overexpression or knock-down of AQP8 in these cells, correlated with increased and

decreased proliferation respectively both at basal levels and when treated with 100μM H_2O_2 (Dalla Sega *et al.*, 2014).

1.3.2.4 Cellular antioxidant systems

Whilst ROS plays a role in cell signalling (1.3.3.2), high levels of ROS are toxic to cells resulting in DNA damage, lipid peroxidation and protein degradation, and their regulation is therefore tightly controlled (reviewed in Valko *et al.*, 2006). Several intracellular mechanisms exist for the purpose of ROS detoxification including, the thioredoxin, peroxiredoxin and glutathione systems, the enzymes SOD and catalase (Figure 1-5) and dietary antioxidants such as vitamins A, C and E.

The thioredoxin system consists of thioredoxin (Trx), thioredoxin reductase (TrxR) and NADPH. In mammalian cells, there are three isoforms of Trx, cytoplasmic Trx (Trx1), mitochondrial Trx (Trx2) and spermatozoa Trx (SpTrx), all of which have a TrxR isoform equivalent. Trx reduce proteins or oxidised peroxiredoxins through transfer of two electrons, the first from cys-32 and then from cys-35 of a conserved active site Cys-Gly-Pro-Cys, followed by the formation of a disulphide bridge between these two adjacent cysteines. Trx is then reduced back to its dithiol form by interaction with TrxR which contains one FAD unit and a c-terminus with a Gly-Cys-Sec-Gly-COOH motif. The selenium and SH group of the neighbouring cysteine donate electrons to oxidised Trx, forming a disulphide bridge in the process. This in turn is reduced by the donation of electrons from NADPH to TrxR via the FAD unit (reviewed in Nordberg and Arner, 2001). It is worth noting that while the Trx system is important as an antioxidant it also has other roles. So, whilst Trx1 is found in the cytoplasm, it can also be excreted from the cell or translocated to the nucleus where it serves different functions (Nakamura *et al.*, 1997). For example, in the cytoplasm Trx inhibits activity of the transcription factor nuclear factor kappa-light-chain-enhancer of activated B-cells (NF-κB), whereas in the nucleus it promotes its ability to bind to DNA (Hirota *et al.*, 1999).

Linked to the thioredoxin system are the antioxidants peroxiredoxins (Prx). Prx are highly abundant in mammalian cells and like Trx are also implicated in H_2O_2 cell signalling. In mammalian cells six isoforms have been identified (PrxI-VI), which can be divided into three classes, 1-Cys Prx, typical 2-Cys Prx and atypical 2-Cys Prx. PrxI, PrxII and PrxVI are localised to the cytosol, PrxIII and PrxV to the mitochondria (with PrxV additionally found in peroxisomes) and PrxIV is found extracellularly.

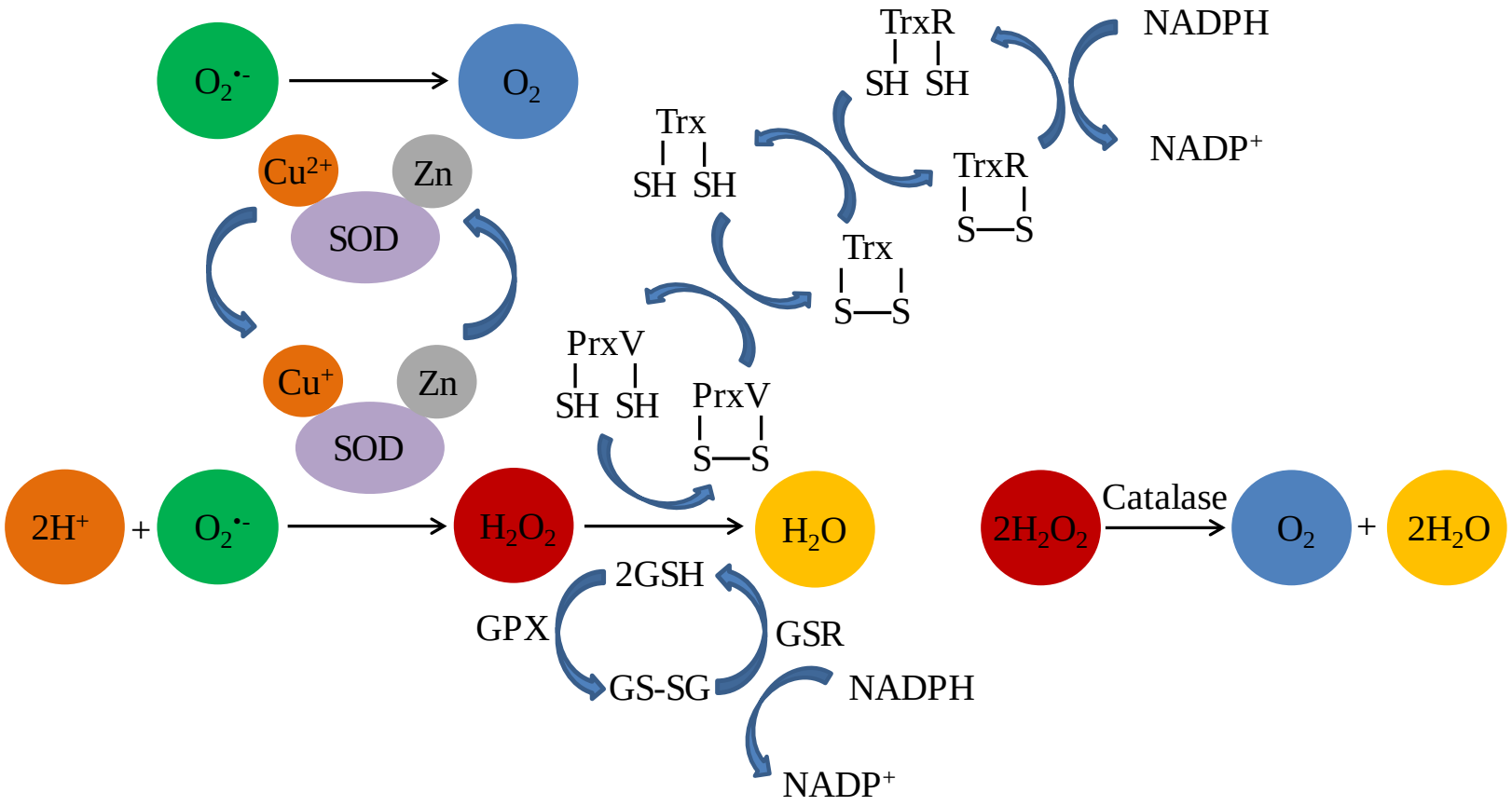

Figure 1-5. Cellular antioxidant systems. Schematic diagram showing the major antioxidant systems in cells. Superoxide ($O_2^{\bullet-}$) is reduced by the catalytic action of superoxide dismutase (SOD) to hydrogen peroxide (H_2O_2), which can then be reduced to water via the actions of the glutathione system or the action of peroxiredoxins (Prx). Prx are reduced by thioredoxin (Trx), which in turn is reduced by thioredoxin reductase (TrxR) and both TrxR and glutathione reductase (GSR) are reduced by nicotinamide adenine dinucleotide phosphate (NADPH). Additionally, H_2O_2 can be converted to oxygen and water by the action of the enzyme catalase. Glutathione (GSH), glutathione peroxidase (GPX).

All Prx isoforms have a conserved active site, which in PrxII is centred around cys-51 and includes pro-44, which limits access to the oxidised sulphenic acid group on the cysteine preventing further oxidation, thr-48, which forms a hydrogen bond with non-conserved residue 45 which in turn forms a hydrogen bond with cys-51 and arg-127 which stabilises the thiolate form of cys-51. In all three Prx classes, cys-51 is initially oxidised to form the sulphenic acid intermediate. Typical 2-Cys Prx (PrxI-IV) are homodimers (with two identical active sites) and contain an additional conserved cysteine in the c-terminus region. Following oxidation of the active site cysteines two disulphide bridges are formed between these cysteines and the c-terminus cysteines of the corresponding dimer. Atypical 2-Cys-Prx (PrxV) is monomeric, which following oxidation of its active cysteine forms a disulphide bridge with another cysteine residue further along its polypeptide chain, whilst 1-Cys-Prx (PrxVI) does not contain an additional cysteine and maintains a sulphenic acid group following oxidation (reviewed in Rhee *et al.*, 2005)). Both typical and atypical 2-Cys-Prx are only reduced by Trx, whilst 1-Cys-Prx is reduced by the glutathione system (Manevich *et al.*, 2004) and ascorbate (Monteiro *et al.*, 2007).

The glutathione system comprises of glutathione (GSH), glutathione peroxidase (GPX) glutathione reductase (GSR) and NADPH. GSH is synthesised in the cytosol by γ-glutamylcysteine synthetase and GSH synthetase (reviewed in Meister and Anderson, 1983) and is the most abundant thiol in mammals, with concentrations ranging from 1-11mM in they cytosol, 3-11mM in the nucleus and 5-11mM in the mitochondria (reviewed in Valko *et al.*, 2006). GSH is oxidised by H_2O_2 in the presence of the selenium containing enzyme GPX to form glutathione disulphide (GSSG). Initially H_2O_2 oxidises the selenium of Sec in GPX generating a selenic acid group on the Sec residue (R-SeOH), which in turn is reduced by GSH to form GS-SeR, which then reacts with another GSH to generate GSSG (reviewed in Masella *et al.*, 2005). GSR contains a FAD unit which when reduced by NADPH, breaks a disulphide bond on the conserved cys-58 and cys-63 residues of GSR, by the formation of a covalent bond with cys-63. $NADP^+$ is then released and replaced by another NADPH, GSSG binds to GSR whereupon cys-58 breaks the disulphide bond releasing one GSH, before cys-63 and cys-58 reform a disulphide bond releasing the other GSH (Berkholz *et al.*, 2008).

Catalase consists of four identical polypeptide chains surrounding a haem group which is the active site. In mammalian cells, it is normally found in the peroxisome where it

catalyses the reaction of H_2O_2, via a two-step reaction. On entering the active site, H_2O_2 donates an oxygen to the haem group, which then reacts with another H_2O_2 molecule, ultimately generating one oxygen and two water molecules (reviewed in Chelikani *et al.*, 2004).

Whilst Prx, GSH and catalase are involved in the reduction of H_2O_2, SOD are responsible for catalysing the dismutation of $O_2^{\bullet-}$ to H_2O_2 and oxygen (McCord and Fridovic.I, 1969). Three forms of SOD exist in humans, the manganese containing mitochondrial SOD (Mn-SOD) which comprises four identical 22-kDa subunits each containing a Mn ion, cytosolic Cu/Zn-SOD containing a Cu-His(61)-Zn active site (Djinovic *et al.*, 1991) in both of its two identical 16-kDa subunits and extracellular SOD (EC-SOD), which like cytosolic SOD also contains a copper and zinc active site, but is a glycoprotein composed of four 30-kDa subunits (Carlsson *et al.*, 1995). SOD catalysed dismutation of $O_2^{\bullet-}$ occurs via reduction of the metal cation generating O_2, which then reduces a second $O_2^{\bullet-}$ to O_2^{2-} which then reacts with $2H^+$ to generate H_2O_2.

1.3.3 Cellular functions of ROS

1.3.3.1 The role of ROS in innate immunity

The role of ROS in innate immunity was established in the 1960's and 70's, when it was discovered that ROS was generated by phagocytes, as a consequence of a previously identified glycolytic 'respiratory burst'. Initially, it was believed that the ROS generated was H_2O_2 (Iyer *et al.*, 1961) but it was later discovered that the $O_2^{\bullet-}$ was the initial product (Babior *et al.*, 1973). During the same period, it was noted that the phagocytes of patients suffering chronic granulomatous disease (a disease characterised by recurrent pyogenic infections) did not generate a 'respiratory burst' and that cytochrome b_{558} was absent from these patients (Segal *et al.*, 1978). Identification of other subunits of the NOX2 complex followed, although it was not until 1993 that the final cytosolic subunit, $p40^{phox}$ was identified (Wientjes *et al.*, 1993). Whilst still a matter of debate, it is believed that ROS is responsible for the direct killing of microorganisms, for example by lipid peroxidation or through inhibition of microbial virulence factors, and indirectly via pH modulation and changes in ion concentrations of the phagosome interior (reviewed in Bedard and Krause, 2007). H_2O_2 may additionally be important in directing granulocyte migration to the site of infection, via activation of Src family kinase, Lyn (Yoo *et al.*, 2011). NOX2 generated ROS has also been shown to be

important in generating a neutrophilic chemoattractant gradient through the inhibition of the phosphatase and tensin homolog (PTEN) and the resulting accumulation of PIP3 (Kuiper *et al.*, 2011). Whilst NOX2 was initially discovered in phagocytic cells due to its role in innate immunity, the discovery of the other NOX isoforms and the development of more sensitive ROS probes showing that these isoforms also generated low levels of ROS in non-phagocytic cells, led to questions concerning their role.

1.3.3.2 The role of ROS as a cell signalling molecule

The role of ROS in signalling was only appreciated following the publication of a study in the late 1980's indicating H_2O_2 was responsible for the tyrosine phosphorylation of insulin receptor substrate 1 in a rat hepatoma cell line (Heffetz and Zick, 1989) and concentration dependent proliferation/inhibition of proliferation, in human fibroblasts (Murrell *et al.*, 1990). Since then, the role of ROS as cell signalling molecules has become established and is recognised in diverse biological functions such as hypoxic response, autophagy, cell growth and differentiation, stem-cell renewal, wound healing and apoptosis. Whilst $O_2^{\bullet-}$ has been shown to be involved in cell signalling, for example in the activation of ERK via peroxisome proliferator-activated receptor-γ activation in the mouse myoblast cell line C2C12 (Huang *et al.*, 2002), its rapid dismutation to H_2O_2 by SOD, means that the majority of ROS signalling appears to be mediated by H_2O_2.

The direct mechanism by which this occurs involves the oxidation of cysteine (or methionine) residues on redox sensitive proteins. Physiological pH, means that approximately 10% of sulphurs on the cysteine residue exist as a thiolate ion (S^-) (although this may be increased due to the local electrostatic environment) rather than a thiol group (SH), allowing for greater reactivity with H_2O_2. Oxidation of the thiolate ion by H_2O_2, results in its conversion to SO^-, which then generates a conformational change in the attached protein and resultant activation/inactivation. Hyperoxidation to SO_2^- or SO_3^-, can also occur, but as this is generally irreversible in the case of SO_3^-, the SO^- ion on the protein normally forms a disulphide (S-S) or sulphenic-amide (S-N) bond, with another SH group. Termination of the signal is achieved through reduction of the protein by the glutathione or thioredoxin (Trx) system (1.3.2.4). However, proteins involved in redox signalling, including phosphatases such as PTEN, protein tyrosine phosphatase 1B (PTP1B), CDC25 and MAPK, kinases and transcription factors, occur at much lower concentrations than that of cellular antioxidants. Furthermore, the known rate constants of target phosphatases are significantly lower than that of antioxidants

such as Prx and Gpx (Sohn and Rudolph, 2003, Denu and Tanner, 1998). As a result, it appears that any direct signalling by H_2O_2 would be negated by H_2O_2's reaction with cellular antioxidants before signalling could be instigated.

Consequently, it was proposed that transduction of cell signalling could be facilitated by the antioxidants themselves via a redox relay. In this model, H_2O_2 initially oxidises Prx, which is abundant in the cell and has been brought into close contact with the target protein. The target protein is then oxidised by Prx, before it can itself be reduced by Trx. Alternatively, in a variation on this model, the oxidised Prx is reduced by the Trx, which in turn oxidises the target protein. Yet another proposal, termed the 'floodgate model' (which also involves co-localisation of Prx), suggested that Prx could be inactivated either by hyperoxidation to SO_2^-, or post-translational modification, which would then allow direct activation/inactivation of the target protein by H_2O_2.

Experimental evidence exists for both models. In the yeast *Saccharomyces cerevisiae*, oxidant receptor peroxidase-1 (which operates as an antioxidant), reacts with H_2O_2, before transducing the signal to a target transcription factor (Delaunay *et al.*, 2002), whilst in HeLa cells Gpx4 also activated roGFP2 when part of the fusion protein (roGFP2-Gpx4), upon activation by H_2O_2 (Gutsche *et al.*, 2009). Additionally, in the AML cell line U937 and in HeLa cells, Prx1 was shown to transduce a H_2O_2 signal to activate the ASK1/p38^{MAPK} pathway (Jarvis *et al.*, 2012). With respect to the floodgate model, growth factor stimulation of NOX in various cell lines has been shown to promote localised Src mediated Prx1 inactivation, which would presumably allow H_2O_2 activation/inactivation of target proteins in the Prx1 inactive area (Woo *et al.*, 2010). Interestingly, in mouse embryonic fibroblasts it was shown that peroxiredoxin 1 protected PTEN inactivation by H_2O_2 protected the cells from RAS activation of AKT, which was reduced at high concentrations of H_2O_2, offering support to the idea of local Prx inactivation as a signalling mechanism (Cao *et al.*, 2009). Nonetheless, although the high concentration and reactivity of Prx seem to exclude direct oxidation of signalling proteins by H_2O_2, this mechanism cannot be ruled out (Marinho *et al.*, 2014). This is because whilst most of the H_2O_2 in direct signalling may be nullified by the action of antioxidants, a proportion will react with the target protein. Application of experimentally obtained kinetics for PTP1B and tyrosine-protein phosphatase non-receptor type 11 (PTPN11) analysed by mathematical modelling that accounted for both

their oxidation and reduction during signalling indicated that PTP1B, but not PTPN11, was compatible with a direct signalling mechanism (Brito and Antunes, 2014).

Regardless of mechanism, it is important to note that the reactivity of ROS mean that its role as a signalling molecule is likely to be localised to the subcellular compartment in which it is generated, dependent on NOX isoform and likely tissue specificity (1.3.2.2). In addition to the stimulation of NOX2 as part of an immune response, NOX isoforms are also stimulated by a variety of ligands such as pro-epidermal growth factor (Bae *et al.*, 1997), platelet-derived growth factor (Sundaresan *et al.*, 1995), tumour necrosis factor α (Lo and Cruz, 1995) and angiotensin II (Ushio-Fukai *et al.*, 1999). This stimulation and resultant ROS production then effect changes in phosphatases, kinases and transcription factors as part of their signalling role. Protein tyrosine phosphatases (PTP) contain a conserved His-Cys-$(X)_5$-Arg-Ser/Thr (with the exception of CDC25 which does not contain the Ser/Thr residue) motif in the active catalytic domain, which hydrolyses phosphotyrosine via the nucleophilic cysteine present in this active site (reviewed in Jackson and Denu, 2001). ROS inactivates PTP's by reaction with this same cysteine, which is selected in preference to other cysteines due to the nucleophilic charge caused by its proximity to the arginine residue. In the case of PTPB1, oxidation by H_2O_2 of the cysteine thiolate group generates a SO^- group, which is stabilised in the active cleft, prior to regeneration of the active enzyme (Denu and Tanner, 1998). A similar process occurs with the oxidation of PTEN and CDC25 by H_2O_2, only in this case oxidation of cysteine in the active site is stabilised by the formation of a disulphide bridge, between cys-124 and cys-71 in PTEN (Kwon *et al.*, 2004) and cys-377 and cys-330 in CDC25C (Savitsky and Finkel, 2002). Of note from a RAS perspective, PTEN is a known inhibitor of the PI3K/AKT pathway, which promotes cells survival (1.2.2.2) thus oxidation of PTEN results in increased activation of this pathway (Leslie *et al.*, 2003). Additionally, RAS is also direct target of ROS, with S-glutathionylation (the addition of glutathione to an oxidised cysteine residue) of cys-118 having been shown to increase RAS activity in vascular smooth muscle cells (Adachi *et al.*, 2004). Conversely, CDC25 is the active domain in GEFs important in activating RAS (1.2.2.1) and are also responsible for activating CDKs important in cell cycle progression. ROS mediated CDC25 cyclin D dependent cell cycle arrest under exposure to high levels of H_2O_2 (Pyo *et al.*, 2013), demonstrating perhaps, the importance of ROS subcellular localisation and relative ROS concentration in ROS signalling. Whilst the His-Cys-$(X)_5$-

Arg-Ser/Thr conserved motif establishes an active site for redox signalling in PTP, no similar motif has been elucidated for the site of redox signalling in protein kinases. This further complicates the picture, as both kinase activation and inactivation have been reported as a consequence of redox signalling. So, for example, S-glutathionylation, as a result of redox signalling, has been reported to inhibit the RAF/MEK/ERK pathway, PKC and cAMP-dependent protein kinase. Conversely, ROS signalling has been shown to lead to both activation and deactivation of Src kinase, dependent on both the subcellular location of Src and the relative levels of the activating/deactivating ROS, whilst tyrosine kinase receptors such as epidermal growth factor receptor have also been shown to be activated by ROS (reviewed in Corcoran and Cotter, 2013).

ROS is also important in the regulation of transcription factors. H_2O_2 has been shown to upregulate the transcription of transcription factors such as c-JUN, c-FOS, TP53 and HIF-1α, increase translation of transcription factors such as nuclear-related factor 2 (Nrf2) and specificity protein 1 (SP1) and target degradation of transcription factors, via the ubiquitin proteasome pathway or via post translational modifications such as acetylation of activator protein 1 (AP-1) or decreased hydroxylation of HIF-1α. Additionally ROS can induce proteolytic release of transcription factors such as NOTCH or sterol regulatory element-binding protein 1 from anchor proteins, allowing translocation to the nucleus, or directly increase affinity of transcription factor binding to DNA such as with heat shock factor 1 (reviewed in Marinho *et al.*, 2014).

1.3.3.3 The role of ROS in normal haematopoiesis

HSC reside in the bone marrow (1.1.1.1) and their quiescence is known to be negatively regulated by ROS. Forkhead box O (FOXO) transcription factors are involved in cell-cycle arrest and apoptosis and are activated in response to oxidative stress whereupon they translocate to the nucleus (Essers *et al.*, 2004). Translocation of FOXO4 to the nucleus has been shown to be a function of redox signalling, where oxidation of cys-239 by ROS mediates the formation of disulphide bonds with nuclear import receptor transportin-1, which in turn allows nuclear localisation (Putker *et al.*, 2013). FOXO deactivation occurs as a result of phosphorylation in response to activation of the PI3K/AKT pathway (1.2.2.2), resulting in their export from the nucleus and subsequent degradation in the cytoplasm (Brunet *et al.*, 1999). Studies in murine HSC have shown that deletion of FOXO3a, which upregulates transcription of Mn-SOD (Kops *et al.*, 2002), results in decreased HSC renewal (Miyamoto *et al.*, 2007) which is mediated by

the tumour suppressor protein ataxia-telangiectasia mutated (ATM) (Yalcin *et al.*, 2008), and is accompanied by elevated ROS levels and myeloid lineage expansion (Tothova *et al.*, 2007). Deletion of ATM in mice resulted in BM failure which was restored following treatment with antioxidants (Ito *et al.*, 2004). In a different study, isolation of murine HSC into ROS high and ROS low populations showed that the ROS low population maintained self-renewal capacity following serial transplantations, whilst the self-renewal capacity of the ROS high population was exhausted following the third serial transplantation. Treatment of the ROS high HSC with the antioxidant NAC, the p38 inhibitor SB203508 or rapamycin (a mTOR inhibitor), restored self-renewal activity (Jang and Sharkis, 2007). Interestingly, the ROS high population in this study also exhibited a decreased ability to adhere to cells containing calcium sensing receptors, whilst NOX generated ROS has additionally been implicated in osteoclast differentiation in human mesenchymal cells, further emphasising a potential regulatory role of ROS, in the BM niche (Huang *et al.*, 2009).

Whilst these increased ROS levels are associated with HSC losing quiescence, it has also been shown, in the human megakaryocytic cell line MO7e, that haematopoietic cytokines, such as GM-CSF, IL-3, SCF and TPO all increase ROS levels (Sattler *et al.*, 1999). In megakaryopoiesis, ROS has been shown to increase platelet production and maturation in the CML cell line MEG-01 and primary human megakaryocytes (O'Brien *et al.*, 2008), which in murine models is mediated by the transcription factor NF-E2 (Motohashi *et al.*, 2010). Following lineage commitment, megakaryocyte progenitors undergo endomitosis (chromosomal replication in the absence of cell division), which in murine cells is potentially mediated by NOX1-derived ROS (McCrann *et al.*, 2009). In human HSC, NOX-derived ROS has also been shown to be crucial for megakaryocyte differentiation via activation of ERK, AKT and JAK2 (Sardina *et al.*, 2010), whilst another study revealed the importance of cytochrome P450 2E1-generated ROS in megakaryocyte differentiation in human HSC (Tang *et al.*, 2014). As noted above, increased ROS in HSC has been associated with expanded myelopoiesis. Interestingly, a recent study using murine CMP, showed that higher levels of ROS actually impeded megakaryopoiesis, instead directing differentiation of CMP into GMP (Shinohara *et al.*, 2014). Finally, ROS has also been shown to induce differentiation of the promonocytic cell line, U937, into macrophages (Yamamoto *et al.*, 2009), and the differentiation of primary human monocytes into dendritic cells (Del Prete *et al.*, 2008).

1.3.3.4 The role of ROS in solid tumours and AML

ROS is implicated in numerous diseases including atherosclerosis, Alzheimer's, Parkinson's, diabetes, ischaemia, rheumatoid arthritis and cancer (reviewed in Valko *et al.*, 2007). One of the first studies implicating ROS in carcinogenesis was performed in mice subcutaneously injected with C3H mouse fibroblasts, that had been previously cultured *in vitro* with neutrophils (12-O-tetradecanoylphorbol-13-acetate (TPA) stimulated or unstimulated) or with the ROS generating enzyme XO and hypoxanthine. In this study approximately 20% of mice treated with these cells developed tumours within 13-22 weeks compared to none of the control mice (Weitzman *et al.*, 1985). In 1991, analysis of H_2O_2 production in human melanoma, colon, pancreatic, neuroblastoma, breast and ovarian cancer cell lines, revealed constitutively active H_2O_2 production over a 4h period, generating H_2O_2 levels similar to those observed in TPA stimulated neutrophils, suggesting increased ROS production may be a feature of transformation (Szatrowski and Nathan, 1991). Later, studies in patients with liver disease suggested ROS plays a part in hepatocarcinogenesis (Valgimigli *et al.*, 2002), and levels of Cu/Zn-SOD are significantly lower in hepatoma tissue than normal human liver tissue (Liaw *et al.*, 1997). Further, homozygous deletion of Cu/Zn-SOD in mice results in decreased lifespan, with 70% developing hepatocarcinoma or benign nodular hyperplasia (Elchuri *et al.*, 2005), whilst homozygous deletion of Mn-SOD in mice is lethal within two weeks of birth (Van Remmen *et al.*, 2003). In the same study, heterozygous deletion of Mn-SOD resulted in increased incidence of haemangioma and adenocarcinoma and significant increases in the incidence of lymphoma. Currently, elevated ROS levels have been reported in many solid tumours and the role they play in tumourigenesis is complex and multifaceted (reviewed in Galadari *et al.*, 2017). Haematologically, a study which collected blood samples from ALL and CML patients samples and compared them with normal blood samples showed elevated levels of ROS in both ALL and CML patients (Devi *et al.*, 2000), whilst studies in our group have additionally revealed elevated levels of NOX generated ROS in AML patient samples when compared with healthy controls (Hole *et al.*, 2013).

The role of ROS in DNA damage

Physiologically ROS is important both in innate immunity (1.3.3.1) and as a signalling molecule (1.3.3.2), with both intra and extracellular ROS levels tightly maintained through cellular antioxidant systems (1.3.2.4). Increased levels of ROS or decreased

levels of cellular antioxidants can cause oxidative stress leading to overactivation of signalling pathways, hyperoxidation of signalling proteins (1.3.3.2), lipid peroxidation (1.3.3.1), structural alterations in protein structures resulting in change of function, as well as damage to DNA and RNA. Reactions of ROS with DNA generate numerous oxidised bases, including 8-hydroxy-2-deoxyguanosine (8-OHdG) which causes G:C to T:A DNA transversions (reviewed inCooke *et al.*, 2003). Increased levels of 8-OHdG have been observed in patients with breast cancer (Matsui *et al.*, 2000), gastric carcinomas (Borrego *et al.*, 2013), lung cancer (Gackowski *et al.*, 2005) and colorectal cancer (Obtulowicz *et al.*, 2010). In leukaemia a study of 116 Chinese children with either ALL or AML revealed significantly elevated levels of 8-OHdG, whilst 8-OHdG levels were also significantly elevated in relapsed AML adult patients (Zhou *et al.*, 2010). 8-OHdG levels were also significantly elevated in the murine cell line 32D transfected with FLT3 with an internal tandem duplication (ITD) compared to FLT3-wild type (WT) (Stanicka *et al.*, 2015). Furthermore, 32D cells containing FLT3-ITD showed a 75% increase in DNA double strand breaks (DSB) compared to WT cells, which was reduced by 30% in cells with $p22^{phox}$ knocked-down. FLT3-ITD is a common mutation in AML (Table 1) and has been shown to be responsible for increased levels of NOX4 generated ROS in the AML cell line Mv4;11(Jayavelu *et al.*, 2016b). These studies suggest that ROS induced DNA damage may be important in the initiation of both solid tumours and in leukaemogenesis.

ROS increased proliferation in cancer

In transformed cell lines, ROS has been shown, in several studies to contribute to increased proliferation. Overexpression of NOX1 in mouse fibroblast cells led to increased superoxide production and proliferation (Suh *et al.*, 1999), whilst in the human colon cancer cell line, HT29-D4 and the prostate cancer cell line DU145, NOX1 and NOX5 generated $O_2^{\bullet-}$ respectively, was associated with an increased proliferative rate in these cells (de Carvalho *et al.*, 2008, Brar *et al.*, 2003). Previous work in our group has shown that NOX2 induced ROS, generates increased proliferation in mutant RAS expressing HPC (Hole *et al.*, 2010) and in AML cell lines and in patient AML blasts (Hole *et al.*, 2013). Additionally, overexpression of NOX isoforms is common in many cancers with overexpression of NOX1 being observed in colon and stomach cancers, NOX2 in CML, NOX4 in ovarian, liver and breast cancer, NOX5 in breast,

colon, lung and prostate cancers as well as melanoma and DUOX2 in colorectal cancers (reviewed in Roy *et al.*, 2015, Graham *et al.*, 2010)

ROS and its role in metastasis

ROS has also been linked to metastasis via processes such as epithelial-mesenchymal transition (EMT), Wnt signalling, PTP signalling and p21-activated kinase 1 signalling (reviewed in Sosa *et al.*, 2013). In particular, EMT, a process in which epithelial cells gain migratory properties, have been shown to have a ROS dependent component. For example, treatment of rat proximal tubular epithelial cells with H_2O_2 results in TGF-β1 activation of the MAPK pathway and EMT initiation (Rhyu *et al.*, 2005). Additionally, matrix metalloproteinase (MMP) an enzyme important in the breakdown of the extracellular matrix, has also been reported to be upregulated in breast cancer and to induce EMT (Lochter *et al.*, 1997). MMP3 generates mitochondrial ROS via RAC-1 and inhibition of this ROS with NAC in murine mammary epithelial cells blocked MMP3 induction of EMT (Radisky *et al.*, 2005). Additionally, RAC-1 generated ROS is important in VEGF signalling which has been shown to induce angiogenesis in endothelial cells via the ROS sensitive adaptor protein p66Shc (Oshikawa *et al.*, 2012). VEGF is also a crucial regulator in tumour angiogenesis, is upregulated in many human cancers, with cytokines, hypoxia and increased ROS all leading to increased VEGF levels (reviewed in Sosa *et al.*, 2013).

ROS disrupts cell signalling in cancer

The role of ROS as a signalling molecule important for cellular proliferation, differentiation and survival is discussed in detail above (1.3.3.2). Unsurprisingly, increased levels of ROS in cancer cells has been shown to lead to aberrant signalling of these pathways. The role of the ROS activated RAS/RAF/MEK/ERK pathway in cell cycling (1.2.2.2) and AML was discussed previously (1.2.2.3), whilst ROS activation of the JNK and $p38^{MAPK}$ pathways has been shown to have both pro and anti-oncogenic effects dependent on context (reviewed in Wagner and Nebreda, 2009). Overexpression of mutant RAS has been shown to lead to increased levels of extracellular ROS (Hole *et al.*, 2010), known to activate the $p38^{MAPK}$ pathway (Kulisz *et al.*, 2002), which in turn upregulates $p16^{INK4A}$ and inhibits CDK, as well as inducing apoptosis as part of the cellular response to oxidative stress. However, whilst mutant H-RAS expression has been shown to induce cell cycle arrest in primary human fibroblasts, several ROS

producing cell lines have been shown to upregulate glutathione S-transferase (GSTM) which inhibits $p38^{MAPK}$ activation. This silencing of $p38^{MAPK}$ then, suggests a mechanism by which cancer cells may escape ROS induced apoptosis (Dolado *et al.*, 2007). In support of this, whilst expression of $H\text{-}RAS^{G12V}$ in human HPC led to activation of $p38^{MAPK}$, a corresponding increase in $p16^{INK4A}$ expression was not observed, suggesting this mechanism becomes decoupled in these cells (Hole *et al.*, 2010). Furthermore, in AML blasts, high ROS levels associated with increased proliferation, which did not correlate with increased $p38^{MAPK}$ activation, although GSTM expression did not appear to mediate this effect. These studies suggest then that suppression of this ROS induced pathway maybe multimodal (Hole *et al.*, 2013).

The tumour suppressor PTEN (reviewed in Kitagishi and Matsuda, 2013), which is inhibited by ROS, is an inhibitor of the RAS targeted PI3K/AKT pathway (1.3.3.2). Activation of the transcription factor FOXO promotes apoptosis and it is upregulated by ROS and inhibited by AKT. Upregulation of FOXO additionally upregulates Mn-SOD which is an important feature in HSC self-renewal (1.3.3.3). Therefore, under normal cellular conditions a balance between ROS activation of FOXO and ROS inhibition of PTEN maintains cellular homeostasis. However excessive ROS can lead to hyperactivation of the PI3K pathway, a common feature of many cancers, resulting in increased cell survival, VEGF production, secretion of MMP (reviewed in Gao and Schottker, 2017) and inactivation of FOXO (reviewed in Tothova and Gilliland, 2007). In AML, constitutive activation of the PI3K/AKT pathway is frequently observed (Xu *et al.*, 2003, Altomare and Testa, 2005), however the role of FOXO is less clear. A recent study revealed that FOXO1 expression in osteoblasts mediated β-catenin initiated AML (Kode *et al.*, 2016), whilst a study of AML patient samples showed that 40% exhibited FOXO activation, that upon inhibition resulted in myeloid differentiation and AML cell death (Sykes *et al.*, 2011). Additionally, in both CML and AML the BCR-ABL fusion protein and FLT3-ITD have been shown to lead to phosphorylation of AKT resulting in increased activation of NOX, and increased ROS production (reviewed in (Jayavelu *et al.*, 2016a), which may in turn reinforce PI3K/AKT activation.

The role of ROS on transcription factors in cancer

Other ROS regulated transcription factors important in cancer development include Nrf2, NF-κB, TP53 and HIF-1α. Nrf2 governs the expression of numerous antioxidant

genes including *GSR* and *PRX* and is considered the master regulator of cellular antioxidant response. Nrf2 binds to Kelch-like ECH-associated protein (KEAP1) in the cytosol under normal conditions, but under conditions of oxidative stress Nrf2 levels are increased and ROS attenuates binding of KEAP1 to Nrf2, leading to its translocation to the nucleus. Aberrant activation of Nrf2 as a result of mutations to Nrf2 or KEAP1 are frequently reported in numerous cancers (reviewed in Taguchi and Yamamoto, 2017), with high levels of Nrf2 also reported in AML (Rushworth *et al.*, 2008). Whilst the resulting increase in antioxidants are protective to cells under normal conditions, paradoxically they are believed to give cancer cells increased protection against chemotherapeutic agents. Like Nrf2, NF-κB is bound in an inhibitory form to, nuclear factor of kappa light polypeptide gene enhancer in B-cells inhibitor alpha (IκBα), until activation of IκBα by ROS results in dissociation of the complex, translocation of NF-κB to the nucleus and activation of target genes involved in proliferation, metastasis, angiogenesis and apoptotic inhibition (reviewed in Gao and Schottker, 2017). NF-κB has been much studied in AML, due to its role in chemoresistance (Rushworth *et al.*, 2010) and it has also been shown to be responsible for high levels of Nrf2 observed in primary human AML cells and AML cell lines (Rushworth *et al.*, 2012). The tumour suppressor gene TP53 has been found to be mutated in most cancers and is frequently mutated in AML (Table 1) (reviewed in Renneville *et al.*, 2008). Nearly 50% of all malignancies involve mutation of TP53 and in cancers such as lung, triple negative breast, serous ovarian and oesophageal it is as high as 80% (reviewed in Duffy *et al.*, 2017). There is a complex interplay between ROS and TP53 protein levels. ROS can both induce TP53 expression via activation of various pathways such as $p38^{MAPK}$, and suppress TP53 expression through oxidation of cysteine residues. Furthermore, activation of TP53 can result in activation of TP53 inducible protein-3, a pro-apoptotic protein which increases ROS levels (Polyak *et al.*, 1997), or the upregulation of antioxidant genes such as GPX1 and Mn-SOD (reviewed in Vurusaner *et al.*, 2012). Therefore, there appears to be a balance, whereby lower levels of ROS induce an antioxidant response in TP53, whereas higher levels induce apoptosis (Sablina *et al.*, 2005).

The role of anti-oxidants and pro-oxidants in cancer treatment

This pro-oxidant/anti-oxidant interplay is an important feature of ROS in cancers and has implications for treatment in AML with both anti-oxidant treatment and pro-

oxidant treatment offering therapeutic potential (reviewed in Hole *et al.*, 2011). As discussed above, high ROS levels are observed in cancer cells and in AML which can lead to a pro-proliferative phenotype. Anti-oxidant treatment might therefore be expected to relieve this proliferative burden and as a prophylactic reduce cancer incidence. However, studies involving antioxidant treatment and epidemiological studies have shown mixed results (reviewed in Poprac *et al.*, 2017, Yasueda *et al.*, 2016). Whilst a variety of reasons have been postulated for this, one major argument against the use of antioxidants is that chemotherapeutic agents typically generate ROS as part of their cytotoxic effect and anti-oxidants serve only to reduce the ROS burden. Consequently, the use of pro-oxidants to augment chemotherapy have been examined in a number of clinical trials and have proved promising in treating a variety of cancers (reviewed in Gorrini *et al.*, 2013). Arsenic trioxide has transformed survival rates in patients with APL (reviewed in (McCulloch *et al.*, 2017) and has also been used in the treatment of lung cancer. However, as discussed above, cancer cells often upregulate the production of antioxidants, and downregulate pro-apoptotic pathways such as TP53, as a response to high ROS, allowing them to escape apoptosis. In addition, it has been shown that both cancer stem cells (Diehn *et al.*, 2009, Kim *et al.*, 2012) and LSC (Lagadinou *et al.*, 2013) exhibit low ROS levels, suggesting that even if treatment with pro-oxidants eliminates the bulk of cancer cells, cancer stem cells or LSC may survive and relapse occur. Interestingly a recent study showed apoptosis of LSC but not HSC as a result of selenium activated ATM-TP53 production of ROS (Gandhi *et al.*, 2014), suggesting that a pro-oxidant approach to eliminating LSC may be feasible.

NADPH is a link between ROS and metabolism in cancer

Activation of ATM by ROS also promotes glucose-6-phosphate dehydrogenase (G-6-PD) activity, the first step of the pentose phosphate pathway (PPP) (1.4), which also generates NADPH (Cosentino *et al.*, 2011). Given that major cellular antioxidant systems, ultimately rely on NADPH to provide their reducing power (Figure 1-5) it is perhaps not surprising that ROS in both normal and aberrant cellular processes is inextricably linked with metabolism. In the cytosol NADPH is primarily generated through the PPP (1.4.4), whilst a number of mechanisms exist for mitochondrial NADPH generation (reviewed in Ciccarese and Ciminale, 2017), which include the serine synthesis pathway (SSP) (via the folate cycle) (reviewed in Yang and Vousden, 2016) and the action of IDH1 and IDH2. IDH1 and IDH2 are commonly mutated in

AML (reviewed in Dang *et al.*, 2010), although in this context NADPH is consumed, and D-2-hydroxyglutarate generated leading to stabilisation of HIF-1α (Zhao *et al.*, 2009). HIF-1α as a target of ROS is controversial, however it is overexpressed in many cancers where it induces expression of numerous glycolytic genes and will be discussed in more detail later (1.4.2.1). Of note, Nrf2 activation has also been shown to modulate metabolism in lung cancer cell lines, through the upregulation of enzymes involved in the NADPH production, notably G-6-PD, IDH1 and malic enzyme 1 (Mitsuishi *et al.*, 2012). Furthermore, TP53 is also important in regulating metabolism. Homozygous deletion of TP53 in mice results in decreased oxygen consumption resulting from decreased mitochondrial respiration occurring as a consequence of reduced TP53 activated 'synthesis of cytochrome c oxidase 2 (SCO2)' production (Matoba *et al.*, 2006), resulting in decreased mitochondrial ROS production. Additionally both glucose transporter (GLUT) 1 and 4 and the glycolytic enzyme phosphoglycerate mutase (PGAM) have all been reported to be inhibited by TP53 expression (reviewed in Zhao *et al.*, 2016a) leading to decreased glycolysis and potentially increased metabolism via the PPP and SSP. Finally, TP53 also upregulates TP53-induced glycolysis and apoptosis regulator (TIGAR) an enzyme which has an active domain similar to PFKFB (1.5.2). TIGAR catalyses the reaction of fructose-2,6-bisphosphate (F-2,6-BP) to fructose-6-phosphate (F-6-P), which inhibits glycolysis, redirects metabolites into the PPP, generating NADPH (Bensaad *et al.*, 2006).

1.4 Metabolism

Broadly defined, cellular metabolism involves a series of catabolic or anabolic chemical reactions which generate or use energy as part of this process. In chemotrophs this energy is obtained through the oxidation of nutrients, with the energy typically stored in the form of ATP. Whilst in higher organisms a plethora of enzymatically catalysed metabolic reactions occur, which are all part of different interconnecting metabolic pathways with multitudinous feedback mechanisms. These pathways are evolutionarily highly conserved with the citric acid cycle, for example, essentially a feature in all terrestrial life. There are three main classes of molecules involved in metabolism, carbohydrates, proteins and lipids that are either catabolised to generate energy or energy stores or used by anabolic pathways in the synthesis of, for example, nucleotides and structural molecules such as cell membranes. In mammals, a triumvirate of glycolysis (1.4.3), the citric acid cycle (1.4.4) and the ETC (1.3.2.1) are central to the

generation of ATP, with glycolysis and the citric acid cycle contributing 2 ATP molecules each and the ETC generating up to 34 ATP molecules in a process collectively termed aerobic respiration (reviewed in Mikawa *et al.*, 2015).

1.4.1 The Warburg effect

A key requirement of aerobic respiration is that sufficient cellular oxygen levels are available, as under anaerobic conditions oxidative phosphorylation cannot occur and instead cellular energy demands are solely met through the less efficient process of glycolysis and the generation of lactate. Initially, it was Otto Warburg who observed that aerobic glycolysis was a hallmark feature of cancer cells (Warburg, 1956), an effect to which he ascribed defective mitochondria as being the cause, a hypothesis that is now known in most cancers to be incorrect (reviewed in DeBerardinis and Chandel, 2016). Instead, it has been shown that mitochondrial respiration is often necessary in tumourigenesis (Weinberg *et al.*, 2010). Given its ubiquity and despite its inefficiency when compared with oxidative phosphorylation, it is clear that the Warburg effect must offer cancer cells some competitive advantage, although its exact ontology remains unclear. One hypothesis contends that whilst inefficient, aerobic glycolysis generates ATP at a rate 10-100 times faster than oxidative phosphorylation, therefore supplying cancer cells with energy at a faster rate. Additionally, this increased glycolytic flux could potentially generate more nucleotides, amino acids and lipids for biosynthesis and perhaps more pertinently would, via the PPP and SSP (1.4.4), generate more NADPH to deal with the increased ROS levels common in many cancer cells (reviewed in Liberti and Locasale, 2016) and the impact of this on ROS signalling pathways (1.3.3.2 and 1.3.3.4). Alternative proposals suggest that the increase in excreted lactate as a result of aerobic glycolysis generates a more acidic microenvironment which breaks down stromal membrane structures, increasing cancer cell motility and metastasis.

1.4.2 Regulation of metabolic pathways

Changes of cellular ROS levels in both normal cell signalling (1.3.3.2 and 1.3.3.3) and as cell signalling following cellular transformation (1.3.3.4) result in changes in numerous signalling pathways controlling multiple cellular functions including growth, proliferation and differentiation. A number of these signalling pathways, in turn, exercise regulatory control over various metabolic pathways, which in turn via several feedback mechanisms modulate ROS levels (Figure 1-6). Increased RAS expression activates the PI3K/AKT/mTOR pathway (1.2.2.2 and 1.3.3.4) and activation of mTOR

is known to activate both nucleotide biosynthesis and lipid synthesis (reviewed in Efeyan *et al.*, 2012) as well as HIF-1α, which upregulate glycolysis via the activation of numerous glycolytic genes (1.4.2.1). In addition to HIF-1α, other ROS activated transcription factors are important in metabolic regulation such as STAT3, which has been shown to upregulate glycolysis in hepatocellular carcinoma cell lines (Li *et al.*, 2017b), FOXO3A, which inhibits glycolysis via activation of tuberous sclerosis 1 protein (Khatri *et al.*, 2010) and NF-κB which was shown to upregulate GLUT3 in mouse embryonic fibroblasts (Kawauchi *et al.*, 2008). Nuclear localisation of the glycolytic enzyme pyruvate kinase muscle 2 (PKM2) is also ROS mediated, where it acts as a co-factor in the activation of c-MYC (1.4.3). RAS also activates c-MYC (1.2.2.2) which is overexpressed in greater than 50% of human cancers and c-MYC has been shown to activate glycolysis via the upregulation of GLUT, the glycolytic enzymes hexokinase (HK), phosphoglucose isomerase (PGI), phosphofructokinase (PFK), glyceraldehyde-3-phosphate dehydrogenase (GAPDH), phosphoglycerate kinase (PGK), PKM2, as well as lactate dehydrogenase A (LDHA), pyruvate dehydrogenase kinase 1 (PDK1) (1.4.3) and PFKFB3 (1.5) (reviewed in Hsieh *et al.*, 2015). Increased glutaminolysis is also a target of c-MYC, which upregulates the glutamine transporter ASCT2 and a key enzyme glutaminase. Additionally, c-MYC was shown to upregulate both phosphoglycerate dehydrogenase (PHGDH) which catalyses the first step of the SSP, serine hydroxymethyltransferase, part of the folate cycle as well as several genes involved in fatty acid metabolism and the citric acid cycle (reviewed in DeBerardinis and Chandel, 2016).

In contrast TP53 (which is frequently mutated in cancer) is known to inhibit glycolysis through inhibition of GLUT1, GLUT4 and PGAM and through activation of TIGAR and SCO2 (1.3.3.4). Inhibition of glycolysis also occurs due to the regulatory role of miRNA. For example, miR-195-5p inhibits GLUT3, miR-143 inhibits HK2 and miR-155 inhibits HIF-1α. Furthermore, TP53 induces miR-34a which suppresses HK1, HK2, GPI and PDK1, as well as sirtuin 1, which activates FOXO1, NF-κB and in a positive feedback loop TP53 (reviewed in Zhao *et al.*, 2016a)

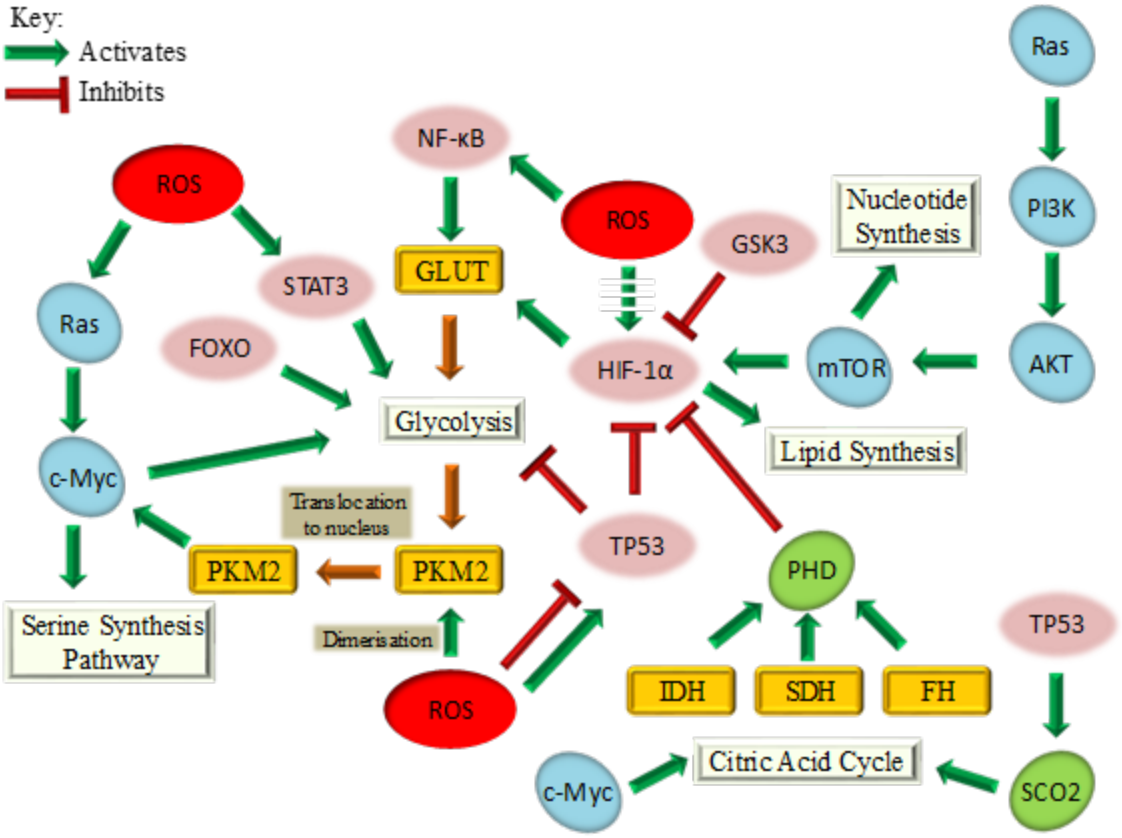

Figure 1-6. Regulation of metabolic pathways. Schematic illustration outlining some of the regulatory mechanism involved in glycolysis and other key metabolic pathways. Transcription factors are in pink and signalling pathways in blue. Reactive oxygen species (ROS), forkhead box O (FOXO), pyruvate kinase muscle 2 (PKM2), signal transducer and activator of transcription (STAT), nuclear factor kappa-light-chain-enhancer of activated B-cells (NF-κB), glucose transporter (GLUT) hypoxia inducible factor-1 alpha (HIF-1α), tumour suppressor protein 53 (TP53), glycogen synthase kinase 3β (GSK-3β), isocitrate dehydrogenase (IDH), succinate dehydrogenase (SDH), fumarate hydratase (FH), protein kinase B (AKT), mammalian target of rapamycin (mTOR), phosphoinositide 3-kinase (PI3K), synthesis of cytochrome c oxidase 2 (SCO2) and prolyl-hydroxylase domain (PHD).

1.4.2.1 Hypoxia Inducible Factor-1 alpha (HIF-1α)

HIF-1α is a transcription factor whose stabilisation and translocation to the nucleus, as a result of low oxygen tension, leads to increased expression or suppression of hundreds of genes via binding to the hypoxia response element (HRE) of promoters (reviewed in Greer *et al.*, 2012)). It is a heterodimer consisting of the subunits HIFα and HIFβ (sometimes referred to as aryl hydrocarbon receptor nuclear translocator (ARNT), which contain a helix-loop-helix domain, as well as a PER-ARNT-SIM domain. Three isoforms of HIF-α exist in humans, all of which contain an oxygen-dependent degradation domain containing two preserved proline residues, which under conditions of normoxia are hydroxylated by prolyl-hydroxylase domain (PHD) enzymes. PHD requires O_2 for its catalytic activity, with the hydroxy-HIF-α, being recognised by von Hippel-Lindau tumour suppressor protein's (pVHL) β-domain, which targets it for ubiquitylation and degradation by 26s proteasome. Additionally, factor inhibiting HIF (FIH), in the presence of O_2, also hydroxylates HIF-α at Asn803 of the C-terminal transactivation domain, which prevents association of HIF-α with transcriptional activators. Under hypoxic conditions Asn803 is not hydroxylated and HIF-α is stabilised, whereupon it dimerises with HIF-β, translocates to the nucleus and interacts with transcriptional co-activators p300/CBP.

HIF-1α is important in the differentiation of a several tissues, including those involved in osteogenesis and haematopoiesis (1.1.1.1) (Takubo *et al.*, 2010), where it is important in maintaining LT-HSC in the HSC niche (Kocabas *et al.*, 2015). It is also required for embryogenesis in mice as homozygous deletion is embryonically lethal by day 10.5, whilst mice lacking HIF-2α are either embryonically unviable or die shortly after birth (reviewed in Semenza, 2012). Furthermore, knockdown of HIF-2α was shown to impede the repopulating ability of human HPC *in vivo,* resulting in increased ROS levels and increased endoplasmic reticulum stress, and suggesting a regulatory role in haematopoiesis (Rouault-Pierre *et al.*, 2013). HIF-1α is implicated in a number of diseases, performing a protective role in coronary artery disease, limb ischemia and wound healing, whilst contributing to disease in pulmonary artery hypertension, sleep apnea and cancer. Increased levels of HIF-1α are seen in numerous cancers including bladder, breast, colon, lung, pancreas and prostate and it is known to activate transcription of genes involved in stem cell maintenance, immortalisation, EMT, immune evasion, vascularisation and glucose metabolism.

HIF-1α is downregulated by TP53 and GSK3 and upregulated by mTOR following activation of the PI3K/AKT pathway, which in turn upregulates the glycolytic enzymes HK, aldolase (ALDO), PGK, enolase (ENO) and PKM2, as well as GLUT, LDHA and PDK1 (reviewed in Semenza, 2010a). Additionally, PHD2 activity (and thus HIF-1α inhibition) is activated by IDH, SDH and fumarate hydratase which are all enzymes involved in the citric acid cycle. HIF-2α is also implicated in cancer biology through regulation of c-MYC, angiogenesis and the promotion of metastasis and chemoresistance (reviewed in Zhao *et al.*, 2015).

Whilst the role of HIF-1α is well established in solid tumours, in leukaemia the literature is less certain. Increased expression of HIF-1α has been reported in all leukaemias, including AML (Gao *et al.*, 2015), and is associated with chemoresistance (Song *et al.*, 2014). Inhibition of HIF-1α with echinomycin using a xenogenic model of AML in NOD-SCID mice prevented serial transplantation of AML (Wang *et al.*, 2011), whilst a syngeneic AML mouse model showed elimination of LSC (without impact on HSC) and cured 40-60% of the mice with relapsed AML (Wang *et al.*, 2014). Mechanistically, HIF-1α has been shown to lead to progression of leukaemia through activation of both the NOTCH and Wnt pathways and inhibition of tumour suppressor genes such as TP53 (reviewed in Deynoux *et al.*, 2016). HIF-2α has also been reported as important in AML disease maintenance with one study reporting that knock-down of HIF-2α in AML patient samples resulted in a decreased ability of these cells to engraft in mouse models (Rouault-Pierre *et al.*, 2013). However, HIF-1α has also been shown to lead to the differentiation of AML cell lines through binding and activation of C/EBP and c-MYC and miRNA suppression (1.4.2), whilst *in vivo*, mouse models have shown accelerated development of AML as a result of HIF-1α knock-down (Velasco-Hernandez *et al.*, 2014) or conditional deletion or HIF-1α and HIF-2α (Vukovic *et al.*, 2015).

The interplay of ROS and HIF-1α is also controversial (reviewed in Hagen, 2012). Initially it was reported that mitochondrial ROS was required for HIF-1α stabilisation under conditions of hypoxia (Guzy *et al.*, 2005, Mansfield *et al.*, 2005) and that this may occur as a result of PHD inhibition by ROS (Pan *et al.*, 2007). However a lack of consensus over whether mitochondrial ROS production was enhanced or reduced under conditions of hypoxia along with the finding that inhibition of PHD require high levels of H_2O_2 suggested this mechanism was unlikely (Masson *et al.*, 2012). Furthermore, the

same study reported that the greater sensitivity of FIH to ROS inhibition meant that, whilst this was a more likely mechanism of HIF-1α inactivation, the extremely slow reversibility of the reaction precluded it from any short-term role in hypoxic response. However, other sources of ROS such as NOX and XO may be important in HIF-1α regulation. NOX4 generated ROS has been reported to promote transcription of HIF-1α (Bonello *et al.*, 2007), whilst a recent review highlights that mitochondrial ROS released from the intermembrane space is increased under conditions of hypoxia and that this is important in HIF-1α stabilisation and tumourogenesis (reviewed in Sabharwal and Schumacker, 2014). Furthermore, whilst the low affinity of PHD and slow reversibility of FIH inhibition by ROS make it unlikely to function as a regulatory molecule in normal hypoxic response, it could be hypothesised that the increased levels of ROS found in many cancers are able inhibit PHD, whilst inactivation of HIF-1α by FIH may not be a requirement of transformed cells. Finally, it has been shown that intermittent hypoxia increases activity of XO an enzyme important in the catabolism of purines and a major source of cellular ROS (Nanduri *et al.*, 2013). XO activation leads to increased ROS, which induces Ca^{2+} activation of PKC, migration of $p47^{phox}$and $p67^{phox}$ to the cell membrane, resulting in activation of the NOX2 complex (1.3.2.2). Interestingly, knock-down of XO or NOX2 completely ablated HIF-1α protein expression in cell lines suggesting a ROS dependent, but mitochondrial independent, component to its stabilisation (Nanduri *et al.*, 2015).

1.4.3 The glycolytic pathway

The glycolytic pathway involves the metabolic breakdown of glucose into pyruvate via a series of intermediary steps (Figure 1-7) with the overall reaction being summarised as:

$$C_6H_{12}O_6 + 2NAD^+ + 2ADP + 2P_i \rightarrow 2C_3H_3O_3 + 2NADH + 2ATP + 2H^+ + 2H_2O$$

where $C_6H_{12}O_6$ is glucose, NAD is nicotinamide adenine dinucleotide, 2ADP is adenosine diphosphate, P_i is inorganic phosphate and $C_3H_3O_3$ is pyruvate.

Glucose (from digested saccharides or synthesised via gluconeogenesis) is taken up into the cell via GLUT, which are integral membrane proteins consisting of 12 transmembrane helices with both the C and N-termini located in the cytosol. The active binding site is located on the 7^{th} transmembrane domain containing the QLS (glutamine-leucine-serine) motif and between the 10^{th} and 11^{th} transmembrane domains and a N-

glycosylation site either on the 1st or 5th extracellular loop. Fourteen isoforms of GLUT have been identified in humans, GLUT's 1, 3, 5, 6 and 9 are primarily expressed in haematopoietic cells, with GLUT1 and GLUT3 primarily responsible for glucose transport and GLUT5 the transport of fructose (reviewed in Vrhovac *et al.*, 2014).

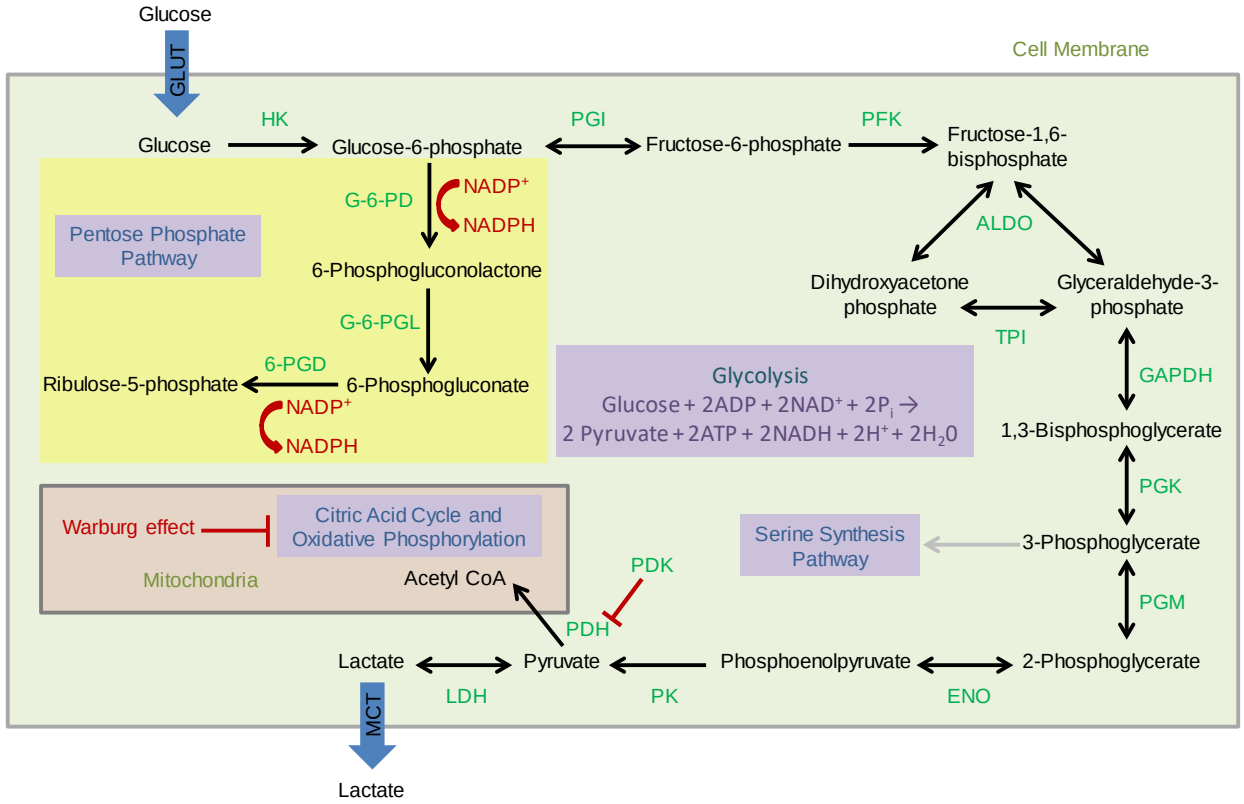

Figure 1-7. Glycolysis. Schematic illustration of the glycolytic reactions, showing the glycolytic intermediates, as well as the first three NADPH generating steps of the pentose phosphate pathway (PPP) catalysed by glucose-6-phosphate dehydrogenase (G-6-PD), gluconolactonase (G-6-PGL) and 6-phosphogluconate dehydrogenase (6-PGD) (yellow box). Glucose is transported across the cell membrane by glucose transporters (GLUT) before being catalysed to glucose-6-phosphate by hexokinase (HK). The other non-reversible steps in glycolysis are catalysed by phosphofructokinase (PFK) and pyruvate kinase (PM), shown by single headed arrow. Double headed arrows indicate reversible reaction. Pyruvate can be converted in to lactate by lactate dehydrogenase (LDH) or into acetyl CoA by pyruvate dehydrogenase (PDH) which is inhibited by pyruvate dehydrogenase kinase (PDK). Lactate can be secreted from the cell by monocarboxylic transporters (MCT). Phosphoglucose isomerase (PGI), aldolase (ALDO), triosephosphate isomerase (TPI), glyceraldehyde phosphate dehydrogenase (GAPDH), phosphoglycerate kinase (PGK), phosphoglycerate mutase (PGM), enolase (ENO), adenosine-5-diphosphate (ADP), adenosine-5-triphosphate (ATP), nicotinamide adenine dinucleotide (NAD), NAD phosphate (NADPH) and inorganic phosphate (P_i).

The first glycolytic step is irreversible and involves the phosphorylation of glucose to glucose-6-phosphate (G-6-P) by ATP and is catalysed by the enzyme HK. There are five isoforms of HK, with HK1 being ubiquitously expressed and HK2 mostly expressed in heart, skeletal and adipose tissues. Both these isoforms are inhibited by G-6-P, can bind to the outer mitochondrial membrane and use ATP derived from the ETC thus linking oxidative phosphorylation with glycolysis (reviewed in Wilson, 2003). The next step is the reversible isomerisation of G-6-P to fructose-6-phosphate, catalysed by PGI. PGI is a dimer with two α/β sandwich domains which is also known as neuroleukin in its role as a neurotrophic factor and is secreted by cancer cells where it is known as autocrine motility factor (AMF) (Jeffery *et al.*, 2000). The third glycolytic reaction, the phosphorylation of F-6-P to fructose-1,6-bisphosphate (F-1,6-BP) by ATP, is one of the rate limiting irreversible steps in glycolysis and is catalysed by the enzyme PFK (Xie *et al.*, 2016). PFK occurs as three isoforms PFK-muscle, PFK-liver (PFK-L) and PFK-platelet (PFK-P) and whilst synthesised as a monomer is only active in tetrameric form. It contains two binding sites for ATP, a catalytic binding site which has an association constant (K_a) of 0.15mM and an inhibitory allosteric binding site with a K_a of 2.5mM. PFK is additionally inhibited by phosphoenolpyruvate (PEP), palmitoyl-CoA, citrate and lactate and is activated by adenosine monophosphate, the signalling molecule cyclic adenosine monophosphate and the metabolite F-2,6-BP, whose role will be discussed further below (1.5). Hormonal regulation by insulin, serotonin and epinephrine occur as a result of phosphorylation of PFK by protein kinases, which stabilise its tetrameric active form (reviewed in Al Hasawi *et al.*, 2014).

The six carbon unit of F-1,6-BP is subsequently split into two three carbon units, either glyceraldehyde-3-phosphate (G-3-P) or its isomer dihydroxyacetone phosphate (DHAP), in a reversible reaction catalysed by ALDO. In humans there are three isoforms of ALDO, and in addition to its role in glycolysis it is also involved in Wnt signalling (Caspi *et al.*, 2014), and the assembly and activity of vacuolar proton-translocating ATPases, important in proton transport and endocytosis) (Lu *et al.*, 2007). Isomerisation reactions between G-3-P and DHAP are catalysed by triose-phosphate isomerase (TPI). TPI is inhibited by binding of PEP to its catalytic binding site, which results in increased flux into the PPP and away from glycolysis (Gruning *et al.*, 2014). Continuation along the glycolytic pathway involves reversible

oxidative phosphorylation of G-3-P to 1,3-bisphosphoglycerate (1,3-BPG) by GAPDH which also reduces nicotinamide adenine dinucleotide (NAD^+) to NADH (required for oxidative phosphorylation (1.3.2.1)) as part of this reaction. GAPDH is additionally involved in apoptosis (as a result of NO induced S-nitrosylation) (Hara *et al.*, 2005) and also potentially as a ROS sensor, in which S-glutathionylation of GAPDH leads to its inactivation and cycling of glycolytic intermediates into the PPP to generate NADPH (Peralta *et al.*, 2015). Notably, GAPDH has also been implicated as a positive regulator of mTOR where, under conditions of high glucose, the GTPase RAS homolog enriched in brain, is released and mTOR activated (1.2.2.2) (Lee *et al.*, 2009).

The first ATP generating glycolytic reaction is catalysed by PGK, a reversible reaction which transfers a phosphate group from 1,3-BPG to ADP to generate 3-phosphoglcerate (3-PG) and ATP. PGK exists as two isoforms, PGK1 which is ubiquitously expressed and PGK2 which is confined to sperm cells (Bowler, 2013). The phosphate group in 3-PG is then moved via a reversible reaction catalysed by the enzyme (PGAM) to generate 2-phosphoglycerate (2-PG). PGAM exists as three isoforms, PGAM1 which is ubiquitous, PGAM2 found predominantly in muscle tissue and PGAM3 found mainly in cardiac and skeletal tissue. Expression of PGAM is negatively regulated by TP53 (1.3.3.4), decreased expression of PGAM increases 3-PG levels which inhibit 6-phosphogluconate dehydrogenase (6-PGD) the enzyme that catalyses the third step of the PPP, by binding to its active site and decreases 2-PG levels which decreases PHGDH activity, which catalyses the first step of the SSP (Hitosugi *et al.*, 2012). The enzyme ENO catalyses the penultimate glycolytic reaction through the reversible dehydration reaction of 3-PG to PEP. ENO occurs in humans in three isoforms, ubiquitous ENO1, ENO2 found mainly in neuron tissue and ENO3 found mainly in muscle tissue and is a metalloenzyme requiring magnesium to be catalytically active. ENO1 is additionally found on the surface of haematopoietic cells where it acts as a plasminogen receptor (reviewed in Diaz-Ramos *et al.*, 2012).

The final step of the glycolytic pathway is irreversible and involves the conversion of PEP to pyruvate catalysed by pyruvate kinase (PK), which requires the transfer of a phosphate group from PEP to ADP to generate ATP. PK has been the subject of numerous excellent reviews and its role in tumour initiation and progression much

studied (Mazurek, 2011, Tamada *et al.*, 2012, Yang and Lu, 2013). In humans, PK exists as four isoforms encoded by two distinct genes, PKL expressed mainly in liver cells and PKR expressed mainly in erythrocytes are encoded by the *PKL/R* gene whilst, PKM1 expressed predominantly in neuron and muscle tissue and PKM2 which is expressed particularly in proliferating cells is encoded by the *PKM2* gene. PKM1 exists as a tetramer and has a strong affinity for PEP, is not allosterically regulated or subject to phosphorylation. PKM2 exists in both tetramer and dimer with a strong or weak affinity for PEP respectively. High levels of tetrameric form correlate with high levels of lactate production, whereas high levels of the dimeric form correlate with increased nucleic acid synthesis. Association of the tetrameric form is induced by F-1,6-BP and serine whereas dissociation into the dimeric form occurs due to increased levels of numerous amino acids and lipids. Conversely, high levels of ROS have also been shown to induce PKM2 dimerization via oxidation of cys358 (Anastasiou *et al.*, 2011), as has phosphorylation by fibroblast growth factor receptor 1 (Hitosugi *et al.*, 2009). Interestingly PKM2 dimer form has been shown to translocate to the nucleus (Wang *et al.*, 2015) where it promotes activation of HIF-1α genes, acts as a co-activator of β-catenin induced expression of c-MYC and phosphorylates STAT3 (1.1.4) (reviewed in Dong *et al.*, 2016).

Under aerobic conditions, the fate of pyruvate in normal cells is oxidative decarboxylation, catalysed by the enzyme pyruvate dehydrogenase (PDH), to form acetyl CoA, and entry into the citric acid cycle (1.4.4). Under hypoxic conditions stabilisation of HIF-1α (1.4.2.1) leads to transactivation of a gene encoding PDK1, which phosphorylates PDH leading to its inactivation (Kim *et al.*, 2006a). HIF-1α, also upregulates LDH expression, which catalyses the conversion of pyruvate into lactate and oxidises NADH in the process (reviewed in Miao *et al.*, 2013).

1.4.3.1 Glycolysis and cancer

As discussed above (1.4.1), a key aspect of cancer cell metabolism is the Warbug effect. This elevated rate of glycolytic flux and subsequent lactate secretion even in the presence of sufficient oxygen is common to most cancers and dysregulation of all steps of the glycolytic pathway have been shown to contribute to this phenotype.

GLUT1 is ubiquitously expressed in human tissues, has a high affinity for glucose and high levels of expression are associated with many cancers, whilst

overexpression of other isoforms have also been linked to tumours specific to their tissue expression (reviewed in Barron *et al.*, 2016). A recent meta-study of GLUT1 overexpression found that it correlated with unfavourable overall survival, increased metastasis and larger tumour size (Yu *et al.*, 2017b). In AML, upregulation of GLUT1 mRNA (Song *et al.*, 2016) and the fructose transporter GLUT5 (Chen *et al.*, 2016b) have been recently reported to be associated with poor outcome in AML patients. Song *et al* similarly identified HK2 overexpression as a feature of AML patients who failed to show remission. HK2 is frequently overexpressed in many cancers including brain (Wolf *et al.*, 2011), pancreatic (Anderson *et al.*, 2017), colorectal (Katagiri *et al.*, 2017) and liver (Guo *et al.*, 2015) and in a recent meta-study was associated with poor prognosis in gastric liver and colorectal but not pancreatic cancer (Wu *et al.*, 2017). PGI also known as AMF is secreted by cancer cells and is associated with EMT transition in breast (Ahmad *et al.*, 2011) and colorectal cancers (Tsutsumi *et al.*, 2009), whilst decreased proliferation in the AML cell line, KG-1, was observed upon knock-down of PGI with shRNA (You *et al.*, 2014).

The role of PFK in cancer appears to be mainly determined by changes in its regulation, as a consequence of inhibition and activation by several other metabolites, particularly F-2,6-BP (1.5). However, increased expression of the PFK-L isoform correlates with increased glycolysis in breast cancer cell lines (Zancan *et al.*, 2010) and is associated with poor OS in lung cancer patients where it is regulated via miRNA-128 and AKT signalling (Yang *et al.*, 2016). All three isoforms of ALDO have also been shown to be elevated in different cancers where increased metastasis and poor prognosis is associated with increased expression of ALDO(A) in both lung (Chang *et al.*, 2017) and pancreatic (Ji *et al.*, 2016) cancers, ALDO(B) in colorectal cancer (Li *et al.*, 2017c) and ALDO(C) in oesophageal cancer (Tao *et al.*, 2017). Proteomic studies revealed elevated levels of ALDO(A), ALDO(C) and ENO1 in the chemoresistant leukaemia cell line K562/A02 when compared with parental K562 cells and in the case of ENO1 this was confirmed by western blot (Shi *et al.*, 2015). Elevated levels of ENO2 have also been reported in patients with ALL where it is associated with lower OS (Liu *et al.*, 2016), whilst proteomic studies have also suggested elevated levels of TPI can occur in human lung squamous cancer (Li *et al.*, 2006).

GAPDH is also frequently upregulated in numerous solid tumours including lung, breast, gastric, liver, brain, renal and pancreatic (reviewed in Guo *et al.*, 2013), whilst increased PGK1 expression is observed in breast cancer where it is associated with poor OS (Sun *et al.*, 2015) and colon cancer where it is associated with increased metastasis (Ahmad *et al.*, 2013). PGAM is also upregulated in colorectal, breast, lung and liver cancers (reviewed in Jiang *et al.*, 2014), and in both AML and CML patient samples (Hitosugi *et al.*, 2012).

The role of PK in solid tumours, and in particular the isoform PKM2 whose expression is elevated in most cancers, has been the subject of much study (reviewed in Wong *et al.*, 2013). As introduced above PKM2 upregulation allows control of glycolytic flux via it tetramer to dimer ratio. Knock-down of PKM2 in cancer cell lines lead to decreased glycolysis and proliferation, whilst increased expression of PKM2 led to increased xenograft establishment (Christofk *et al.*, 2008). Expression of PKM1/PKM2 isoforms occurs due to alternative splicing, where c-MYC induced upregulation of heterogenous nuclear ribonucleoprotein leads predominantly to expression of PKM2 (David *et al.*, 2010). Additionally, HIF-1α (1.4.2.1), increases expression of PKM2, whilst PKM2 interacts with HIF-1α via prolyl hydroxylase 3 (PHD3) leading to transactivation of HIF-1α target genes. Increased mTOR activity (1.2.2.2) also leads to increased PKM2 expression, whilst increase in PTEN (1.3.3.2) inhibits PKM2 expression. Increased levels of PKM2 have been found in patients with lung (Schneider *et al.*, 2002), and colon (Eigenbrodt *et al.*, 1997) cancers, whilst a more recent study showed increased PKM2 levels in sixteen different tumour types, although this was only due to an isoform switch in glioblastoma (Desai *et al.*, 2014). In contrast to solid tumours, little work has been done on PKM2 in leukaemia. One study suggested increased PKM2 phosphorylation (and associated dimer formation) may be a function of LSC's (Sturgill and Guzman, 2014), whilst a recent study reported that conditional expression of Runx1-ETO in the AML cell line U937, resulted in downregulation of PKM2 (Yan *et al.*, 2017).

PDK activity and expression has been shown to be upregulated in cancer as a result of HIF-1α and c-MYC activation (Kim *et al.*, 2006a), whilst TP53 has also been shown to be a negative regulator of PDK2 both *in vitro* and *in vivo* (Contractor and Harris, 2012). Increased PDK1 expression is observed in non-small cell lung cancer tissues (Liu and Yin, 2017), overexpression of PDK2 is seen in cervical cancers

where it significantly correlates with metastasis (Lyng *et al.*, 2006), whilst PDK3 is overexpressed in colon cancers (Lu *et al.*, 2011). Given the observation that the Warburg effect increases glucose uptake, decreased oxidative phosphorylation resulting from increased PDK activity results either in increased conversion of pyruvate into lactate, or increased diversion of glycolytic intermediary metabolites into other metabolic pathways. LDH is a tetramer which exists as five isoforms, comprising of two subunits LDHA and LDHB in different combinations and encoded by the *LDHA* and *LDHB* genes. LDHA has the greater affinity for pyruvate and isoforms predominant in this protein strongly catalyse the pyruvate to lactate reaction and it is over expressed. The isoform LDH5 is composed of four LDHA subunits and is upregulated in head and neck squamous cell cancer (HNSCC) (Koukourakis *et al.*, 2009), non-small-cell lung cancer (Koukourakis *et al.*, 2003) and is associated with metastasis in colorectal cancer (Koukourakis *et al.*, 2005). A recent study involving 204 patients with acute leukaemia also reported that LDH plasma levels were significantly elevated compared to healthy controls and were also increased in relapse patients compared to those in CR (Hu *et al.*, 2016). Monocarboxylate transporters (MCT) are responsible for transporting lactate across the cell membrane, with MCT1 involved in both import and export, MCT2 import and MCT4 primarily export of lactate, with all these isoforms reported to be overexpressed in different tumours (reviewed in Baltazar *et al.*, 2014). Interestingly in lung adenocarcinoma cells expressing mutant K-RAS, shRNA knock-down of LDHB resulted in decreased proliferation *in vitro* and *in vivo* and elevated expression of LDHB was additionally observed in K-RAS mutated tumour tissue of patients with lung cancer, although not in other tumour types containing this mutation (McCleland *et al.*, 2013). LDHB preferentially catalyses the lactate to pyruvate reaction and may provide a mechanism (especially in combination with changes in MCT expression) by which extracellular lactate can be recycled by some cancers into metabolic pathways used in biosynthesis (4.4.2).

1.4.3.2 Glycolytic inhibitors

Given all glycolytic enzymes have been shown to be dysregulated in cancer, a considerable body of research exists with a view to targeting these or associated enzymes. As increased glucose uptake facilitated by overexpression of GLUT is a feature of many cancers, inhibition of these proteins represents an attractive target in

cancer therapy. WZB117 is a polyphenolic ester which specifically inhibits GLUT1, it has been shown to decrease glucose uptake and proliferation in lung and breast cancer cell lines, whilst a xenograft model of human lung cancer showed a 70% reduction in size with a daily dose of 10mg/kg (Liu *et al.*, 2012). Natural flavonoids such as Naringenin have been shown to inhibit glucose uptake in the AML cell line U937, whilst Kaempferol inhibited both glucose uptake and lactate uptake in the breast cancer cell line MCF7 (reviewed in (Granchi *et al.*, 2016). Other synthetic GLUT1 inhibitors such as enolic anilide fasentin 32, STF-31 as well as a series of methyl-ketoxime and thiazolidinedione derivatives have also been shown to reduce glucose uptake and decrease proliferation in cell lines.

HK, which catalyses the first step in glycolysis has also been targeted. 2-Deoxyglucose was one of the first drugs used to target this pathway, it is metabolised by HK to 2-deoxyglucose-6-phosphate which cannot be metabolised by PGI resulting in the inhibition of isoforms HK I, II and III. However, HK IV is not inhibited and the 2-deoxyglucose-6-phosphate can be metabolised through the PPP. Clinical trials using 2-DG alone were shown not to be effective, however in combination with other chemotherapeutic agents treatment efficacy was enhanced (reviewed in Zhao *et al.*, 2013). Another HK inhibitor 3-bromopyruvate (which is also known to inhibit GAPDH) has been shown to be effective both *in vitro* and *in vivo* in various cancers, including AML and ALL (Akers *et al.*, 2011) and was recently granted FDA orphan drug status in the treatment of liver cancer (reviewed in Granchi *et al.*, 2014). Lonidamine specifically targets HK II which is frequently upregulated in cancers. However, despite showing efficacy in pre-clinical trials, phase II and phase III clinical trials showed no significant improvement in OS and were terminated in 2006 due to hepatotoxicity, although interest in its use has recently been revived (reviewed in Cervantes-Madrid *et al.*, 2015). Targeting of PGAM has also recently been investigated using MJE3, which inhibited proliferation in breast cancer cell lines and PGAMI-004A which inhibited proliferation of both the AML cell line KG-1 and AML and CML cells from patients (Hitosugi *et al.*, 2012).

LDH inhibition has also been the target of much research, due to the increased expression of LDHA in many cancers, the potential role of lactate acidosis in metastasis (reviewed in Han *et al.*, 2013) and the fact that its inhibition would have limited toxicity on normal cells, where pyruvate is typically converted to acetyl CoA.

Compounds such as gossypol (AT-101) is currently undergoing phase I clinical trials in patients with prostate cancer (Liu *et al.*, 2009) and phase II clinical trials in patients with lung cancer (Baggstrom *et al.*, 2011). FX-11 (a gossypol derivative) and galloflavin have also been shown to be effective in xenograft models and hepatocellular cell lines respectively. Using a similar rationale as for LDH, the lactate transporters MCT have also been targeted for inhibition. MCT inhibitors such as α-cyano-4-hydroxy-cinnamate and AR-C155858 (developed by AstraZeneca) blocked proliferation in glioblastoma cell lines and activated T-cells respectively, whilst the inhibitor AZD3965 is currently in phase I clinical trials for the treatment of diffuse large B cell lymphoma (reviewed in Doherty and Cleveland, 2013).

Dichloroacetate (DCA), which inhibits PDK, has also been widely studied, sensitising prostate cancer cell lines to radiation (Cao *et al.*, 2008), inhibiting breast cancer metastasis both *in vitro* and *in vivo* (Sun *et al.*, 2010) and inducing apoptosis in endometrial cancer cell lines (Wong *et al.*, 2008). Phase I clinical trials in glioblastoma showed DCA was well tolerated in patients (Dunbar *et al.*, 2014), whilst in AML combination treatment of DCA and arsenic trioxide in AML cell lines showed synergistic apoptotic effects (Emadi *et al.*, 2015). Furthermore, treatment of one patient with refractory AML, with DCA 11 days and arsenic trioxide for 9 days was tolerated, before treatment was discontinued following enrolment in an AML specific trial. Recently, gene expression studies showed elevated expression levels of PDK in BM AML patient samples compared with BM from healthy individuals, with *in vitro* studies in Runx1-eto expressing AML cells showing decreased glycolytic phenotype when treated with both DCA and another PDK inhibitor AZD7545 (Kizilkaya and Reckzeh, 2016).

1.4.4 The citric acid cycle, serine synthesis and pentose phosphate pathway

Following conversion of pyruvate into acetyl CoA, which takes place in the mitochondrial matrix, the reaction of this metabolite with oxaloacetate to make citrate is catalysed by citrate synthase, which is the first step in the citric acid cycle. The citric acid cycle is a series of metabolic reactions that involving oxidation/reduction reactions, which generate NADH and FADH via the transfer of hydride ions, thus providing electrons for the ETC (1.3.2.1) which is a major source of cellular ROS (reviewed in Wallace, 2012). Fumarate hydratase, SDH and IDH are frequently mutated in cancer, with IDH mutations frequently reported in AML

(Table 1) (1.3.3.4). SDH mutations lead to increased succinate levels and inhibition of PHD (1.4.2.1) as well as DNA methylation and epigenetic dysregulation. FH catalyses the reaction of fumarate to malate, therefore its inactivation leads to increased levels of fumarate which activate NRF2 (1.3.3.4). Mutations in IDH2 are known to cause epigenetic dysregulation and blocks in cellular differentiation. AG-221 has been shown to inhibit this mutant IDH2 in AML cells *in* vitro and *in* vivo and is currently undergoing phase I/II clinical trials (Yen *et al.*, 2017). Whilst not an inhibitor of the citric acid cycle, the compound IACS-10759, which targets complex I of the ETC (1.3.2.1) was recently shown to inhibit ATP production and oxygen consumption in isolated mitochondria at single digit nanomolar concentrations, whilst increasing median survival by greater than 50 days in AML xenograft models (Protopopova *et al.*, 2015) and is currently in phase I clinical trials in AML patients.

The SSP branches from the glycolytic pathway at the glycolytic intermediate 3-PG, where it is converted into 3-phosphohydroxypyruvate by the enzyme PHGDH, followed by conversion to phosphoserine by phosphoserine aminotransferase 1 and finally to serine by the action of the enzyme phosphoserine phosphatase (reviewed in Yang and Vousden, 2016)). Regulation of the SSP is achieved through 2-PG which activates PHGDH whilst serine activates the tetrameric form of PKM2 leading to increased glycolysis and decreased levels of 2-PG (1.4.3). Importantly serine can enter the folate cycle, which provides another route for the generation of NADPH, which has been shown to contribute to tumour growth *in vivo* (Ye *et al.*, 2014). Overexpression of PHGDH has been reported in melanomas, colorectal and breast cancers, whilst knock-down of PHGDH inhibits growth of the leukaemia cell line, HL-60 (Polet *et al.*, 2016).

The PPP generate nucleotides for biosynthesis and is a major source of cellular NADPH an important cellular antioxidant (1.3.2.4). The first step involves the dehydrogenation of G-6-P to 6-phosphogluconolactone (6-PG) catalysed by G-6-PD and the conversion of $NADP^+$ to NADPH (reviewed in Patra and Hay, 2014). Gluconolactonase catalyses the hydrolysis of 6-PG to 6-phosphogluconate, which is then catalysed by 6-PGD to ribulose-5-phosphate (Ru-5-P) alongside the generation of a second NADPH. Ru-5-P can then be converted into ribose-5-phosphate (R-5-P) by the enzymatic action of ribulose-5-phosphate isomerase. R-5-P, which can then be used in the synthesis of nucleotides. Alternatively, where redox homeostasis and

not nucleotide synthesis is the major requirement of the cell Ru-5-P can be catalysed by ribulose-5-phosphate epimerase, into xyulose-5-phosphate (X-5-P) and via a series of further metabolic reactions back into the glycolytic intermediates F-6-P and G-3-P. G-6-PD is the rate limiting step of the PPP and is regulated by the $NADP^+$/NADPH ratio, RAS/PI3K signalling and phosphorylation by Src, whilst 6-PGD is inhibited by 3-PG (Hitosugi *et al.*, 2012).

In cancer, aberrant RAS signalling (1.2.2.2) or activation of Src (1.3.3.2) can promote activation of the PPP. Mutant K-RAS^{G12D} has been shown to increase flux through the PPP in murine models of pancreatic cancer (Ying *et al.*, 2012), whilst PI3K augmented upregulation of NRF2 in several cancer cell lines generated increased PPP flux (Mitsuishi *et al.*, 2012). G-6-PD has also been shown to be upregulated in prostate cancer, which was reported to be modulated by mTOR activation (Tsouko *et al.*, 2014). In AML, a recent study showed upregulation of G-6-PD mRNA in approximately 60% of patients, although it was not correlated with OS or relapse (Chen *et al.*, 2016c). Targeting of xenograft mice injected with the cell line K562 with the antimalarial drug dihydroartemisinin and the 6-PGD inhibitor Physicon resulted in decreased tumour growth, whilst primary leukaemia cells isolated from the PB of AML patients showed significantly decreased viability, with no toxicity observed in haematopoietic cells isolated from the PB of healthy individuals (Elf *et al.*, 2017).

1.5 The role of 6-Phosphofructo-2-kinase/fructoste-2,6-bisphosphatase (PFKFB) in metabolism

PFKFB is a bifunctional enzyme that catalyses the reaction of F-6-P to F-2,6-BP in both directions (Figure 1-8). In humans there are several isoforms encoded by four different genes. The *PFKFB1* gene contains 17 exons, with alternative splicing generating three different isoforms predominantly associated with liver, muscle and foetal tissue. Alternative splicing of *PFKFB2* generates two different isoforms both associated with heart tissue. The gene for *PFKFB3* contains 19 exons and via alternative splicing generate six different isoforms, although only two are substantively different, the ubiquitous isoform and the inducible isoform. The ubiquitous isoform is distributed in numerous tissues whilst the inducible isoform is named due to its upregulation under conditions of hypoxia. The gene for *PFKFB4*

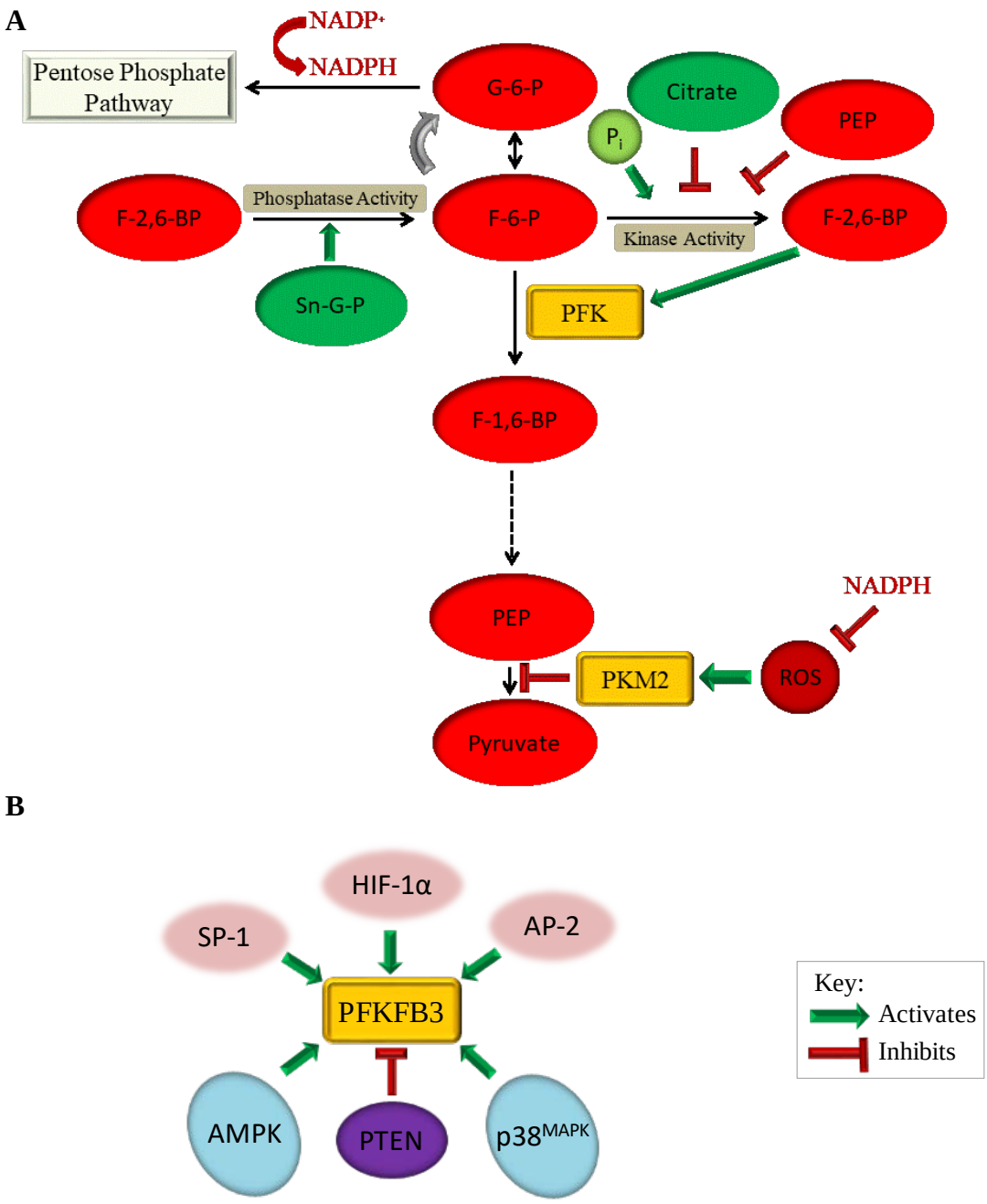

Figure 1-8. 6-Phosphofructo-2-kinase/fructoste-2,6-bisphosphatase (PFKFB) regulation and glycolysis. (A) Schematic illustration of main effectors and inhibitors of PFKFB, both as a phosphatase catalysing fructose-2,6-bisphosphate (F-2,6-BP) to fructose-6-phosphate (F-6-P) and as a kinase catalysing F-6-P to F-2,6-BP. F-2,6-BP activates phosphofructokinase (PFK) increasing glycolytic flux. Phosphoenolpyruvate (PEP) and citrate inhibit the kinase activity of PFKFB. Reactive oxygen species (ROS) increases PKM2 dimerisation, which inhibits the conversion of PEP to pyruvate. Sn-glycerol-3-phosphate (Sn-G-P) activates PFKFB phosphatase activity. Decreased kinase activity and increased phosphatase activity of PFKFB decreases glycolytic flux and potentially leads to increase flux through the pentose phosphate pathway, generating NADPH. Phosphorylation, S-gluathionylation and methylation all modulate PFKFB activity. **(B)** Activators and inhibitors of PFKFB3 which shows a kinase to phosphatase activity of 740:1. Transcription factors (pink) and signalling pathways (blue). Glucose-6-phosphate (G-6-P), inorganic phosphate (P_i), fructose-1,6-bisphosphate (F-1,6-BP), specificity protein 1 (SP1), activator protein 2 (AP-2), hypoxia inducible factor-1 alpha (HIF-1α), phosphatase and tensin homolog (pTEN), 5'adenosine monophosphate-activated protein kinase (AMPK) p38 mitogen-activated protein kinase ($p38^{MAPK}$).

contains 14 exons, several different splice alternatives have been identified, and although originally discovered in testes tissue it is also found in other tissues. The crystal structures of the liver form of PFKFB1 (Lee *et al.*, 2003), PFKFB2 (Crochet *et al.*, 2017), the inducible form of PFKFB3 (Kim *et al.*, 2006b) and PFKFB4 (Hasemann *et al.*, 1996) have all now been determined. Whilst the catalytic domain of each isoform is highly conserved (85% homology), differences in the N-terminus and C-terminus impact on their respective kinetic properties (Cavalier *et al.*, 2012). The N-terminus of PFKFB is responsible for catalysing the synthesis of F-2,6-BP from F-6-P and ATP, whilst the C-terminus catalyses its degradation in the reverse direction. The kinase to phosphatase (k/p) activity of each isoform is a key determinant in its metabolic role and whilst the k/p activity of PFKFB1 (liver), PFKFB2 and PFKFB4 are 1.2, 1.8 and 0.9 respectively, the k/p of PFKFB3 has been determined as 740, which is elevated to 3000 upon phosphorylation by AMPK (Marsin *et al.*, 2002), resulting in increased PFKFB3 kinase activity, increased F-2,6-P levels, increased activation of PFK and increased glycolytic flux. Kinase activity is additionally stimulated by inorganic phosphate, inhibited by PEP, citrate and sn-glycerol-3-phosphate (important in the synthesis of glycerophospholipids), which additionally promotes its phosphatase activity (reviewed in Ros and Schulze, 2013). Importantly, the product of this kinase activity is F-2,6-BP, which is a powerful allosteric activator of PFK (Pilkis *et al.*, 1981), a rate limiting step in glycolysis (1.4.3).

1.5.1 PFKFB3

The structure of the inducible isoform of PFKFB3 consists of a polypeptide chain, comprising of a six-stranded β-sheet and seven α helices which form the N-terminus and a six-stranded β-sheet with eight α helices forming the C-terminus. The functional form of PFKFB3 is a homodimer with the N-termini forming a twelve-stranded interlinked β-sheet, whilst the C-termini remain separate. The active binding site for ATP occurs between residues 168-179 and for F-6-P between residues 72 and 84. Compared with other isoforms, the PFKFB3 isoform has a serine at position 80 and a lysine at position 79, which allow a hydrogen bond to form between Tyr81 and Asp185, restricting the flexibility of the F-6-P loop, enhancing binding of the substrate and providing a rationale for the increased kinase activity of PFKFB3 (Kim *et al.*, 2006b).

1.5.1.1 Regulation of PFKFB3

PFKFB3 expression has been shown to be negatively regulated by PTEN (Figure 1-8B). Mouse embryonic fibroblast cells with PTEN knock-down show 3-fold increases in F-2,6-BP concentration levels, which were ablated upon reintroduction of PTEN, whilst increased PFKFB3 protein levels were also observed in the knock-down cells (Cordero-Espinoza and Hagen, 2013). The 5' promoter region of *PFKFB3* gene contains SP-1 and AP-2 domains (Navarro-Sabate *et al.*, 2001), and is therefore a target of these transcription factors, which have roles in cell differentiation, growth, proliferation and apoptosis, and are additionally modulated by ROS (1.3.3.2). Additionally, the *PFKB3* gene contains a serum response element, which is activated by the $p38^{MAPK}$ pathway (1.2.2.3) (Novellasdemunt *et al.*, 2013), and a HRE (Obach *et al.*, 2004) which is a target of HIF-1α (1.4.2.1).

From an oncogenic perspective, increased aerobic glycolysis is known to decrease extracellular pH, through increased lactate production (1.4.3) which is important in metastasis. One study, using the DB-1 cell line showed increased AMPK activation under conditions of low pH resulted in both increased protein expression of PFKFB3 and increased phosphorylation of PFKFB3 at Ser-461, leading to increased glycolysis (Mendoza *et al.*, 2012). Interestingly however, AMPK activation in colorectal cancer cell lines showed increased GLUT1, HKII and PFKFB3 expression and glycolysis immediately following activation, but long term activation resulted in cell death (Yu *et al.*, 2017a).

1.5.1.2 Post-translational modifications of PFKFB3

In addition to phosphorylation of Ser-461 by AMPK (1.5.1.1), increased sonic hedgehog signalling (which is associated with increased tumour size and progression in breast cancer) was shown to lead to increased glycolysis and proliferation in breast cancer cell lines, not as a function of increased expression of PFKFB3, but due to phosphorylation of Ser-461 (Ge *et al.*, 2015b). In the AML cell line U937, methylation of Arg-131 and Arg-134 were also shown to increase PFKFB3 kinase activity (Yamamoto *et al.*, 2014). Other post-translational modifications such as by IκB kinase β (IKKβ) have been shown to downregulate PFKFB3. As discussed previously (1.3.3.4), ROS stimulated IKKβ phosphorylates IκB proteins, resulting in their dissociation from NF-κB and its translocation to the nucleus where it regulates genes involved in proliferation and apoptosis. However it was also shown, in HEK

293T cells, that IKKβ can also directly phosphorylate PFKFB3 at Ser-269 leading to its inhibition and decreased glycolytic flux (Reid *et al.*, 2016). S-glutathionylation of PFKFB3 has also been shown to occur under conditions of high ROS, resulting in decreased kinase activity (Seo and Lee, 2014). HeLa cells treated with exogenous H_2O_2 showed S-glutathionylation of PFKFB3, decreased levels of F-2,6-BP and increased concentrations of Ru-5-P and X-5-P. Resolution of the crystal structure revealed this modification occurred at Cys-206, followed by the formation of a hydrogen bond at Gln-199. Alternatively, downregulation of miR-206 and increased mRNA and protein expression of PFKFB3, was shown to be a feature of oestrogen receptor alpha positive breast cancer cells (Ge *et al.*, 2015a). Here it was shown that miR-206 downregulated PFKFB3 expression, and therefore decreased glycolysis, via direct interaction with the PFKFB3 mRNA.

1.5.1.3 PFKFB3 and its inhibition in cancer

Immunohistochemical staining for PFKFB3 expression has shown elevated levels of this enzyme in colon, prostate, breast, lung, pancreatic, ovarian, kidney and thyroid tumour tissue (Atsumi *et al.*, 2002), whilst staining of 111 HNSCC tissues, also revealed elevated expression in nearly all samples (Li *et al.*, 2017a). Analysis of 40 astrocytic glioma brain tissue samples showed protein levels of PFKFB3 are markedly elevated in high grade astrocytomas (Kessler *et al.*, 2008), whilst mRNA levels of all *PFKFB* isoforms have been shown to be upregulated in malignant gastric tissue (Bobarykina *et al.*, 2006). Overexpression of PFKFB3 has also been shown to dysregulate circadian clock genes, which in turn enhance PFKFB3 expression in tongue cancer (Chen *et al.*, 2016a). In the breast cancer cell lines T47D and MCF7, PFKFB3 expression and phosphorylation at Ser-461, were both shown to increase in response to progestin (Novellasdemunt *et al.*, 2012). In AML a recent study has shown that knock-down of the tumour suppressor protein, tuberous sclerosis 2 leads to elevated expression of PFKFB3 in AML cell lines via activation of mTOR (Feng and Wu, 2017). Furthermore, treatment of these cells with the PFKFB3 inhibitor 1-(4-pyridinyl)-3-(2-quinolinyl)-2-propen-1-one (PFK-15) and rapamycin showed synergistic suppression of proliferation.

PFK-15 is an analogue of the PFKFB3 inhibitor 3-(3-pyridinyl)-1-(4-pyridinyl)-2-propen-1-one (3PO) and shows improved pharmokinetic properties compared to 3PO (Clem *et al.*, 2013). 3PO has previously been shown to inhibit proliferation,

alongside glucose uptake and cellular F-2,6-BP levels, in the Jurkat T-cell leukaemia cell line and solid tumour cell lines as well as inhibiting tumour growth in murine xenograft models of Lewis lung carcinoma, MDAMB231 breast adenocarcinoma and HL-60 promyelocytic leukaemia (Clem *et al.*, 2008). PFK-15 has been shown to both, inhibit proliferation and induce apoptosis in gastric cancer cell lines, and decrease tumour growth *in vivo* (Zhu *et al.*, 2016). In HNSCC xenograft models, PFK-15 has also been shown to be effective in suppressing tumour growth and metastasis (Li *et al.*, 2017a).

Administration of Oestradiol to breast cancer patients increases glucose uptake and has been linked to increased PFKFB3 expression (Imbert-Fernandez *et al.*, 2014). Treatment of breast cancer cell lines with both Oestradiol and another analogue of 3PO, 1-(pyridine-4-yl)-3-(7-(trifluoromethyl)-quinolin-2-yl)-prop-2-en-1-one (PFK158), or Oestradiol in cell lines with PFKFB3 knocked-down, resulted in decreased F-2,6-BP levels and glucose uptake. PFK158 (which is currently undergoing phase I clinical trials) has also been shown to be effective against chemoresistant ovarian cancer cell lines (Mondal *et al.*, 2015), whilst treatment of A375 melanoma xenograft bearing mice in combination with the RAS inhibitor Vemurafenib resulted in >80% tumour inhibition and 50% tumour regression (compared to 80% inhibition and no regression in the stand alone therapy) (Telang *et al.*, 2015).

1.5.1.4 Moonlighting functions of PFKFB3

In addition to PFKFB's role in glycolysis (1.5), the isoform PFKFB3 also plays a role in cell cycle regulation and autophagy. Localisation of PFKFB3 to the nucleus was first observed in HeLa and HCT116 cell lines (Yalcin *et al.*, 2009a), whilst a later study revealed PFKFB3 catalysed production of F-2,6-BP in the nucleus, which promoted the phosphorylation of protein p27 by CDK1 leading to its degradation and inhibition of cell cycle arrest (Yalcin *et al.*, 2014).

Links between autophagy and PFKFB3 were first made in T-cells of patients with rheumatoid arthritis, where decreased glucose metabolism and autophagy was observed compared to control. Analysis of expression of glycolytic genes revealed decreased expression of *PFKFB3* mRNA, which was confirmed at a protein level (Yang *et al.*, 2013), alongside increased levels of NADPH. A further study suggested

that starvation of HeLa cells resulted in phosphorylation of $p38^{MAPK}$ by ROS, stabilisation of HIF-1α and increased expression of GLUT3, whilst at the same time increasing proteasome degradation of PFKFB3. This proposed mechanism increases cellular glucose uptake whilst shifting metabolism away from glycolysis and into the PPP and is observed alongside an decrease in autophagy (Desideri *et al.*, 2014). However, another study involving pharmacological inhibition of PFKFB3 in colon adenocarcinoma cell lines showed decreased cellular glucose uptake, alongside increased levels of ROS and increased autophagy (Klarer *et al.*, 2014). These apparently contradictory results may reflect different cellular responses to differing concentrations of ROS (i.e. S-glutathionylation (1.5.1.2), or differences in regulatory mechanisms between the cell lines (i.e. TIGAR (1.5.2)) or be reflective of different experimental conditions, such as glucose availability, impacting differently on the cellular responses. However, they do suggest that PFKFB3 may be central in managing an intricate balance between cellular metabolic requirements and redox regulation.

1.5.2 TP53-induced glycolysis and apoptosis regulator (TIGAR)

TIGAR is an enzyme encoded by the gene *C12orf5* which is induced by TP53 (Jen and Cheung, 2005). It contains an active binding site which is closely related to the phosphatase site of PFKFB and catalyses the hydrolysis of F-2,6-BP and F-1,6-BP to F-6-P (Li and Jogl, 2009). Consequently, it has been shown that TIGAR can be rapidly induced by TP53 in response to cellular stress, leading to decreased glycolysis and cellular ROS, as a result of the diversion of metabolites into the PPP (Bensaad *et al.*, 2006). Furthermore, knock-down of PFKFB3 has been shown to induce TIGAR expression via AKT signalling in HeLa cells (Simon-Molas *et al.*, 2016). TIGAR has been shown to be highly expressed in a number of cancers including breast (Won *et al.*, 2012), nasopharyngeal (Zhao *et al.*, 2016b) and glioblastoma (Wanka *et al.*, 2012). Recently TIGAR overexpression has been shown to be associated with poor prognosis in patients with cytogenetically normal AML (Qian *et al.*, 2016) and CLL (Hong *et al.*, 2016).

1.6 Aims and Objectives

In the last twenty years, it has become increasingly clear that ROS play a significant role in cellular signalling, particularly pathways associated with growth, differentiation and survival. In many cancers ROS levels have been shown to be elevated, leading to aberrant signalling in these pathways. Work in our group has previously reported increased levels of NOX2-derived ROS in HPC infected with mutant RAS, AML cell lines and AML blasts. Furthermore, this increased ROS was shown to be correlated with a pro-proliferative phenotype. Coupled with this, mRNA microarray and Metacore pathway analysis of mutant RAS expressing HPC identified significant ROS-dependant up-regulation of genes associated with glycolysis, linking ROS production to the possible induction of the Warburg effect (which increases the rate of aerobic glycolysis in transformed cells). There is however, no direct evidence demonstrating a role for ROS in modulating metabolism in AML, nor what impact this may have on proliferation of these cells.

Therefore, the main aims of this study are to:

(i) *Determine ROS dependent changes in glucose uptake, extracellular lactate secretion and proliferation in AML models.*
To address this the effect of ROS modulation on glucose and lactate levels will be assayed, both in HPC expressing mutant RAS and in AML cell lines.

(ii) *Determine the ROS-dependent transcriptional and translational changes affecting glycolytic enzymes in AML models.*
Previously generated mRNA microarray data will be subjected to a supervised analysis focussing on glycolytic enzymes.
Correspondingly, the effect of ROS on the protein expression of glycolytic enzymes in the above AML models will be determined by immunoblotting.

(iii) *Determine ROS dependent perturbations of metabolites in AML models.*

The impact of ROS levels on the concentrations of cellular metabolites in AML cell lines and AML patient blasts will be determined using a variety of mass spectrometry platforms.

(iv) *Determine the mechanism by which any ROS-dependent changes in glycolysis occur.*

Overexpression, knock-down and chemical inhibition will be used to attempt to elucidate the mechanism through which ROS mediates changes in glycolytic activity in experimental models of AML.

2 Materials and Methods

2.1 Materials and reagents

Materials are grouped by supplier and listed in alphabetical order below.

Ampicillin, 7-aminoactinomycin (7-AAD), boric acid, bovine serum albumin fraction V (BSA), Bradford's reagent, calcium chloride ($CaCl_2$), catalase, chloroquine, cobalt chloride ($CoCl_2$), deoxyribonuclease (DNAse), Dimethylsulphoxide (DMSO), diphenyleneiodonium (DPI), Dulbecco Modified Eagle Medium (DMEM), ethanol, ethylene glycol-bis(2-aminoethylether)-N,N,N',N'-tetraacetic acid (EGTA), ethylenediaminetetraacetic acid (EDTA), glucose, glucose oxidase (GOX), glycerol, Iscove's Modified Dulbecco's Medium (IMDM), isopropanol, kanamycin, L-glutamine, magnesium chloride ($MgCl_2$), 2-mercaptoethanol, poly-L-lysine solution, polyethylene glycol sorbitan (Tween-20), Ponceau S solution, potassium dihydrogen phosphate (KH_2PO_4), Roswell Park Memorial Institute 1640 medium (RPMI), sodium chloride (NaCl), sodium orthovanadate (Na_3VO_4) sodium phosphate (Na_2HPO_4), triethylammonium bicarbonate (TEAB) lysis buffer (composed of 0.5M TEAB 5mL, 0.05% *w/v* SDS 50 µL, Protease Inhibitor Cocktail 100 µL, Phosphatase Inhibitor Cocktail P0044, Phosphatase Inhibitor Cocktail P5726, sucrose, tris(hydroxymethyl)aminomethane (Tris), Tris-borate EDTA (TBE) buffer (composed of 89mM Tris, 89mM boric acid, 2mM EDTA), tris(hydroxymethyl)aminomethane (Tris), 4-(1,1,3,3-tetramethylbutyl)phenyl-polyethylene glycol (X100 Triton), were purchased from Sigma-Aldrich, Poole, U.K.).

Agarose, dithiothretiol (DTT), Hank's Balanced Salt Solution (HBSS), human Granulocyte Colony-Stimulating Factor (G-CSF), human Granulocyte-Macrophage Colony Stimulating Factor (GM-CSF), 4-(2-hydroxyethyl)-1-piperazineethanesulfonic acid (HEPES) human interleukin-3 (IL-3), human interleukin-6 (IL-6), Phosphate Buffered Saline (PBS), human Stem Cell Factor (SCF), streptomycin, Super-Optimal medium (SOC) (comprising 0.5% *w/v* yeast extract, 2% *w/v* tryptone, 10mM NaCl, 2.5mM KCl, 10mM $MgCl_2$, 10mM $MgSO_4$ and 20mM glucose), trypsin were purchased from Invitrogen, Paisley, U.K.

Anti-CD34 magnetically labelled microbeads, Fc receptor blocking agent, Mini-MACS Kit, MS Column were purchased from Miltenyi Biotec, Bisley, U.K. Human Fms-like tyrosine kinase-3 ligand (FLT3) were purchased from Peprotech, London, U.K. Complete mini EDTA-free protease inhibitor tablets, 30% iron saturated human transferrin were purchased from Roche, Welwyn Garden City, U.K. Bacto-Tryptone™, Bacto-yeast™, Ficoll-Pacque™ were purchased from BD Biosciences, Oxford, U.K. Gentamycin were purchased from Sanofi-Aventis, Guildford, U.K.. Heparin were purchased from Leo Laboratories Ltd, Princes Risborough, U.K. Tris-acetate-EDTA (TAE buffer) (composed of 40mM Tris, 20mM acetic acid, 1mM EDTA) were purchased from Thermo-Scientific, Loughborough, U.K. Seakem CTG™ Agarose powder were purchased from Lonza, Nottingham, U.K. Peq Green were purchased from Peqlab, Lutterworth, U.K. Retronectin were purchased from Takara Bio, Paris, France. 2-(N-(7-nitrobenz-2-oxa-1,3-diazol-4-yl) amino)-2-D-deoxyglucose (2-NBDG) and Trizol™ were purchased from Life Technologies, Glasgow, U.K. 3-Benzyl-7-(2-benzoxazolyl) thio-1,2,3-triazolo (4,5-d) pyrimidine (VAS-2870) were purchased from ENZO-life sciences, Exeter, U.K. Magnesium acetate was purchased from Fisons Scientific Equipment, Loughborough, U.K. Benzonase were purchased from Novagen, Nottingham, U.K. 3-(3-pyridinyl)-1-(4-pyridinyl)-2-propen-1-one (3PO), 1-(pyridine-4-yl)-3-(7-(trifluoromethyl)quinolin-2-yl)-prop-2-en-1-one (PFK158) were purchased from Axon Medchem, Groningen, Netherlands. Recombinant Human HIF-1α protein were purchased from Abcam, Cambridge, UK. Foetal bovine serum (FBS) was purchased from Labtech, Heathfield, U.K. Tissue culture grade water was purchased from Hameln pharmaceuticals, Gloucester, U.K. Cytarabine (ARA-C) was purchased from University Hospital of Wales pharmacy, Cardiff, U.K. Plasticware was purchased from Iwaki Biosciences, Iwaki, Japan and Nunc, Roskilde, Denmark unless otherwise stated.

2.1.1 Antibodies

Antibodies used in this study are listed below in alphabetical order along with the clone number, application, concentration used and manufacturer.

Table 2. List of antibodies used in this study. Antibodies are listed in alphabetical order. BIOSS (Aachen, Germany), CST (Cell Signalling Technology, Leiden, Netherlands), MBL Life science (Nagoya, Japan), Merck Millipore (Feltham, U.K.), Santa-Cruz (Heidlberg, Germany) Serotec (Oxford, U.K.), GE Healthcare (Little Chalfont, U.K.). Abbreviations: murine (Mu), rabbit (Rb) monoclonal antibody (mAb), polyclonal antibody (pAb), flow cytometry (FC), western blot (WB), concentration ($Conc^n$).

Antibody	Clone	Use	$Conc^n$	Manufacturer
Beta actin	Mu mAb 8226	WB	0.5ng/µL	Abcam
Aldolase (A) ALDO(A)	Rb mAb D73H4	WB	1ng/µL	CST
Aldolase (C) ALDO(C)	Rb pAb	WB	10ng/µL	Abcam
Anti-mouse HRP	Sheep	WB	2ng/µL	GE Healthcare
Anti-rabbit HRP	Sheep	WB	2ng/µL	GE Healthcare
CD34-PE	Mu mAb 8G12?	FC	5ng/µL	BD Biosciences
CD45-PerCP	Mu mAb MEM28	FC	1ng/µl	Abcam
Enolase 1 (ENO1)	Rb mAb D2S1A	WB	1ng/µL	CST
Fructose-1,6-bisphosphatase 1 (FBP1)	Rb mAb EPR4620	WB	1ng/µL	Abcam
Glyceraldehyde-3-phosphate dehydrogenase (GAPDH)	Rb mAb D16H11	WB	0.5ng/µL	CST
Glucose transporter 3 (GLUT3)	Rb mAb EPR10508(N)	WB	1ng/µL	Abcam
Glucose transporter 5 (GLUT)5	Mu mAb 12F2	WB	2ng/µL	Abcam
Hexokinase 1 (HK1)	Rb mAb C35C4	WB	2ng/µL	CST
Histone H1	Mu mAb AG4	WB	2ng/µL	Serotec
Hypoxia-inducible factor 1-alpha (HIF-1α)	Mu mAb 54	WB	10ng/µL	BD Biosciences
Immunoglobulin G1-PE (IgG1-PE)	Mu mAb MOPC-31C	FC	5ng/µL	BD Biosciences
Lactate dehydrogenase (A) (LDH(A))	Rb mAb C4B5	WB	1ng/µL	CST
Monocarboxylate transporter 4 (MCT4)	Rb pAb	WB	1ng/µL	Abcam

NOX2-PE	Mu mAb 7D5	FC	5ng/µL	MBL
$p38^{MAPK}$	Rb pAb	WB	2ng/µL	CST
Phospho-$p38^{MAPK}$	Rb mAb (Thr180/Tyr182) D3F9	WB	2ng/µL	CST
Phosphofructokinase (P) (PFK(P))	Rb mAb D2E5	WB	1ng/µL	CST
6-phosphofructokinase/ fructose-2,6-biphosphatase 3 (PFKFB3)	Rb mAb D7H4Q	WB	1ng/µL	CST
Phospho-6-phosphofructokinase/ fructose-2,6-biphosphatase 3 (phospho-PFKFB3)	Rb pAb (Ser 466)	WB	2ng/µL	BIOSS
Phosphoglucose isomerase (PGI)	Rb mAb EPR11663(B)	WB	5ng/µL	Abcam
Phosphoglycerate mutase 1 (PGAM1)	Rb mAb D3J9T	WB	2ng/µL	CST
Phosphoglycerate kinase (PGK)	Rb mAb EPR14908	WB	2ng/µL	Abcam
Pyruvate kinase (M) 1 (PK(M)1)	Rb mAb D30G6	WB	1ng/µL	CST
Pyruvate kinase (M) 2 (PK(M)2)	Rb mAb D78A4	WB	1ng/µL	CST
H-RAS	Rb pAb	WB	10ng/µl	Santa-Cruz
N-RAS	Mu mAb OP25	WB	10ng/µL	Merck
Triphosphate isomerase (TPI)	Rb mAb EPR12149(B)	WB	1ng/µL	Abcam
α-Tubulin	Rb mAb EP1332	WB	1ng/µL	Abcam

2.2 Recombinant DNA methodology

Full length human cDNA encoding PFKFB3 variant 2 (NCBI reference sequence NM-001145443.2) (Figure 2-1A) flanked by DNA sequences for *Bam*H1 and *Eco*R1 restriction sites (to allow directional subcloning into the PINCO vector (Figure 2-1B)), and *XbaI* and *HpaI* (to allow directional subcloning into the pHIV vector (Figure 2-1C) (2.2.3.2) was purchased from Eurofins MWG (Ebersberg, Germany). The sequence was supplied in the pEX-K4 expression vector containing sequences for kanamycin resistance (pEX-K4 PFKFB3).

Five shRNA sequences complementary to PFKFB3 (TRC2 N0000314690, TRC2 N0000314746-8, TRC2 N0000381874 (appendix 1)), were purchased from Mission^{TM}, Sigma-Aldrich in the TRC2-pLKO.5-puro lentiviral vector expressing puromycin and ampicillin resistance (Figure 2-1D), which had been transformed into DH5α-T1^{R} competent *Escherichia coli* (*E.coli)* cells. TRC2-pLKO.5-puro non-mammalian shRNA control plasmid DNA, dissolved in TE buffer (500ng/µL), expressing puromycin and ampicillin resistance was purchased from Mission^{TM}, Sigma-Aldrich.

Five shRNA sequences complementary to HIF-1α (TRC N0000003808-11, TRC N0000010819 (appendix 2)) in TRC1-pLKO.5-puro lentiviral vector DNA and expressing puromycin and ampicillin resistance (Figure 2-1E), dissolved in TE buffer (500ng/µL), were purchased from Mission^{TM}, Sigma-Aldrich. TRC1-pLKO.5-puro non-mammalian shRNA control plasmid DNA, dissolved in TE buffer (500ng/µL), expressing puromycin and ampicillin resistance had previously been purchased from Mission^{TM}, Sigma-Aldrich, and THP-1 cells previously infected with this control.

In addition, full length cDNA encoding N-RAS^{G12D} (kindly provided by Alan Hall, University College of London, U.K.) and H-RAS^{G12V} (kindly provided by Julian Downward, CRUK London Research Institute, U.K.) had previously been sub-cloned by blunt cloning into the *Bam*H1 site of the retroviral expression vector PINCO (gift of Pier Pelicci, European Institute of Oncology, Milan, Italy), which co-expresses green fluorescent protein GFP from an internal cytomegalovirus (CMV) promoter (Grignani *et al.*, 1998) and into the PINCO vector expressing DsRed (kindly provided by Dr. Alex Tonks, Cardiff University, U.K.). Control PINCO

vectors (expressing GFP or DsRed alone) for N-RAS^{G12D} and H-RAS^{G12V} experiments had also been previously generated by insertion of non-mammalian encoding DNA (1.2Kb) into the PINCO plasmid, to prevent excessive expression of reporter genes. Plasmid DNA had subsequently been transformed into competent *E.coli* cells and was available in our laboratory. The integrity of N-RAS^{G12D} and H-RAS^{G12V} in the PINCO plasmid had previously been checked by sequencing and by functional assay (Hole, 2010).

2.2.1 Transformation of competent *E.coli* with recombinant plasmid DNA

To generate sufficient plasmid DNA for transfection, DNA amplification was performed in chemically competent *E.coli* One Shot Stabl3^{TM} cells (Invitrogen, Loughborough, UK). Cells were thawed on ice, 20ng (5µL) of cDNA (see 2.2) added, then incubated on ice for 30 min, at 42^{o}C for 30sec then on ice for a further 2 min. SOC media (250µl) (Invitrogen), prewarmed to 42^{o}C, was added and cells shaken at 225 rpm at 37^{o}C for 1h.

Selective Luria-Bertani (LB) broth was made using Bacto-Tryptone (10g) (BD Bioscience), Bacto-yeast extract (5g) (BD Bioscience), NaCl (10g) (Sigma) dissolved in dH_2O (1L) and autoclaved. LB agar was made as for LB broth but with the addition of agarose (15g) (Invitrogen). Transformed *E.*coli cells (50µL) was spread over kanamycin (Sigma) or ampicillin (Sigma) (50µg/mL) selective LB agar plates (30mL) and incubated overnight at 37^{o}C. A single isolated colony was selected to inoculate kanamycin (Sigma) or ampicillin (Sigma) (50µg/mL) selective LB broth (5mL). The broth was shaken at 225rpm, 37^{o}C for 7h, diluted in kanamycin (Sigma) or ampicillin (Sigma) (50µg/mL) selective LB broth, before incubation overnight at 37^{o}C on a rotary shaker (225rpm). Prior to isolation of recombinant plasmid DNA (2.2.2), inoculated broth (850µL) was added to glycerol (150µL) (Sigma) and stored at -80^{o}C.

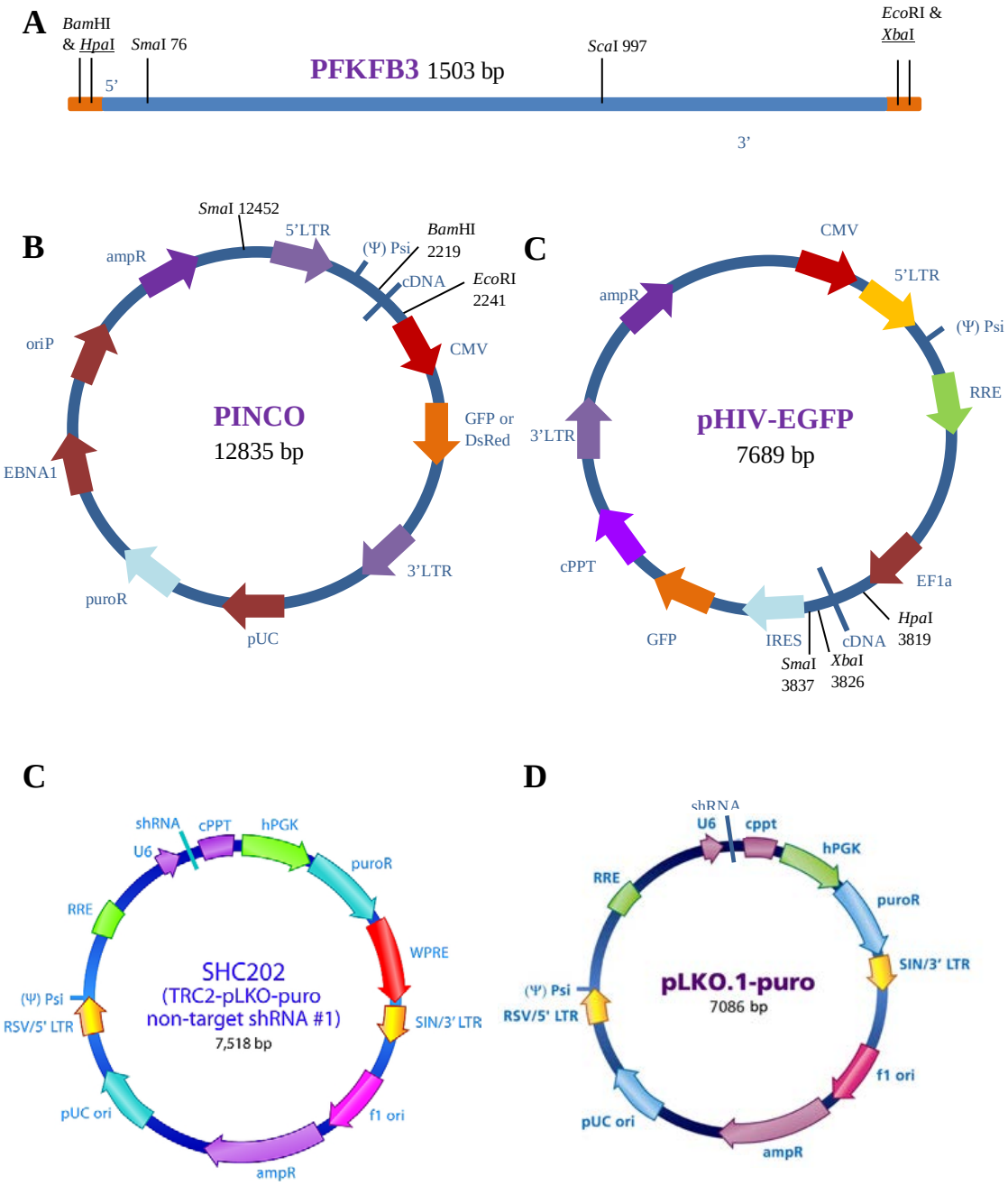

Figure 2-1. Plasmid vectors and PFKFB3 sequence used in study. Vector maps showing sequences of interest of (A) PFKFB3 (var2) (blue represents PFKFB3 gene, green represents additional DNA sequence, coding for restriction sites shown, to allow subcloning of gene) (B) PINCO, (C) pHIV-EGFP, (D) p-LKO.2-puro, (E) p-LKO.1-puro and (E) PFKFB3. Black lines show digestion sites for restriction enzymes. U6 (RNA polymerase III U6 promoter) , cppt (central polypurine tract), hPGK (human phosphoglcerate kinase eukaryotic promoter), puroR (puromycin resistance), SIN3'LTR (3'self inactivating long terminal repeat), f1 ori (f1 origin of replication), ampR (ampicillin resistance), pUC ori (pUC origin of replication), RSV 5'LTR (Rous Sarcoma virus 5' long terminal repeat), ΨPsi (RNA packaging signal), RRE (Rev response element), WPRE (woodchuck hepatitis post-transcriptional regulatory element), CMV (cytomegalovirus promoter), GFP (green fluorescent protein) DsRed (red fluorescent protein), pUC (pUC prokaryotic control sequence), EBNA1 (Epstein-Barr virus nuclear antigen 1), oriP (Epstein-Barr virus origin of replication), EF1a (human elongation factor-1 alpha) IRES (internal ribosome entry site).

2.2.2 Isolation and quantitation of recombinant plasmid DNA

Transformed *E.coli* cells (2.2.1) in selective LB broth (150mL) was centrifuged at 6,000g, 4^{o}C for 15 min and plasmid DNA was extracted by alkaline lysis and salt precipitation, using the QIAGEN HiSpeed Plasmid Maxi Kit (QIAGEN, Manchester, UK), according to the manufacturer's instructions. Briefly, the bacterial pellet was lysed in proprietary buffer P1 (containing RNase A) (10mL) and proprietary buffer P2 (10mL), mixed by inversion, incubated at room temperature (RT) for 5 min, before addition of proprietary buffer P3 (10mL). Lysate was transferred to a QIA filter cartridge, incubated at RT for 10 min, then the lysate filtered into a HiSpeed Maxi tip (previously equilibrated with proprietary QBT buffer (10mL) and allowed to pass through the resin by gravity flow. The tip was washed with proprietary QC buffer x2 (30mL). Plasmid DNA was eluted with 15mL of proprietary QF buffer, precipitated using 10.5mL of isopropanol (Sigma) and incubated at RT for 5 min. The elute was passed through a QIA precipitator using a 30mL syringe to isolate the plasmid DNA, washed with 70% *v/v* ethanol (2mL) (Sigma) and air dried by syringing air through the precipitator. The plasmid DNA was then collected by passing TE buffer (1mL) through the precipitator, the collected elute was then passed through the precipitator once more to maximise DNA recovery. The isolated plasmid DNA was then quantified using a NanoDrop ND-1000 spectrophotometer (Thermoscientific, Loughborough, UK), according to the manufacturer's instructions and DNA purity measured by confirming the A260/280 ratio range was between 1.8-2.

2.2.3 Generation of retroviral and lentiviral vectors encoding PFKFB3

2.2.3.1 Excision and isolation of PFKFB3 DNA

To express PFKFB3 in haematopoietic cells, this gene was directionally subcloned into the PINCO retroviral expression vector. Initially, PFKFB3 DNA was excised from the pEX-K4 vector prior to ligation into either the PINCO vector (co-expressing DsRed as a reporter gene) or the pHIV vector (conferring puromycin resistance). PFKFB3 DNA was excised from the pEX-K4 vector using *Bam*H1 high fidelity (HF) (50U) and *EcoI*R1 HF (50U) restriction enzymes, or *XbaI* HF (80U) and *HpaI* HF (75U) restriction enzymes (NEB, Ipswich, UK) (Figure 2-1B&C). Plasmid DNA (pEX-K4 PFKFB3) (5µg) was incubated with restriction enzymes and

NEB buffer 4 (NEB) (composed of 5mM potassium acetate, 2mM tris-acetate, 1mM magnesium acetate and 0.1mM dithioreitol) for 1h at 37ºC in a water bath.

To separate the PFKFB3 'insert' agarose gel electrophoresis was performed using low melting point agar. Seakem CTG™ Agarose powder (1g) (Lonza) was dissolved in TAE buffer (100mL) (Thermoscientific) and 25mL poured into a flat-bed electrophoresis tank. DNA gel loading dye (Thermoscientific) was added at a ratio of 1:6 to the digest DNA, loaded onto the gel and electrophoresed at 40V for 3h. DNA was visualised using a UV longwave transilluminator (UVP high performance, Cambridge, U.K.) and the fragment corresponding to the PFKFB3 insert was excised from the gel using a scalpel. DNA was extracted from the gel using a QIAquick™ gel extraction kit (QIAGEN), according to the manufacturer's instructions. Briefly, proprietary buffer QG was added in the ratio 3:1 to the gel, incubated at 50^0C for 10 min, isoproponal (Sigma) added at a 1:1 ratio to the gel and the mixture added to a QIAquick column and centrifuged for 1 min at 12,782g. QG buffer (500µL) was added to the column and centrifuged as above to ensure removal of agarose traces. Proprietary PE buffer (750µL) was added to the column, incubated for 4 min and centrifuged as above. DNA was eluted using proprietary EB buffer (50µL). The isolated plasmid DNA was then quantified using a NanoDrop ND-1000 spectrophotometer, according to the manufacturer's instructions and DNA purity measured by confirming the A260/280 ratio range was between 1.8 - 2.

2.2.3.2 Ligation of PFKFB3 DNA into retroviral or lentiviral vectors

To allow subcloning of PFKFB3 DNA, linearization of the target vectors (PINCO or pHIV) was performed. PINCO vector (5µg) was added to tissue culture grade sterilised water (35µLµ) (Hameln), NEB buffer 3 (5µL) (NEB) (composed of 100mM NaCl, 50mM Tris-HCl, 10mM $MgCl_2$, 1mM DTT) prior to addition of the restriction enzymes *Eco*RI (20U) and *Bam*HI (20U). The pHIV vector (2µg) was added to tissue culture grade sterilised water (38.5µL) (Hameln), NEB buffer 4 (5µL) (NEB), 1% *v/v* BSA (Sigma) in PBS (Invitrogen), prior to addition of the restriction enzymes *Hpa*I (20U) and *Xba*I (20U). Controls, with the restriction enzymes replaced with water were also performed. The vector and restriction enzyme mix (or controls) were then incubated for 1h at 37ºC, and the DNA purified using a Qiaquick purification kit (Qiagen), according to the manufacturer's

instructions. The linearized vector DNA was then quantified using a NanoDrop ND-1000 spectrophotometer as above. To confirm linearization of the vectors agarose powder (0.8g) (Invitrogen) was dissolved in TBE buffer (100mL) (Sigma) and 25mL poured into a flat-bed electrophoresis tank with Peq Green (1µL) (Peqlab). The control and digested vector DNA was loaded onto the gel alongside a NEB 1Kb ladder and electrophoresed for 1h at 80V. Gels were visualised by ultraviolet light in a LAS-3000 digital imaging device to confirm different migration rates through the gel (data not shown). Subcloning of the PFKFB3 DNA sequence into the PINCO and pHIV vectors was subsequently achieved by incubating insert and vector DNA at a molar ratio of 1:10 (8µL) with T4 DNA ligase (20U) (NEB) and T4 DNA ligase reaction buffer (1µL) (NEB) (composed of 50mM Tris-HCl, 10mM $MgCl_2$, 1mM ATP and 10mM DTT) at 16^{o}C for 4h. Plasmid DNA was subsequently transformed into competent *E.coli* cells (2.2).

2.2.3.3 Verification of PFKFB3 ligation

To verify successful ligation and orientation of the PFKFB3 DNA, a 'test digest' was performed using the restriction enzymes *Sma*I (20U/µL) (NEB) for the pHIV subcloned vector and *Sca*I (10U/µL) (NEB) for the subcloned PINCO vector (Figure 2-1A-C). Plasmid DNA (0.1-1µg) was incubated with and without the restriction enzyme (1µL), CutSmart^{TM} buffer (1µL) (NEB) (composed of 5mM potassium acetate, 2mM tris-acetate, 1mM magnesium acetate and 100µg/mL BSA) and dH_2O (8µL) for 70 min at 25^{o}C in a water bath. The DNA was electrophoresed and visualised as above (2.2.3.2) and compared with expected fragment sizes calculated using pDraw32 v.1.1.128 (Acaclone software).

To confirm integrity of the PFKFB3 sequence in the vectors, DNA sequencing was performed by Eurofins MWG Operon's SMARTSeq KIT sequencing service. Vector DNA containing the PFKFB3 insert (750-1500ng) was mixed with 2µL of primer (Table 3) (20pmol/µL) and sent to Eurofins for direct sanger sequencing (5.3.3.1).

Table 3. Primers used for direct sequencing. Table shows the primers used for sequencing of the PINCO and pHIV vectors containing PFKFB3 (var.2) DNA. P1 and P2 were used for the sequencing of the PINCO vector and P3-5 for the pHIV vector. Full sequence results can be found (appendix 3&4)

Primer	Target vector of sequence	Sense	Sequence
P1	PINCO	Forward	5’ TAG AAC CTC GCT GGA AAG GA 3’
P2	PINCO	Reverse	5’ TTA TGT AAC GCG GAA CTC CA 3’
P3	pHIV	Forward	5’ TGG AAT TTG CCC TTT TTG AG 3’
P4	PFKFB3	Forward	5' AGA AGC CAT GGA CGA CTT CA 3'
P5	PFKFB3	Forward	5' GGA AGG CGC TCA ATG AGA TC 3'

2.3 Cell culture and cryopreservation

All tissue culture work was carried out in a Class II biosafety cabinet and waste disinfected with bleach or autoclaved. Cells were cultured under aseptic conditions at 37°C in 5% CO_2 unless otherwise specified.

2.3.1 Cryopreservation of cells

Cryopreserved cells were thawed by immersion in 37°C water bath for 2 min followed by dropwise addition of 5mL culture medium over 3 min. Cell suspension was then centrifuged at 270g for 5 min and resuspended in appropriate growth medium at the recommended density as below (2.3.3). Cryopreservation of cells was achieved by adding 500µL of IMDM (Sigma) (supplemented with 10% *v/v* FBS (Labtech), 2mM L-glutamine (Sigma) and 20µg/mL gentamycin (Sanofi-Aventis)) and additionally containing 30% *v/v* FBS (Labtech) and 20% *v/v* DMSO (Sigma) to 500µL of cell suspension of fully confluent cells (e.g. 1 vial frozen per confluent F25 flask) in 1.8mL cryovials (Thermoscientific). Cryovials were placed in Nalgene Mr Frosty™ controlled freezing containers (Thermoscientific), containing 100% isopropanol (Sigma) and stored in -80°C freezer overnight, before transfer of vials to liquid nitrogen storage containers.

2.3.2 Isolation of haematopoietic progenitor cells

Neonatal cord blood was obtained from healthy full-term pregnancies at the Maternity Unit of the University Hospital of Wales in Cardiff, with the informed consent of mothers undertaking Caesarian sections with the approval of research ethics committee in accordance with the 1964 declaration of Helsinki. Cord blood was collected in falcon tubes (50mL) containing 200µL of heparin (1000U/mL) (Leo Laboratories Ltd) and 400µL of PBS (Invitrogen). Initially, in order to estimate the number of $CD34^+$ cells present, immunophenotyping of cord blood was performed and proportion of $CD34^+$ cells was estimated using flow cytometric analysis (2.3.2.1).

Mononuclear cells were isolated from cord blood by density gradient centrifugation using Ficoll-Paque™ (BD Biosciences). Cord blood was diluted with an equal volume of HBSS (Invitrogen) additionally containing HEPES (25mM) (Invitrogen), gentamycin (20µg/mL) (Sanofi-Aventis) and heparin (1U/mL) (Leo Laboratories Ltd). The diluted cord blood was layered (7:5) on top of Ficoll-Paque™ (BD

Biosciences) and centrifuged at 400g for 40 min. The layer of mononuclear cells found at the plasma-Ficoll interface was recovered using syringe and quill, added to RPMI (15mL) Sigma) (containing 5% *v/v* FBS (Labtech) and 1U/mL heparin (Leo Laboratories Ltd)) and centrifuged at 270g for 10 min. Cells were resuspended in RPMI (20mL) (Sigma), (190µL removed and added to zaponin (1.5µL) (Beckman-Coulter, Galway, Ireland) for counting by haemocytometer) and centrifuged at 270g for 10 min. Cells were frozen at approximately 5 x 10^7 cells/mL (2.3.1) prior to isolation of $CD34^+$ using a Mini-MACS $CD34^+$ Progenitor Cell Isolation Kit (Miltenyi Biotec, Bisley, UK), according to the manufacturer's instructions.

Briefly, previously frozen mononuclear cells were thawed (2.3.1) in the presence of 0.45µM filtered FBS (900µL/mL of cells) (Labtech) and DNase (100µg/mL) (Sigma). An equivalent volume of degassed MAC buffer (consisting of PBS (Invitrogen), 0.5% *v/v* BSA and 5mM $MgCl_2$ (both Sigma)) was added dropwise over 3 min and this step repeated twice. Cells were centrifuged at 270g for 10 min, resuspended in MAC's buffer (6.7 x 10^8 cells/mL), and incubated at 4ºC for 15 min in the presence of anti-CD34 antibody (2 x 10^9 cells/mL) and Fc receptor blocking agent (2 x 10^9 cells/mL). Cells were washed in MACs buffer (2 x 10^7 cells/mL), centrifuged at 270g for 5 min, resuspended in MACs buffer (5 x 10^8 cells/mL) and incubated at 4ºC for 15 min in the presence of anti-FC magnetic microbeads (2 x 10^9 cells/mL), washed as above and filtered through a MS separation column (previously equilibrated with MACs buffer) in the presence of a magnetic field. The $CD34^+$ cells were eluted from the column with MACs buffer (1mL) in the absence of a magnetic field, counted by haemocytometer (2.3.4) and cultured according to section (2.3.3.3).

2.3.2.1 Immunphenotyping of cord blood

CD34 is a cell surface marker for HPC (1.1.1.1). Therefore to determine HPC numbers in the sample, cord blood (15µL) was mixed with anti-CD45-peridinin chlorophyll (PerCP) labelled antibody (10µL) (BD Biosciences) and either anti-CD34-phycoerythrin (PE) (BD Biosciences) labelled antibody (10µL) or isotype matched control antibody, IgG1-PE (10µL) (BD Biosciences), then incubated at 4ºC for 30 min. Lysis buffer (BD Biosciences) was added and cells incubated for a further 10 min at RT. Cells were washed with PBS (5mL) (Sigma), centrifuged at 270g for 5 min, resuspended in PBS (200µL) (Sigma) and analysed using an Accuri

C6 flow cytometer coupled with FCS express ver.6 software to determine the proportion of mononuclear cells (PerCP labelled) and $CD34^+$ cells (PE labelled). Flow cytometric analysis is described in (2.12).

2.3.3 Cell culture

2.3.3.1 Cell culture of non-adherent cell lines

The myeloid leukaemic cell lines NOMO-1, THP-1, Mv4;11, KG-1 and U937 were obtained from the European Collection of Authenticated Cell Cultures (ECACC) (Porton Down, Salisbury, UK). NOMO-1, THP-1 and U937 cells were cultured in RPMI (Sigma), supplemented with 10% *v/v* FBS (Labtech), 2mM L-glutamine (Sigma) and 20µg/mL gentamycin (Sanofi-Aventis). Mv4;11 cells were cultured in IMDM (Sigma) supplemented with 10% *v/v* FBS (Labtech), 2mM L-glutamine (Sigma) and 20µg/mL gentamycin (Sanofi-Aventis) and KG-1 cells were cultured in IMDM (Sigma) supplemented with 20% *v/v* FBS (Labtech), 4mM L-glutamine (Sigma) and 20µg/mL gentamycin (Sanofi-Aventis).

Additionally, THP-1 and NOMO-1 cells lentivirally transduced (2.5) with shRNA complementary to NOX2 mRNA and encoding puromycin resistance and control cells (THPSH and NOMOSH) which had been transfected with shRNA coding for a non-mammalian target sequence, were kindly provided by Professor Richard Darley and cultured as for NOMO-1 and THP-1 cells.

Cells were cultured at a cell density of between 1×10^5 and 5×10^5 / mL and passage number did not exceed 20. Cell density was determined prior to subculturing by haemocytometer or flow cytometry (2.3.4).

2.3.3.2 Cell culture of adherent cell lines

The packaging cell lines Phoenix (gift of Garry Nolan, Stanford University School of Medicine, Stanford) or HEK293T (ECACC) were cultured in DMEM (Sigma), supplemented with 10% *v/v* FBS (Labtech), 2mM L-glutamine (Sigma) and 20µg/mL gentamycin (Sanofi-Aventis) and incubated at 37ºC. Confluent cells were detached from plasticware by addition of trypsin (Invitrogen) (500µg/mL), incubation for 5 min at room temperature (RT) followed by equal addition of appropriate growth medium (5mL) and disaggregation. Cells were harvested by

centrifugation at 270g for 5 min, washed in PBS (Invitrogen), counted (2.3.4) and then cultured according to (2.4.1).

2.3.3.3 Cell culture of haematopoietic progenitor cells

Isolated HPC (2.3.2) at an initial cell seeding density of 2 x 10^5 cells/mL were cultured in 'HPC media mix' (IMDM (Sigma) containing 20% *v/v* FBS (Labtech), 1% *v/v* deionised bovine serum albumin fraction V (BSA) (Sigma), 45µM 2-mercaptoethanol (Sigma), 360µg/mL 30% iron saturated human transferrin (Roche) and 100µg/mL streptomycin (Invitrogen)) supplemented with growth factors as described below. Following isolation of HPC (subsequently defined as day 0), cells were cultured (days 0-3) as above with the addition of human growth factors IL-3 (50 ng/mL), IL-6 (25 ng/mL), SCF (50 ng/mL), G-CSF (25 ng/mL), GM-SCF (25 ng/mL) (all purchased from Invitrogen) and Flt3 (50 ng/mL) (Peprotech), subsequently defined as $36S^{hi}$ medium. After day 3, cells were cultured in HPC media mix alone, or with the addition of 5ng/mL of IL-3, SCF, GM-CSF and C-CSF (Invitrogen), subsequently defined as $3S^{lo}$GGM medium. In some experiments HPC were cultured in $3S^{lo}$GGM until day 5 and thereafter in HPC media mix alone. Cell density culture conditions are described in the individual results section (3.3)

2.3.4 Cell counting

Counting by haemocytometer was accomplished by adding 10µL of cells to a haemocytometer counting chamber, containing nine, 100nl cuboids and multiplying the average number of cells per cuboid by 1 x 10^4 to obtain number of cells per mL. Counting by flow cytometry was performed by adding 100uL of cells to a FACS tube, running 25µL through a Accuri C6 flow cytometer and analysing the data using FCS express ver.6 software (2.12). After excluding cell debris based on forward scattered light and side scattered light (FSC/SSC), the number of events was multiplied by 40 to obtain number of cells per mL.

2.3.5 Determination of cell viability using 7-AAD

7-AAD is a molecule that intercalates with DNA resulting in a spectral shift with an emission wavelength (λ) of 647nm. 7-AAD is excluded from live cells but can permeate the membrane of non-viable cells. To determine cell viability, 7-AAD (1µg/mL) (Sigma) was added to cells, incubated at RT for 10 min and analysed using an Accuri C6 flow cytometer in conjunction with FCS express ver.6 software (2.12).

2.4 Generation of recombinant virus

Generation of retrovirus was achieved using Phoenix packaging cells (gift of Garry Nolan, Stanford University School of Medicine, Stanford) and lentivirus was generated using HEK293T cells. Virus was generated using either calcium phosphate transfection (2.4.1) or cationic lipid transfection (2.4.2). Mock culture supernatant was achieved by culturing cells as below, without transfecting DNA. All work was carried out in a class II biosafety cabinet and centrifugation steps performed in sealed safety cups. Incubation of flasks was performed inside a sealed Perspex box. All waste was disinfected with bleach and subsequently autoclaved. Double gloves were worn throughout.

2.4.1 Calcium phosphate transfection

HEK293T or Phoenix cells were cultured in DMEM (Sigma) as above (2.3.3.2) and then transfected with recombinant plasmid DNA. The day prior to transfection cells were counted and seeded at 1 x 10^7 cells / F75 Flask (Phoenix cells) or 7.5 x 10^6 (HEK293T cells) / F75 Flask. For HEK293T cells, culture flasks were pre-treated with 5mL of 0.01% *w/v* poly-L-lysine solution (Sigma), incubated at RT for 30 min, then washed with PBS (Invitrogen).

For retroviral transfection, tissue culture grade sterile water was mixed with 45µg of plasmid DNA (except H-RAS^{G12V} (12µg)) and 45 µL of $CaCl_2$ (2.5M) (Sigma) and added dropwise to 450 µL HEPES buffer (50mM) (Invitrogen) to give a total volume of 900µL, whilst the solution was bubbled with a pipette. The solution was immediately vortexed for 4s and left to precipitate for 20 min. Five minutes prior to transfection, 15 µL of 25 µM chloroquine (Sigma) was added to the Phoenix cultures, then the DNA was added dropwise and the cells were incubated at 37ºC in a humidified incubator with 5% CO_2. After 16h the media was replaced with 8 mL of fresh medium and cells incubated for a further 24h at 33^{o}C. Viral supernatant was collected following centrifugation at 270g to remove cells that had been dislodged from the flask, then snap frozen and stored in liquid nitrogen. In some instances, cells were collected and lysed for analysis of target protein expression (2.9). In addition, where cells were infected with virus encoding for GFP/dsRed expression visual inspection by fluorescent microscope and flow cytometric analysis were performed (2.12).

Lentiviral transfection was achieved using HEK293T cells as above, except 25µg of plasmid DNA was used, alongside 8µg of envelope plasmid DNA (pMD2.G) and 15µg of packaging plasmid DNA (psPAX2).

2.4.2 Cationic lipid transfection

Cationic lipid transfection was achieved using the Lipofectamine 3000^{TM} kit (Invitrogen), according to the manufacturer's instructions. Briefly, cells were seeded at 9 x 10^6 cells/mL in 75cm^2 surface area culture flasks, on the day prior to infection. For retroviral infection, 48µL of proprietary P3000 reagent was mixed with 15µg of plasmid DNA and added to proprietary OptiMEM medium to make a total volume of 2070µL. Proprietary reagent Lipofectamine 3000 (57µL) was then mixed with OptiMEM medium (2025µL), added to the DNA mix and incubated at RT for 15 min. Total flask medium was reduced to 5mL, the DNA added to the cells and incubated at 37ºC with 5% CO_2 for 6h. The flask medium was aspirated, replaced with DMEM (9mL) and incubated at 37ºC with 5% CO_2 for 16h, before the viral supernatant was collected as above. Lentiviral transfection was performed as above except 4.5µg of plasmid DNA was used, alongside 4.8µg pMD2.G and 8.7µg psPAX2.

2.5 Infection of cells

In order to infect cells with virus, 24-well plates were coated with retronectin (30µg/mL) (Takara Bio) and incubated at 4^0C overnight. The retronectin was aspirated and replaced with 250 µL of 1% *v/v* BSA (Sigma) in PBS (Invitrogen) and left for 30 min. The BSA was aspirated and replaced with 1 mL retroviral or lentiviral supernatant. The culture plate was centrifuged at 2272 x g for 2 hours at 12ºC. The supernatant was removed from the wells and replaced with either HPC (2 x 10^5 cells/mL) or cell lines (2-5 x 10^5 cells/mL) and subsequently incubated at 37ºC overnight. For retroviral infection the process was repeated, the cells were removed to an incubator (37ºC, 5% CO_2), the wells were treated with retrovirus as above and the cells returned to the wells and incubated at 37ºC, 5% CO_2 overnight.

Cells expressing GFP or DsRed were assessed alongside mock cultures (2.4) by flow cytometry (2.12) to measure infection rates (for HPC this was day 3 post-isolation (2.3.3.3). Cells were centrifuged at 270g for 5 min, washed in PBS (Invitrogen), centrifuged at 270g for 5 min resuspended in PBS and analysed using an Accuri C6

flow cytometer and FCS express ver.6 software (2.12). Autoflourescence of the mock cultures defined the threshold of GFP/DsRed positivity, which was set at 99%. Infected HPC were additionally probed with an anti-CD34-PE conjugated antibody or with a matched IgG1 isotype control (both BD Bioscience) to confirm homogeneity of the cells. Here cells were treated as above only prior to washing with PBS cells were treated with the antibody (Table 2) and incubated for 30 min at 4ºC.

Cells infected with DNA encoding puromycin resistance were cultured in appropriate media (2.3.3) treated with puromycin (1µg/mL) alongside mock cultures (2.4) and cell viability assessed daily using 7-AAD (2.3.5) until no viable mock culture cells remained, thus establishing a pure population of infected cells.

2.6 Determination of NOX2 expression and detection of superoxide using Diogenes™

2.6.1 Determination of NOX2 expression

To determine expression levels of NOX2 in the NOMO-1 and THP-1 cell lines, cells (50K) were treated with a NOX2 PE conjugated antibody (5ng/µL) or an isotype matched control (Table 2), incubated for 45 min at 4ºC and then analysed by an Accuri C6 flow cytometer in conjunction with FCS express ver.6 software (2.12).

2.6.2 Detection of superoxide using Diogenes™

Superoxide measurement of KG-1, U937, MV4;11, NOMO-1 and THP-1 cell lines was carried out using the chemiluminescent probe Diogenes™ (National Diagnostics, Hessle, U.K.). Cells were counted, centrifuged at 270g for 5 min, washed in PBS (5mL) (Invitrogen), centrifuged at 270g for 5 min and resuspended in standard buffer (KH_2PO_4 (4.58mM), Na_2HPO_4 (8.03mM), NaCl (130mM), KCl (4.43mM), glucose (5.55mM), $MgCl_2$ (0.5mM), $CaCl_2$ (0.45mM), BSA (0.1% *v/v*) all purchased from Sigma) at 1 x 10^6 cells/mL. Cells (150K) were added in triplicate to a white FluoroNunc Maxisorp 96 well plate and Diogenes™ reagent (50µL) added. Luminescence was measured over 2h at 37ºC, using a Chameleon Hidex fluorescent plate reader, according to the manufacturer's instructions. Chemiluminescent traces were plotted according to light emission rate, measured as relative light units (RLU), against time and either peak RLU compared, or the area

under the curve calculated, using the trapezium rule, and given as a measure of total superoxide production during the assay.

2.7 Determination of cellular glucose consumption and lactate secretion

To determine cellular glucose consumption and lactate secretion, cells were counted, seeded and treated, according to the experimental conditions (see individual result sections) before being incubated, at 37ºC, 5% CO_2, for a time as described in the individual result sections.

2.7.1 Glucose and lactate assay of culture media

Post-incubation, cells were counted and centrifuged at 270g for 5 min. Supernatant from the culture media was filtered using Microcon-10 kDa centrifugal filter units (Merck-Millipore, Feltham, UK) at 12,782g for 30 min. The levels of D-glucose and L-Lactate were measured by fluorimetry using a glucose and L-Lactate assay kit (Abcam, Cambridge, UK) coupled with a Chameleon Hidex fluorescent plate reader (Ex/Em 535/590 nm), according to the manufacturer's instructions. Briefly, samples were diluted with proprietary glucose or lactate buffer to a volume of 50µL and added in triplicate to a black 96 well flat bottomed microclear plate (Greiner Bio-One, Stonehouse, UK). Glucose or lactate buffer containing proprietary glucose or lactate probe (0.8% *v/v*) and proprietary glucose or lactate enzyme mix (0.8% *v/v*) were added (50µL) to each well and left to incubate in the dark at RT for 30 min. Fluorescence was measured (Ex/Em 535/590nm) and compared with glucose or lactate standards assayed in duplicate on the same plate. Glucose or lactate concentration of the samples was determined from the linear part of the standard curve generated from the supplied glucose or lactate standards (0–1 nmol/well), according to the equation:

$$y = mx + c$$

where y is the average relative light units recorded by the plate reader for each glucose/lactate standard, x is the concentration of the glucose/lactate standard, c is the point of y-axis intersection obtained from the line of best fit (drawn according to the least square method) and m is the slope of the line of best fit.

2.7.2 Measurement of individual cellular glucose uptake

To determine cellular glucose uptake at the individual cell level, the glucose bioprobe 2-NBDG (Life Technologies) was employed in conjunction with flow cytometry. Cells were washed twice in PBS (Invitrogen) then treated with 2-NBDG (10µM) or PBS alone (to establish a background control) followed by incubation for 10 min (37ºC, 5% CO_2) and two washes in ice cold PBS (Invitrogen). Cells were immediately analysed by flow cytometry using an Acurri C6 flow cytometer in conjunction with FCS express ver.6 software (2.12). 2-NBDG emits fluorescence at a wavelength of 542nM. Having excluded cell debris based on FSC/SSC, the median glucose uptake per cell of the samples was established by subtracting the median value of fluorescence of the background control cells from the median value of fluorescence of the cells treated with 2-NBDG.

2.8 Method for determining effective dose of PFKFB3 inhibitors using CellTiter-Glo™ assay

To determine the half maximal effective concentrations (EC_{50}) of the PFKFB3 inhibitors 3PO and PFK158, a CellTiter-Glo luminescent cell viability assay (Promega, Southampton, UK) was used, according to the manufacturer's instructions. Briefly, cells were cultured in a white 96-well culture plate in the presence of serial dilutions of inhibitor for 24h at 37ºC in a humidified incubator with 5% CO_2. Prior to analysis, the plate was equilibrated at RT for 30 min then proprietary CellTiter-Glo reagent™, was added in equal volume to the culture media, mixed on an orbital shaker for 2 min and incubated at RT for 10 min. Luminescence was measured immediately, at a single time point, using a Chameleon Hidex fluorescent plate reader according to the manufacturer's instructions. Light emission was measured in RLU and plotted against inhibitor concentration to generate a sigmoid curve. The EC_{50} was determined from the sigmoid curve as the concentration corresponding to a 50% change from highest to lowest RLU.

2.9 Determination of cellular protein expression

To determine the expression levels of cellular proteins as a result of different experimental conditions (see individual results sections), HPC or cells from AML-derived cell lines (5 million cells for HPC and Mv4;11 and 2 million cells for THP-1

and NOMO-1 derived cells) were centrifuged at 270g for 5 min and washed in tris-buffered saline (TBS) (composed of 1M Tris-HCl, 130mM NaCl (both Sigma)) (10mL), followed by centrifugation at 270g for 5 min and the supernatant removed and flash frozen in liquid nitrogen. Frozen cells were stored at -80ºC or used below.

2.9.1 Whole cell lysate extraction

Frozen cell pellets (2.9) were thawed on ice in the presence of DNase (1µg) (Sigma). Cells were treated with lysis buffer (composed of 10 mM HEPES-KOH (Invitrogen), 10 mM 2-mercaptoethanol (Sigma), 1mM magnesium acetate (Fisons Scientific Equipment), 0.5 mM EDTA (Sigma), 0.5 mM EGTA (Sigma), 0.25 M sucrose (Sigma), 1 mM Na_3VO_4 (Sigma),1 complete mini EDTA protease inhibitor tablet per 10 mL (Roche), 1% *v/v* x100-Triton (Sigma)) (2 x 10^7 cells/mL), vortexed, incubated on ice for 30 min and subjected to occasional vortexing. The cell lysate was centrifuged at 12,782g for 5 min at 4ºC and the protein concentration of the supernatant determined by Bradford assay (2.9.3).

2.9.2 Nuclear/Cytosol Extraction and Fractionation

THP-1 cells centrifuged at 270g for 5 min, washed in TBS (10mL) as above and the supernatant removed leaving washed cell pellets for nuclear/cytosol fractionation using a kit from Biovision (California, USA), according to the manufacturer's instructions. Briefly, cell pellets were resuspended in proprietary cytosol extraction buffer A (100µL/million cells) containing protease inhibitor cocktail (2µL) and dithiothreitol (1µL). Cells were vortexed (15s), incubated on ice for 10 min, cytosol extraction buffer B (5.5µL/million cells) added, vortexed (5 sec) and incubated on ice for a further minute. Cells were then vortexed for 5s, centrifuged at 12,782g for 8 min at 4ºC and the supernatant (containing the cytosolic extract) collected and stored at -80^{0}C. The remaining cell pellet was washed in PBS (Invitrogen) containing $MgCl_2$ (0.5mM) (Sigma), centrifuged at 12,782g for 3 min at 4ºC, the supernatant discarded and the pellet snap frozen in liquid nitrogen. The samples were subjected to three rapid freeze/thaw cycles in liquid nitrogen followed by addition of Benzonase (25U/µL) (Novagen) at 2µL/million cells. The samples were kept on ice for 60 min before TEAB lysis buffer was added at 10µL/million cells. The samples were kept on ice for a further 30 min, subjected to occasional vortexing, before being centrifuged at 12,782 x g for 10 min at 4ºC and the supernatant stored at -80ºC.

Protein quantification of the nuclear and cytosol extracts was performed, as described below (2.9.3).

2.9.3 Protein concentration quantification

Bradford's reagent (Sigma) was diluted 1:1 with tissue culture grade sterilised water (Hameln) and 190µl added to duplicates of the cell lysate sample (10µl), diluted 20-fold with tissue culture grade sterilised water (Hameln), in a 96-well flat-bottomed plate. The plate was equilibrated to RT for 10 min, then absorbance measured (590nm) using a spectrophotometer (ASYS Hitech, GmbH, Eugendorf, Austria) and compared with BSA protein standards (0-10 µg/mL) assayed in duplicate on the same plate. Protein concentration of the cell lysate was determined from the linear part of the standard curve as described above (2.7). Variation between duplicates of the measured absorbance of the protein standards was limited to a co-efficient of variation (CV) of 5% and variation between cell lysates duplicates limited to 10% CV.

2.9.4 Protein electrophoresis and electroblotting

Proteins were separated by SDS-PAGE using Nu-PAGE 4-12% Bis-Tris Mini Gels (Invitrogen) and electroblotted according to the manufacturer's instructions using proprietary Nu-Page reagents purchased from Invitrogen.

Prior to separation by electrophoresis, denaturation and reduction of disulphide bonds was performed. Protein extracts, from the cell lysates, were incubated at 70^{o}C for 10 min in the presence of Nu-Page x1 LDS buffer (containing lithium dodecyl sulphate) (Invitrogen) and 50mM DTT (Invitrogen). To ensure an equal volume of protein across samples in the final denatured protein extracts, the volume of protein added was adjusted with tissue culture grade sterilised water (Hameln), according to the value determined from the Bradford's assay (2.9.3), to a final concentration of 1µg/µL.

Bis-Tris gels were placed in a X-Cell II^{TM} mini-cell containing x1 running buffer (composed of 50mM 3-(N-morpholino)propanesulfonic acid, 50mM tris base, 0.1% *w/v* sodium dodecyl sulphate and 0.25% antioxidant, and proteins loaded (20µg) on to the gels alongside x1 LDS buffer, containing 5% *v/v* MagicMark XP^{TM}, to allow visualisation of protein molecular weight. Following 200 volts electrophoresis for 50 min gels (x1 or x2) were placed in a X-Cell II^{TM} blotting module, next to a

nitrocellulose membrane in the presence of x1 transfer buffer containing methanol (10% *v/v* for 1 gel or 20% *v/v* for 2 gels) and electroblotted at 30 volts for 60 min. Electroblotted membranes were washed in dH_2O on a plate shaker for 5 min (x2) and proteins visualised using Ponceau S solution (1.3mM Ponceau S, 0.83M ethanoic acid) (Sigma), in order to facilitate cutting of membrane if required. Membranes were subsequently washed as above, incubated on a plate shaker for 60 min in TBS-T (TBS buffer with 0.1% *v/v* Tween-20) and 2% *w/v* milk powder (Marvel), then washed for 15 min in TBS-T and then a further three times for 5 min in TBS-T. Membranes were subsequently used for immunoblotting.

2.9.5 Immunoblotting

Membranes were incubated overnight at 4^{o}C, in 10 mL TBS-T containing 2% *w/v* milk powder, containing antibodies at concentrations described in (Table 2). Membranes were washed with 20mL of TBS-T for 15 min on a plate shaker followed by three subsequent 20 mL washes for 5 min. Subsequent incubation of the membrane occurred at RT on a plate shaker in the presence of TBS-T containing 1% *w/v* milk powder and secondary anti-mouse or anti-rabbit horse radish peroxide conjugated antibody (GE Healthcare), diluted 1:5000, for 60 min. Following incubation, membranes were washed four times in TBS-T as above and target proteins were visualised using the ECL Advance Detection Kit (GE Healthcare), according to the manufacturer's instructions. Chemiluminescence was detected using a LAS-3000 image analyser (Fujifilm UK Ltd) and analysed using AIDA Image Analyser Version 4.19 (Fujifilm UK Ltd). To confirm equal loading of proteins the nitrocellulose membrane was washed and reprobed as above using anti- β-actin or anti- α-tubulin for whole cell protein extraction, or anti- β-actin for cytosol protein extraction and anti-histone H1 for nuclear protein extraction (Table 2). Relative changes in protein expression were measured using AIDA Image Analyser software (Raytest, Straubenhardt, Germany). Briefly, the area of a region of interest was determined and the pixel density of this region compared with equivalent areas of interest. The pixel density of equal sized areas around the comparative areas of interest was used to determine the background signal, which was subtracted prior to comparison, and the relative pixel density levels normalised to the control sample.

2.10 Analysis of microarray data of ROS induced changes in mRNA expression in HPC

Gene expression profiling, using Affymetrix Genechip® whole transcriptome microarray, had previously been performed in our laboratory to determine significant ROS dependent changes in mRNA expression of human HPC expressing mutant N-RAS (N-RAS^{G12D}) compared with control HPC (Hopkins, 2014). Briefly RNA from four transduced cultures (Figure 2-2) was isolated and processed for hybridisation to GeneChip® Human Exon 1.0ST array, before being analysed by Central Biotechnology Services (University of Cardiff, UK), using the Ambion WT Expression Kit, according to the manufacturer's instructions.

In this study, identification of ROS mediated changes in mRNA expression of glycolytic enzymes was achieved by supervised analysis of the gene expression profiling data, using a full extended probe set (probes supported by exon prediction algorithms including GeneID, GenScan, Exoniphy, RNAGene, spgGene and Twinscan), by Partek Genomics Suite software (ver. 6.6, Partek Inc., USA). Raw data files were imported using Affymetrix annotation files and Robust Multi-Array analysis algorithm was used for Exon level expression analysis. Adjustments were made for guanine-cytosine content and probe sequence on pre-background subtracted values, and background correction, quantile normalisation and median polishing (to remove chip effect) performed. Log_2 data transformation was then performed and mRNA expression levels of control HPC were compared with mRNA expression levels of control HPC treated with DPI (100nM) and N-RAS^{G12D} both untreated and treated with DPI. A 2-way ANOVA based on

$$Y_{ijk} = \mu + C_i + C_j + \varepsilon_{ijk}$$

where Y_{ijk} is the k^{th} observation on the i^{th} condition of the j^{th} cord blood replicate (random variability between samples), μ is the common effect for the whole experiment, C_i is the i^{th} condition (experimental treatment e.g. DPI), C_j is the j^{th} cord blood replicate (random variability between samples) and ε_{ijk} is the random error of the k^{th} observation of the i^{th} condition of the j^{th} replicate, was used to identify statistically significant changes in gene expression. Fisher's Least Significance Difference was performed for control vs control + DPI, control vs N-RAS^{G12D} and

N-RAS^{G12D} vs N-RAS^{G12D} + DPI (Figure 2-2), and where possible the Benjamini-Hochberg multiple testing correction was applied or the level of significance was reduced to $p<0.01$.

2.11 Metabolomic analysis of ROS induced changes in metabolites using chromatography-mass-spectroscopy.

Metabolomics can be used to study relative differences in metabolite levels between samples. Metabolon^{TM} (http://www.metabolon.com/) is a company that specialises in performing and analysing metabolomic data generated using ultrahigh performance liquid chromatography-tandem mass spectroscopy (UPLC-MS/MS) and gas-chromatography mass-spectroscopy (GC-MS). Two studies were designed to compare ROS mediated changes in cellular metabolites of both AML-derived cell lines and AML patient blasts.

2.11.1 Strategy for metabolomic study of ROS induced changes in metabolites in AML-derived cell lines

For the cell line study, three cell lines were used:

- THPSH control cells (2.3.3.1) were compared with THPSH cells treated with DPI (100nM) and THP cells in which NOX2 was knocked down using shRNA (THP NOX2-KD);
- NOMOSH control cells (2.3.3.1) were compared with NOMOSH cells treated with DPI (100nM) and NOMO cells in which NOX2 was knocked down using shRNA (NOMO NOX2-KD);
- Mv4;11 control cells (treated with 0.0018% *v/v* DMSO (vehicle control) were compared with Mv4;11 cells treated with GOX, either 10mU/mL or 20mU/mL.

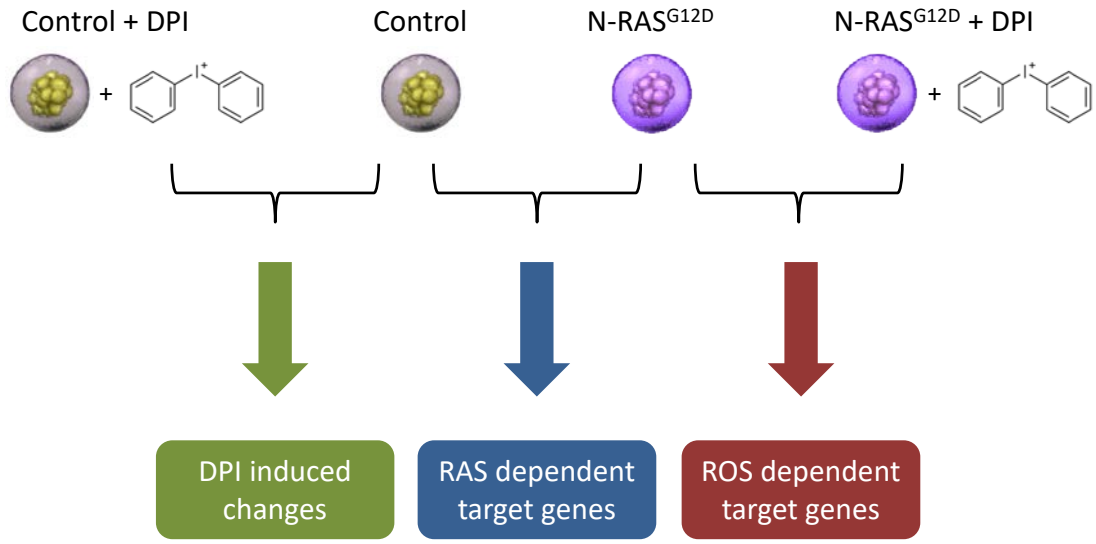

Figure 2-2. Strategy for determining ROS mediated changes in mRNA expression in N-RAS^{G12D}. Control HPC and HPC expressing mutant N-RAS were cultured with or without DPI (100nM) for 18h and isolated RNA investigated using GeneChip^{TM} Human Exon 1.0ST arrays. Significant ROS mediated changes in mRNA expression levels were then determined using Partek Genomics Suite software (ver. 6.6, Partek Inc., USA)

All cells were seeded at 5 x 10^5 under the conditions outlined above and incubated for a further 24h at 37ºC in a humidified incubator with 5% CO_2. Following incubation cells were counted by flow cytometry (2.3.4), viability determined using 7-AAD (2.3.5) and glucose uptake measured using the 2-NBDG bioprobe (2.7.2). Cell samples (of 30 million cells) were required to show > 90% viability and > 10% change in glucose uptake, in order to be processed (see below) and sent for metabolomic analysis. Additionally, NOX2 generated superoxide was determined in the THP and NOMO cell lines using Diogenes™ (2.6.2), to verify that knock-down of NOX2 or DPI treatment decreased superoxide production. Samples fulfilling this criteria, were centrifuged at 270g for 10 min at 4ºC, in conical propylene centrifuge tubes (Scientific Laboratory Supplies, Nottingham, UK), previously treated with 1% *v/v* BSA. Samples meeting the above criteria, were washed in PBS (10mL) (Sigma), centrifuged as before, resuspended in PBS (10mL). 30 million cells were pipetted into a conical propylene centrifuge tubes pre-treated with 1% *v/v* BSA, centrifuged as previously, flash frozen in liquid nitrogen and stored at -80ºC. Quadruplicate samples per condition, were shipped on dry ice to Metabolon™ for analysis. Additionally, cells from each sample were isolated for future determination of relative changes in cellular protein expression and cross reference with other cellular protein extractions from other experiments, determined under equivalent experimental conditions (2.9).

2.11.2 Strategy for metabolomic study of ROS induced changes in metabolites in AML patient blasts

Peripheral blood and bone marrow samples collected from a random cohort of AML patients who had enrolled in UK MRC/NCRI AML 14-17 clinical trials at point of diagnosis, before treatment and following informed consent from patients in accordance with the 1964 Declaration of Helsinki, were used in this study.

Samples (n=36), were selected randomly, thawed (2.3.1), counted and analysed for viability using 7-AAD (2.3.5). Only those samples with a cell count greater than 30 million and a viability greater than 80% were sent for analysis by Metabolon™ (n=20). Additionally, mononuclear cells isolated from healthy individuals (n=6) were also sent to Metabolon™ as a comparative control. Diogenes™ analysis of AML blasts (2.6.2) stratified the patient samples into ROS^{Hi} and ROS^{Lo} producing

AML blasts (Figure 4-14). Samples were not processed to determine glucose uptake, but otherwise all steps were performed as above (2.9).

2.11.3 Metabolomic analysis of studies

Metabolomic analysis of the samples was carried out by Metabolon™ (http://www.metabolon.com/). Briefly, protein removal and metabolite recovery was performed by vigorous shaking in methanol, followed by centrifugation. The extract was divided into five fractions and organic solvent removed using TurboVap™. Quality control was performed using a pooled matrix sample from all experimental samples as a technical replicate, water samples as blanks, solvent samples used in extraction and a cocktail of standards (chosen not to interfere with endogenous compounds) spiked into each sample to aid chromatographic alignment. Instrument variability was determined from the median relative standard deviation of the spiked standards (< 2%) and process variability from the median relative standard deviation of the endogenous metabolites in the pooled standard (<7%).

Cell line samples were analysed using UPLC-MS/MS, utilising Waters ACQUITY UPLC and Thermoscientific Q-Exactive high resolution mass spectrometer interfaced with a heated electrospray ionisation source and Orbitrap mass analyser. Four of the sample aliquots were analysed using either a C18 column (Water UPLC BEH C18-2.1x100mm, 1.7µM) or a HILIC column (Waters UPLC BEH Amide 2.1x150mm, 1.7µM), under the following conditions:

(i) Acidic positive ion conditions, chromatographically optimised for more hydrophilic compounds. Extract gradient eluted from a C18 column using methanol, acetonitrile, water, 0.05% perfluoropentanoic acid (PFPA) and 0.1% formic acid.

(ii) Acidic positive ion conditions, chromatographically optimised for more hydrophobic compounds. Extract gradient eluted from a C18 column using methanol, acetonitrile, water, 0.05% PFPA and 0.01% formic acid.

(iii) Basic negative ion conditions. Extract gradient eluted from a C18 column using methanol, water, and 6.5mM ammonium bicarbonate (pH 8).

(iv) Basic negative ion conditions. Extract gradient eluted from a HILIC column using water, acetonitrile and 10mM ammonium formate (pH 10.8).

AML patient blast sample extracts were analysed as above except analysis (ii) was not performed and analysis of (i) was performed without PFPA. Additionally, GC-MS was performed on one aliquot. Briefly, samples were dried under vacuum for 18h, derivatised under dried nitrogen using bistrimethyl-silyltrifluoroacetamide and separated on a 5% diphenyl / 95% dimethyl polysiloxane fused silica column (20m x 0.18mm ID; 0.18µM film thickness) using helium as a carrier gas (temperature range 60-340^{o}C of 17.5 min). Analysis was performed using a Thermo-Finnigan Trace DSQ fast-scanning single quadropole mass spectrometer using electron impact ionisation.

Raw data was extracted, peak identified and quality control processed using proprietary Metabolon^{TM} hardware, software and biochemical library database. Following normalisation to Bradford protein concentration, log transformation and imputation of missing values with the minimum observed value for each compound, Welch's unequal variance two sample t-test was performed to identify significant differences between the experimental groups. To account for a potentially high false discovery rate (as a consequence of multiple comparisons), a q-value was also calculated, where a lower q-value is an indication of higher confidence in the result.

To better understand variations between samples, principal component analysis (PCA) was employed to provide a global analysis of how closely related or otherwise any given sample is. Samples that cluster together in PCA show greater similarities than those that are more widely distributed (4.3.5.2). Further analysis of differences between samples was provided by subjecting the data to a process of hierarchical clustering. Hierarchical clustering seeks to determine differences between data by grouping together two samples that share the closest values and then recomputing the differences between this newly grouped sample and the other samples based on the largest difference of the two samples in the paired group compared to the other samples. This process is then repeated until all samples are paired and the data is often represented by a dendogram (Figure 4-9B).

2.12 Flow cytometry and data analysis

Isolation of cells to be analysed by flow cytometry was performed as described in individual method sections. A minimum of 10,000 events were collected using an

Accuri C6 flow cytometer. Data analysis was performed using FCS express ver.6 software.

In general, forward scattered light (FSC) was used to determine size and side scattered light (SSC) the granularity. Application of bi-variate gating allowed the exclusion of cell debris and other sub-cellular size detected events. Excitation of fluorescent molecules was achieved using a diode red laser (λ=640nm) and a solid state blue laser (λ=488nm). Emission was detected using 3 standard optical filters, filtering light at a λ of 530-535nm, 540-585nm and >670nm. A list of fluorochromes with their excitation/emission spectra is given in Table 4. Where multiple fluorochromes were employed, 'spill over' of fluorescent signal into detectors of adjacent wavelengths was compensated for, using compensation settings within the FCS express ver. 6 software. Briefly, the median fluorescent intensity of unlabelled and fluorochrome labelled cells was adjusted to equivalence in optical detectors with wavelengths adjacent to detectors designed to detect any given fluorochromes.

Table 4. List of fluorochromes used in this study. Fluorochromes used to label/identify cells are listed in alphabetical order alongside their absorption and emission wavelengths (λ).

Fluorochrome	Absorption λ (nm)	Emission λ (nm)
7-AAD	488	647
DsRed	558	583
GFP	489	508
2-NBDG	465	542
PE	480	570
PerCP	490	675

2.13 Statistical analysis

Significance of difference was determined using one-way ANOVA with Tukey's honestly significance differences test, Student's paired t-test or one sample t-test using Minitab (v17) (Minitab Ltd, Coventry, U.K.). Appropriate statistical tests used are labelled in figure legends.

3 Mutant RAS and NOX2 derived ROS affect glycolysis in human haematopoietic progenitor cells and AML derived cell lines

3.1 Introduction

AML is a heterogeneous haematological malignancy often characterised by a *RAS* mutation (Naoe and Kiyoi, 2013). Using a normal human haematopoietic progenitor cell (HPC) model it has previously been shown that constitutively active *RAS* leads to autonomous proliferation of HPC and overproduction of ROS (Hole *et al.*, 2010). The authors of this study showed that HPC expressing mutant RAS exhibited elevated levels of extracellular superoxide production (as measured by the chemiluminescent probe Diogenes^{TM}), no increases in mitochondrial superoxide production (as measured by MitoSOX) and increased levels of NOX2 protein expression on the plasma membrane when compared to control cells not expressing mutant RAS. Treatment with the NOX inhibitor, diphenyleneiodonium (DPI) and the antioxidant apocynin resulted in the near ablation of superoxide production with concomitant decreases in proliferation, suggesting a NOX dependent mechanism for these *RAS* induced increases in ROS production and proliferation. Overproduction of ROS through NOX activation has also been observed in greater than 60% of AML patient blasts, where it is associated with increased proliferation (Hole *et al.*, 2013). This suggests that these AML blasts are functioning within a highly oxidatively stressed extracellular environment, which may, at least in part, be driving these proliferative increases. To support this hypothesis, Hole *et al* (2013), employed the enzyme glucose oxidase (GOX) to generate hydrogen peroxide (H_2O_2), a major source of ROS (1.3.1), in culture with two AML cell lines (Mv4;11 and KG-1) and observed proliferative increases.

ROS has been implicated in cellular differentiation, growth and survival via its role as a cell signalling molecule. This can occur via inhibition of protein tyrosine phosphatases (PTP's), PTEN and PKC, or through regulation of gene expression via transcription factors such as NFκB, TP53 and HIF-1α and/or through epigenetic modifications of HDAC's and DNMT's (reviewed in Sardina *et al.*, 2012). Previously our group have generated preliminary data which have shown significant

RAS and ROS attributable gene expression changes, in particular those associated with glycolysis and carbohydrate metabolic pathways (Hopkins *et al.*, 2014). RAS has been widely reported to upregulate glycolysis in several solid cancers (Mazurek *et al.*, 2001, Ying *et al.*, 2012, Gaglio *et al.*, 2011, Zheng *et al.*, 2015), which is a hallmark of the Warburg effect (1.4.1). Furthermore, NOX generated ROS has previously been reported to modulate cellular glucose uptake in leukaemic cell lines (Prata *et al.*, 2008). However, the mechanism by which NOX2 generated ROS affects the subsequent metabolism of glucose and how this can affect proliferative changes are unknown. Therefore, this chapter specifically addresses the functional impact that ROS has on glycolysis in AML cells and examines whether this has a correlative effect on proliferation.

3.2 Aims and objectives

The main objective of this chapter is to assess the impact that mutant RAS and NOX2 derived ROS has on glycolysis. This study therefore aims to:

- To determine the effect of mutant RAS on glycolysis.

  HPC will be infected with N-RAS^{G12D} or H-RAS^{G12V} and changes in glycolysis will be assayed by glucose uptake and extracellular lactate production and compared with HPC not expressing mutant RAS (control).

- To determine the effect of NOX2 derived ROS on glycolysis and proliferation using a HPC model.

  HPC expressing mutant RAS will be treated with NOX inhibitors and their effect on glucose uptake, extracellular lactate production and proliferative rate will be assessed.

- To determine the effect of NOX2 derived ROS on glycolysis and proliferation using AML cell lines.

  AML cell lines that generate extracellular ROS will be treated with NOX inhibitors or have NOX2 knocked-down using shRNA and the effect on glucose uptake, extracellular lactate production and proliferative rate will be compared with corresponding control cells. Conversely, the AML cell line, Mv4;11 (which generates low levels of extracellular ROS) will be treated with

H_2O_2 (GOX) and glucose uptake, extracellular lactate production and proliferative rate will be compared with control cells.

3.3 Results

3.3.1 Mutant RAS increases glucose uptake and extracellular lactate generation in human HPC

Infection of HPC ($CD34^+$) with mutant *RAS* has previously been shown to generate an increase in NOX derived ROS production and proliferation compared to control HPC (Hole *et al.*, 2010). As *RAS* is commonly mutated in AML (Naoe and Kiyoi, 2013), HPC infected with mutant RAS were employed to model the effect of this mutation on glycolytic function. Human $CD34^+$ cells were isolated from neonatal cord blood and retrovirally infected with *N-RAS*^{G12D} or *H-RAS*^{G12V} using the PINCO expression vector (gift of Pier Pelicci, European Institute of Oncology, Milan, Italy). This vector encodes GFP which acts as a selectable marker. Control cells expressed GFP alone. Transduced cells were cultured for six days before being analysed for changes in glucose uptake and lactate production as described in the methods (2.7).

3.3.1.1 Expression of mutant RAS in human HPC

To confirm successful gene transduction, infected cells were analysed for GFP expression by flow cytometry 24h post infection. As shown in Figure 3-1A-C, GFP expression levels ranged from 58-76% for control cells, 75-94% for N-RAS^{G12D} and 44-70% for H-RAS^{G12V}, demonstrating successful infection was obtained in these cells. Figure 3-1D shows that 100% of cells expressed the HPC marker $CD34^+$, establishing that nearly all the cultured cells constituted a HPC population.

To establish that RAS protein was overexpressed in the mutant RAS expressing HPC, a western blot was performed. Figure 3-1E shows that in both N-RAS^{G12D} and H-RAS^{G12V}, higher levels of RAS protein can be observed compared to control HPC, indicating that RAS is constitutively expressed in these cells.

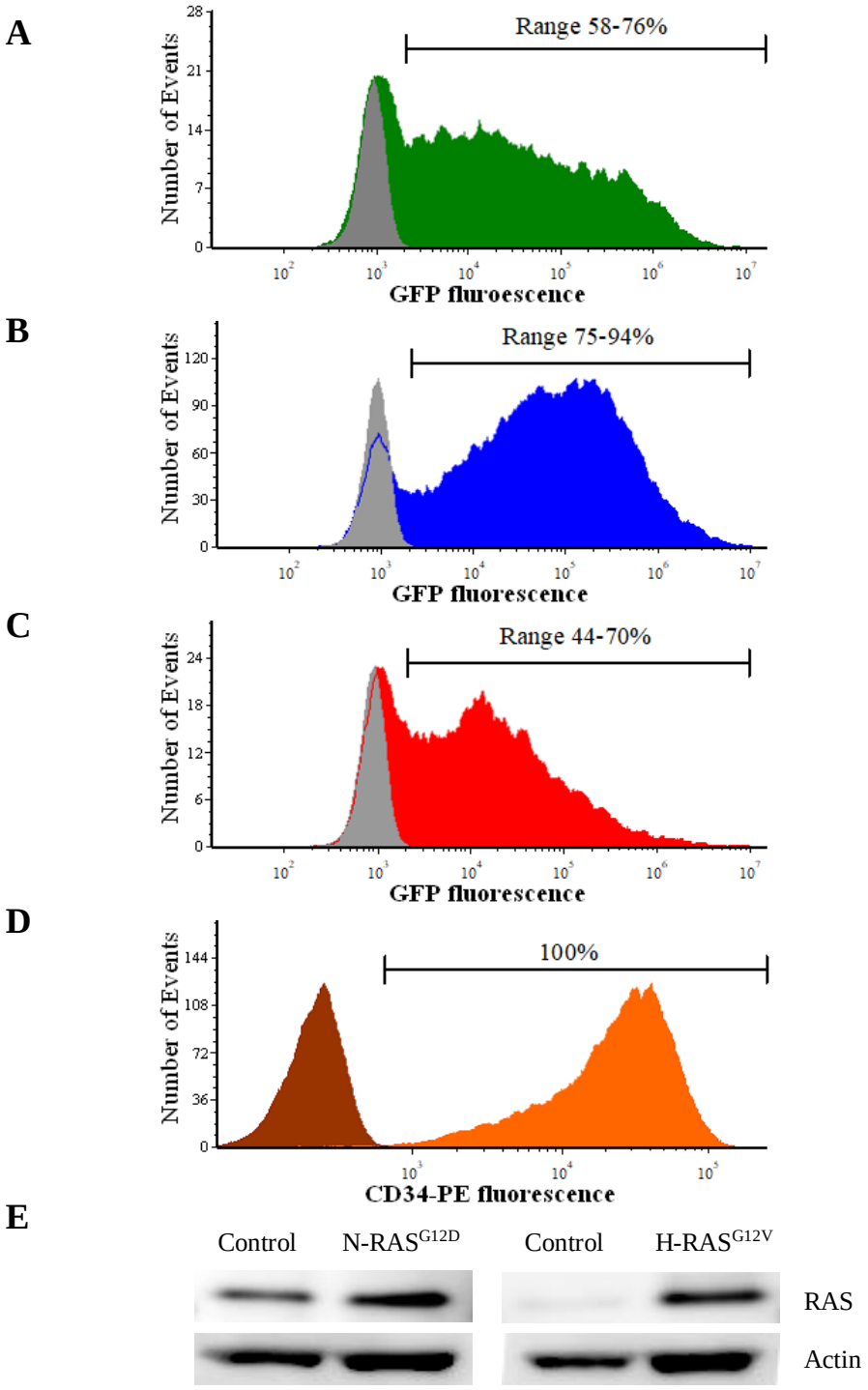

Figure 3-1. Infection of human HPC (CD34$^+$) with mutant RAS. Representative flow cytometric histograms showing percentage of HPC cells expressing GFP in **(A)** Control (green); **(B)** N-RAS^{G12D} (blue) and **(C)** H-RAS^{G12V} (red) transduced cells (n=7). Histograms were gated to exclude cell debris and dead cells based on FSC/SSC. Background auto fluorescence was established using HPC subjected to the equivalent retroviral infection procedure but in the absence of retrovirus (mock HPC) (grey) infected cells. Percentage within the black marker line represents proportion of cells showing fluorescence greater than background autofluorescence at <0.01%. **(D)** Representative flow cytometric histogram showing expression of the HPC marker CD34. Infected cells were analysed for CD34 expression level using anti-CD34 PE. Background non-specific fluorescence (brown) was established using isotype matched control antibody, IgG_1 PE. **(E)** Example western blot analysis of RAS protein expression comparing control and N-RAS^{G12D} and control and H-RAS^{G12V} infected CD34$^+$ cells. Actin was used as a loading control.

3.3.1.2 Mutant RAS promotes increased glucose uptake in human HPC

Increased aerobic glycolysis is a common feature of cancerous cells with concomitant increases in cellular glucose uptake and lactate secretion (reviewed in Mikawa *et al.*, 2015). To examine the impact of mutant RAS expression on glycolysis, this study initially analysed changes in glucose consumption of mutant RAS expressing HPC compared to control HPC. The concentration of glucose retained in the culture medium following three days of growth was determined using a fluorometric D-glucose assay kit. Figure 3-2A shows that the levels of glucose remaining in the culture media were 27% ± 15% less in the media of N-RAS^{G12D} and a significant 45% ±35% ($p=0.023$) less in the media of H-RAS^{G12V} when compared to control. These differences in the concentration of glucose remaining in the culture media indicate that mutant RAS expressing HPC consume glucose at a greater rate than control cells.

It is known that culturing cells in high concentrations of growth factors and cytokines stimulates proliferation and increases glycolysis in excess of that required to support this growth (Bauer *et al.*, 2004). Consequently, it was reasoned that the full effect of mutant RAS on glucose uptake may be masked by use of these growth factors. Therefore, HPC were cultured in the absence of cytokines over three days and the concentration of glucose in the culture media assayed as above. In the absence of growth factors N-RAS^{G12D} HPC showed a significant 2-fold decrease in glucose levels of the culture supernatant compared to control, whilst H-RAS^{G12V} HPC showed a significant 11-fold decrease (Figure 3-2B). This decrease in concentration of glucose in the culture supernatant of both N-RAS^{G12D} and H-RAS^{G12V} HPC, suggests that in the absence of cytokines mutant RAS allows growth-factor independent increases in cellular glucose consumption.

To confirm that these changes in cellular glucose consumption occurred at the single cell level and were not a consequence of increased cellular proliferation, the fluorescent glucose bioprobe 2-(N-(7-nitrobenz-2-oxa-1,3-diazol-4-yl) amino)-2-D-deoxyglucose (2-NBDG) coupled with flow cytometry was employed. 2-NBDG is a fluorescent glucose derivative that is transported into the cell by glucose transporters and is phosphorylated to 2-NBDG-6-phosphate before being broken down into non-fluorescent derivatives (Yoshioka *et al.*, 1996, Yamamoto and Ashida, 2012). 2-

NBDG emits fluorescence at a wavelength of 542nm which has a spectral overlap with GFP emission. Therefore, HPC were alternatively infected with the PINCO retroviral expression vector that was modified to co-express DsRed instead of GFP. Expression levels of DsRed ranged from 18-88% for control, 41-49% for N-RAS^{G12D} and 21-22% for H-RAS^{G12V} (Figure 3-3A). Glucose uptake of HPC expressing mutant RAS were compared with control HPC using the 2-NBDG probe. Figure 3-3B shows typical flow cytometric histograms demonstrating changes in glucose uptake of control, N-RAS^{G12D} and H-RAS^{G12V} infected HPC (DsRed^{+}) compared to uninfected cells (DsRed^{-}). Figure 3-3C shows that H-RAS^{G12V} showed a significant 1.9-fold increase in glucose uptake, whilst a 1.3-fold increase in glucose uptake was observed in N-RAS^{G12D}, although this did not reach significant. When cells were cultured in the absence of cytokines, a significant 2-fold increase in glucose uptake was observed for H-RAS^{G12V}, whilst a non-significant 1-4-fold increase was observed in N-RAS^{G12D} (Figure 3-3D). These data demonstrate that expression of mutant RAS in normal human HPC increases glucose uptake at the individual cell level when compared with control cells and that this increase occurs both in the absence and presence of cytokines.

Taken together, the data above suggests that increased levels of glucose uptake, is associated with expression of mutant RAS in normal human haematopoietic progenitor cells.

A

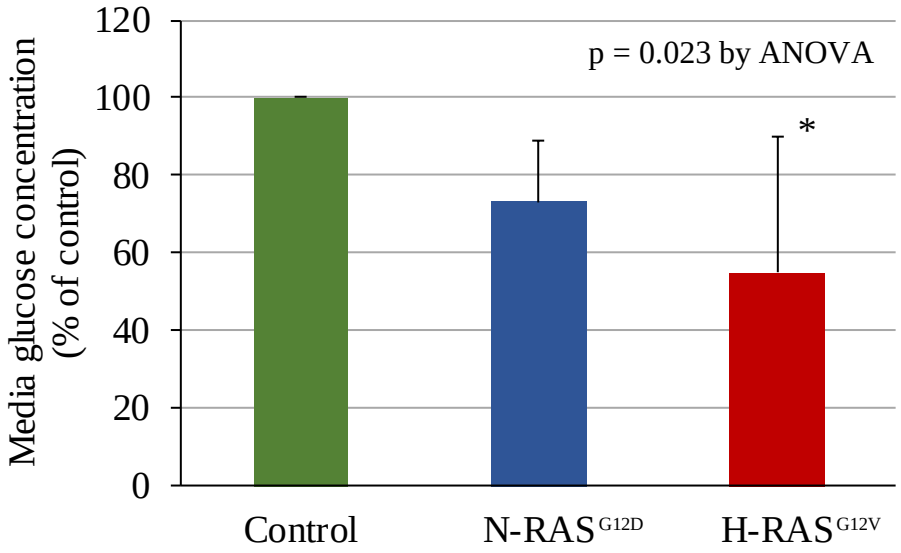

B

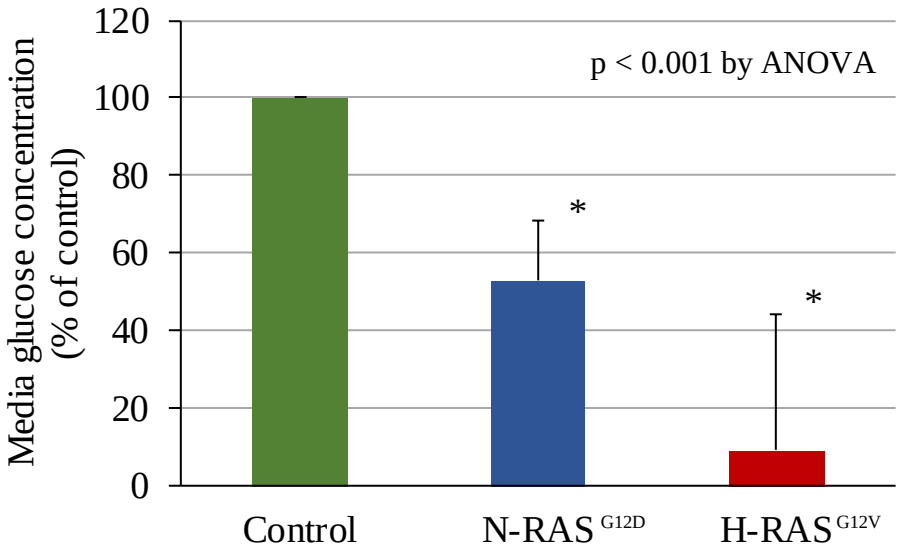

Figure 3-2. Depletion of glucose in culture media of human HPC. Depletion of glucose in culture media (normalised to control) of transduced HPC supplemented **(A)** with growth factors (n=5) **(B)** without growth factors (n=4). Following infection, $CD34^+$ cells were cultured for 3 further days (day 6 of development) at an initial seeding density of 0.5 x 10^5 cells/ml with growth factors (IL3, SCF, G-CSF and GM-CSF), and 1.5 x 10^5 cells/ml without growth factors. Data represents mean ± 1SD. * denotes $p<0.05$ analysed by ANOVA with Tukey's honestly significance difference.

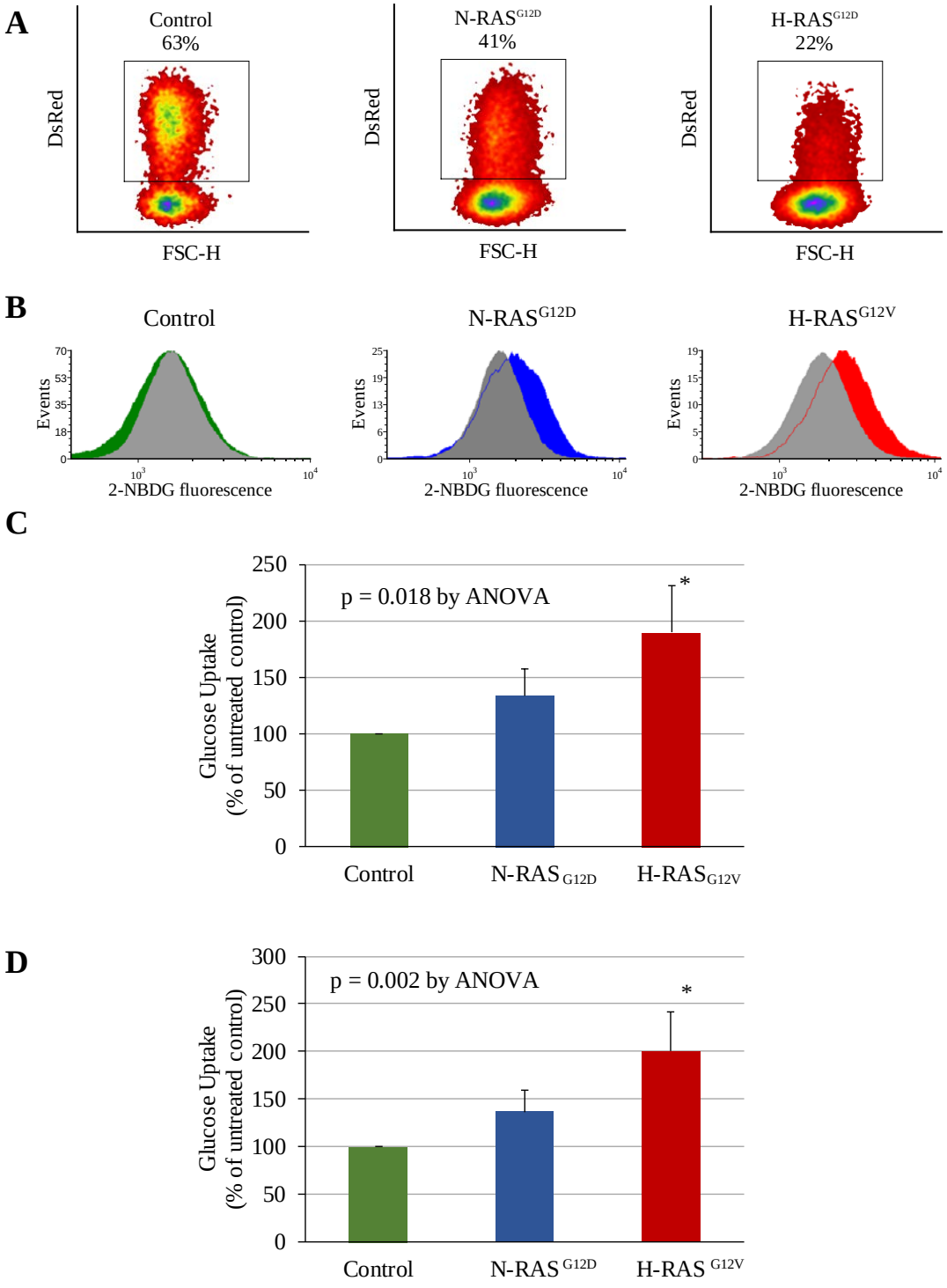

Figure 3-3. Glucose uptake in HPC expressing mutant RAS. **(A)** Representative flow cytometric plots showing percentage of HPC cells expressing DsRed in transduced cells. Data were gated to exclude cell debris based on FSC/SSC. **(B)** Representative flow cytometric histograms showing change in glucose uptake in; control (green); N-RAS^{G12D} (blue); H-RAS^{G12V} (red) DsRed^{+} cells cf. DsRed^{-} cells (grey). **(C, D)** Glucose uptake (normalised to control (green)) in transduced HPC **(C)** supplemented with growth factors (n=3) and **(D)** without growth factors (n=3); control (green), N-RAS^{G12D} (blue), H-RAS^{G12V} (red). Following infection, CD34^{+} cells were cultured for 3 further days (day 6 of development) at an initial seeding density of 0.5 x 10^5 cells/ml with growth factors (IL3, SCF, G-CSF and GM-CSF), and 1.5 x 10^5 cells/ml without growth factors. Data represents mean ± 1SD. * denotes $p<0.05$ analysed by ANOVA with Tukey's honestly significance difference.

3.3.1.3 Mutant RAS promotes extracellular lactate production in human HPC

Alongside increases in glucose uptake, the Warburg effect has also been shown to result in increases in the generation of extracellular lactate (reviewed in Mikawa *et al.*, 2015). To determine whether the observed increases in glucose uptake in mutant RAS HPC (3.3.1.2) were also associated with increased extracellular lactate secretion, a fluorometric L-lactate assay was used to determine media lactate concentration, after three days of growth.

Figure 3-4A shows no significant increase in extracellular lactate production in HPC expressing mutant RAS compared to control was observed when cells were cultured in the presence of cytokines. In contrast, in the absence of cytokines, N-RAS^{G12D} had a 1.3-fold and H-RAS^{G12V} a significant 4-fold ($p=0.002$) increase in extracellular lactate secretion compared to control HPC (Figure 3-4B). This suggests that in the absence of cytokines mutant RAS results in growth factor independent increases in extracellular lactate production. Changes in extracellular lactate production mirror the changes observed in glucose uptake (3.3.1.2) and together suggest that mutant RAS expressing HPC engender increases in glycolytic function via increased cellular glucose uptake and lactate secretion.

A

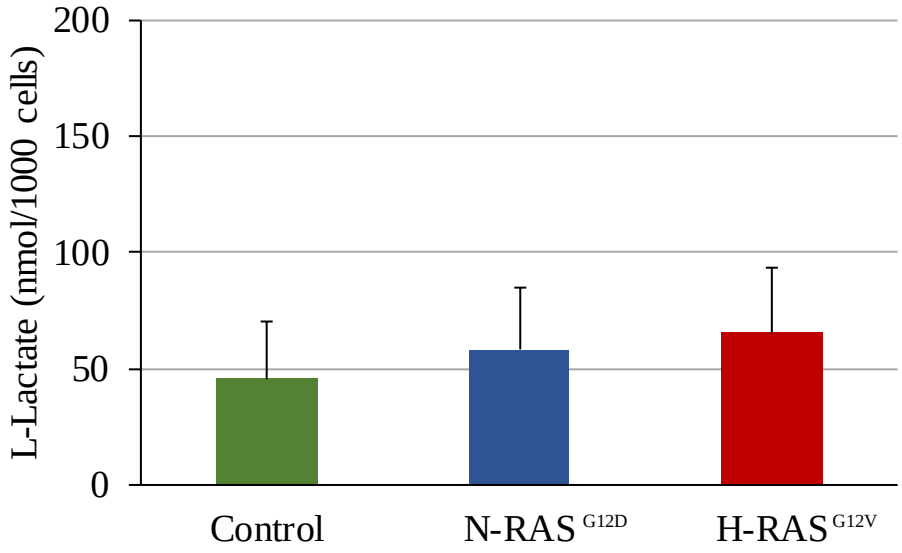

B

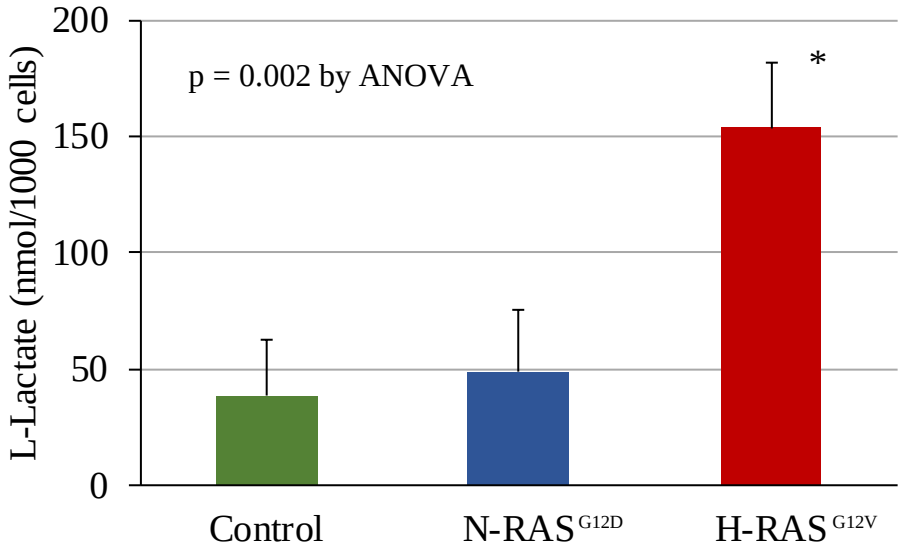

Figure 3-4. Extracellular concentration of L-lactate per 1000 human HPC. Concentration of extracellular L-lactate in culture media of transduced GFP$^+$ HPC, supplemented **(A)** with growth factors (n=5) **(B)** without growth factors (n=4). Following infection, CD34$^+$ cells were cultured for 3 further days (day 6 of development) at an initial seeding density of 0.5 x 10^5 cells/ml with growth factors IL3, SCG, G-CSF and GM-CSF, and 1.5 x 10^5 cells/ml without growth factors. Data represents mean ± 1SD. * denotes $p<0.05$, analysed by ANOVA with Tukey's honestly significance difference.

3.3.1.4 Mutant RAS promotes glucose uptake in HPC of transgenic mice expressing N-RAS^{D12}

Data above suggests *in vitro* expression of mutant RAS in HPC leads to increases in glycolysis. To support this conclusion, glucose uptake was assayed *ex vivo* in HPC harvested from secondary transplants of transgenic mice expressing N-RAS^{D12} driven by an MRP8 promoter, as previously described (Omidvar *et al.*, 2007). MRP8 is primarily expressed by myeloid cells during differentiation and promotes expression of genes in myeloid cells (Nacken *et al.*, 1996). Mice expressing N-RAS^{D12} under control of MRP8 do not develop AML-like disease (Kogan *et al.*, 1998) but when crossed with mice expressing BCL-2 to generate MRP8[BCL-2/NRASD12] mice, human AML-like disease occurs (Omidvar *et al.*, 2007). N-RAS^{D12} mice can therefore be considered a preleukaemic murine model approximating to the human HPC RAS model above. To observe the effect of N-RAS^{D12} on glucose uptake in a pre-leukaemic AML murine model, 2-NBDG was employed to investigate glucose uptake in bone marrow cells derived from N-RAS^{D12} mice. A significant 1.9-fold increase ($p<0.05$) in glucose uptake was observed in N-RAS^{D12} mice compared to wild type control (WT) (Figure 3-5). This suggests that both *in vitro* and *in vivo* expression of mutant N-RAS results in increased cellular glucose uptake when compared to controls cells.

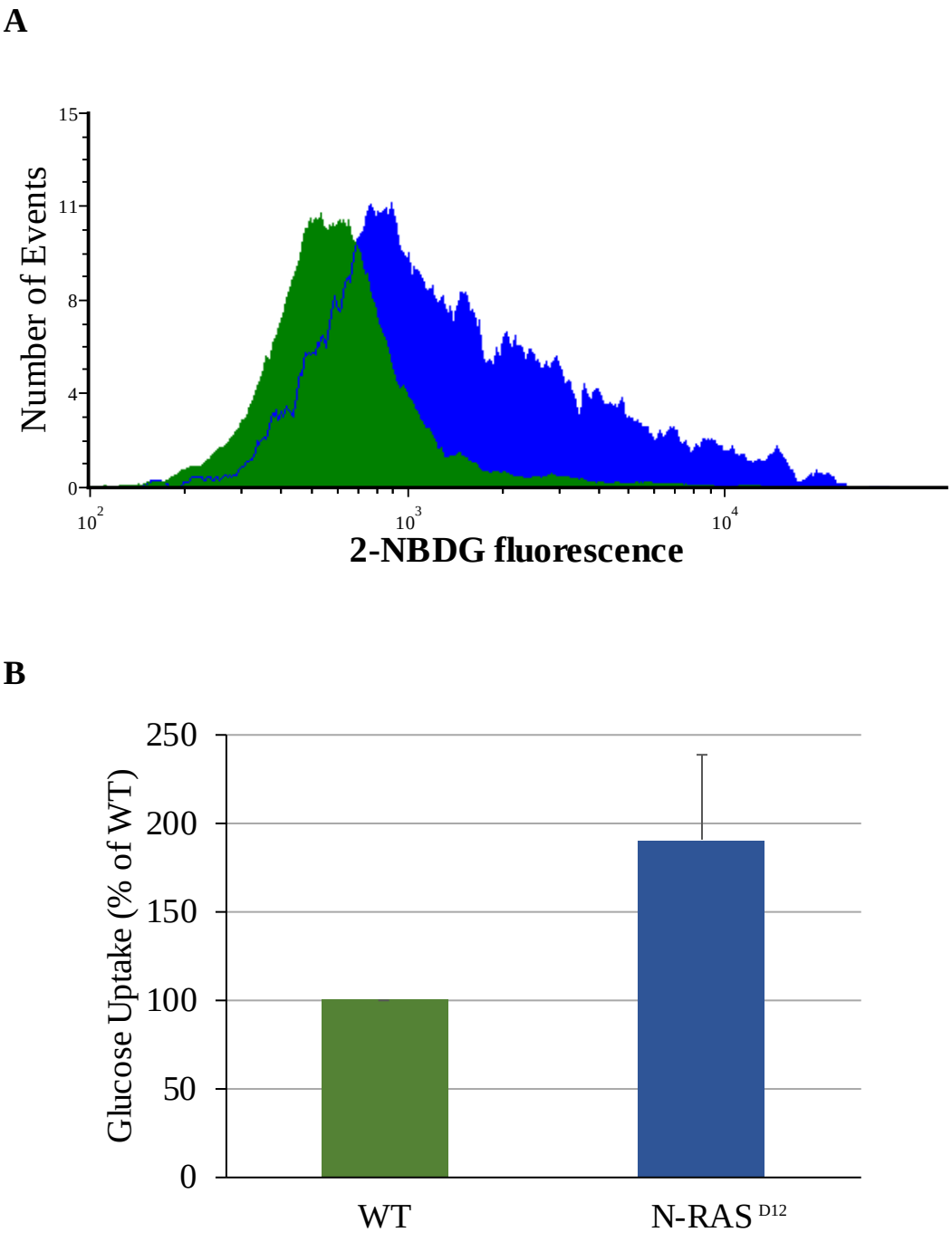

Figure 3-5. Glucose uptake in murine bone marrow cells. (A) Representative flow cytometric histogram showing change in glucose uptake in; WT control (green) compared with N-RAS^{12D} (blue). Histograms were gated to exclude cell debris and dead cells based on FSC/SSC. **(B)** Cellular glucose uptake (normalised to WT control) in N-RAS^{D12} transgenic mice driven by an MRP8 promoter and compared to wild type control (n=8). Cells kindly harvested by Dr. Nadar Omidvar as previously described (Omidvar *et al.*, 2007) Data represents mean ± 1SD. SD = 48%, 95% CI (150% and 231%) calculated by one sample t-test.

3.3.2 ROS affects functional changes in glycolysis in human HPC

The above data suggests expression of mutant RAS, both in human HPC and murine HPC, results in increased glycolysis. Given that previous work in our group has shown that increases in proliferation, as a consequence of mutant RAS, are at least in part attributable to NOX2-derived ROS (Hole *et al.*, 2010), we next determined whether these RAS dependent changes in glycolysis were also mediated by ROS. Therefore, glucose uptake and lactate production were assayed following NOX inhibition in these cultures.

3.3.2.1 Phosphorylation of p38^{MAPK} in mutant RAS expressing HPC

ROS normally induces a stress response in cells leading to inhibition of the cell cycle, modulated as a result of phosphorylation of the p38 mitogen activated protein kinase (p38^{MAPK}) pathway (Kulisz *et al.*, 2002). H-RAS^{G12V} HPC have previously been shown to have increased levels of p-p38^{MAPK} which is ablated upon addition of DPI (Hole *et al.*, 2010). To confirm that this was also true for N-RAS^{G12D} and to validate that the mutant-RAS expressing HPC were experiencing oxidative stress (ROS), western blots were performed to detect the presence of p-p38^{MAPK}. As shown in Figure 3-6 HPC expressed equal levels of p38^{MAPK}, however N-RAS^{G12D} and H-RAS^{G12V} expressed higher levels of phosphorylated p38^{MAPK}, which was decreased upon treatment with DPI. This supports previous data (Hole *et al.*, 2010) that mutant RAS expressing HPC experience increased levels of ROS as determined by phosphorylation of the p38^{MAPK} pathway and that this ROS induced stress response is relieved upon inhibition of NOX2 by addition of DPI.

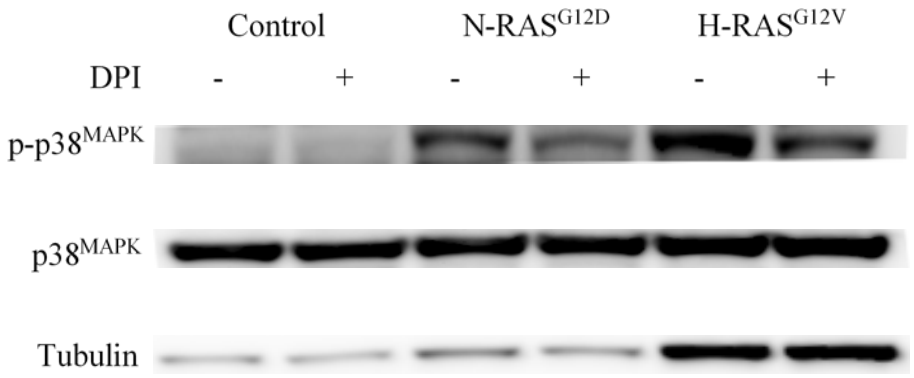

Figure 3-6. Mutant RAS expressing HPC exhibit increased phosphorylation of p38^{MAPK}. Human HPC control, N-RAS^{G12D} and H-RAS^{G12V} were incubated for 24h in the presence and absence of DPI (100nM). Expression and phosphorylation state of p38 was determined by western blot using whole cell lysates derived from these cells and probed with antibodies recognising p-p38^{MAPK} and p38^{MAPK}. Tubulin was used as a loading control.

3.3.2.2 ROS promotes increased glucose uptake in human HPC

HPCs expressing mutant RAS and co-expressing GFP, were treated with 100nM DPI (a concentration that has previously been shown not to affect HPC viability (Hopkins *et al.*, 2014), but which inhibits 90% of NOX2 activity in the HL60 cell line (Hopkins, 2014) for 24h and the concentration of glucose in the cell culture media was assayed as above (3.3.1.2). Figure 3-7A shows that both the untreated N-RAS^{G12D} and H-RAS^{G12V} HPC had a lower concentration of glucose in the culture supernatant after 24h compared to cells not expressing mutant RAS (consistent with data reported above (3.3.1.2) and suggesting increased uptake of glucose by these cells). However, following NOX inhibition of N-RAS^{G12D} and H-RAS^{G12V} with DPI, a respective 1.4-fold and 1.8-fold increase in the concentration of glucose retained in the culture media compared to untreated cells was observed (albeit not statistically significant). Treatment of cells not expressing mutant RAS with DPI had minimal effect; 1.1-fold increase compared to control. Since DPI is reported as a non-specific flavoprotein inhibitor at high concentrations (Aldieri *et al.*, 2008), HPCs were also treated with an alternative, more specific NOX inhibitor (reviewed in Altenhofer *et al.*, 2012) VAS-2870 (5μM), which has been shown to inhibit NOX2-derived ROS in the THP-1 cell line (Dr. Paul Hole, unpublished data). Figure 3-7B shows a 1.4-fold decrease in media glucose levels for N-RAS^{G12D} and a significant 1.9-fold decrease for H-RAS^{G12V} compared with control HPC after 24h. Treatment with VAS-2870 resulted in a 1.2-fold and 1.3-fold increase in the concentration of glucose retained in the culture media for N-RAS^{G12D} and H-RAS^{G12V} respectively, when compared to untreated cultures. Commensurate with above, treatment of HPC not expressing mutant RAS had minimal changes in glucose consumption when treated with VAS-2870; a 1.1-fold increase compared to the untreated cells. These data show that glucose concentration of the culture media is reduced in mutant RAS expressing HPC after 24h compared to control. Furthermore, treatment of mutant RAS expressing HPC with NOX inhibitors partially reverses this effect, suggesting that NOX activity may be driving glucose uptake, although further repeats would be required to demonstrate statistical significance.

Glucose uptake at the single cell level using 2-NBDG was also performed in HPC expressing mutant RAS (co-expressing DsRed), treated with NOX inhibitors. These studies focussed on cells expressing mutant N-RAS^{G12D} since in AML, this is the

most common RAS mutation (Renneville *et al.*, 2008). Control and N-RAS^{G12D} HPC were treated with DPI (100nM), VAS-2870 (5μM) or GSK-NOX2 (3μM). GSK-NOX2 is a specific NOX2 inhibitor a proprietary compound (made available courtesy of GlaxoSmithCline) and has been shown to decrease NOX2-derived ROS in the NOMO-1 cell line (Professor Richard Darley, unpublished data). Figure 3-8A shows typical flow cytometric histograms demonstrating changes in glucose uptake of N-RAS^{G12D} treated with NOX inhibitors compared with the co-cultured, uninfected HPC. When the glucose uptake of untreated N-RAS^{G12D} was compared with separately cultured, untreated control HPC, N-RAS^{G12D} showed a significant 1.4-fold increase in glucose uptake compared with control HPC. Treatment of N-RAS^{G12D} with VAS-2870 showed a near ablation of this mutant RAS induced increase in glucose uptake, whilst GSK-NOX2 reduced increased glucose uptake by half, in the N-RAS^{G12D} when compared to untreated cells (Figure 3-8B). Treatment of control HPC with DPI, VAS-2870 and GSK-NOX2 had little to no effect on glucose uptake, whilst surprisingly DPI also had a minimal effect on glucose uptake at the single cell level in the N-RAS^{G12D} HPC when compared with untreated cells. The failure of DPI to reduce glucose uptake in the N-RAS^{G12D} HPC may be indicative of an off-target effect of this compound (3.4), or may be a statistical anomaly requiring further experimental repeats. Overall these data support the changes in glucose concentration observed in the culture supernatant of these HPC (Figure 3-7). Taken together these data suggests NOX2 derived ROS increases glucose uptake in HPC expressing mutant RAS.

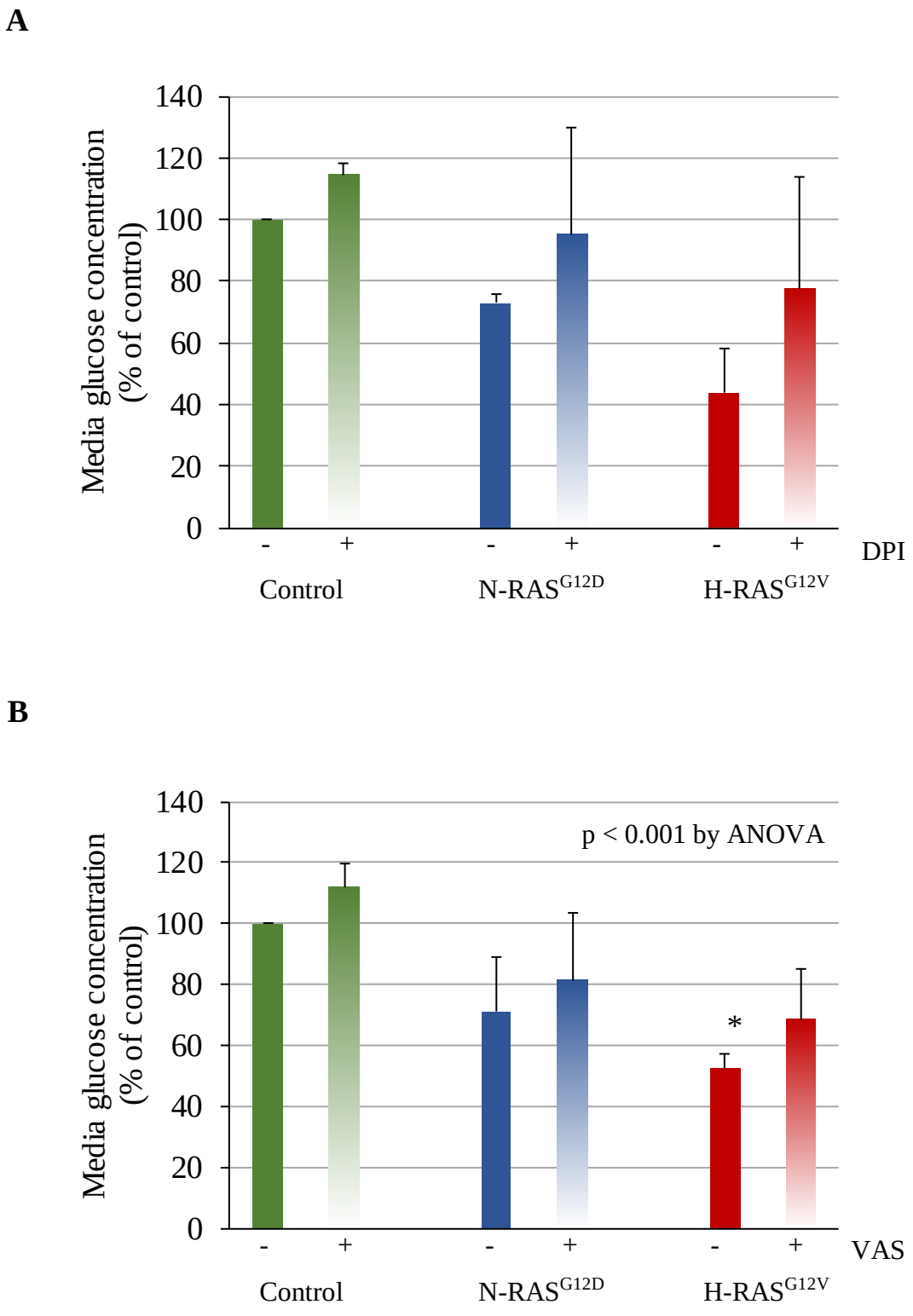

Figure 3-7. ROS induced changes of glucose concentration in culture media in human HPC. Depletion of glucose in culture media (normalised to control) of transduced HPC treated with **(A)** DPI (100nM) and **(B)** VAS-2870 (5μM) (n=3). Cells were counted (day5) and cultured for a further 24h in the presence/absence of inhibitors, without growth factors, at an initial seeding density of 6 x 10^5 cells/ml. Data represents mean ± 1SD. * denotes $p<0.05$, analysed by ANOVA with Tukey's honestly significance difference.

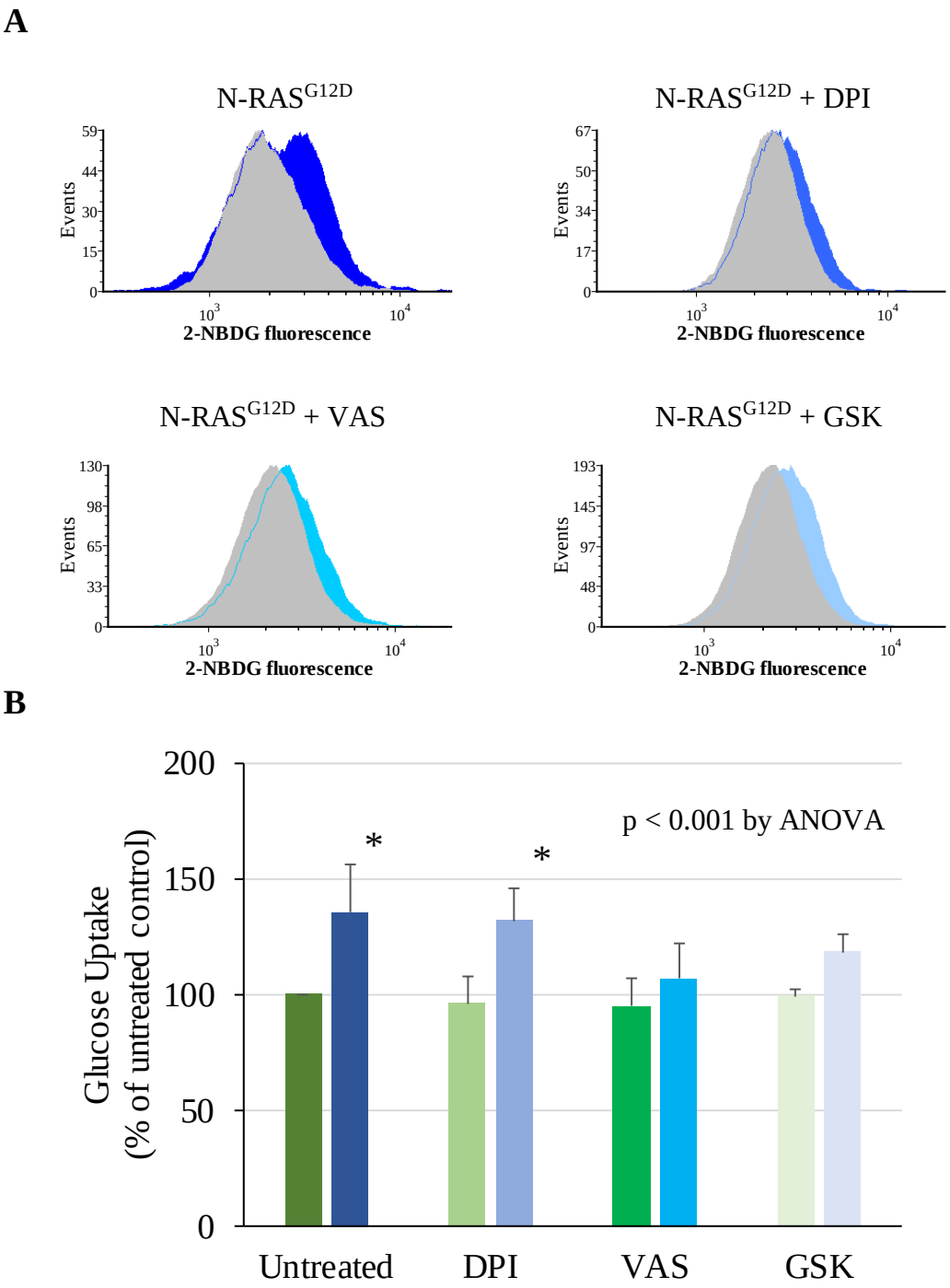

Figure 3-8. ROS induced changes in glucose uptake in human HPC. (A) Representative flow cytometric histograms showing change in glucose uptake in N-RAS^{G12D} (DsRed^{+} cells); untreated (dark blue); + DPI (100nM) (blue); + VAS-2870 (5µM) (sky blue); + GSK-NOX2 (3µM) (light blue) cf. DsRed^{-} cells (grey). Data were gated to exclude cell debris based on FSC/SSC. **(B)** Cellular glucose uptake (normalised to untreated control) in transduced HPC treated with DPI (100nM), VAS-2870 (5µM) and GSK-NOX2 (3µM); control (green), N-RAS^{G12D} (blue). Cells were counted (day5) and cultured for a further 24h in the presence/absence of inhibitors, without growth, factors at an initial seeding density of 6 x 10^5 cells/ml (n=3). Data represents mean ± 1SD. * denotes $p<0.05$ (compared to untreated control HPC (dark green)), analysed by ANOVA with Tukey's honestly significance difference.

3.3.2.3 ROS affects extracellular lactate production in human HPC

Alongside increased glucose consumption, mutant RAS expressing HPC also generate increased extracellular lactate (3.3.1.3). To ascertain whether this increase is a function of increased ROS production, lactate was assayed from cultures treated with NOX inhibitors as above (3.3.1.3). Surprisingly, treatment of these cells with DPI, resulted in 1.5, 2.4 and 1.7-fold increases in extracellular L-lactate production, of control, N-RAS^{G12D} and H-RAS^{G12V} HPC respectively, when compared to untreated controls (Figure 3-9A), although these changes did not reach significance. Treatment with VAS-2870 resulted in no changes in extracellular lactate production (Figure 3-9B). The lack of any significant changes to extracellular lactate production in mutant RAS expressing HPC upon treatment with VAS-2870 suggest that NOX2-derived ROS does not impact on extracellular lactate secretion whilst the increase in extracellular lactate secretion of the cells upon treatment with DPI may be the result of an off-target effect. Overall these data do not support the idea that NOX2-derived ROS is responsible for increases in lactate secretion in mutant RAS expressing HPC.

3.3.2.4 ROS promotes proliferation in human HPC

As previously reported by our group, proliferative decreases occur in mutant RAS expressing HPC treated with DPI over a 48 h period (Hole *et al.*, 2010). To determine whether changes in carbohydrate metabolism observed above, also correlated with changes in proliferation, growth rates were assayed using a haemocytometer. Both N-RAS^{G12D} and H-RAS^{G12V} HPC showed decreased proliferation when treated with DPI whilst control HPC growth remained unchanged (Figure 3-10A). To verify that these proliferative changes were a result of NOX-derived ROS the above experiment was repeated using VAS-2870. Similar to treatment with DPI, no proliferative changes occurred in the control HPC, whilst a 1.4-fold reduction in proliferation occurred in N-RAS^{G12D} and H-RAS^{G12V}, which reached significance for H-RAS^{G12V} (Figure 3-10B). This suggests that the decreases in glucose uptake observed above, corresponded with ROS associated proliferative changes observed here and previously, and that these proliferative changes in mutant RAS expressing HPC were at least in part a function of NOX2-derived ROS.

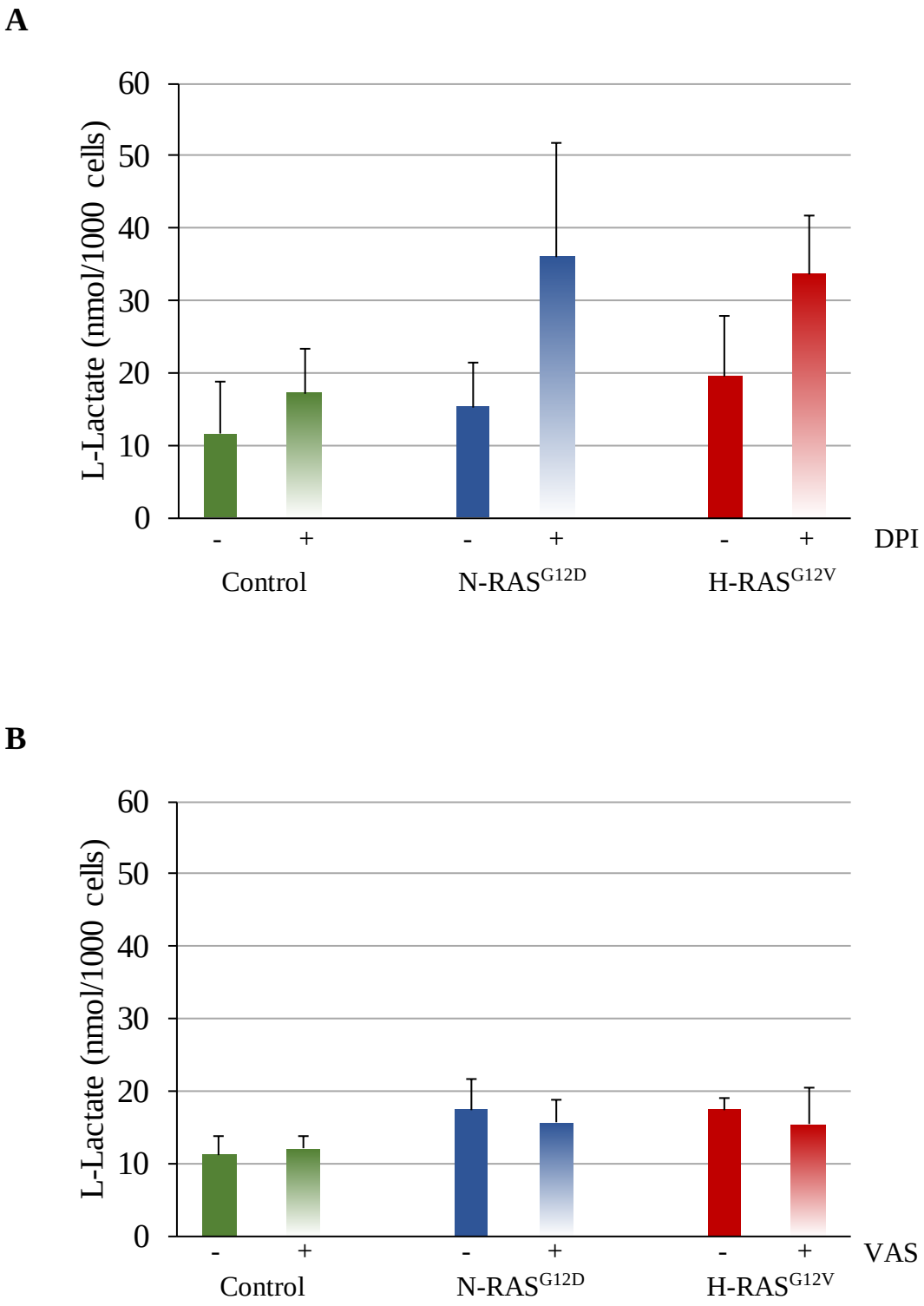

Figure 3-9. ROS induced changes in extracellular L-lactate production in human HPC. Concentration of extracellular L-lactate in culture media of transduced CD34^{+} cells, treated **(A)** with DPI (100nM) (n=3) or **(B)** with VAS-2870 (5µM) (n=4). Cells were counted (day5) and cultured for a further 24h, in the presence/absence of inhibitors, without growth factors at an initial seeding density of 6 x 10^5 cells/ml. Data represents mean ± 1SD.

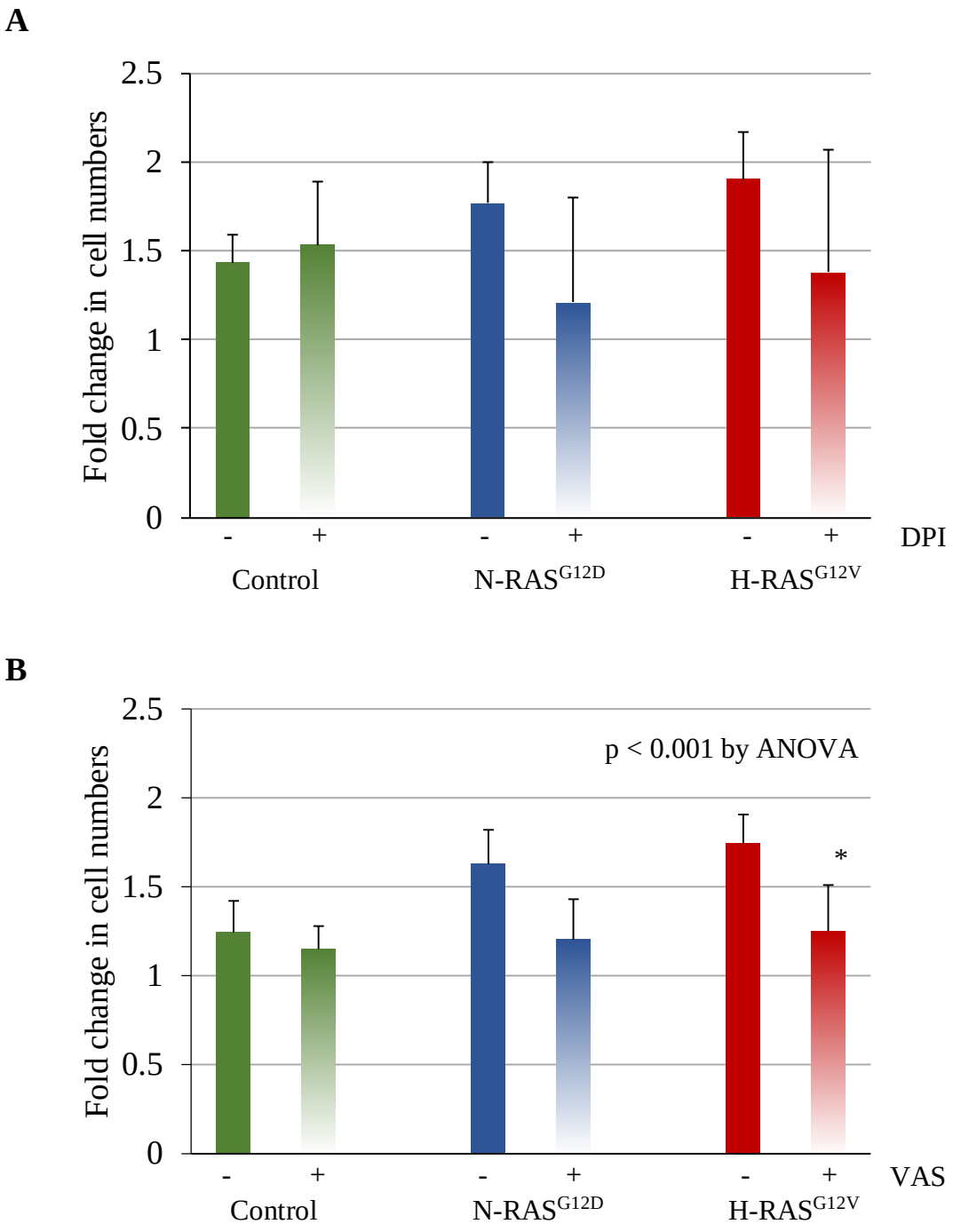

Figure 3-10. ROS induced changes in proliferation of human HPC. Fold change in cell numbers of transduced HPC, treated with **(A)** DPI (100nM) (n=3) or **(B)** VAS-2870 (10μM) (n=4). Cells were counted (day5) and cultured for a further 24h in the presence/absence of inhibitors, without growth factors at an initial seeding density of 6 x 10^5 cells/ml Data represents mean ± 1SD. * denotes $p<0.05$, analysed by ANOVA with Tukey's honestly significance difference.

3.3.3 ROS affects functional changes in glycolysis in AML cell lines

The data above suggest that NOX-derived ROS affects functional changes in glycolysis in human HPC transformed with mutant RAS. To investigate further the role of ROS on glycolysis in AML, changes in this pathway were assayed in AML derived cell lines with varying ability to produce NOX2 derived extracellular ROS. Changes in glucose uptake and extracellular lactate production as a result of chemical inhibition or NOX2 knock-down using shRNA were determined.

Extracellular superoxide generated by NOX2 is rapidly converted to H_2O_2 *in vivo,* by superoxide dismutase (SOD) (Hole *et al.*, 2011). Glucose oxidase (GOX) an enzyme which catalyses the production of H_2O_2 (Hole *et al.*, 2013) can be used to mimic the effect of NOX2-derived ROS in AML cell lines that don't generate detectable extracellular superoxide. These cell lines make good models to study glycolysis, as treatment with exogenous ROS, generated through the addition of GOX, allows tighter control over levels of cellular exposure to H_2O_2.

3.3.3.1 Determination of NOX2 derived ROS in AML cell lines

An assay to detect extracellular superoxide production using the chemiluminescent probe Diogenes^{TM} was used to screen a selection of AML cell lines for their ability to produce ROS. Figure 3-11A shows extracellular superoxide levels were detected at much higher levels in the NOMO-1 and THP-1 cell lines, compared with the cell lines Mv4;11, KG-1 and U937. The specificity of the Diogenes^{TM} probe for superoxide has previously been validated (Hole *et al.*, 2010), as the presence of SOD in culture quenches Diogenes^{TM} chemiluminescence, whilst treatment with catalase (which decomposes H_2O_2 but not superoxide) does not. This suggests that a major source of ROS in NOMO-1 and THP-1 cell lines is superoxide.

As NOX2 is a major source of extracellular superoxide production, knock-down of NOX2 (NOX2-KD) using shRNA provides a good method for examining the effects of endogenous NOX2-derived ROS. THP-1 and NOMO-1 cells lentivirally transduced with shRNA complementary to NOX2 mRNA and encoding puromycin resistance were kindly provided by Professor Richard Darley and were compared with control cells (THPSH and NOMOSH) which had been transfected with shRNA coding for a non-mammalian target sequence. NOX2 is a transmembrane protein (Bedard and Krause, 2007), so to confirm NOX2-KD, NOX2 expression was

determined by flow cytometry using an anti-NOX2 PE-conjugated antibody (Figure 3-11B). To confirm a functional reduction in superoxide production, NOX2-KD cells were assayed using Diogenes^{TM}. Superoxide production in THP cells with NOX2 knocked-down, was almost completely ablated compared to THPSH, whilst NOMO NOX2-KD cells showed a 30% reduction in superoxide production compared with NOMOSH (Figure 3-11C). To confirm that treatment of THPSH and NOMOSH cells with DPI also resulted in a decrease in NOX2 derived superoxide THPSH and NOMOSH cells treated with DPI (100nM) were additionally assayed using Diogenes^{TM}. THPSH and NOMOSH cells showed a 90% and 70% reduction in superoxide production respectively (Figure 3-11C).

ROS has previously been shown to result in phosphorylation of p38^{MAPK} pathway as part of a stress response in HPC expressing mutant RAS, which is alleviated following inhibition of ROS (3.3.2.1). To confirm this mechanism in AML cell lines, western blots were performed on NOMO-1 and THP-1 with NOX2 knocked-down or treated with DPI (100nM) and compared with control cells. Figure 3-12A shows that both the NOMO NOX2-KD and THP NOX2-KD cells showed decreased phosphorylation of p38^{MAPK} compared with NOMOSH and THPSH controls, whilst treatment with DPI also resulted in decreased phosphorylation of this protein in THPSH cells. Expression levels of p38^{MAPK} showed no changes compared to control in either NOX2-KD cells or those treated with DPI. This alteration in phosphorylation state of p38^{MAPK} indicates that NOMO-1 and THP-1 cells experience a stress response arising from NOX2 derived ROS.

Western blot analysis to determine the phosphorylation state of p38^{MAPK} was also undertaken for Mv4;11 cells treated with GOX which constitutively generates H_2O_2 in the culture media. Figure 3-12B shows that GOX treated Mv4;11 cells showed increased phosphorylation of p38^{MAPK} compared to control and no changes in protein expression of p38^{MAPK} upon treatment with GOX. These data show that addition of exogenous ROS to Mv4;11 cells results in increased phosphorylation of p38^{MAPK}.

Overall, these data demonstrate that AML cell lines producing endogenous ROS or subjected to exogenous H_2O_2 induced phosphorylation of p38^{MAPK} and that the levels of endogenous ROS can be repressed by chemical inhibition or shRNA knock-down targeting the NOX2 oxidase.

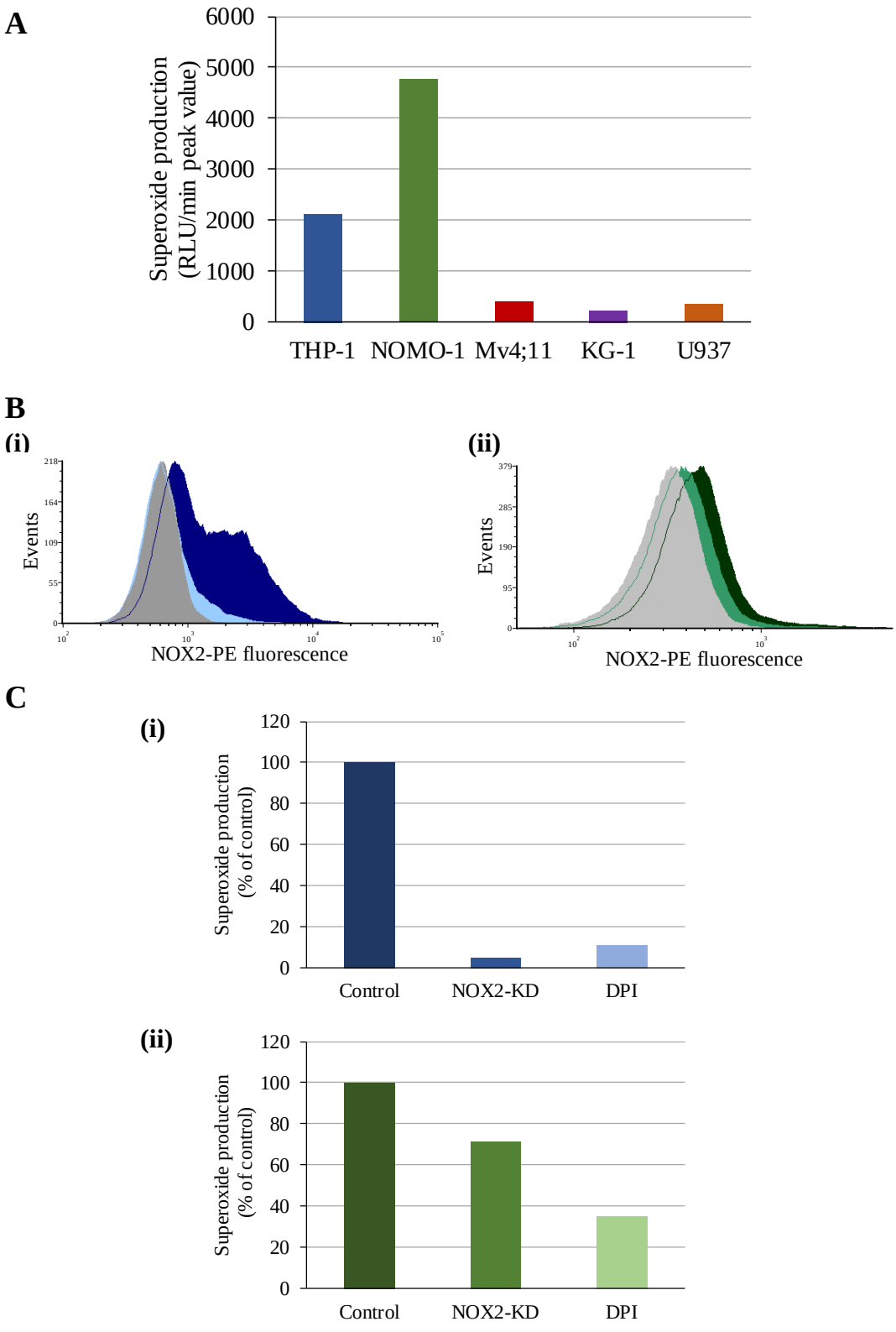

Figure 3-11. Superoxide production in AML cell lines. (A) Peak superoxide production (relative luminescent units/min (RLU/min)) in a panel of AML derived cell lines measured using Diogenes™. **(B)** Cell surface NOX2 expression in **(i)** THPSH (control) (dark blue), THP NOX2-KD (light blue) and **(ii)** NOMOSH (control) (dark green) NOMO NOX2-KD (light green) determined using an anti-NOX2-PE conjugated antibody and compared to IgG_1 isotype control (grey). **(C)** Superoxide production (normalised to control) in **(i)** THPSH (control) (dark blue), THP NOX2-KD (blue) THPSH treated with DPI (100nM) (mid blue) and **(ii)** NOMOSH (control) (dark green), NOMO NOX2-KD (green), NOMOSH treated with DPI (100nM) (mid green).

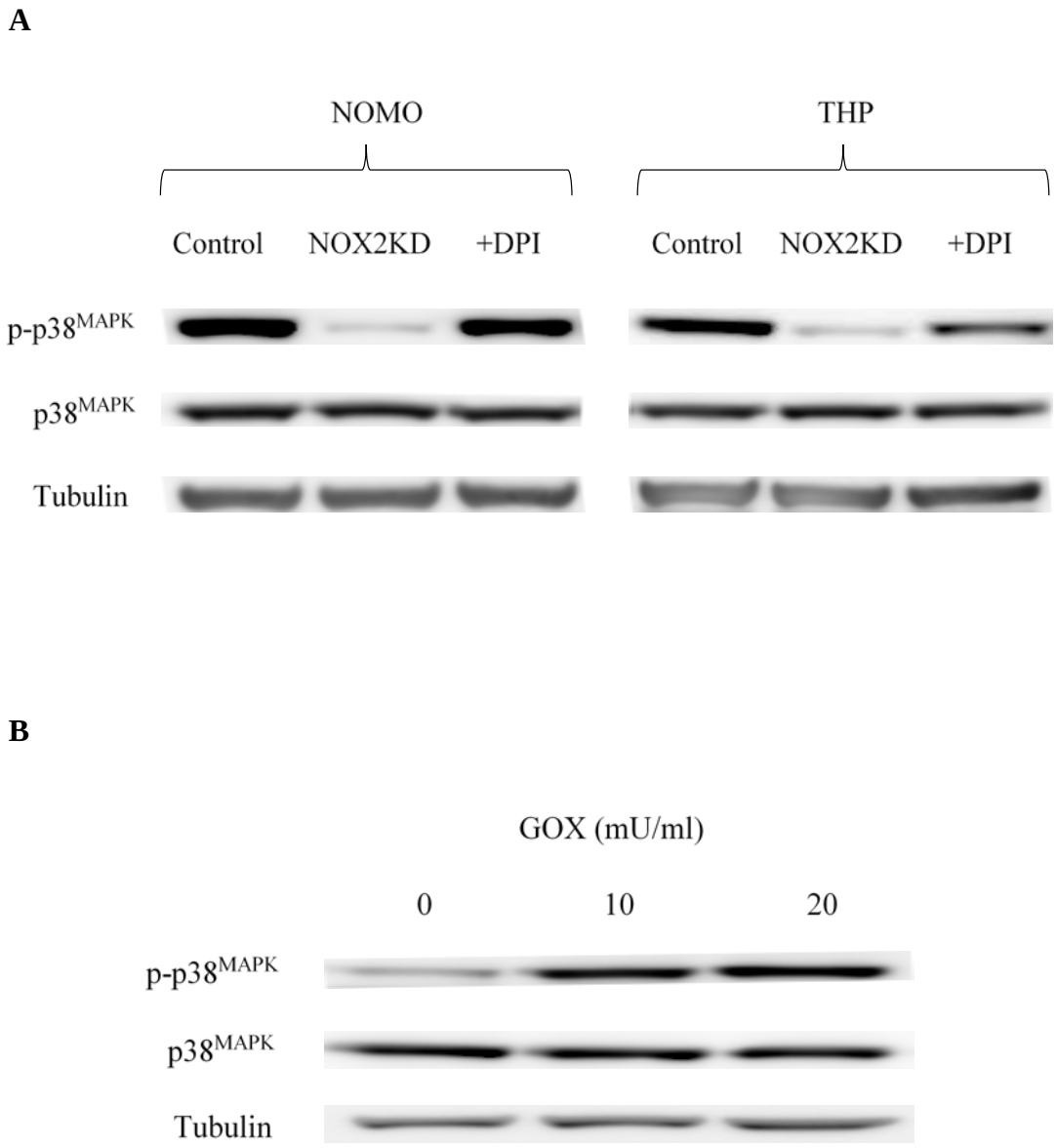

Figure 3-12. AML cell lines exhibit ROS induced stress response of p38^{MAPK} pathway. AML cell lines were incubated for 24h under the conditions described. Expression and phosphorylation state of p38^{MAPK} was determined by western blot using whole cell lysates derived from these cells and probed with antibodies recognising p-p38^{MAPK} and p38^{MAPK} in **(A)** NOMOSH and THPSH control cells, compared with NOMO NOX2 KD and THP NOX2 KD cells and NOMOSH and THPSH incubated in the presence and absence of DPI (100nM) and **(B)** Mv4;11 cells treated with GOX. Tubulin was used as a loading control.

3.3.3.2 ROS promotes glucose uptake in AML cell lines

To investigate further the impact that ROS has on glycolysis in AML, cellular glucose uptake in the THP and NOMO cell lines, was measured using 2-NBDG. Glucose uptake levels in these cells were then compared with the glucose uptake of cells in which NOX2 had been knocked-down using shRNA, or chemically inhibited. To ensure that knock-down of NOX2 or treatment with chemical inhibitors did not affect cell viability, cells were stained with 7-aminoactinomycin D (7-AAD) and analysed by flow cytometry. Figure 3-13 shows that knock-down of NOX2 with shRNA or chemical inhibition did not impact on the viability of THP or NOMO cells. This suggests that any changes in glucose uptake in the cells were a result of experimentally controlled variables and not the viability of the cells.

Knock-down of NOX2 in THP cells showed a significant 1.5-fold decrease in cellular glucose uptake compared to control. Pharmacological inhibition with DPI, VAS-2870 and GSK-NOX2 also resulted in significant 4-fold, 1.2-fold and 1.2-fold respective decreases, in glucose uptake compared to control (Figure 3-14A). In NOMO cells, NOX2 knock-down generated a significant 1.3-fold decrease in glucose uptake, whilst treatment with DPI resulted in a significant 1.6-fold decrease in glucose uptake (Figure 3-14B). These results show that decreases in the levels of extracellular ROS experienced by these cell lines results in decreases in cellular glucose uptake and that NOX2 generated ROS is, in part, responsible for changes in these levels of glucose consumption.

Given that cellular glucose uptake can be decreased by inhibition of extracellular ROS, it was reasoned that increasing levels of exogenous ROS would result in an increase in glucose uptake. To test this, Mv4;11 cells were treated with different concentrations of GOX (hence H_2O_2) and the amount of cellular glucose uptake measured, as above, using 2-NBDG. To test whether GOX did not affect the viability of the cells, treated cells were incubated with 7-AAD, analysed by flow cytometry and compared with control. No changes in cell viability was observed in the cells treated with GOX compared for control (Figure 3-15A). Treatment of the Mv4;11 cells with 10mU/ml and 20mU/ml of GOX resulted in a significant 1.2-fold and 1.3-fold increase in glucose uptake respectively (Figure 3-15B). These data show that

increased extracellular H_2O_2 levels result in an increase in glucose uptake in the Mv4;11 cell line.

Together, these data demonstrate that ROS is an important mediator of glucose uptake in these AML cell lines and that NOX2 generated ROS is an important contributor to these changes.

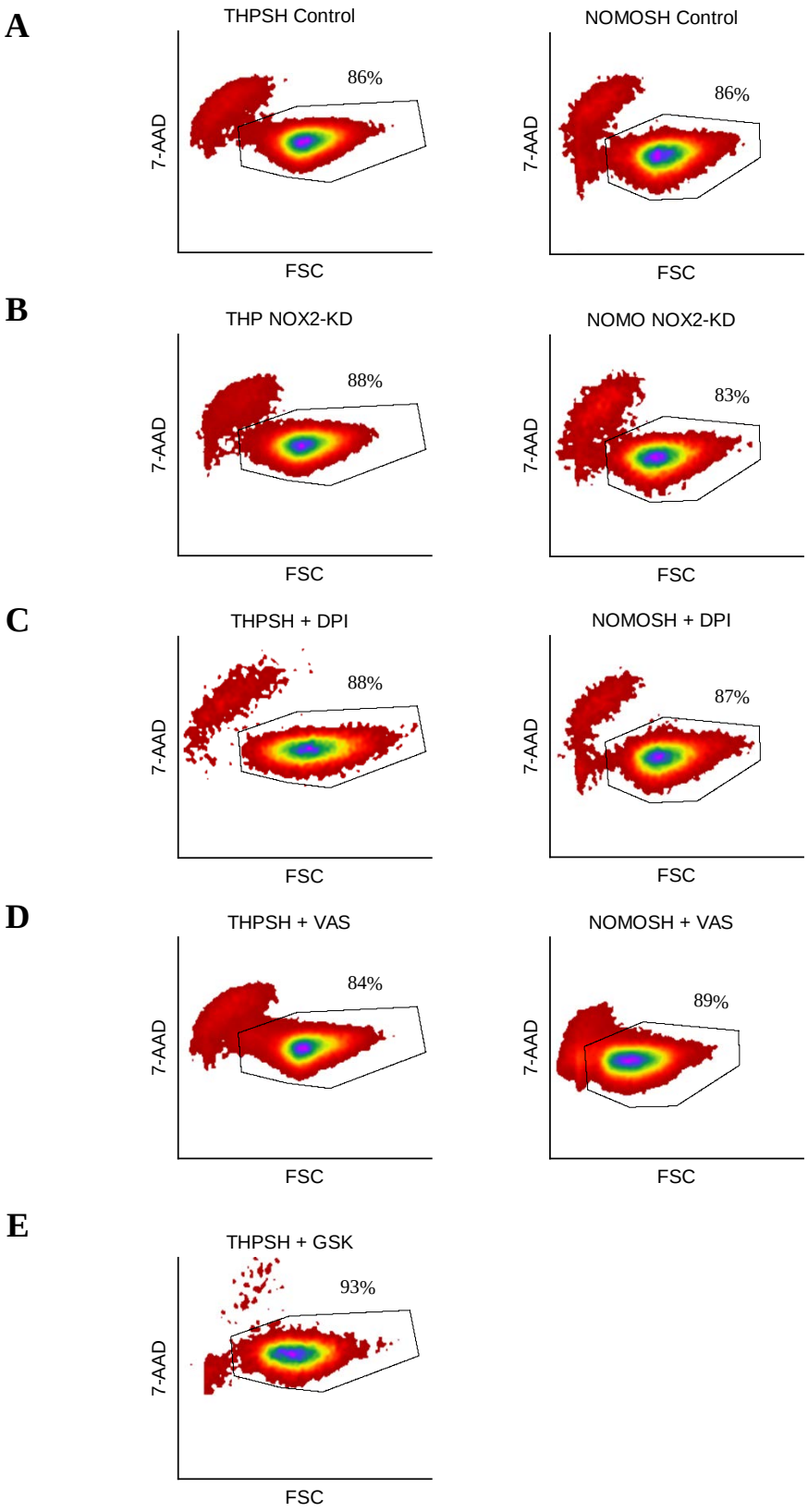

Figure 3-13. Viability of THP-1 and NOMO-1 cells. Representative flow cytometric density plots showing percentage of viable THP and NOMO cells infected with **(A)** shRNA control, **(B)** NOX2KD shRNA; or control cells treated with **(C)** DPI (100nM) **(D)** VAS-2870 (5µM) **(E)** GSK-NOX2 (3µM) (THP only) and cultured for 24h, in the presence/absence of inhibitors, (initial seeding 5 x 10^5 cells/ml). Data were gated to exclude cell debris based on FSC/SSC. Cells were incubated with 7-AAD, gated areas show proportion of viable cells.

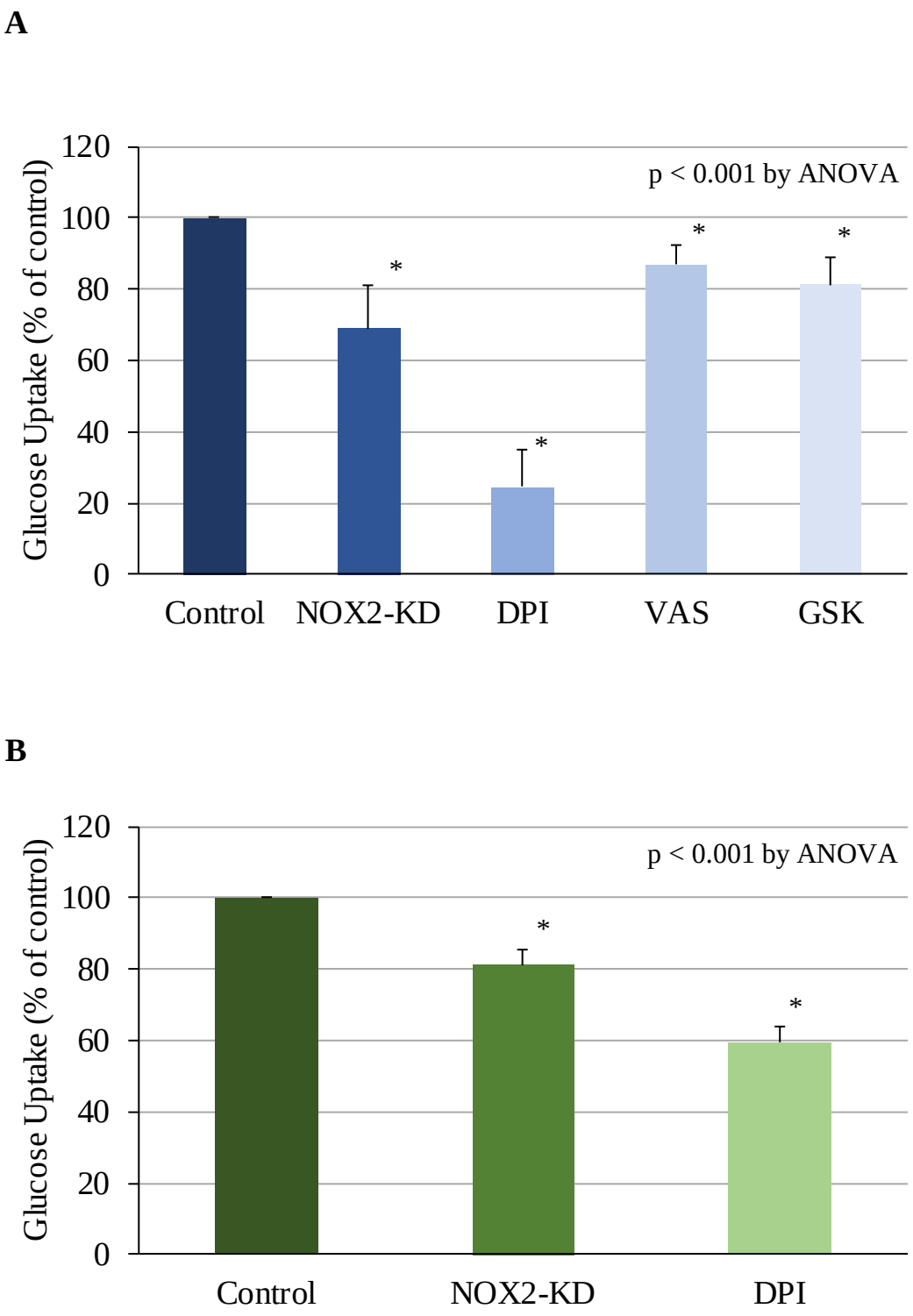

Figure 3-14. NOX derived ROS induced changes in glucose uptake in ROS generating AML cell lines. Cellular glucose uptake (normalised to control). **(A)** THP; control (non-mammalian encoding shRNA) (dark blue), NOX2-KD (blue), treated with DPI (100nM) (mid blue), VAS-2870 (5μM) (light blue) GSK-NOX2 (3μM) (pale blue) (n≥3). **(B)** NOMO; control (non-mammalian encoding shRNA) (dark green), NOX2-KD (green), treated with DPI (100nM) (mid green) (n≥3). Cells were seeded at 5 x 10^5 cells/ml and cultured for 24h, in the presence/absence of inhibitors. Data represents mean ± 1SD. * denotes $p<0.05$ analysed by ANOVA with Tukey's honestly significance difference.

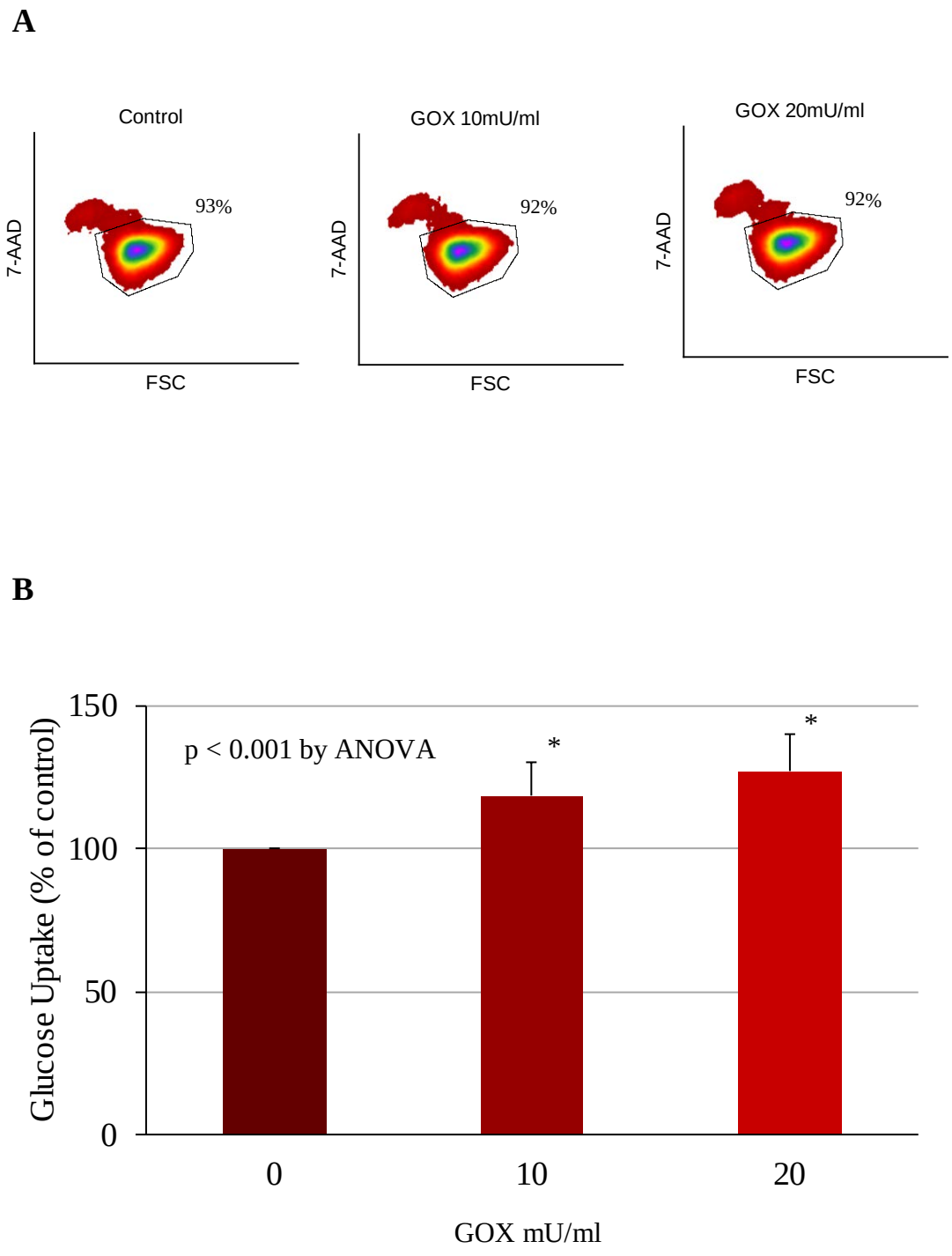

Figure 3-15. Exogenous ROS induced changes in glucose uptake in the AML derived cell line Mv4;11. (A). Representative flow cytometric density plots showing percentage of viable GOX treated (10mU/ml and 20mU/ml) Mv4;11 cells compared for untreated control. Data were gated to exclude cell debris based on FSC/SSC. Cells were incubated with 7-AAD, gated area shows proportion of viable cells. **(B)** Cellular glucose uptake (normalised to control) of Mv4;11 cells treated with GOX. Cells were seeded at 5 x 10^5 cells/ml and cultured for 24h in the presence/absence of GOX ($n \geq 17$). Data represents mean ± 1SD. * denotes $p<0.05$ analysed by ANOVA with Tukey's honestly significance difference.

3.3.3.3 ROS affects extracellular lactate production in AML cell lines

To examine whether these ROS induced changes in glucose uptake in AML cell lines occurred contiguously with changes in extracellular lactate production, cells were cultured as in 3.3.3.2, and the levels of lactate in the culture media assayed as above (3.3.1.3).

Figure 3-16A shows that THP cells with NOX2 knocked-down showed a 2.4-fold increase in extracellular lactate production compared with control. Knock-down of NOX2 in NOMO cells resulted in 1.3-fold increase in extracellular lactate compared to control, whilst treatment with the NOX inhibitor VAS-2870 generated a 1.7-fold increase (Figure 3-16B). These results suggest that inhibition of NOX2 generated ROS, result in an increase in the production of extracellular lactate. This ROS dependent increase in extracellular lactate, alongside decreases in glucose uptake, whilst unexpected, agree with the ROS induced changes observed in extracellular lactate production in HPC (3.3.2.3).

In THP and NOMO cells decreases in ROS lead to decreases in cellular glucose uptake, whilst simultaneously increasing extracellular lactate production. To test the effect of increases in levels of exogenous ROS on AML cell lines Mv4;11 cells were cultured and treated with GOX, as in 3.3.3.2, and the concentration of lactate in the culture supernatant assayed as above. Surprisingly, treatment with 10mU/ml of GOX resulted in a 1.3-fold increase in extracellular lactate production, whilst treatment with 20mU/ml of GOX caused a 1.6-fold increase (Figure 3-16C). In the context of Mv4;11 cells, increases in ROS lead to increases in both cellular glucose uptake (Figure 3-15B) and extracellular lactate levels (Figure 3-16C) which emulate the mutant RAS induced changes observed in HPC (Figure 3-4).

Paradoxically, these data, together with the data generated from the HPC model, suggests that whilst ROS alters extracellular lactate secretion, in an AML context it may not do so in a manner consistent with the Warburg effect. Instead, from a ROS perspective, it appears that changes in extracellular lactate production are likely both cell and context dependent (3.4).

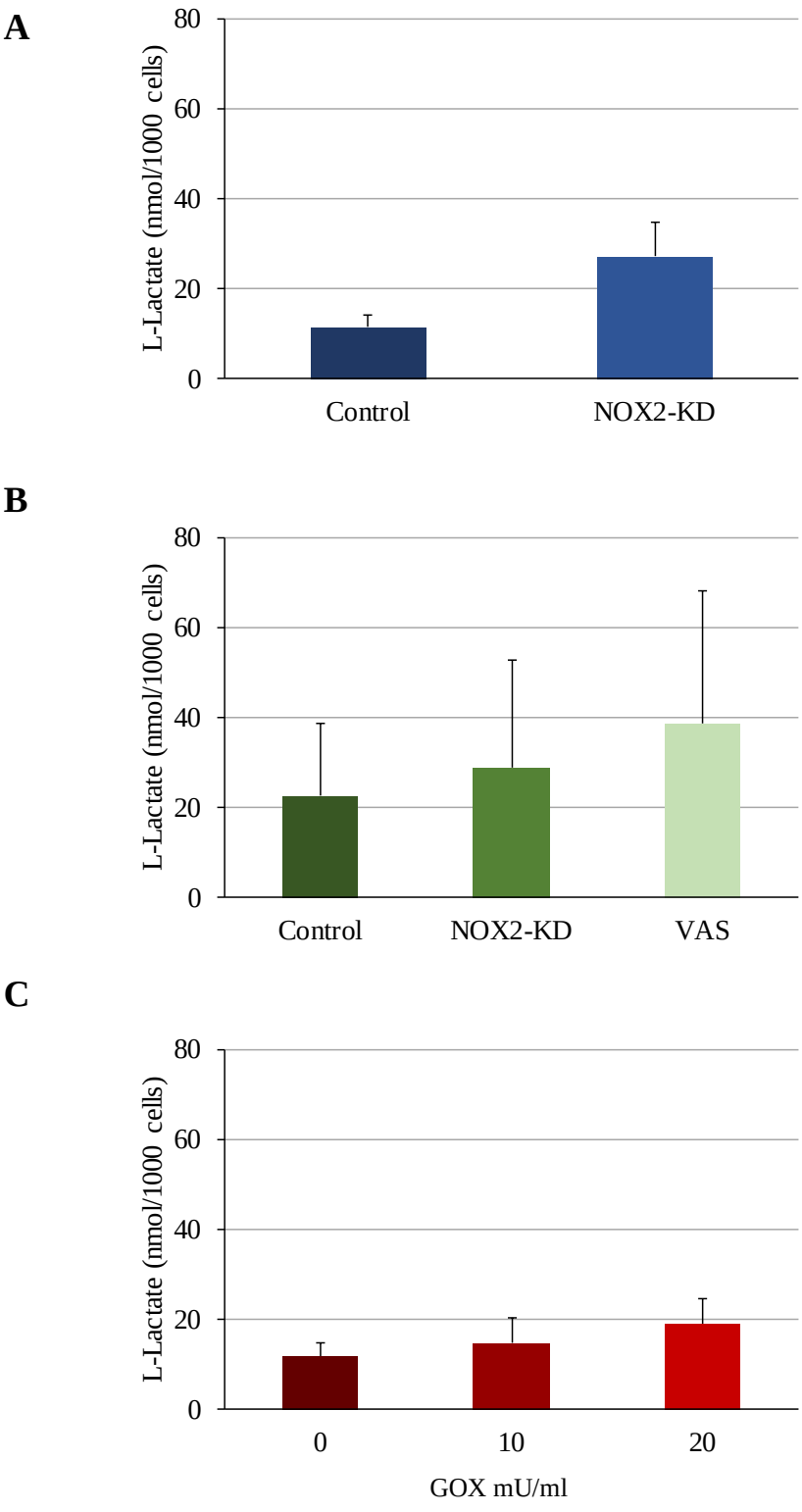

Figure 3-16. ROS induced changes in extracellular lactate production in AML derived cell lines. Concentration of extracellular L-lactate in the culture media of AML cell lines **(A)** THP; control (non-mammalian encoding shRNA) (dark blue), NOX2-KD (blue) (n=3) **(B)** NOMO; control (non-mammalian encoding shRNA) (dark green), NOX2-KD (green), treated with VAS (5µM) (light green) (n=6). **(C)** Mv4;11 cells treated with GOX (n=3). Cells were seeded at 5 x 10^5 cells/ml and cultured for 24h, in the presence/absence of inhibitors/GOX. Data represents mean ± 1SD.

3.3.3.4 ROS promotes proliferation in AML cell lines

It has previously been reported that elevated ROS levels, lead to proliferative increases in both AML blasts and the AML cell lines Mv4;11 and KG-1 (Hole *et al.*, 2013). To examine whether these ROS dependent changes were also observed in the THP-1 and NOMO-1 cell lines, cells cultured as in 3.3.3.2 were counted by both haemocytometer and flow cytometry.

Knock-down of NOX2 in THP cells resulted in a significant 1.3-fold decrease in proliferation compared to control. Pharmacological inhibition with DPI or VAS-2870, resulted in a 1.2-fold and 1.1-fold decrease respectively. Interestingly treatment with GSK-NOX2 had no effect on proliferation (Figure 3-17A), although it is worth noting that whilst, at these concentrations, this compound works well in *in vitro* assays of superoxide production, its longer-term stability under culture conditions has not been demonstrated. Knock-down of NOX2 in NOMO cells resulted in a significant 1.2-fold decrease in proliferation compared to control. Treatment with DPI resulted in a significant 1.3-fold decrease, whilst treatment with VAS-2870 yielded a 1.2-fold decrease in proliferation compared to control, although this did not reach significance (Figure 3-17B). These data show that in these AML cell lines, NOX2 derived ROS can promote the proliferative rate of these cells.

To examine whether the addition of exogenous ROS would lead to an increase in proliferation, Mv4;11 cells were treated with GOX. Figure 3-17C shows that Mv4;11 cells experienced a significant 1.5-fold and 1.4-fold increase in proliferation, when treated with 10mU/ml and 20mU/ml of GOX respectively. This shows that increases in exogenous ROS in the Mv4;11 cell line result in increases in proliferation of these cells.

Taken together these data shows that, in AML cell lines, levels of extracellular ROS influence the proliferative rate of these cells.

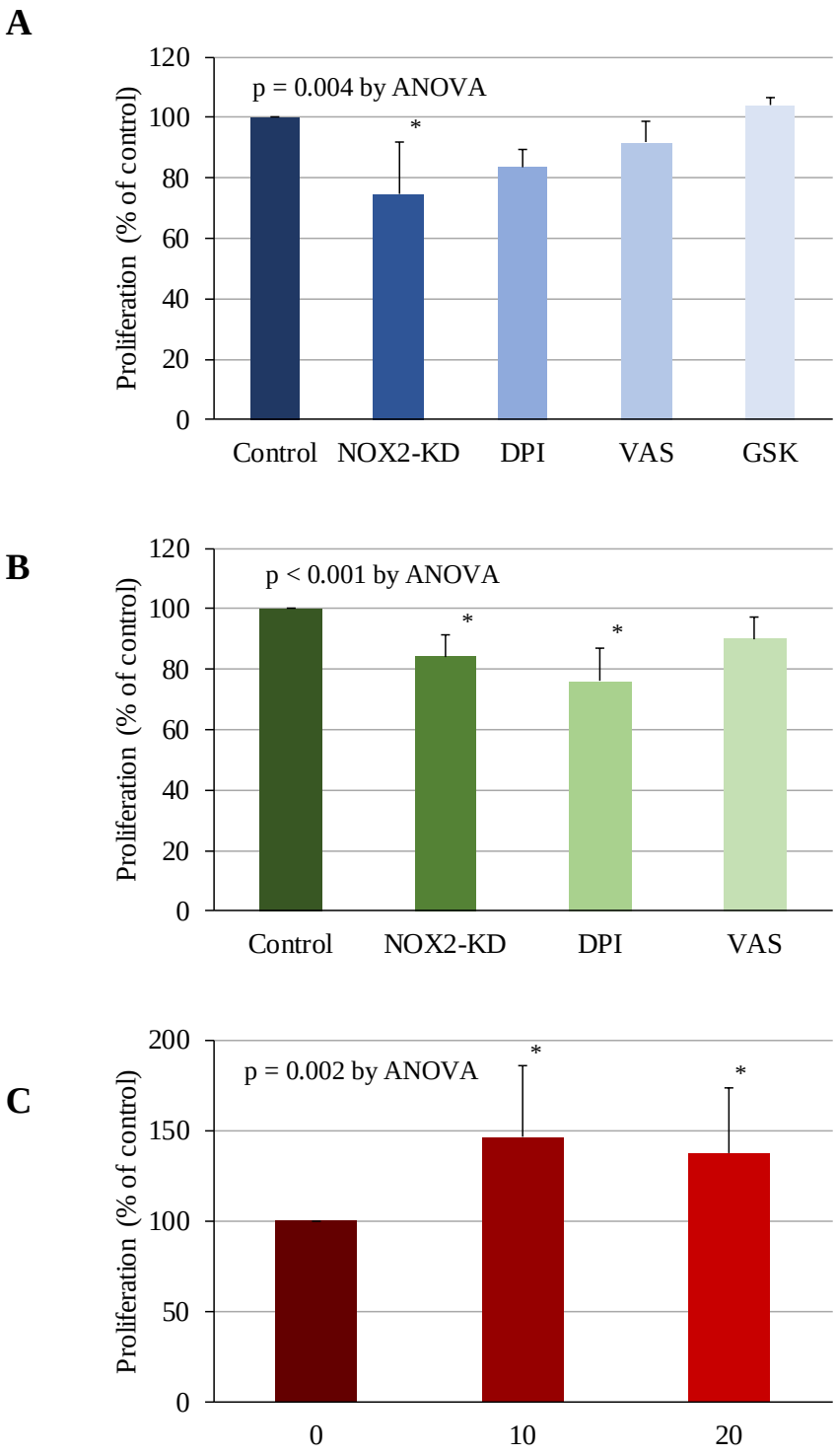

Figure 3-17. ROS promotes proliferation in AML-derived cell lines. Percentage proliferative change (normalised to control) in the AML cell lines **(A)** THP; control (non-mammalian encoding shRNA) (dark blue), NOX2-KD (blue), treated with DPI (100nM) (mid blue), VAS-2870 (5µM) (light blue) GSK-NOX2 (3µM) (pale blue) (n≥3). **(B)** NOMO; control (non-mammalian encoding shRNA) (dark green), NOX2-KD (green), treated with DPI (100nM) (mid green); VAS-2870 (5µM) (light green) (n≥3). **(C)** Mv4;11 cells treated with GOX (n≥6). Cells were seeded at 5 x 10^5 cells/ml and cultured for 24h, in the presence/absence of inhibitors/GOX. Data represents mean ± 1SD. * denotes $p<0.05$, analysed by ANOVA with Tukey's honestly significance difference.

3.4 Discussion

The data presented in this chapter indicates that both mutant RAS and NOX2 derived ROS impact on glycolysis. Specifically, mutant RAS expressing HPC showed increases in both glucose uptake and lactate secretion compared to normal HPC and murine N-RAS^{12D} HPC also showed elevated levels of glucose uptake compared to control. Inhibition of NOX2 in these cells with DPI or VAS-2870, resulted in a decrease in both glucose uptake and proliferation. Surprisingly, increased lactate secretion was observed in mutant RAS expressing HPC treated with DPI, whilst no changes were observed in HPC treated with VAS-2870. Additionally, two AML derived cell lines generating NOX2 derived ROS showed decreased glucose uptake and proliferation upon knock-down or chemical inhibition of NOX2, although lactate secretion was increased. Finally, the addition of exogenous ROS to the AML derived cell line Mv4;11, resulted in increased glucose uptake, lactate secretion and proliferation. The data presented is summarised in Table 5.

Mutational RAS activation accounts for approximately 15-30% of AML cases (reviewed in Naoe and Kiyoi, 2013) and oncogenic *RAS* is widely reported to be linked to increases in glycolysis, though little is known in the context of AML. Specifically, Racker *et al.*, 1985 were the first to show, that rat cells transfected with oncogenic RAS showed a 6-fold increase in lactate production compared to control. More recently Zheng *et al.*, 2015 reported a 2.4-fold increase in intracellular lactate levels in human breast epithelial cells transformed with the H-RAS oncogene. Mechanistically, RAS is known to stabilise c-MYC and HIF-1α and activate the PI3K/AKT pathway, all of which have been associated with increased expression of glycolytic enzymes and increased glycolytic flux (reviewed in Chesney and Telang, 2013). Studies examining glycolytic rate in AML are relatively scarce. A very small study involving 23 patient samples suggested high glycolytic metabolism correlated with an increased overall survival rate, all be it with increased drug resistance (Herst *et al.*, 2011). However, a recent, larger, metabolomic study of 400 AML patients compared with 446 healthy controls, identified elevated levels of the glycolytic intermediates 3-phosphoglycerate, pyruvate and lactate as conferring a poor prognosis for survival (Chen *et al.*, 2014).

Table 5. Summary of data presented in chapter 3. Table shows a summary of the changes in glucose uptake, lactate secretion and proliferation of human haematopoietic progenitor cells (HPC) infected with mutant RAS, murine bone marrow (BM) cells and AML cell lines compared with appropriate control cells, as presented in chapter 3. * represents data that showed significant changes compared to controls. n/a indicates that this data was not measured. Details of individual test conditions and the statistical analysis can be found in the appropriate results section of the chapter. Mutational status of RAS in NOMO-1, THP-1 and Mv4;11 was obtained from the Catalogue of Somatic Mutations in Cancer **http://cancer.sanger.ac.uk/cell_lines/gene/analysis?**

Cell	RAS mutation	Treatment	Glucose Uptake	Lactate Secretion	Proliferation
Human HPC	N-RAS^{G12D}	None	Increased	Increased	n/a
	H-RAS^{G12V}	None	Increased*	Increased*	n/a
Murine BM cell	N-RAS^{12D}	None	Increased	n/a	n/a
Human HPC	None	DPI	Unchanged	Increased	Unchanged
		VAS-2870	Unchanged	Unchanged	Unchanged
		GSK-NOX2	Unchanged	n/a	n/a
	N-RAS^{G12D}	DPI	Unchanged	Increased	Decreased
		VAS-2870	Decreased*	Unchanged	Decreased
		GSK-NOX2	Decreased*	n/a	n/a
NOMO-1	K-RAS^{G13D}	NOX2-KD	Decreased*	Increased	Decreased*
		DPI	Decreased*	n/a	Decreased*
		VAS	n/a	n/a	Decreased
THP-1	N-RAS^{G12D}	NOX2-KD	Decreased*	Increased	Decreased*
		DPI	Decreased*	n/a	Decreased
		VAS	Decreased*	Increased	Decreased
		GSK-NOX2	Decreased*	n/a	Unchanged
Mv4;11	None	GOX (10mU/ml)	Increased*	Increased	Increased*
		GOX (20mU/ml)	Increased*	Increased	Increased*

Previous work in our group suggests that mutant RAS expressing HPC's are decoupled from normal proliferative regulatory mechanisms, exhibiting elevated growth factor independent survival and proliferation compared with normal human HPC (Hole *et al.*, 2010). Data presented here shows that overexpression of mutant RAS in HPC also leads to changes in the glycolytic function of these cells, with both cellular glucose uptake (3.3.1.2) and lactate secretion (3.3.1.3) significantly increased, consistent with the Warburg effect. This suggests a correlation between increased aerobic glycolysis in mutant RAS expressing HPC and an increased proliferative rate in these cells.

In support of this, the increase in the proliferative rate of mutant RAS expressing HPC described above (Hole *et al.*, 2010) was found to be linked to increases in NOX2-derived ROS and data presented here show that increased levels of ROS result in increased proliferation and glucose uptake in HPC expressing mutant RAS. Specifically, treatment of both N-RAS^{G12D} and H-RAS^{G12V} with a panel of NOX inhibitors resulted in decreased proliferation (3.3.2.4) and decreased glucose uptake in all cases (3.3.2.2). Additionally, in the ROS generating AML cell lines investigated, chemical inhibition or NOX2 knock-down with shRNA also resulted in significant decreases in proliferation (3.3.3.4) and cellular glucose uptake (3.3.3.2), whilst treatment of Mv4;11 cells (which do not generate significant levels of NOX2 derived ROS) with exogenous ROS instigated significant increases in proliferation (3.3.3.4) and cellular glucose uptake (3.3.3.2). In support of this role for NOX derived ROS as a modulator of glycolytic activity NOX activated ROS production has been reported to increase glucose transporter-1 activity in leukaemic cell lines (Prata *et al.*, 2008). Further, a recent study (Zeng *et al.*, 2016) reported that NOX4 generated ROS promoted glycolysis, glutaminolysis and increased pentose phosphate pathway (PPP) activity in non-small cell lung cancer cell lines. Additionally, Hole *et al.*, 2013 reported that over 60% of AML patient blasts showed increased levels of ROS, which correlated with increased proliferation in these cells. Overall, data presented here and elsewhere, is congruent with the hypothesis that elevated ROS increases glucose uptake which generates an increased proliferative rate.

Interestingly however, whilst elevated ROS led to increases in cellular glucose uptake corresponding increases in extracellular lactate were only observed in the

GOX treated Mv4;11 cells (3.3.3.3). Chemical inhibition of NOX2 in mutant RAS expressing HPC showed elevated levels of lactate secretion upon treatment with DPI, whilst treatment with VAS-2870 showed no significant effect (3.3.2.3). It is recognised that at micro-molar concentrations, DPI inhibits not only NOX but also mitochondrial respiration through the inhibition of NAPDH cytochrome P450 oxidoreductase, as well as, nitric oxide synthase, and xanthine oxidase (reviewed in Aldieri *et al.*, 2008). Additionally, it has been reported (Riganti *et al.*, 2004), that DPI inhibits not only the citric acid cycle but also the PPP, the first step of which regenerates NADPH, an important reducing agent for ROS. Inhibition of the citric acid cycle could potentially explain increases in extracellular lactate as an accumulation of pyruvate (the final product of glycolysis) would also generate proportional increases in the concentration of intracellular lactate. Similarly, the PPP offers an alternative pathway by which glucose may be metabolised and its inhibition would potentially also lead to an accumulation of pyruvate and *de facto*, lactate. However, this DPI inhibition of the PPP and of mitochondrial respiration was instigated at micro-molar concentrations of DPI and a recent study (Bulua *et al.*, 2011) suggests that at nano-molar concentrations (comparable with those used in this study), inhibition of NOX but not mitochondrial respiration is observed. Nonetheless, whilst off-target effects of DPI (4.4.1.1) offer one plausible explanation for increased lactate secretion, apparent ROS dependent increases in extracellular lactate secretion observed in AML cell lines treated with VAS-2870 or with NOX2 genetically knocked-down (3.3.3.3), suggest other potential rationale for these results.

One hypothesis for the observed changes in lactate secretion involve the enzyme pyruvate kinase. Lactate is generated because of enzymatic conversion of phosphoenolpyruvate to pyruvate by pyruvate kinase followed by its subsequent conversion to lactate by lactate dehydrogenase A (1.4.3); and both its production and transport are subject to several regulatory mechanisms. Whilst lactate production is increased in many cancers as a result of the upregulation of the M2 isoform of pyruvate kinase (PKM2) (Tamada *et al.*, 2012) and activation of HIF-1 α (Luo *et al.*, 2011), ROS promotes dissociation of PKM2 from its active tetrameric form to an inactive dimeric form (Anastasiou *et al.*, 2011). This results in the accumulation of phosphoenolpyruvate and other glycolytic intermediates and a reduction in lactate

production. Increased tetrameric PKM2 as result of decreased ROS via chemical inhibition or NOX2 knock-down, could then potentially explain the lactate increases observed above.

An alternative hypothesis that explains the decoupling of ROS induced increases in glucose uptake from lactate secretion, involves the recycling of lactate to generate increased NADPH. The anti-oxidant capacity of cells is partly dependent on the glutathione and thioredoxin systems (1.3.2.4) which requires the donation of electrons from nicotinamide adenine dinucleotide (NADH) or nicotinamide adenine dinucleotide phosphate (NADPH) for its antioxidant effect (reviewed in Hole *et al.*, 2011). An important mechanism for re-generating NADPH is via the conversion of glucose-6-phosphate to 6-phosphogluconolactone, the first step of the PPP (1.4.4). Additionally the PPP is an important metabolic pathway for generating nucleotides for biosynthesis and is known to be dysregulated in a number of cancers (reviewed in (Patra and Hay, 2014). Given the correlation between ROS and proliferation observed above (3.3.2.4 and 3.3.3.4) it is conceivable that lactate rather than being transported out of the cell could instead be diverted into the PPP, resulting in a negative correlation between ROS and lactate secretion.

Regardless of the mechanism by which these ROS induced changes in lactate secretion occur, taken together with the observed changes in glucose uptake and proliferation, it appears that changes in cellular ROS levels are an important feature in modulating glycolytic function in both mutant RAS expressing HPC and in AML cell lines. Given that changes in glycolytic metabolism have been reported in AML patients (Herst *et al.*, 2011, Chen *et al.*, 2014), the next chapter examines changes in the expression of glycolytic genes and the levels of glycolytic metabolites because of ROS modulation in order to determine the mechanisms by which these changes occur.

4 Determination of the effect of ROS on glycolytic gene expression and glycolytic metabolites

4.1 Introduction

Having observed functional changes in glycolysis as a result of the expression of mutant *RAS* and/or exposure to increased levels of exogenous ROS, it was postulated that modulation of expression or activity of a number of enzymatic proteins involved in carbohydrate metabolism may explain this phenomenon. In support of this, previous transcriptome analysis Hopkins *et al.*, 2014 showed significant ROS induced changes in global messenger RNA (mRNA) levels using the HPC model. More specifically, Metacore^{TM} pathway analysis of these data identified glycolysis as the most dysregulated pathway (Hopkins, 2014). It is well established that glycolysis is dysregulated in many solid cancers and nearly all the enzymes in the glycolytic pathway have been implicated in this dysregulation (reviewed in Hu *et al.*, 2014). Haematological malignancies by contrast are less well studied. A study by Ryland *et al.*, 2013 showed increased expression of glyceraldehyde phosphate dehydrogenase (GAPDH) in chronic lymphocytic leukaemia patients compared to healthy controls; increased glycogen synthase has been reported in AML patients (Bhanot *et al.*, 2015); and most recently increased mRNA levels of glucose transporter 1 (GLUT1), hexokinase II (HK2) and HIF1-α were reported in AML patients who did not enter remission following treatment compared to both healthy controls and those showing complete remission (Song *et al.*, 2016). However, within an AML context, no studies on the effect of ROS on glycolytic gene expression have been reported. Therefore, this chapter examines changes in glycolytic enzyme expression in mutant RAS expressing HPC, with specific focus on ROS induced changes and using whole cell metabolomics to explore ROS modulated changes in metabolite concentration.

4.2 Aims and objectives

The main objective of this chapter is to determine the effect of NOX2-derived ROS on mRNA and protein expression levels of glycolytic enzymes and resultant changes in the relative abundancies of key carbohydrate metabolites. To achieve this, this chapter has the following aims:-

- To determine the effect of ROS on mRNA levels of glycolytic enzymes. A supervised analysis, specifically focussing on glycolytic enzymes, of the previously generated microarray data (Hopkins *et al.*, 2014) will be performed to identify any significant changes in mRNA expression.
- To determine the effect of ROS on protein expression levels of glycolytic enzymes in human HPC expressing mutant RAS. Western blots will be performed on cell lysates of mutant RAS expressing HPC, both untreated and treated with DPI and compared to control HPC.
- To determine the effect of ROS on protein expression levels of glycolytic enzymes in AML cell lines. Western blots will be performed on cell lysates of ROS generating cell lines in which NOX2 has been inhibited or knocked-down, and compared with control. Additionally, western blots will be performed on cell lysates of Mv4;11 cells subjected to increased exogenous ROS levels, to determine any changes in protein expression of glycolytic enzymes.
- To determine ROS-induced changes in key carbohydrate metabolite levels. ROS generating AML cell lines with NOX2 inhibited or knocked-down and Mv4;11 cells subjected to increased exogenous ROS (and controls) will be sent to Metabolon^{TM} for ultra-performance liquid chromatography-tandem mass spectrometry (UPLC-MS/MS) analysis for global metabolite quantitation. Additionally, MS will be employed to identify significant ROS induced changes in metabolite concentrations of AML patient blasts characterised as low/high ROS producers.

4.3 Results

4.3.1 Mutant RAS and ROS induce changes in mRNA expression of genes involved in carbohydrate metabolism in human HPC

Previous work in our laboratory, employing Affymetrix Genechip® whole transcriptome microarray coupled with an unsupervised analytical approach on the Core Probe set list[1] has shown significant ROS dependent changes in mRNA expression of human HPC expressing mutant N-RAS (N-RAS^{G12D}) compared with control HPC (Hopkins *et al.*, 2014). Further, Metacore^{TM} pathway analysis of these changes identified glycolysis as the most dysregulated pathway. To refine the analysis and identify which glycolytic enzymes showed significant changes in mRNA expression, a supervised approach (focussing on enzymes involved in carbohydrate metabolism), using the full extended probe set[2] of the above microarray data was performed. To achieve this, gene expression profiling data was analysed using Partek Genomics Suite software (ver. 6.6, Partek Inc., USA). Raw data files were imported using Affymetrix annotation files and Robust Multi-Array analysis algorithm was used for background correction, normalisation and median polishing (to remove chip effect); $\log_2$ data transformation was then performed (see methods for full details, 2.10). Figure 4-1 shows the glycolytic enzymes whose mRNA expression significantly changed in N-RAS^{G12D} compared to control and N-RAS^{G12D} treated with DPI compared with the untreated N-RAS^{G12D} cells; but which were not significant for control HPC treated with DPI compared with untreated control. As shown in Figure 4-2 the relative mRNA expression levels of these enzymes for each condition, is represented in box plots. These data show that several glycolytic genes have a ROS-dependent change in their mRNA expression.

[1] Core probe set list refers to probes validated from RefSeq database containing complete coding sequence information.
[2] Full probe set list refers to probes supported by exon prediction algorithms including GeneID, GenScan, Exoniphy, RNAGene, spgGene and Twinscan.

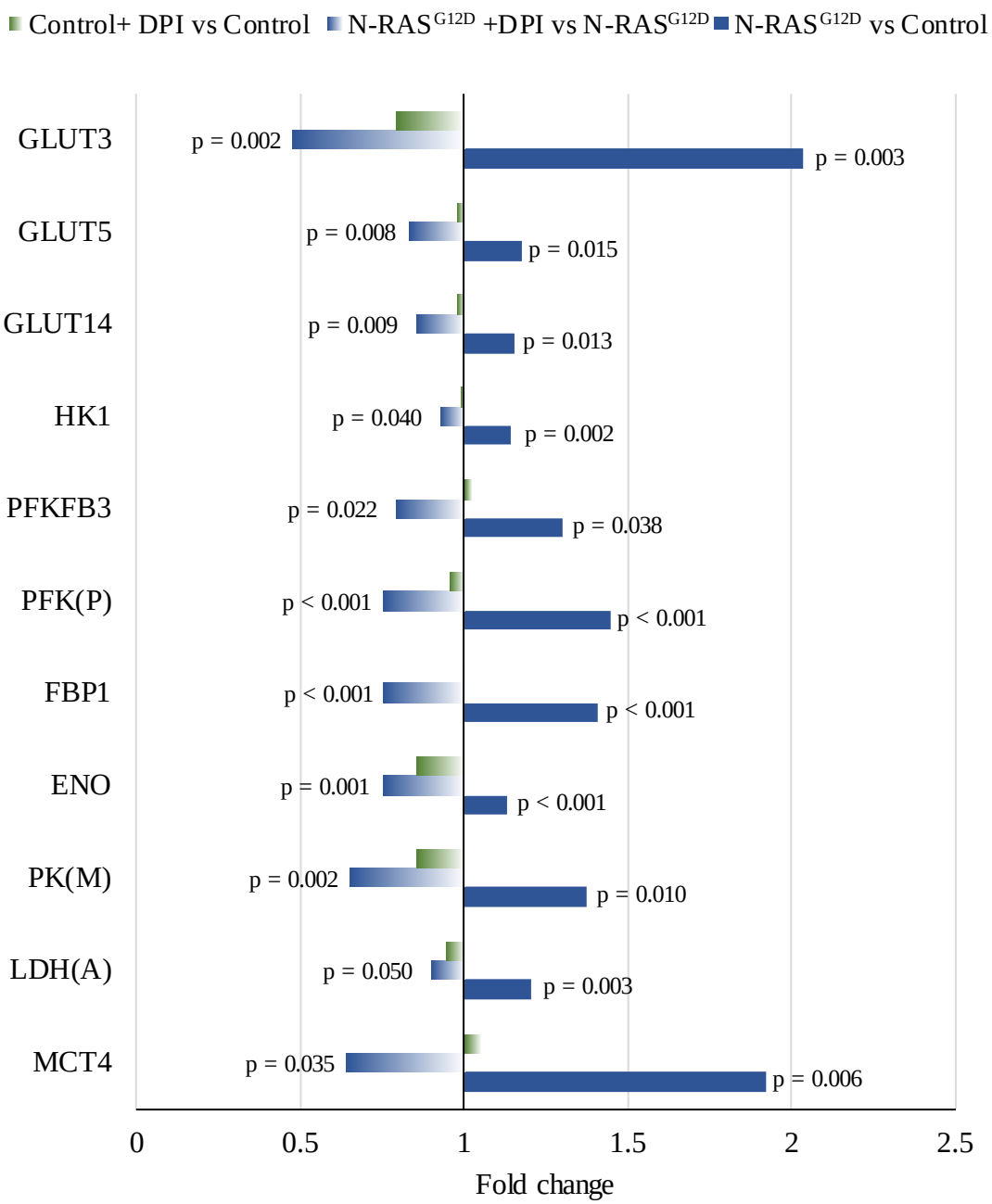

Figure 4-1. ROS dependent fold changes in mRNA expression of glycolytic enzymes in human HPC. Fold changes in mRNA expression for N-RAS^{G12D} transduced HPC compared to control HPC (blue), N-RAS^{G12D} HPC treated with DPI (100nM) compared to untreated N-RAS^{G12D} (blue gradient) and control HPC treated with DPI (100nM) compared for untreated control HPC (green gradient). DPI treatment occurred for 24 h at 37ºC, 5% CO_2. GLUT3 (glucose transporter 3), GLUT5 (glucose transporter 5), GLUT14 (glucose transporter 14), HK1 (hexokinase 1), PFKFB3 (6-phosphofructo-2-kinase/fructose-2,6-biphosphatase 3), PFK(P) (phosphofructokinase platelet), FBP1 (fructose-1,6-bisphosphatase 1), ENO **(**enolase), PK(M) (pyruvate kinase muscle), LDH(A) (lactate dehydrogenase A), MCT4 (monocarboxylate transporter 4). Data represents mean fold change of n=4; p-value calculated by 2-way ANOVA with Benjamini-Hochberg multiple testing correction (see methods).

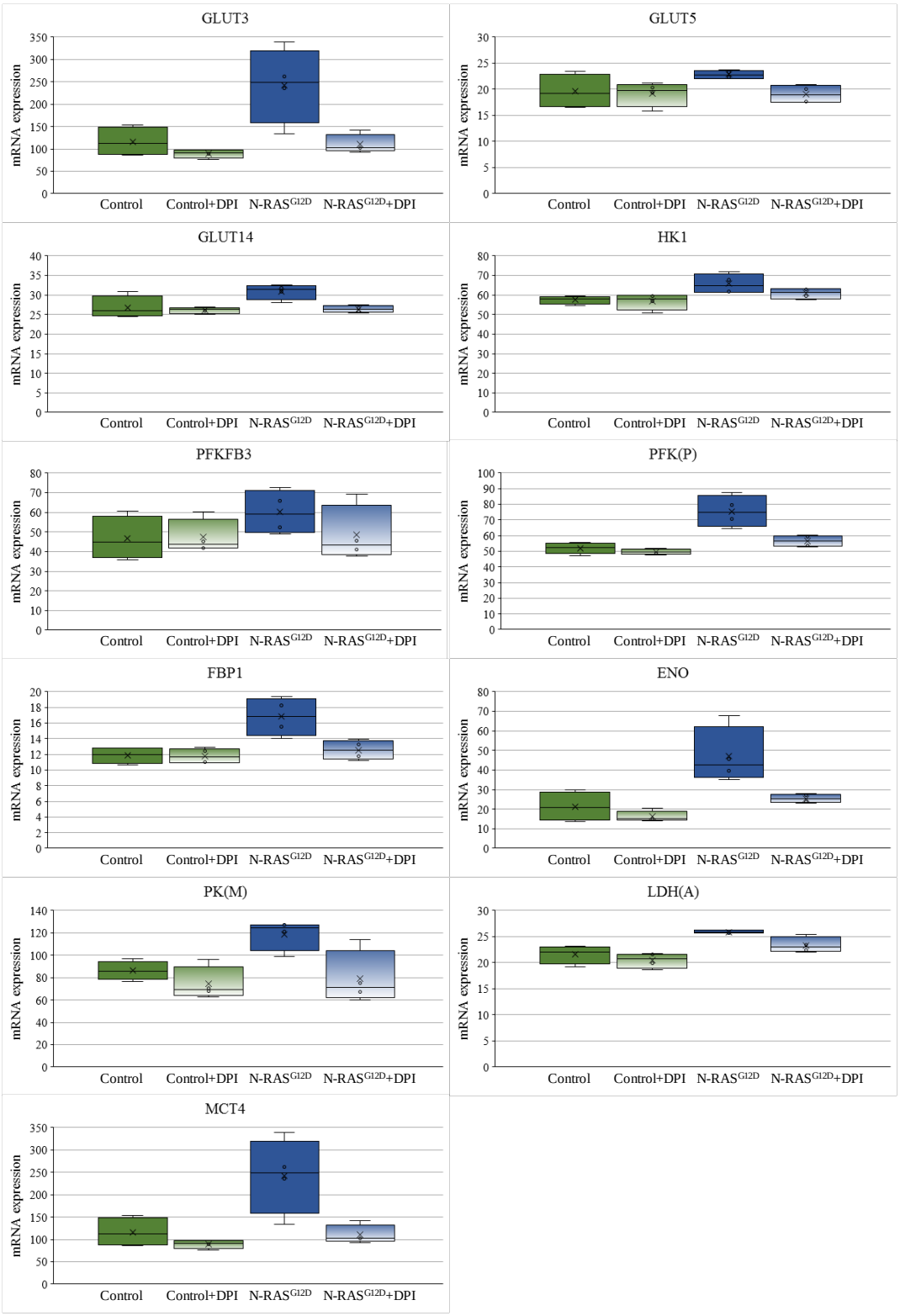

Figure 4-2. mRNA expression levels of glycolytic enzymes significantly altered by ROS. Normalised log_2 expression of mRNA in control HPC (green), control HPC treated with 100nM DPI (green gradient), N-RAS^{G12D} HPC (blue) and N-RAS^{G12D} HPC treated with DPI (blue gradient). DPI treatment occurred for 24 h at 37ºC, 5% CO_2. GLUT3 (glucose transporter 3), GLUT5 (glucose transporter 5), GLUT14 (glucose transporter 14), HK1 (hexokinase 1), PFKFB3 (6-phosphofructo-2-kinase/fructose-2,6-biphosphatase 3), PFK(P) (phosphofructokinase platelet), FBP1 (fructose-1,6-bisphosphatase 1), ENO **(**enolase), PK(M) (pyruvate kinase muscle), LDH(A) (lactate dehydrogenase A), MCT4 (monocarboxylate transporter 4). Box plots represent median quartile ranges, x represents mean value (n=4).

4.3.2 Mutant-RAS and ROS induce changes in protein expression of glycolytic enzymes in HPC

The data above show changes in mRNA expression of glycolytic enzymes as a result of mutant N-RAS expression and that these changes are in part ROS mediated. However it is well established that mRNA levels do not necessarily correspond with protein expression levels (reviewed in Vogel and Marcotte, 2012). Therefore, to determine if changes in expression of mRNA translated into changes in the biologically functional proteins, western blot analysis was performed in human HPC and AML cell lines.

4.3.2.1 Mutant RAS and ROS modifies protein expression of key glycolytic enzymes in human HPC

Changes in mRNA expression of glycolytic enzymes, were observed in response to modulating exposure of mutant RAS expressing cells to various levels of ROS (4.3.1). To determine whether these responses translated to changes on protein expression of glycolytic enzymes in human HPC, western blots were performed. Figure 4-3A shows that increases in levels of protein expression were seen in H-RAS^{G12V} compared with control for glucose transporter 3 (GLUT3), glucose transporter 5 (GLUT5), hexokinase 1 (HK1), phosphoglucose isomerase (PGI), 6-phosphofructo-2-kinase/fructose-2,6-biphosphatase 3 (PFKFB3), phosphofructokinase platelet (PFK(P)), aldolase C (ALDO(C)), phosphoglycerate kinase (PGK), pyruvate kinase muscle 1 (PK(M)1) and lactate dehydrogenase A (LDH(A)) and were most marked with GLUT3, PFKFB3, PFK(P) and PGK. In N-RAS^{G12D} increased protein expression was observed in GLUT3, GLUT5, PGI, PFKFB3, PFK(P), ALDO(C) and PK(M)1 compared to control HPC (Figure 4-3A). These data indicate that numerous changes occur in expression of enzymatic glycolytic proteins as a result of expression of mutant RAS in HPC. Interestingly the most marked changes in expression occur predominantly with enzymes involved in catalysing the initial stages of glycolysis or in transporting glucose into the cell (4.4).

Having confirmed that mutant RAS expressing HPC elicit a ROS induced response in p38^{MAPK} (Figure 3-12), the effect of ROS inhibition on expression of glycolytic enzymes was also determined. Figure 4-3 shows that the only observable ROS dependent change occurred upon treatment of N-RAS^{G12D} HPC with DPI (100nM)

for 24h, which resulted in a 3-fold decrease in expression of PFKFB3 compared with untreated cells. No other ROS associated changes were observed in the panel of glycolytic enzymes tested, either in N-RAS^{G12D} or H-RAS^{G12V}. No changes in PFKFB3 expression or any glycolytic enzyme tested, were seen in the DPI treated control HPC compared with untreated cells. Overall, this suggests that the increase in PFKFB3 expression observed in N-RAS^{G12D} compared with control HPC is operating as a result of a ROS dependent mechanism. Interestingly this decrease in PFKFB3 expression was not observable in H-RAS^{G12V} upon treatment with DPI compared to untreated H-RAS^{G12V} (Figure 4-3). This suggests that either increased PFKFB3 expression functions independently of ROS in these cells, or that the concentration of DPI was not sufficient to quash the effect of ROS on this enzyme, in these cells.

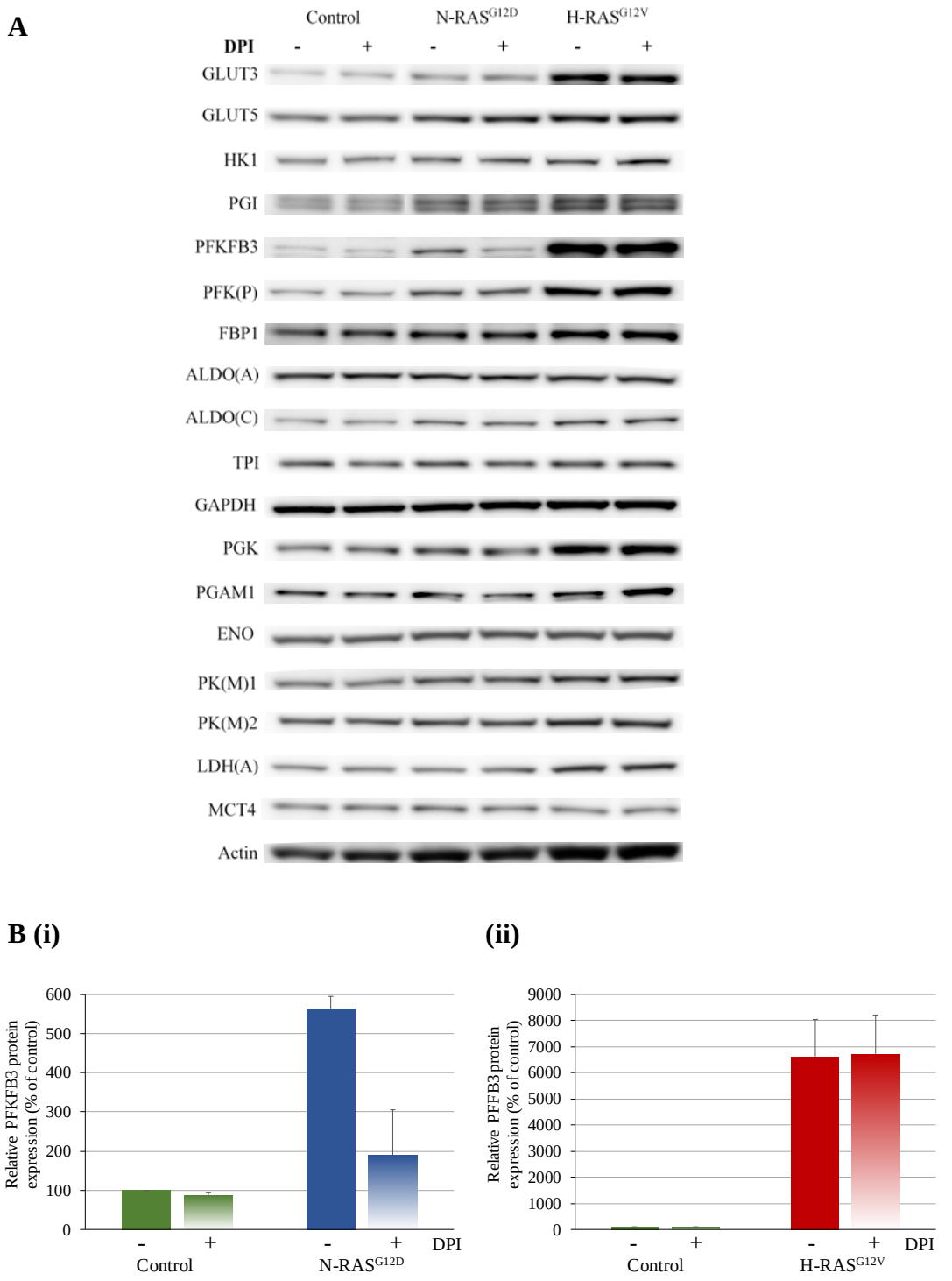

Figure 4-3. Mutant RAS and ROS dependent changes in protein expression of glycolytic enzymes. Human HPC control, N-RAS^{G12D} and H-RAS^{G12V} were incubated for 24h in the presence or absence of DPI (100nM) followed by whole cell protein extraction. **(A)** Example western blots showing expression of GLUT3, GLUT5, HK1, PGI (phosphoglucose isomerase), PFKFB3, PFK(P**)**, FBP1, ALDO(A) (aldolase A), ALDO(C) (aldolase C), TPI (triphosphate isomerase), GAPDH (glyceraldehyde phosphate dehydrogenase), PGK (phosphoglycerate kinase), PGAM1 (phosphoglycerate mutase 1), ENO, PK(M)1 (pyruvate kinase muscle 1), PK(M)2 (pyruvate kinase muscle 2), LDH(A) and MCT4. Actin was used as a loading control. (**B)** Relative protein expression (as measured by pixel density of equivalent regions of interest (ROI) between different samples on the same blot then normalised to control) of PFKFB3 in control HPC c.f. **(i)** N-RAS^{G12D} and **(ii)** H-RAS^{G12V} HPC (n=2) determined by western blot using whole cell lysates from these cells and densitometry analysed using AIDA software. Data represents mean ± 1SD.

4.3.3 ROS affects PFKFB protein expression in AML cell lines

The data above suggests that increased ROS levels leads to increased expression of PFKFB3 in N-RAS^{G12D} expressing cells. In order to observe the effect of ROS on glycolytic enzymes in other AML contexts, western blots were performed on THP-1 and NOMO-1 (AML cells which generate extracellular ROS (Figure 3-11)) and the AML cell line Mv4;11 treated with GOX.

4.3.3.1 Inhibition of ROS leads to a decrease in expression of PFKFB3 in the AML cell line THP-1

Previously it was shown that chemical inhibition of ROS production and knock-down of NOX2 in the AML cell lines NOMO-1 and THP-1, resulted in a decrease in glucose uptake (Figure 3-14). To determine whether this change was accompanied by changes in protein expression of glycolytic enzymes, western blots were performed in these cell lines. Western blot analysis in THP-1 cells, on a panel of glycolytic enzymes, show the only significant change occurred in PFKFB3 expression, which was reduced by 60% in THP NOX2-KD cells compared to THPSH control and 40% in THPSH control treated with DPI (100nM) for 24h compared to untreated control (Figure 4-4A and B(i)). Interestingly in NOMO-1 cells, which also generate extracellular ROS no changes in PFKFB3 expression were observed (see 4.4.1) (Figure 4-4A and B(ii)), although a decrease in expression of FBP1 was seen when compared with control (Figure 4-4A). Together these data suggest that ROS can elicit changes in expression of glycolytic enzymes in these AML cell lines, and together with the data from 4.3.2.1, suggest that PFKFB3 expression may be a function of ROS regulation.

4.3.3.2 Treatment of Mv;411 with exogenous ROS leads to an increase in expression of glycolytic enzymes.

Treatment of Mv4;11 cells with GOX was previously shown to increase the glucose uptake of these cells (Figure 3-15). To determine whether the addition of exogenous ROS led to changes in protein expression of glycolytic enzymes in MV4:11 cells, western blots were performed on cells treated with GOX for 24h and compared with untreated control. Figure 4-5A demonstrates that Mv4;11 cells treated with increasing levels of GOX had increased protein expression of HK1, PFKFB3 and PFK(P) compared with untreated controls. PFKFB3 expression was increased 3.5-

fold in Mv4;11 cells treated with 10mU/ml GOX and a significant 10-fold increase ($p<0.05$) when treated with 20mU/ml GOX compared to untreated cells (Figure 4-5B(i)). Additionally, PFK(P) was increased 1.6-fold and 8.4-fold (Figure 4-5B(ii)) and HK1 increased 1.2-fold and 1.6-fold (Figure 4-5C(iii)) in Mv4;11 cells treated with 10mU/ml and 20mU/ml GOX respectively, compared with the untreated cells.

To confirm that this increase in expression of HK1, PFKFB3 and PFK(P) was directly related to increases in H_2O_2 levels incurred through the addition of GOX, Mv4;11 cells were additionally treated with GOX in the presence of catalase which decomposes H_2O_2 (Hole *et al.*, 2010). Western blot analysis showed that treatment with GOX led to an increase in protein expression of these enzymes, which was suppressed upon addition of catalase (Figure 4-6). This indicates that increased levels of exogenous H_2O_2 in Mv4;11 cells lead to increases in expression of glycolytic enzymes.

Taken together with 4.3.3.1 these data show that modulation of ROS levels in AML cell lines modifies the expression of several glycolytic enzymes and commensurate with data for N-RAS^{G12D} HPC (4.3.2.1) suggests modulation of ROS frequently alters levels of PFKFB3 expression.

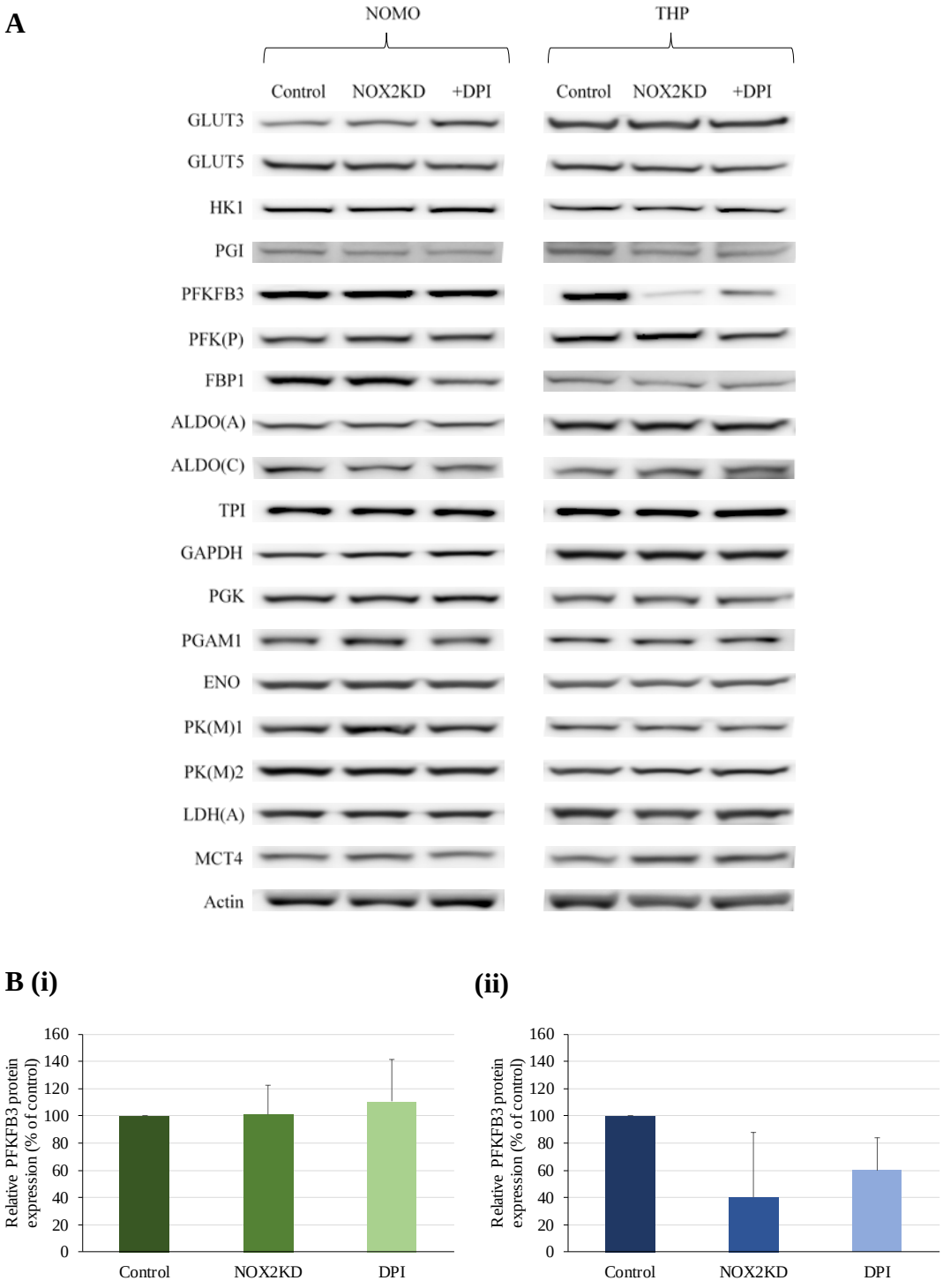

Figure 4-4. ROS dependent changes in protein expression of glycolytic enzymes in the AML derived cell lines NOMO-1 and THP-1. NOMO-1; control (non-mammalian encoding shRNA), NOX2-KD, NOMO-1 control treated with DPI (100nM) and THP-1; control (non-mammalian encoding shRNA), NOX2-KD, THP-1 control treated with DPI were incubated for a further 24h followed by whole cell protein extraction. **(A)** Example western blots showing expression of GLUT3, GLUT5, HK1, PGI, PFKFB3, PFK(P), FBP1, ALDO(A), ALDO(C), TPI, GAPDH, PGK, PGAM1, ENO, PK(M)1, PK(M)2, LDH(A) and MCT4. Actin was used as a loading control. (**B)** Relative protein expression (as measured by pixel density of equivalent ROI between different samples on the same blot then normalised to control) of PFKFB3 in **(i)** NOMO and **(ii)** THP cells (n=3) determined by western blot using whole cell lysates from these cells and densitometry analysed using AIDA software. Data represents mean ± 1SD.

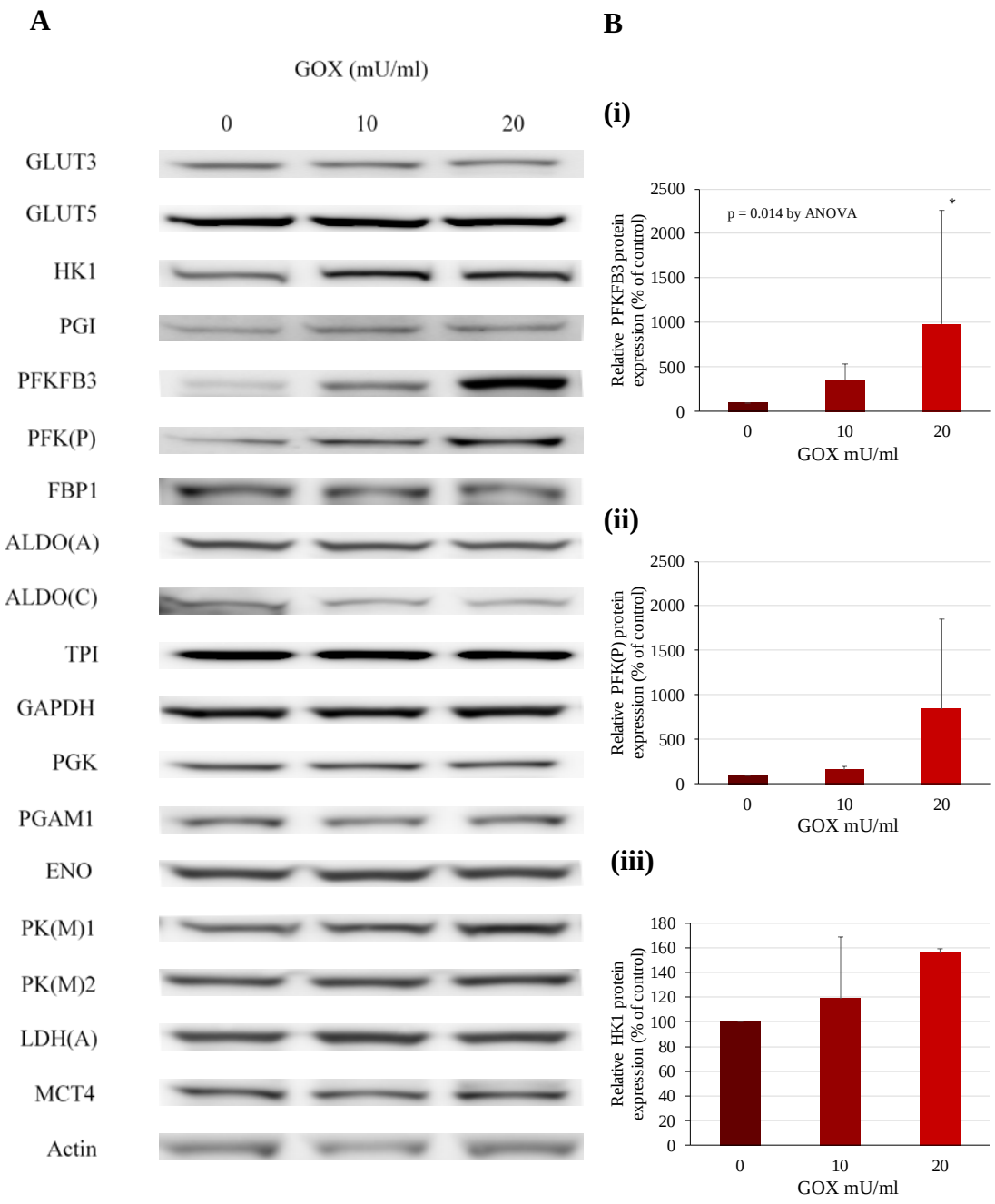

Figure 4-5. ROS dependent changes in protein expression of glycolytic enzymes in the AML derived cell line Mv4;11. Mv4;11 cells treated with GOX (10mU/ml or 20mU/ml) were incubated for a further 24h followed by whole cell protein extraction. **(A)** Example western blots showing expression of GLUT3, GLUT5, HK1, PGI, PFKFB3, PFK(P), FBP1, ALDO(A), ALDO(C), TPI, GAPDH, PGK, PGAM1, ENO, PK(M)1, PK(M)2, LDH(A), MCT4. Actin was used as a loading control. (**B)** Relative protein expression (as measured by pixel density of equivalent ROI between different samples on the same blot then normalised to control) of **(i)** PFKFB3 (n=5), **(ii)** PFK(P) (n=3), **(iii)** HK1 (n=3) determined by western blot using whole cell lysates from these cells and analysed by AIDA image analyser. Data represents mean ± 1SD. * denotes $p<0.05$ analysed by ANOVA with Tukey's honestly significance difference.

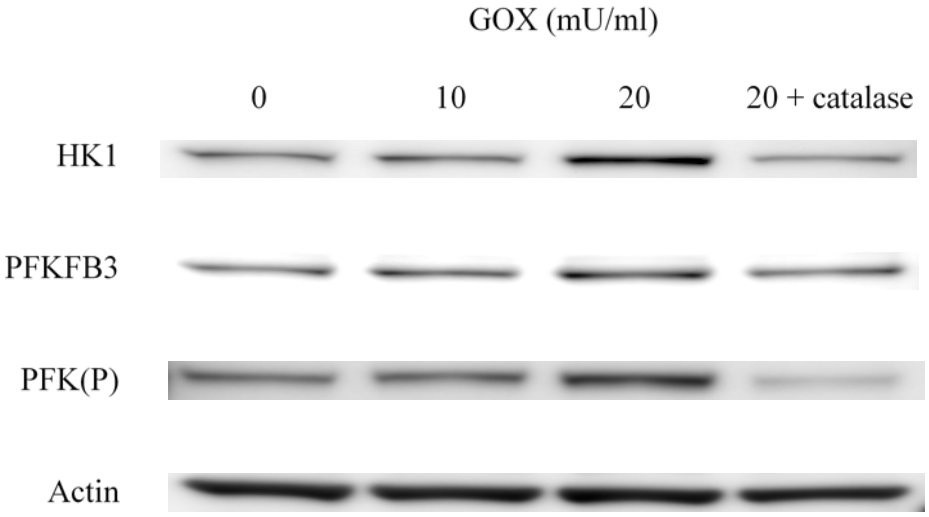

Figure 4-6. Exposure of MV4;11 cells to exogenous ROS increases protein expression of HK1, PFKFB3 and PFK(P). Mv4;11 cells were treated with GOX (10mU/ml or 20mU/ml) or GOX (20mU/ml) and catalase (100μg/ml) and incubated for a further 24h prior to whole cell lysis. Western blots show expression of HK, PFKFB3 and PFK(P). Actin was used as a loading control.

4.3.4 Post translational modifications and translocation of PFKFB3 in mutant RAS expressing HPC and AML cell lines.

The data above suggests that changes in ROS levels result in changes in protein expression of PFKFB3 (a key regulatory enzyme in glycolysis (1.5)), in N-RAS^{G12D} HPC and in some AML cell lines. Since phosphorylation (Novellasdemunt *et al.*, 2013) and nuclear translocation of PFKFB3 (Yalcin *et al.*, 2009a) has been shown to play a role in glycolytic flux and cell cycle progression, western blots were analysed to determine ROS induced changes in these key regulatory functions.

4.3.4.1 ROS does not induce phosphorylation of PFKFB3

It has previously been reported that in COS-7 cells (a cell line derived from colon cancer), increased phosphorylation of PFKFB3 at Ser461 results in increased lactate production and increased proliferation (Bando *et al.*, 2005) and increases in F-2,6-BP in the breast cancer cell line T47D (Novellasdemunt *et al.*, 2012). Phosphorylation of PFKFB3 has also been shown to increase its kinase activity (Marsin *et al.*, 2002). To determine whether ROS induced phosphorylation of PFKFB3 occurred in mutant RAS expressing HPC, whole cell lysates of untreated and DPI treated cells were analysed by western blot using an antibody recognising phosphorylated PFKFB3 (p-PFKFB3). As shown in Figure 4-7A, N-RAS^{G12D} HPC, but not H-RAS^{G12V} HPC treated with DPI have reduced expression of p-PFKFB3 compared to untreated cells, with a relative change similar to that observed for PFKFB3. No changes in p-PFKFB3 expression of control HPC treated with DPI were observed. These data indicate that in N-RAS^{G12D} HPC, ROS had no effect on phosphorylation of PFKFB3 as the relative ROS induced changes in p-PFKFB3 and PFKFB3 are broadly equivalent.

To determine whether ROS affected phosphorylation of PFKFB3 in AML cell lines, western blot analysis on whole cell lysates of THP NOX2-KD cells, THPSH cells treated with DPI and Mv4;11 cells treated with GOX compared with control cells was performed. Figure 4-7B and C show that in all cases no changes in phosphorylation of PFKFB3 occurred when compared to control cells. However, ROS inhibition and knockdown in THP-1 cells decreased expression of total PFKFB3 protein and Mv4;11 cells treated with GOX showed increased levels of total PFKFB3 protein compared to untreated control. Given the ROS dependent

changes in total PFKFB3 protein levels, it might be expected that if ROS was exhibiting no effect on PFKFB3 phosphorylation, pPFKFB3 protein levels would exhibit an equivalent pattern. The failure of pPFKFB3 protein levels to mirror the changes observed in total PFKFB3 protein levels indicates that ROS may prevent phosphorylation of this enzyme in AML cell lines (see 4.4).

Overall, whilst N-RAS^{G12D} HPC did show a decrease in p-PFKFB3 expression upon treatment with DPI in agreement with decreases in total PFKFB3 protein expression, data from the AML cell lines indicate that ROS may prevent phosphorylation of this enzyme, suggesting a role for ROS in the phosphorylation of PFKFB3 that is context dependent (see 4.4).

4.3.4.2 ROS does not cause translocation of PFKFB3 to the nucleus in THP-1

It has been shown previously in a number of cell lines, that PFKFB3 translocates to the nucleus (Yalcin *et al.*, 2006). Ectopic expression of PFKFB3 in the nucleus of cervical, colon and breast cancer cell lines led to increased cell proliferation without impacting on the overall glycolytic rate (Yalcin *et al.*, 2009a). This led the authors to speculate that in this context PFKFB3 may, in addition to its role in regulating glycolytic rate, also have a regulatory role in cell cycle progression. In order to examine whether ROS played a role in nuclear translocation of PFKFB3 in the AML cell line THP, cytosol/nuclear fractionated lysates of THP NOX2-KD, THPSH cells treated with DPI and untreated THPSH control cells were isolated. Western blot analysis shows that no PFKFB3 protein expression was observed in the nuclear fractions of either the ROS inhibited cells or control cells (Figure 4-8). This suggests that ROS does not play a role in translocation of PFKFB3 to the nucleus. Furthermore, the failure to detect expression of PFKFB3 in the nucleus of control cells suggests that in THP-1 cells, nuclear translocation of PFKFB3 is not a factor in cell cycle progression.

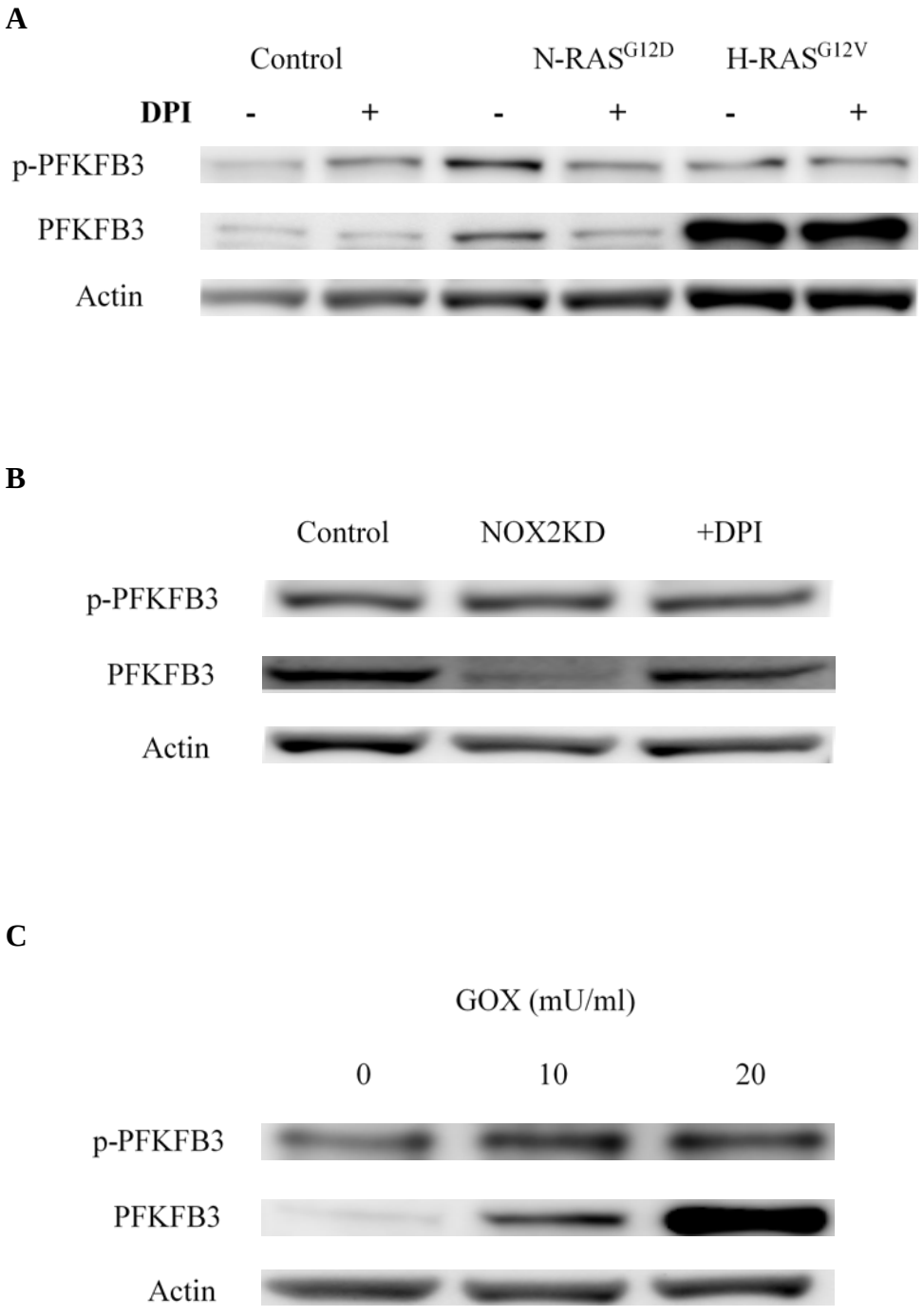

Figure 4-7. ROS induced phosphorylation of PFKFB3. Example western blot showing expression of p-PFKFB3 using whole cell lysates derived from **(A)** control, N-RAS^{G12D} and H-RAS^{G12V} HPC treated and untreated with DPI (100nM) and incubated for a further 24h; **(B)** THPSH, THP NOX2-KD and THPSH cells treated with DPI (100nM) and incubated for a further 24h; **(C)** Mv4;11 untreated and treated with 10mU/ml and 20mU/ml GOX and incubated for a further 24h. Actin **(A)** and histone **(B)** and **(C)** were used as loading controls (n=2).

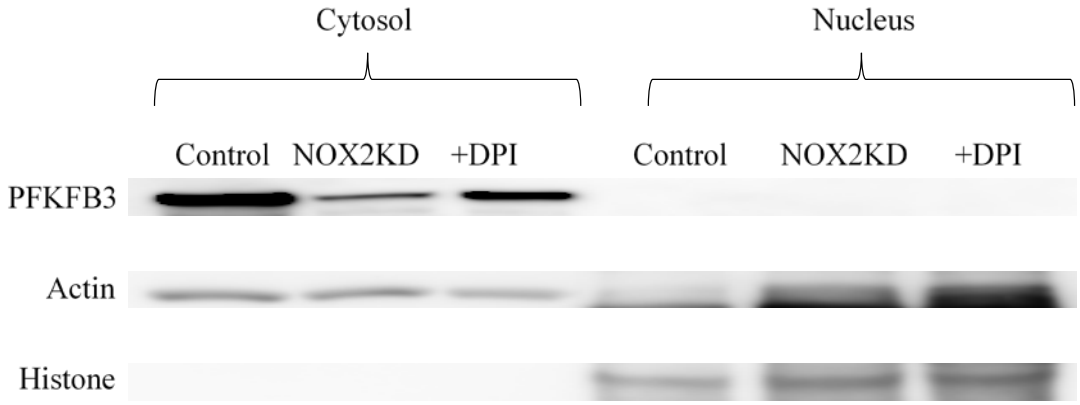

Figure 4-8. PFKFB3 is not observed in the nucleus of THP-1 cells. Cytosol/nuclear fractionated lysates of THPSH control, THP NOX2-KD and THPSH cells treated with 100nM DPI and incubated for a further 24h were analysed by western blot using an antibody recognising PFKFB3. Histone and Actin were used as loading controls. N.B. bands observed slightly below the molecular weight of actin in the nuclear fraction are likely the result of non-specific binding of the histone antibody, the failure to detect PFKFB3 in the nuclear fraction indicates a lack of cytosolic contamination.

4.3.5 Biochemical metabolite concentrations are changed in models of AML

Using mass spectrometry as an analytical tool, the relatively new field of metabolomics is providing insights, both in establishing biomarkers of disease in patients (Wang *et al.*, 2013) and as a research tool in determining relative changes in metabolite concentrations in disease models (Bhanot *et al.*, 2015). Through manipulation of ROS in AML cell lines, changes in glucose uptake (3.3.3.2), lactate output (3.3.3.3), proliferation (3.3.3.4) and protein expression of glycolytic enzymes (4.3.3.1 and 4.3.3.2), have been observed in these cells. To understand dynamically the impact these ROS induced changes had on metabolite concentrations in metabolic pathways related to glycolysis, cell line samples in which ROS had been chemically manipulated or NOX2 genetically knocked-down, were prepared as previously described (2.11.1) and analysed by Metabolon™ (http://www.metabolon.com/) a company specialising in the analysis of the metabolome (2.11).

4.3.5.1 Sample preparation and quality control for GCMS

Mass spectrometry (using a variety of platforms, see 2.11.3) was performed on quadruplicate samples of NOMO and THP cells untreated, treated with DPI (100nM) for 24h and with NOX2 knocked-down. Further, Mv4;11 cells untreated or treated with GOX for 24h were also included in the study. Prior to mass spectrometry analysis, Diogenes™ assay was performed to confirm superoxide production and inhibition in the THP and NOMO samples as previously demonstrated (data not shown: 3.3.3.1). Additionally, the cells were analysed to confirm that the changes in glucose uptake and proliferation observed in (3.3.3.2,3.3.3.4) were also replicated in these samples. Samples needed to show a minimum 10% change in both proliferation and glucose uptake (data not shown). Additionally, samples were stained with 7AAD to determine viability of the cells (2.3.5), with a minimum of 90% viability being set as a prerequisite for further analysis.

4.3.5.2 Principal component analysis indicates differences between AML cell lines and cell line treatments.

To better understand the overall biochemical variations between each sample, principal component analysis (PCA) can be employed to provide a global analysis of how closely related or otherwise any given sample is. As shown in Figure 4-9A, PCA performed by Metabolon^{TM}, show that sample type (e.g. cell line) was one of the largest determining factor in differences of biochemical metabolite composition between samples. However, the PCA clearly shows that treatment of both NOMO and THP cell lines with DPI changed the global metabolite composition of these cells as evidenced by separation of the treated replicated samples from the control, an effect also observed between NOX2-KD cells and the SH control. In contrast, the smallest variation observed was in the Mv4;11 cells treated with GOX. Taken together, these data indicate that whilst cell line origin was the largest determining factor in changes in global biochemical metabolite variation, exposure to ROS affects the metabolome or global biochemical metabolite composition.

To support these data, hierarchical clustering (performed by Metabolon^{TM}) as shown in Figure 4-9B, also demonstrates that the largest variation between samples occurred between different cell lines, with treatment providing the next largest variation and differences between replicates showing the least variation.

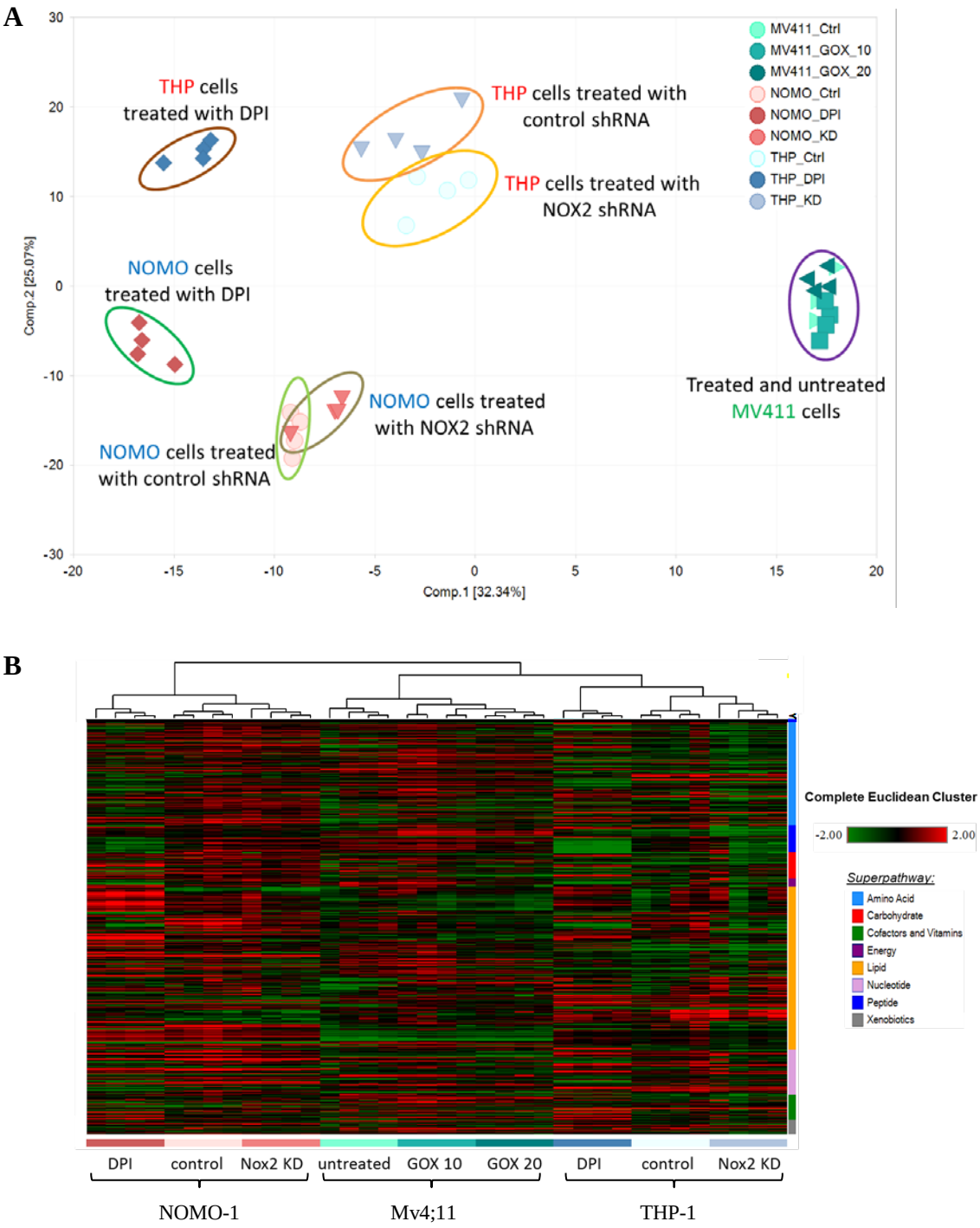

Figure 4-9. Variation in biochemical metabolites between samples analysed by Metabolon™. **(A)** PCA analysis representing variation between samples, where circles represent control, squares represent DPI treated cells (100nM) NOMO (red), THP (blue) and GOX treated cells (10mU/ml) Mv4;11 (green) and triangles represent NOX2-KD cells NOMO(red), THP (blue) and GOX treated cells (20mU/ml) Mv4;11 (green). All cells chemically treated were incubated for 24h following treatment. **(B)** Dendrogram representing variation between samples subjected to hierarchical clustering analysis, NOMO (red), THP (blue), Mv4;11 (green). All calculations were performed by Metabolon™, samples were loaded equally across the platform, normalised to Bradford protein concentration, each biochemical is then rescaled to set the median equal to l, imputation of missing values (if any) with minimum value for each compound is performed and data log transformed. Green represents lower and red higher concentration of biochemical relative to median value. Graphs constructed by Metabolon™ (n=4).

4.3.5.3 ROS affects change in relative concentrations of biochemical metabolites of the glycolytic pathway

The data above (4.3.5.2) suggests ROS induced changes in global biochemical metabolite levels in AML cell lines. To determine whether ROS induced changes in glycolytic metabolites, the above dataset was analysed specifically for metabolites within this pathway.

Knock-down of NOX2 results in changed glycolytic metabolite profile.

The data above (4.3.3.1) have demonstrated that knock-down of NOX2 in the THP cell line decreases PFKFB3 expression, a key regulatory enzyme in glycolysis (1.5.1). To ascertain whether NOX2KD additionally changed glycolytic metabolite levels, mass spectrometry was performed on THP and NOMO cells with NOX2 knocked-down and the data analysed by Metabolon^{TM}. In THP cells, knock-down of NOX2 using shRNA resulted in a reduction of the glycolytic metabolites, F-1,6-BP (1.4-fold), dihydroxyacetone phosphate (DHAP) (2-fold), and a significant reduction of pyruvate (1.3-fold, p=0.016) and lactate (1.9-fold, p=0.003) compared to control cells. Interestingly a non-significant increase was observed in F-6-P (5.2-fold) and in 3-PG (1.2-fold) (Figure 4-10). In NOMO NOX2-KD cells, a reduction in the metabolites F-6-P (2.5-fold), F-1,6-BP (2.3-fold) and DHAP (1.3-fold) was observed compared to control, which reached significance for F-1,6-BP (p=0.005), whilst 3-PG showed a non-significant increase (1.2-fold) (Figure 4-10). Taken together these data are supportive of the idea that lower levels of ROS, result in decreased glucose uptake in these cell lines, in agreement with the observations in (3.3.3.2).

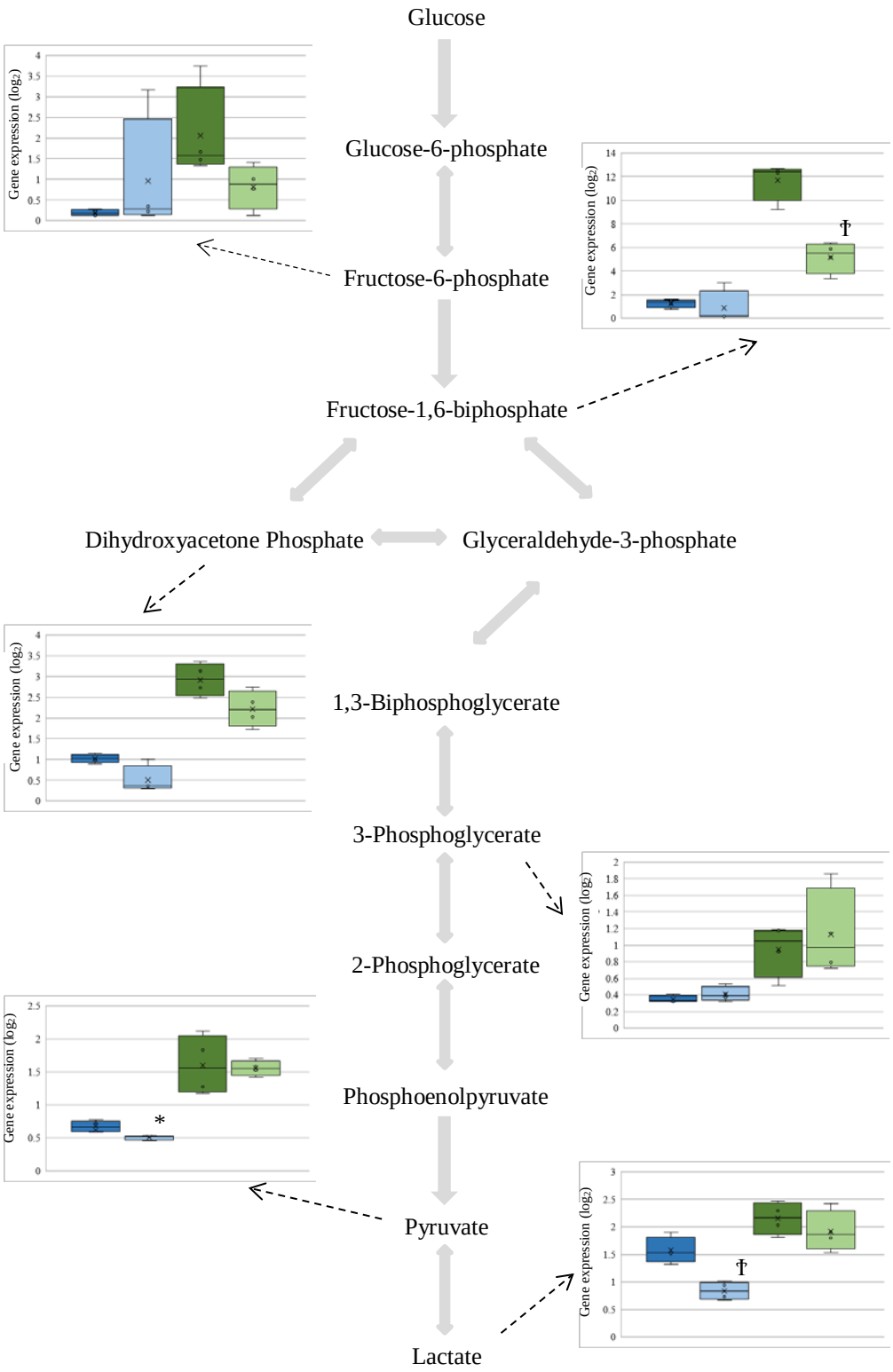

Figure 4-10. Changes in glycolytic intermediates in AML derived cell lines with NOX2 knocked-down. Schematic diagram of glycolysis, showing variation in glycolytic metabolite levels, as detected by mass spectrometry, in THPSH (dark blue), THP NOX2-KD (blue), NOMOSH (dark green), NOMO NOX2-KD (green) cells. Data shows relative values following normalisation to Bradford protein concentration, log transformation and imputation of missing values with the minimum observed value for each compound (n=4). Box plots represent median quartile ranges, x represents mean value. * denotes $p<0.05$ and † denotes $p<0.005$ for NOX2-KD cells compared with SH control as analysed by Welch's two sample t-test.

Chemical inhibition of NOX2 results in changed glycolytic metabolite profile.

Decreased protein expression of the glycolytic enzyme PFKFB3 was found to be reduced in THP cells treated with DPI, whilst a decrease in expression of FBP1 was observed in NOMO cells treated with DPI, when compared with control cells (4.3.3.1). To examine whether DPI altered glycolytic metabolite levels, mass spectrometry was performed by Metabolon^{TM} on both THP and NOMO samples treated with DPI (as previously described, 3.3.3.2) and compared with the levels in untreated cells. Treatment of THP cells with DPI (100nM) for 24h resulted in a significant decrease in lactate (2.2-fold, p=0.001), whilst decreases were also observed in F-6-P (1.5-fold) and F-1,6-BP (1.2-fold), compared with untreated cells. Interestingly significant increases in both pyruvate (4.4-fold, p<0.0001) and 3-PG (8.1-fold, p=0.002) were also observed (Figure 4-11), which may be the result of off target effects of the DPI (4.4). NOMO cells showed significant decreases in the glycolytic metabolites F-6-P (3.8-fold, p=0.004), F-1,6-BP (4-fold, p=0.0001), DHAP (2-fold, p=0.0005) and lactate (2.9-fold, p<0.0001), upon treatment with DPI. No change in the relative amounts of pyruvate was observed, whilst analogous to the results observed in THP a significant increase in 3-PG (3.6-fold, p=.002) was also seen (Figure 4-11). The significant decrease in glycolytic metabolites in NOMO cells treated with DPI alongside the significant decrease in lactate and decreases in F-6-P and F-1,6-BP in the THP cells are supportive of an overall decrease in glucose uptake as seen in (3.3.3.2).

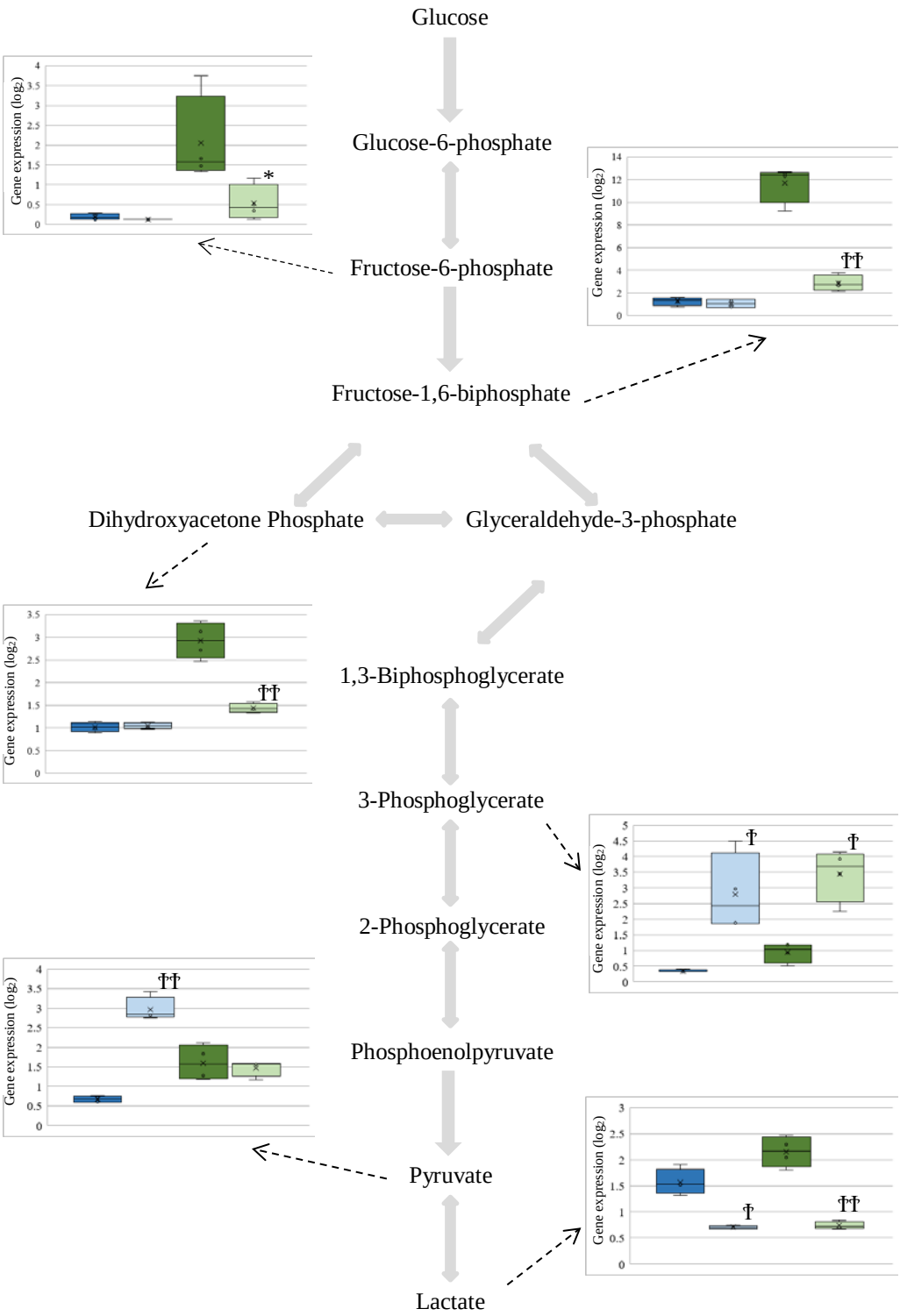

Figure 4-11. Changes in glycolytic intermediates in AML derived cell lines with NOX2 chemically inhibited. Schematic diagram of glycolysis, showing variation in glycolytic metabolite levels, as detected by mass spectrometry, in THPSH (dark blue), THPSH + DPI (100nM) (light blue), NOMOSH (dark green), NOMOSH + DPI (100nM) (light green) cells. All cells incubated for 24h following DPI treatment. Data shows relative values following normalisation to Bradford protein concentration, log transformation and imputation of missing values with the minimum observed value for each compound (n=4). Box plots represent median quartile ranges, x represents mean value. * denotes $p<0.05$, † denotes $p<0.005$ and †† denotes $p<0.001$ for DPI treated cells compared with untreated control as analysed by Welch's two sample t-test.

Increased exogenous ROS in Mv4;11 cells results in changed glycolytic metabolite profile.

When Mv4;11 cells were treated with exogenous ROS increases in protein expression levels of the glycolytic enzymes HK1, PFK(P) and PFFKFB3 were all observed (4.3.3.2). To further detail how ROS impacted on metabolism in these cells, mass spectrometry was performed (as previously described, 2.11.3) on Mv4;11 cells treated with 10mU/ml and 20mU/ml of GOX, incubated for a further 24h and compared with untreated cells. The addition of GOX 10mU/ml to the cell line Mv4;11 resulted in a significant increase in the glycolytic metabolite pyruvate (1.3-fold, p=0.001), although interestingly this increase is not observed at the higher dose (GOX 20mU/ml). Additionally, decreases in F-6-P (1.4-fold), DHAP (1.2-fold) and 3-PG (1.8-fold) were also observed, although none of these changes reached significance. Treatment with the higher dose (GOX 20mU/ml) resulted in a significant (1.5-fold, p=0.02) decrease in intracellular lactate levels, whilst a non-significant decrease in 3-PG (2.4-fold) was additionally observed. Conversely a non-significant increase in F-1,6-BP (1.2-fold) was also detected (Figure 4-12). Whilst significant increases in pyruvate are observed in Mv4;11 cells treated with GOX 10mU/ml, the absence of any change in pyruvate levels, alongside the significant decrease in intracellular lactate levels in Mv4;11 cells treated with higher dose of GOX, does not offer support to the idea of an increase in glycolytic flux in these cells. It is worth noting however, that increases in extracellular lactate levels were observed in Mv4;11 cells treated with both the lower and higher levels of GOX, and therefore the failure to detect increases in glycolytic metabolite intermediaries maybe a function of enhanced lactate export (4.4).

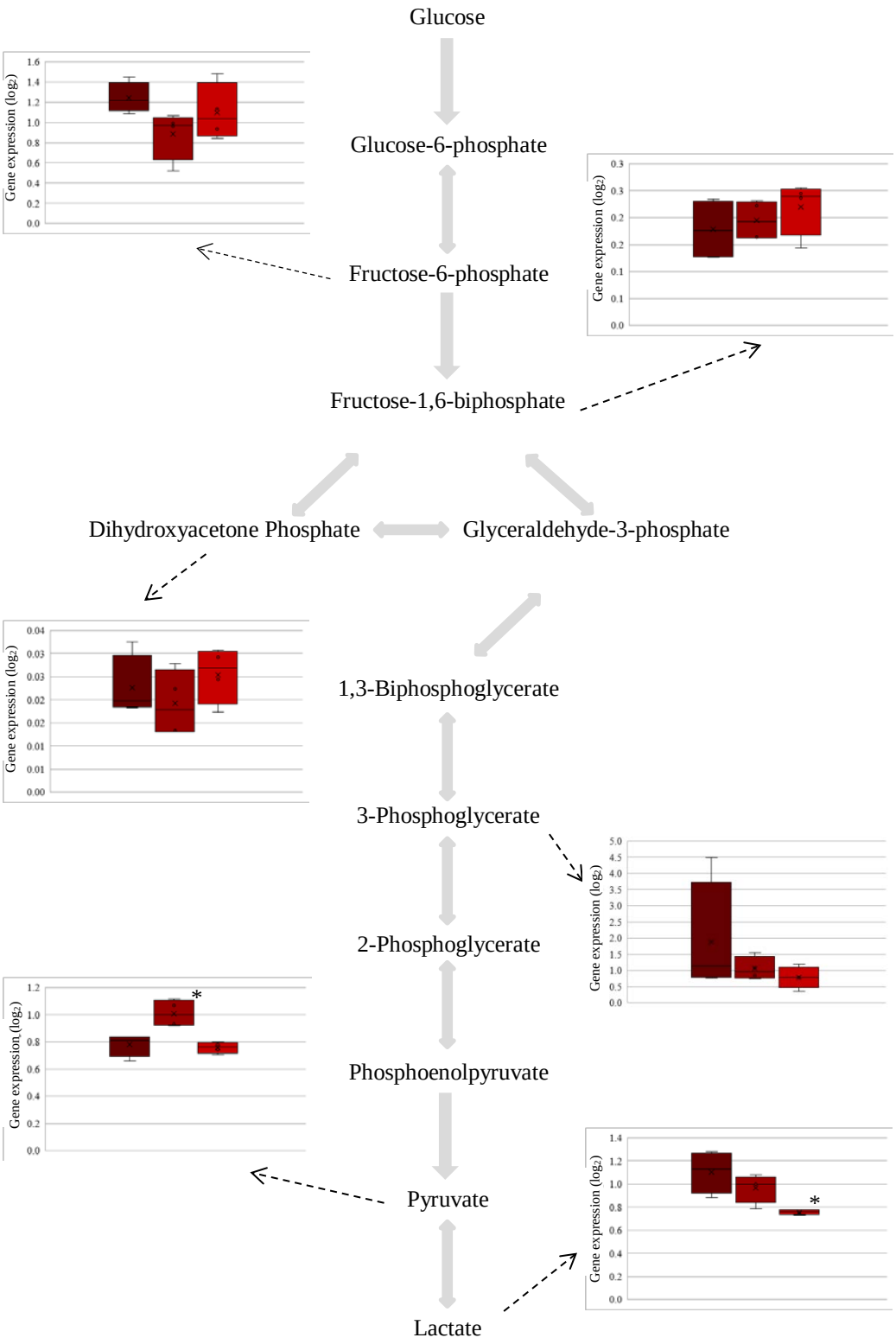

Figure 4-12. Changes in glycolytic intermediates in Mv4;11 cells experiencing increased exogenous ROS. Schematic diagram of glycolysis, showing variation in glycolytic metabolite levels, as detected by mass spectrometry, in Mv4;11 cells; untreated (dark red), treated with GOX (10mU/ml) (red) and GOX (20mU/ml) (light red). Cells incubated for 24h following treatment. Data shows relative values following normalisation to Bradford protein concentration, log transformation and imputation of missing values with the minimum observed value for each compound (n=4). Box plots represent median quartile ranges, x represents mean value. * denotes $p<0.05$ for GOX treated cells compared with untreated control as analysed by Welch's two sample t-test.

4.3.5.4 ROS induces changes in metabolite levels of other metabolic pathways

The mass spectrometry data above shows changes in concentrations of glycolytic metabolites as a result of changes in ROS levels, which are broadly supportive of the ROS induced changes in glucose uptake observed in 3.3.3.2. Glycolysis is only one component of cellular metabolism, with many other metabolic pathways feeding into and branching off from glycolytic intermediates (1.4.4). Whilst a detailed analysis of ROS induced changes in these pathways is beyond the scope of this study, some significant changes are worthy of note.

DPI treatment results in decreases in fumarate, a key intermediate in the citric acid cycle

Otto Warburg initially ascribed his observation that cancer cells exhibited increased aerobic glycolysis to defective mitochondrial function in these cells (Warburg, 1956), although a number of subsequent studies have shown functional mitochondria is important in cancer cell metabolism (reviewed in Wallace, 2012). The citric acid cycle commences from the reaction of acetyl CoA with oxaloacetate to form citrate. Acetyl CoA is generated following the decarboxylation of pyruvate catalysed by the enzyme pyruvate dehydrogenase, whilst oxaloacetate is regenerated from the citric acid cycle. Importantly the metabolic step which converts succinate to fumarate involves the reduction of flavin adenine dinucleotide which generates the proton gradient necessary for oxidative phosphorylation. Furthermore, it has been shown that whilst HSC require fumarate hydratase (the enzyme that catalyses this step) for self-renewal and maintenance, LSC do not (Guitart *et al.*, 2017). Therefore, ROS induced changes in fumarate levels may be indicative of changes in the cellular rates of oxidative phosphorylation. Analysis of the mass spectrometry data by Metabolon^{TM} showed no significant changes in fumarate levels were observed in either THP or NOMO cells with NOX2 knocked-down, however treatment of both cell lines with DPI resulted in a significant 4.2-fold ($p<0.0001$) and 2.4-fold ($p=0.009$) decrease in fumarate respectively. Treatment of Mv4;11 cells with GOX 10mU/ml showed no change in fumarate levels, although a treatment dose of 20mU/ml resulted in a significant 1.5-fold reduction ($p=0.024$) (Figure 4-13A). These data suggest that genetic silencing of NOX2 in THP and NOMO cells does

not affect the rate of oxidative phosphorylation, whilst the changes observed through chemical inhibition of NOX2 with DPI may be the result of an off-target effect.

ROS induces changes in 6-phosphogluconolactone, a key intermediate in the PPP.

One potential explanation for increased aerobic glycolysis in cancer cells is a facilitation of increased flux through the PPP, which generates nucleotides for biosynthesis and a recent paper (Chen *et al.*, 2016c) reported that PPP enzymes were upregulated in 61% of AML patients. The rate limiting step in the PPP is the conversion of glucose-6-phosphate to 6-phosphogluconolactone (6-PG) and this is also the step that generates NADPH, which combats oxidative stress (reviewed in Patra and Hay, 2014). Therefore, the mass spectrometry data from the samples, was analysed by Metabolon^{TM} for changes in 6-PG levels, in order to assess the impact of ROS on this pathway. Knock-down of NOX2 in NOMO and THP cells resulted in a non-significant decrease (1.2-fold) and a non-significant increase (3.3-fold) in 6-PG, respectively. Inhibition of these cell lines with DPI both generated decreases in 6-PG levels, 1.3-fold in the THP cells and 2.2-fold in NOMO and this was significant in the NOMO cells ($p=0.004$). Treatment of Mv4;11 cells with GOX (10mU/ml) resulted in a significant ($p=0.033$) 1.8-fold increase in 6-PG, whilst treatment with 20mU/ml of GOX showed a non-significant 1.3-fold increase (Figure 4-13B). Whilst the observed increase in 6-PG in THP NOX2-KD cells is inconsistent with the idea of ROS induced increases in the PPP, overall these data are supportive of the idea that increased ROS levels result in increased PPP metabolism.

ROS induces changes in other significant metabolites.

In addition to the changes in metabolic pathways identified above, mass spectrometry analysis of the samples revealed significant ROS dependent changes in amino acid levels and metabolites involved in sphingolipid metabolism, which are important in biosynthesis.

Knock-down of NOX2 in THP cells decreased levels of nineteen of the twenty amino acids, and this was significant for eleven of them. NOMO NOX2-KD cells showed significant decreases in proline and aspartate, although significant increases in serine, asparagine and isoleucine were also observed. Treatment of THP cells with

DPI, resulted in a decrease in sixteen of the twenty amino acids, of which eleven were significant, whilst treatment of NOMO cells with DPI showed a decrease in all twenty amino acids, which were significant for sixteen. Additionally, treatment of Mv4;11 cells with GOX (10mU/ml) led to increase in eighteen of the twenty amino acids, six of which were significant, although treatment at the higher dose (GOX 20 mU/ml) led to a depletion of amino acids, five of which were significant (Table 6). These data suggest that increased levels of ROS lead to increases in cellular levels of amino acids.

Significant reductions in a number of metabolites involved in sphingolipid metabolism were observed in both THP and NOMO cells which had NOX2 knocked-down, although this was not observed in cells treated with DPI, whilst conversely addition of exogenous ROS to Mv4;11 cells resulted in significant increases of metabolites involved in sphingolipid metabolism (data not shown).

Overall these data suggest that ROS has significant impacts not only on the glycolytic function of cells but also on a number of other metabolic pathways.

A

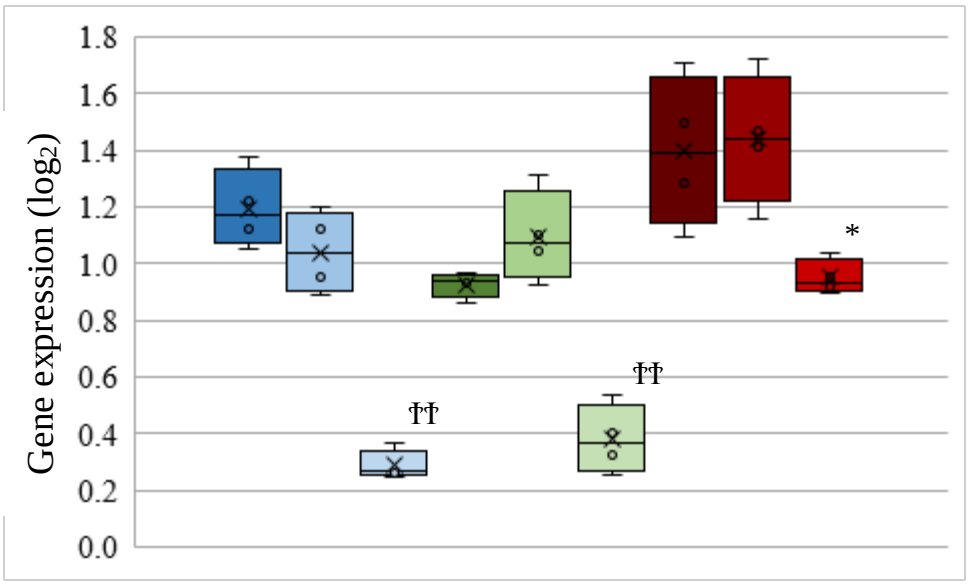

B

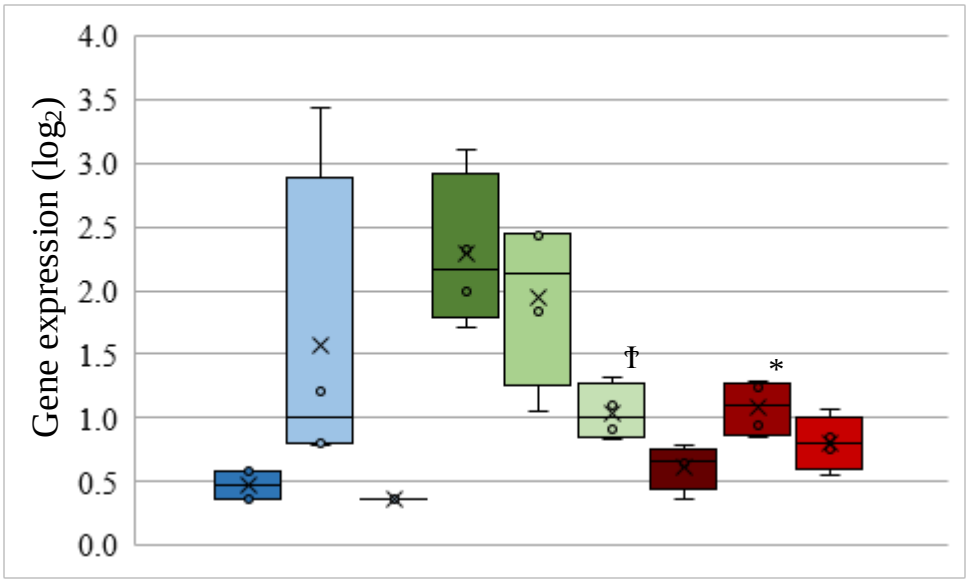

Figure 4-13. ROS induced changes in fumarate and 6-phosphogluconolactone. Box plots showing relative changes in metabolite levels, as detected by mass spectrometry of **(A)** fumarate and **(B)** 6-phosophogluconolactone in THPSH (dark blue), THP NOX2-KD (blue), THPSH treated with DPI (100nM) (light blue), NOMOSH (dark green), NOMO NOX2-KD (green), NOMOSH treated with DPI (100nM) (light green), Mv4;11 untreated (dark red), Mv4;11 treated with GOX (10mU/ml) (red) and GOX (20mU/ml) (light red) cells. All cells incubated for further 24h following chemical treatment. Data shows relative values following normalisation to Bradford protein concentration, log transformation and imputation of missing values with the minimum observed value for each compound (n=4). * denotes $p<0.05$, † denotes $p<0.005$ and †† denotes $p<0.001$ for DPI or GOX treated cells compared with untreated control as analysed by Welch's two sample t-test.

Table 6. ROS induced variation in amino acid metabolite levels in AML-derived cell lines Table shows mean fold changes in amino acids, as detected by mass spectrometry, in THPSH and NOMOSH cells, THP and NOMO cells with NOX2 genetically silenced, THPSH and NOMOSH cells treated with DPI (100nM) and Mv4;11 cells untreated and treated with GOX. All cells incubated for further 24h following treatment. Data shows relative values following normalisation to Bradford protein concentration, log transformation and imputation of missing values with the minimum observed value for each compound (n=4). Boxes shaded green indicate significant decreases and boxes shaded red indicate significant increases ($p<0.05$) performed using Welch's two sample t-test.

	THP-1		NOMO Cell Lines		MV411 Cells	
	NOX2 KD vs Control	DPI vs Control	NOX2 KD vs Control	DPI vs Control	GOX 10mU/ml vs Control	GOX 20mU/ml vs Control
Glycine	0.75	1.31	1.02	0.84	1.11	0.85
Serine	0.78	0.37	1.19	0.63	1.09	0.72
Threonine	0.77	0.83	1.1	0.51	1.28	1
Alanine	0.75	0.57	1.19	0.43	0.98	0.73
Asparagine	0.67	0.64	1.25	0.48	1.13	0.86
Glutamate	0.75	0.95	0.95	0.9	1.06	0.82
Glutamine	0.16	1.64	1.27	0.42	1.14	0.73
Histidine	0.81	0.74	1.16	0.72	1.28	0.97
Phenylalanine	0.79	0.51	1.06	0.65	1.18	0.91
Tryptophan	0.8	0.63	1.12	0.7	1.23	1.03
Leucine	0.77	0.64	1.07	0.71	1.16	0.86
Methionine	0.83	0.63	1.14	0.86	1.2	0.82
Cysteine	0.52	1.08	0.83	0.79	1.19	0.97
Proline	0.74	0.89	0.88	0.71	1.23	1.03
Aspartate	1.38	0.54	0.77	0.41	0.84	0.64
Arginine	0.93	1.32	1.06	0.86	1.09	0.78
Isoleucine	0.82	0.89	1.13	0.84	1.28	1.03
Valine	0.85	0.73	1.06	0.73	1.28	0.95
Lysine	0.86	0.84	0.91	0.63	1.15	0.89
Tyrosine	0.74	0.47	1.11	0.68	1.18	0.92

4.3.6 AML patient samples show ROS induced changes in biochemical metabolite concentrations

The metabolomic data above suggests that changes in cellular metabolite levels can occur as a consequence of ROS modulation in AML. To determine whether changes in biochemical metabolite levels vary between AML patients stratified according to production of ROS and compared to normal human mononuclear cells, AML blasts from 20 AML patients were sent to Metabolon^{TM} for metabolomic analysis. As shown in Figure 4-14, Diogenes^{TM} analysis of AML blasts stratified the patient samples into ROS^{Hi} and ROS^{Lo} producing AML blasts.

PCA on patient samples and controls as shown in Figure 4-15 demonstrate that the global biochemical metabolite composition of control samples differentiated from patient samples. Further, patient samples deemed high ROS^{Hi} producers predominantly clustered separately from those deemed ROS^{Lo}. These data indicate that variations in global biochemical metabolite composition are a consequence of both AML and the ROS produced by AML blasts.

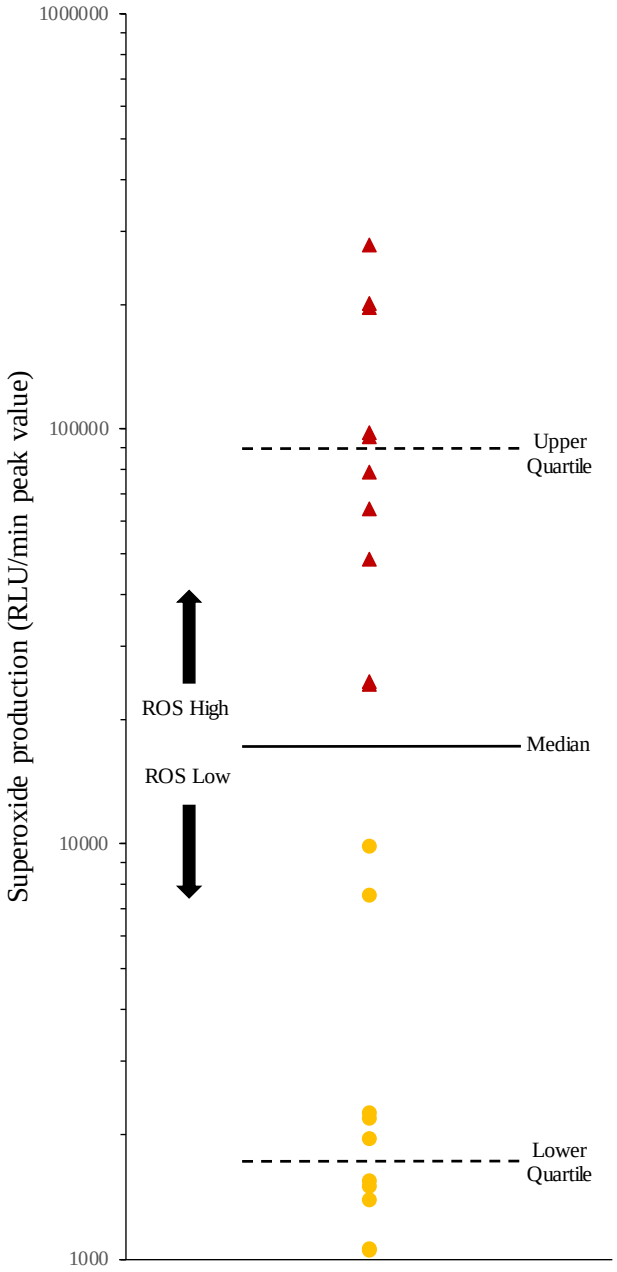

Figure 4-14. Superoxide production in AML patient blasts. Peak superoxide production (relative luminescent units/min (RLU/min)) in a panel of AML patient blasts measured using Diogenes™. Blasts were stratified by median into ROS^{Hi} (red triangle, n=10) and ROS^{Lo} (yellow circle, n=10) blasts.

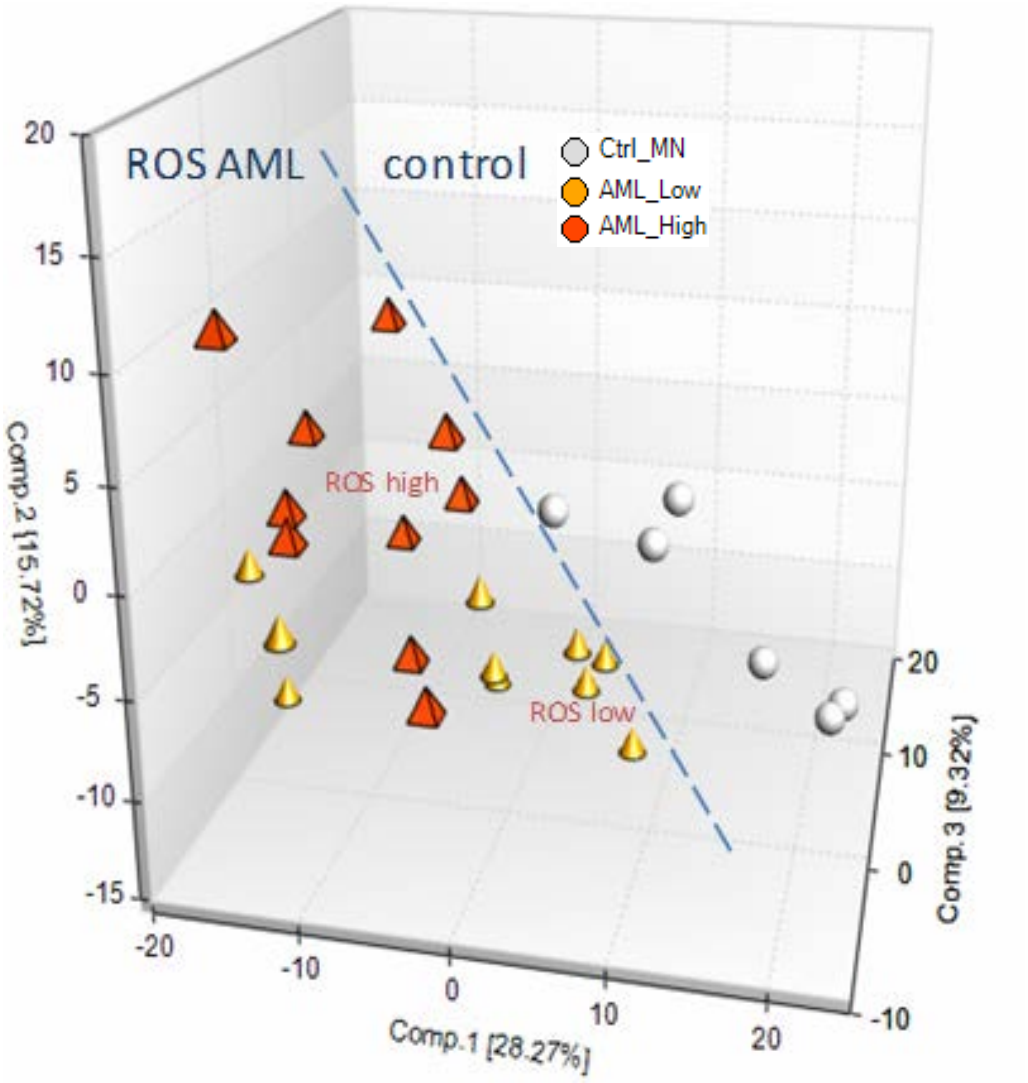

Figure 4-15. PCA showing variation between samples in biochemical metabolites analysed by MS. White circles represent healthy human mononuclear control cells (Ctrl_MN), yellow cones represent AML blasts with low ROS (AML_Low) and red pyramids represent AML blasts with high ROS (AML_High). All calculations were performed by Metabolon™, samples were loaded equally across the platform, normalised to Bradford protein concentration, log transformed and imputation of missing values (if any) with minimum value for each compound (n=4). Graph constructed by Metabolon™.

4.3.6.1 AML patient samples show changes in glycolytic metabolite levels and this is modulated by ROS

Having determined variation in global metabolite levels between AML patient blasts and healthy controls, the mass spectrometry data was analysed further to determine variations in glycolytic metabolites. AML blasts show increased levels of glucose uptake (2.6-fold) and significantly increased levels (2.4-fold) of intracellular lactate ($p=0.004$) compared to mononuclear controls. Significantly decreased levels of the glycolytic intermediates, F-1,6-BP (1.3-fold, $p=0.006$), 3-PG (1.6-fold, $p=0.045$), 2-PG (1.5-fold, $p=0.007$) and pyruvate (1.4-fold, $p=0.003$) were also observed alongside a non-significant decrease in G-6-P (1.3-fold). Additionally, a non-significant increase in F-6-P (1.2-fold) and a significant (2-fold) increase in DHAP ($p=0.012$), was also seen (Figure 4-16). Overall, the increase in glucose uptake and significant increase in lactate output in AML blasts are supportive of the idea of increased glycolysis in AML patients.

To determine ROS induced changes in glycolytic metabolites in AML patients, the data was analysed between ROS^{Hi} and ROS^{Lo} AML blasts. Significant increases were observed in glucose (2.4-fold, $p=0.008$), G-6-P (2-fold, $p=0.01$) and F-6-P (1.9-fold, $p=0.018$) metabolite levels in the ROS high blasts. Increases were also observed in the metabolite levels of F-1,6-BP (1.6-fold), DHAP (1.5-fold), 2-PG (1.3-fold) of ROS high blasts when compared with ROS low blasts, although these were not significant. Conversely, there were non-significant decreases in the metabolite levels of 3-PG (1.5-fold), PEP (1.5-fold) and pyruvate (1.4-fold) in the ROS high blasts compared to the ROS low blasts (Figure 4-17). Interestingly, intracellular lactate levels showed only a 1.1-fold increase in the ROS high blasts compared to the ROS low blasts, which may be a function of increased lactate excretion or alternative ROS induced mechanism (4.4). Overall, the significant increase in intracellular glucose levels, alongside the increase in a number of glycolytic intermediates in ROS high blasts are supportive of a ROS induced increase in glycolysis in AML patients.

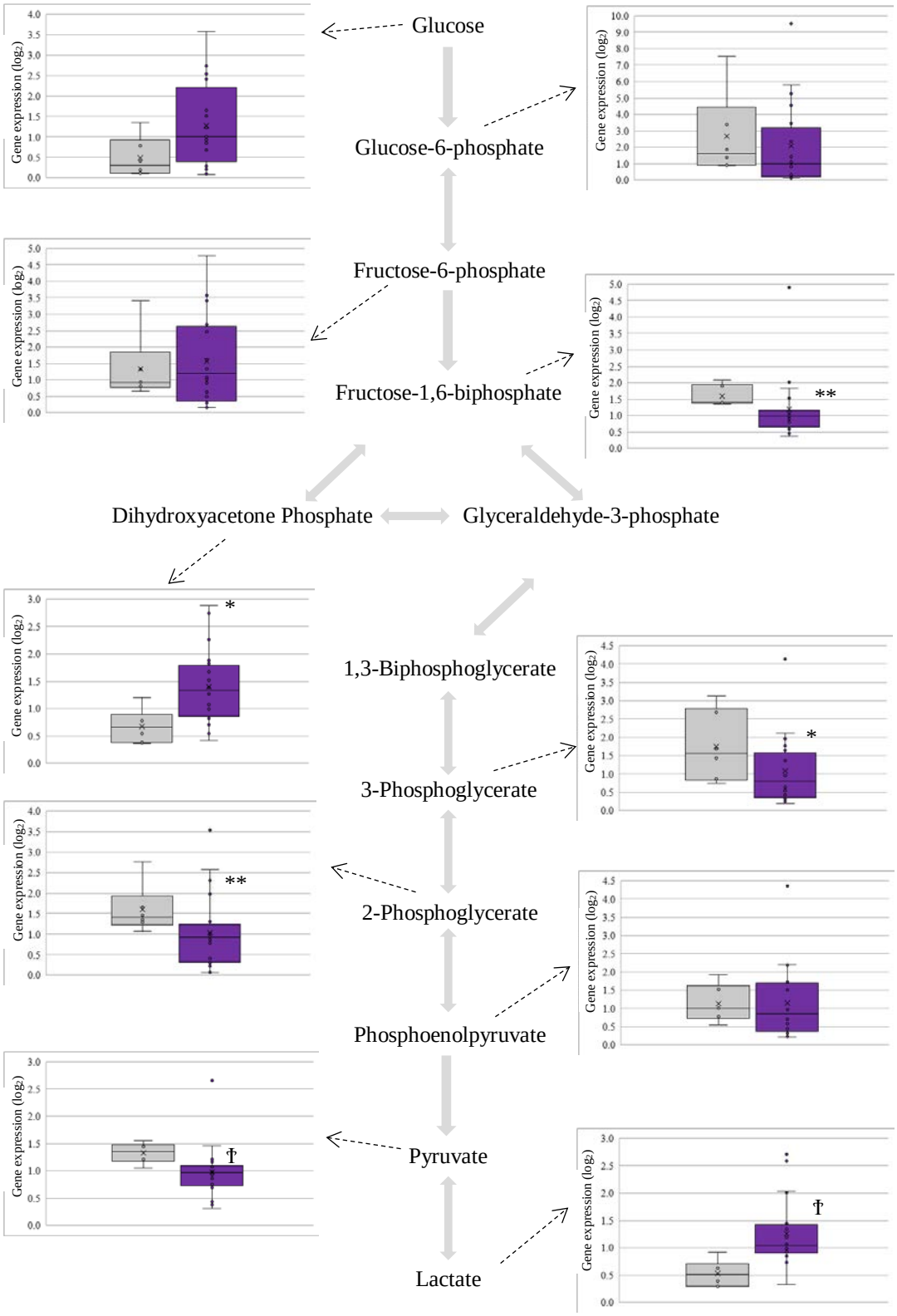

Figure 4-16. Changes in glycolytic intermediates in AML patient samples compared with healthy controls. Schematic diagram of glycolysis, showing variation in glycolytic metabolite levels, as detected by mass spectrometry, in healthy human mononuclear cells (grey) and AML patient blasts (purple). Data shows relative values following normalisation to Bradford protein concentration, log transformation and imputation of missing values with the minimum observed value for each compound (n=6 control, n=20 AML blasts). Box plots represent median quartile ranges, x represents mean value, • or ◦ represent individual data points. * denotes $p<0.05$, ** denotes $p<0.01$ and Ŧ denotes $p<0.005$ as analysed by Welch's two sample t-test.

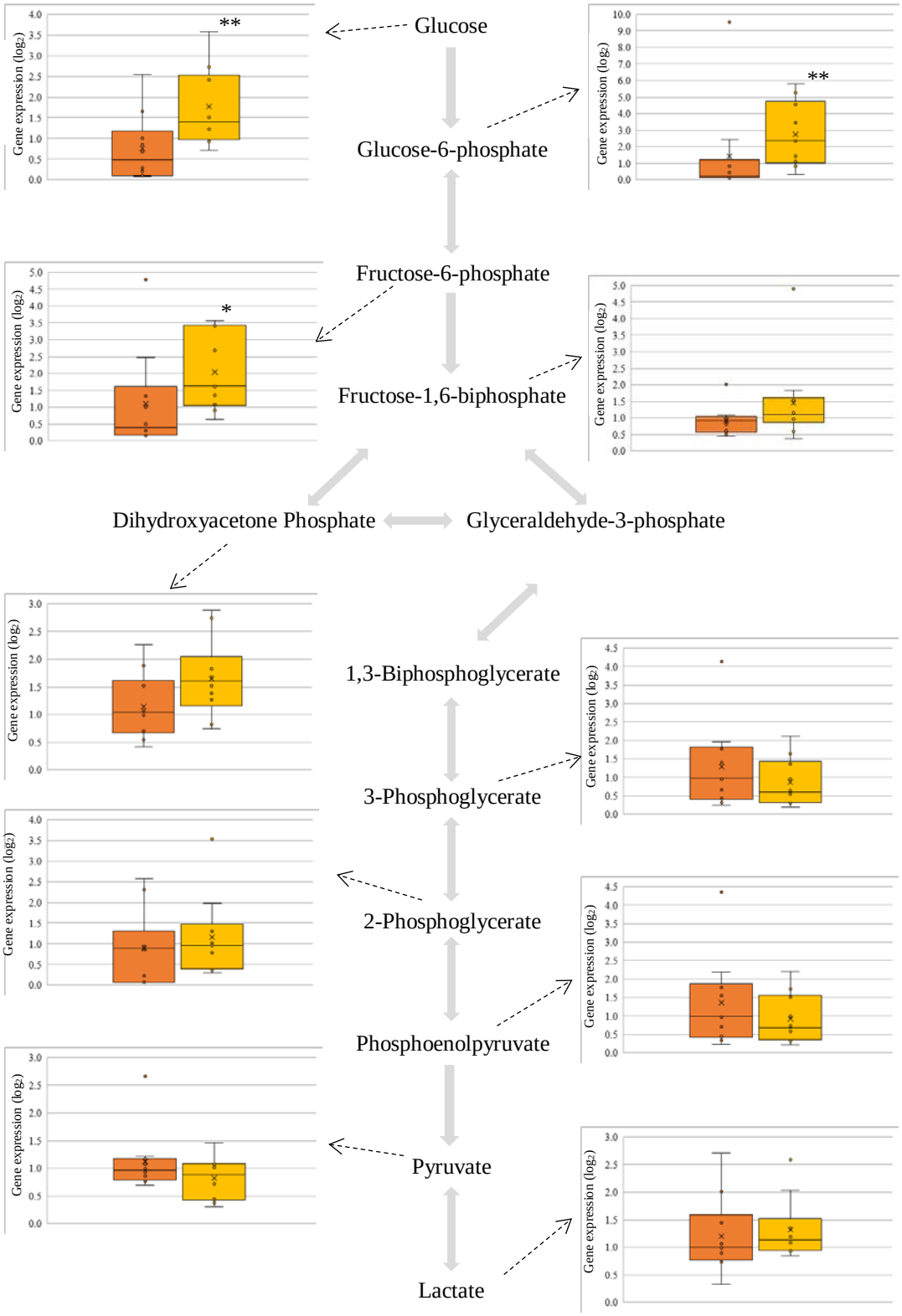

Figure 4-17. Changes in glycolytic intermediates in ROS high AML blast compared with ROS low AML blasts. Schematic diagram of glycolysis, showing variation in glycolytic metabolite levels, as detected by mass spectrometry, in ROS low AML blasts (orange) and ROS high AML blasts (yellow); Data shows relative values following normalisation to Bradford protein concentration, log transformation and imputation of missing values with the minimum observed value for each compound (n=10). Box plots represent median quartile ranges, x represents mean value, • or ◦ represent individual data points. * denotes $p<0.05$ and ** denotes $p<0.01$ as analysed by Welch's two sample t-test.

4.3.6.2 AML patient samples show changes in pentose phosphate pathway metabolite profile

As described earlier (4.3.5.4), the PPP generates nucleotides for biosynthesis and NADPH an important antioxidant. AML cell lines showed ROS dependent changes in 6-PG the first intermediate of the PPP pathway. Further metabolism along this pathway generates ribose-5-phosphate (R-5-P), a key metabolite in the synthesis of nucleotides and xylulose-5-phosphate (X-5-P) (reviewed in Samland and Sprenger, 2009). Therefore, to examine whether AML blasts show changes in PPP metabolites and to determine if ROS is a factor in these changes, the mass spectrometry data was analysed by Metabolon^{TM}, for changes in these metabolites. AML blasts showed non-significant increases in 6-PG (1.2-fold) and X-5-P (2.2-fold), whilst a significant increase in R-5-P (3.7-fold, $p=0.004$) was observed when compared to mononuclear controls (Table 7). Interestingly when the ROS high blasts were compared with the ROS low blasts a non-significant decrease in both 6-PG (2.5-fold) and R-5-P (1.3-fold) was observed, however a significant 2-fold ($p=0.002$) increase in X-5-P was also seen (Table 8). These data suggest that AML patient blasts show increased utilisation of PPP compared to healthy controls, although the data on the impact of ROS on this pathway is more equivocal.

Table 7. Variation in PPP metabolite levels in AML patient samples compared with healthy controls. Table shows median and mean fold changes in detectable PPP metabolites in AML patient blasts compared with healthy human mononuclear cells , as detected using gas chromatography mass spectrometery. Boxes shaded dark purple indicate significant differences performed on the mean ($p<0.05$) using Welch's two sample t-test, q-values represent the false discovery rate.

Metabolite	AML blasts vs human mononuclear control cells			
	Median Fold Change	Mean Fold Change	p-value	q-value
6-Phosphogluconolactone	0.62	1.17	0.2238	0.0618
Ribose-5-phosphate	3.91	3.73	0.0042	0.0021
Xyulose-5-phosphate	2.11	2.20	0.0532	0.0184

Table 8. Variation in PPP metabolite levels in ROS high AML blasts compared with ROS low AML blasts. Table shows median and mean fold changes in detectable PPP metabolites in ROS high AML blasts compared with ROS low AML blasts, as detected using gas chromatography mass spectrometery. Boxes shaded dark yellow indicate significant differences performed on the mean ($p<0.05$) using Welch's two sample t-test, q-values represent the false discovery rate.

Metabolite	ROS high vs ROS low AML blasts			
	Median Fold Change	Mean Fold Change	p-value	q-value
6-Phosphogluconolactone	1.01	0.40	0.6552	0.479
Ribose-5-phosphate	1.10	0.77	0.3167	0.3269
Xyulose-5-phosphate	2.82	2.03	0.0022	0.0288

4.4 Discussion

This chapter presented data which supports the hypothesis that changes in aerobic glycolysis are mediated by increased levels of ROS in both mutant-RAS expressing HPC and in AML derived cell lines. Further, it was also demonstrated that these effects are potentially mediated by changes in several proteins involved in carbohydrate metabolism with strongest changes observed in PFKFB3. Finally, metabolomic analysis of levels of glycolytic metabolites in cell line models and AML patient samples offer further evidence to support ROS modulating glycolytic activity in AML.

4.4.1 The effect of RAS and ROS on glycolysis and PFKFB3 expression

Oncogenic *RAS* has been widely reported to show increased glycolytic activity and is linked with increased activity of GLUT1, PFK1, GAPDH and PKM2 (reviewed in Chesney and Telang, 2013). Recent work by Song *et al.*, 2016 and Chen *et al.*, 2016b have also shown increased expression of GLUT1 and GLUT5 mRNA respectively, within an AML context. A new analysis of previously generated microarray data by our group, specifically focussing on glycolytic enzymes, showed increased mRNA transcription of several glycolytic enzymes in N-RAS^{G12D} HPC compared to control HPC (4.3.1). Furthermore, this increased mRNA expression of glycolytic enzymes is decreased in N-RAS^{G12D} HPC when ROS is inhibited by treatment of the cells with DPI. However, as noted previously, changes in mRNA expression do not necessarily correlate with increased protein expression. Analysis of mutant-RAS expressing HPC showed increased protein expression of several glycolytic enzymes (most markedly GLUT3, PFK(P) and PFKFB3), but only PFKFB3 showed a ROS dependent change in protein expression and then only in N-RAS^{G12D} HPC (Figure 4-3). The discrepancy between N-RAS^{G12D} and H-RAS^{G12V} HPC may reflect an alternate mechanism for PFKFB3 overexpression in H-RAS^{G12V} compared with N-RAS^{G12D} or may be a result of a sub-optimal DPI dose in these cells, which generate significantly more ROS than their N-RAS^{G12D} counterparts (Hole *et al.*, 2010).

PFKFB3 catalyses the reaction of F-6-P to F-2,6-BP (1.5.1). F-2,6-BP is a powerful allosteric activator of PFK which catalyses F-6-P to F-1,6-BP (reviewed in Ros and Schulze, 2013) a rate limiting step in glycolysis (Xie *et al.*, 2016) and increased

PFKFB3 expression has been shown to increase glucose uptake and cellular lactate generation in a number of solid tumour cell lines. Heterozygotic genomic deletion of PFKFB3 in mouse lung fibroblasts resulted in decreased F-2,6-BP production and decreased lactate secretion (Telang *et al.*, 2006); chemical inhibition of PFKFB3 in Jurkat T cell leukaemia cells results in decreased proliferation, glucose uptake and lactate secretion (Clem *et al.*, 2008) and a recent study showed glucose uptake and lactate secretion was decreased upon chemical inhibition of PFKFB3 in HNSCC cell lines (Li *et al.*, 2017a). PFKFB3 mRNA expression has been shown to be upregulated in a number of solid tumours including colon, breast, prostrate, ovary and thyroid (Atsumi *et al.*, 2002) and a recent study showed increased immunohistochemical staining of PFKFB3 in 111 head and neck squamous cell carcinoma patient samples when compared with normal surrounding tissue (Li *et al.*, 2017a).

Here, inhibition of NOX2-derived ROS in the THP-1 cell line resulted in decreased expression of PFKFB3, whilst analysis of other glycolytic enzymes showed no ROS associated changes in protein expression levels. This suggests that ROS modulates PFKFB3 expression in these cells and is a key player in ROS induced changes in glycolysis. Additionally, increased exogenous ROS levels, in the Mv4;11 cell line, resulted in increased protein expression of PFKFB3, as well as increased HK1 and PFK(P) expression (Figure 4-5). Furthermore, treatment of this cell line with both GOX and catalase (which decomposes H_2O_2, but not superoxide) did not increase protein expression of these enzymes, providing further evidence that it is NOX-derived ROS that modulates expression levels of this protein (4.3.3.2). Curiously, knock-down of NOX2 in the NOMO-1 cell line did not result in changes in expression levels of any of the glycolytic enzymes tested whilst chemical inhibition with DPI resulted in decreased expression but only of FBP1 (Figure 4-4). NOMO-1 cells generate much higher levels of superoxide than THP-1; furthermore, whilst knock-down of NOX2 in these cells decreased superoxide production by 30%, THP NOX2-KD cells showed a 90% decrease in superoxide production (3.3.3.1). Whilst chemical inhibition of NOMO-1 cells with DPI decreased superoxide production by 65%, it is worth noting that this reduction would still mean these cells were generating superoxide levels similar to those generated in untreated THP-1 cells. These much higher levels of superoxide production in NOMO-1 cells, coupled with

a less efficient knock-down of NOX2, may offer one possible explanation for the absence of decreased PFKFB3 expression. Alternatively, FBP1 (an enzyme involved in gluconeogenesis, which catalyses the reaction F-1,6-BP to F-6-P, the reverse step of the glycolytic reaction catalysed by PFK), showed decreased expression levels in DPI treated NOMO-1 cells, which could suggest that the mechanism by which ROS modulates glycolytic change may vary between cell lines.

In N-RAS^{G12D} HPC and the THP-1 and Mv4;11 cell lines, changes in protein expression of PFKFB3 were observed in conjunction with changes in NOX2 derived ROS levels. PFKFB3 has additionally been shown to translocate to the nucleus of cell lines (Yalcin *et al.*, 2006), leading to increased cellular proliferation (Yalcin *et al.*, 2009a). Given that ROS modulation resulted in proliferative changes in mutant RAS expressing HPC (3.3.2.4) and AML derived cell lines (3.3.3.4), nuclear expression of PFKFB3 was examined in THP-1 cells. No expression of PFKFB3 was found in either the nucleus of the ROS inhibited THP-1 cells or the THP control cells, demonstrating that PFKFB3 does not translocate to the nucleus and that this mechanism is not involved in proliferative changes in these cells. It has also been reported that phosphorylation of PFKFB3 at Ser-461 increases glycolytic flux (Novellasdemunt *et al.*, 2013). Here, analysis of p-PFKFB3 expression in N-RAS^{G12D} HPC demonstrated that ROS did not lead to changes in phosphorylation of this protein, as chemical inhibition of ROS in these cells resulted in similar relative changes in expression of both p-PFKFB3 and total PFKFB3. Conversely in AML cell lines, whilst ROS leads to changes in PFKFB3 expression in both THP-1 and Mv4;11 cells, no changes were observed in the relative expression levels of p-PFKFB3, which may suggest a ROS induced inhibition of phosphorylation in these cells. The discrepancy between these results and those observed in N-RAS^{G12D} HPC may well reflect a lack of specificity with this antibody and there are issues with detecting phosphorylated proteins by western blot (Campa and Kypta, 2011). However, given the variety of ROS related post-translational modifications to PFKFB3 reported in the literature (1.5.1.2) and the potential impact on metabolic regulation (4.4.2), further examination of the data described above may be warranted.

Further evidence that NOX2-derived ROS affects glycolysis was provided through metabolomic analysis. Metabolomic data from patient samples showed significant

increases in cellular glucose, G-6-P and F-6-P levels in ROS^{Hi} compared with ROS^{Lo} AML blasts (Figure 4-17), supportive of ROS induced increases in glucose uptake in these cells.

4.4.1.1 The effect of ROS and PFKFB3 expression on cellular lactate levels

Whilst data presented above and in chapter 3 demonstrates a clear association between increased ROS levels and increased glucose uptake, the link between increased ROS and increased lactate is less clear. Metabolomic analysis of THP-1 cells, in which NOX2 was knocked-down or chemically inhibited with DPI, showed that intracellular lactate levels are significantly decreased compared to control (4.3.5.3), supportive of the idea that ROS associated increases in PFKFB3 expression are synonymous with increased glycolysis. Supportive of this, in NOMO NOX2-KD cells, which showed no observable changes in PFKB3 expression compared to control, no changes in intracellular lactate levels were seen. However, treatment of NOMO-1 cells with DPI (which also show no changes in PFKFB3 expression) did lead to a significant decrease in intracellular lactate levels. This decrease may be a function of the decreased FBP1 expression (which could result in decreased lactate recycling (4.4.2)), or may be an off-target effect.

Contrary to the hypothesis that decreased ROS results in decreased intracellular lactate levels is that, in Mv4;11 cells, exposure to increased exogenous ROS, resulted in either, no change in intracellular lactate levels (GOX 10mU/ml) or a significant decrease in intracellular lactate levels (GOX 20mU/ml). One possible explanation for this discrepancy is that ROS may affect the rate at which these cells transport lactate across the cellular membrane. Supportive of this, is the observation that Mv4;11 cells subjected to increased exogenous ROS show increased levels of lactate secretion (3.3.3.3). Monocarboxylic transporters (MCT) are responsible for the transfer of lactate across the plasma membrane and the isoform MCT4 has been shown to be overexpressed in highly glycolytic tissues, induced by hypoxia and overexpressed in a number of tumour types (reviewed in Baltazar *et al.*, 2014). Interestingly, the microarray data in $N\text{-}RAS^{G12D}$ HPC (4.3.1) show ROS dependent increases in MCT4 expression in mutant RAS expressing HPC. However, no ROS associated changes in MCT4 protein expression were observed either in mutant RAS expressing HPC or cell lines. Overexpression of other MCT isoforms have been

reported in a several cancers however, therefore it remains possible that the ROS induced increases in lactate secretion observed in the Mv4;11 cell line, are a result of upregulation of one of these alternate isoforms.

4.4.2 The effect of ROS and PFKFB3 expression on the Pentose Phosphate Pathway

Further complexity in determining the effect of ROS on lactate generation, is the observation that ROS inhibition, in both the THP-1 and NOMO-1 cell lines and mutant RAS expressing HPC, leads to an increase in extracellular lactate (3.3.2.3, 3.3.3.3). One frequently cited hypothesis for increased aerobic glycolysis in cancer cells is the accumulation of glycolytic intermediates important in biosynthesis (reviewed in Mayers and Vander Heiden, 2015). One important metabolic pathway for nucleotide biosynthesis is the PPP (1.4.4) and as noted previously (3.4), one potential explanation for the increase in extracellular lactate in ROS inhibited THP-1 and NOMO-1 cells may involve increased recycling of lactate into the PPP, which is known to be dysregulated in a number of cancers (reviewed in Patra and Hay, 2014). Additionally, the first step of the PPP (G-6-P to 6-PG) generates NADPH an important molecule in relieving the cellular oxidative stress generated by excess ROS. Data discussed above (4.4.1) demonstrated that AML ROS^{Hi} blasts had significantly higher levels of G-6-P and F-6-P than ROS^{Lo} blasts, whilst both THP-1 cells and Mv4;11 cells showed no equivalent changes in pPFKFB3 expression because of ROS modulation, such as those observed in PFKFB3 expression. Given that it has been reported (Novellasdemunt *et al.*, 2013), that phosphorylation of PFKFB3 at Ser-461 generates an increase in glycolytic flux, these data suggest that increased ROS may lead to both an increase in glucose uptake (as a result of increased PFKFB3 expression) whilst simultaneously modulating glycolytic flux via phosphorylation of PFKFB3 and diverting intermediates into the PPP. Interestingly, metabolomic data from THP-1 and NOMO-1 cells treated with DPI and in NOMO NOX2-KD cells, shows decreased levels of 6-PG, whilst Mv4;11 cells treated with GOX show increased levels of 6-PG (4.3.5.4), data supportive of this idea. Whilst AML blasts showed higher levels of PPP intermediates than human mononuclear cells (Table 7), the data for ROS^{Hi} compared with ROS^{Lo} blasts was more equivocal. X-5-P (xyulose-5-phosphate) levels showed a significant 2-fold increase in ROS^{Hi} blasts compared to ROS^{Lo} blasts supportive of the idea that increased ROS results in

increased flux through the PPP. However, both 6-PG and R-5-P levels were reduced in ROS^{Hi} compared with ROS^{Lo} blasts, although this did not reach significance (Table 8). Taken together these data indicate that increased levels of ROS may result in a metabolic shift into the PPP to relieve cellular oxidative stress, which is at least partially enabled by lactate recycling, an idea further supported by the decreased expression of FBP1 in NOMO-1 cells treated with DPI (4.3.3.1). Futhermore, lactate is a known inhibitor of PFK (Leite *et al.*, 2007), this suggests that in cells with lower ROS levels, cellular NADPH requirements will be reduced and in order to maintain energy production via glycolysis, the need for cells to excrete lactate will be increased. These data then suggest another potential ROS related glycolytic regulatory mechanism, that balances the energy requirements of cells with the need to provide molecules for biosynthesis and manage oxidative stress.

In contrast, the argument that increased ROS leads to an increase in PPP flux is not supported by the observation that THP NOX2-KD cells show a 3.3-fold increase in 6-PG levels compared to control cells (4.3.5.4). However, given that these cells show a larger decrease in PFKFB3 protein expression when NOX2 is knocked-down compared with chemical inhibition with DPI (Figure 4-4A), this anomaly could be the result of a larger decrease in the conversion of F-6-P to F-1,6-BP in the NOX2-KD cells compared to the DPI treated cells, resulting in an accumulation of glycolytic intermediates above this step. This idea is supported by the 5.2-fold increase in F-6-P observed in THP NOX2-KD cells, which contrasts with a reduction in this metabolite in THP-1 and NOMO-1 cells treated with DPI and in NOMO NOX2-KD cells (4.3.5.3). This suggests that the impact of ROS on glycolysis and the PPP may vary between cell lines and variations in glycolytic and PPP metabolites may be dynamically affected by cellular ROS levels.

4.4.3 The effect of ROS on 3-phosphoglycerate levels and serine synthesis

Whilst the metabolomic data presented above broadly supports the hypothesis that inhibition of ROS in THP and NOMO cell lines results in decreases in glycolytic intermediates (4.3.5.3), one anomaly is that levels of 3-PG are increased in both cell lines when NOX2 is knocked-down and significantly increased upon treatment with DPI. 3-PG has previously been shown to inhibit the enzyme 6-phosphogluconate dehydrogenase which catalyses the third step of the PPP (Hitosugi *et al.*, 2013) and

is also the first step in the serine synthesis pathway (SSP) which also generates NADPH (see below). Consequently, when cellular ROS levels are increased, decreases in this glycolytic intermediate (as observed above) would enable, via the SSP and relieved inhibition of the PPP, increased generation of NADPH to relieve oxidative stress. PGAM, which catalyses the conversion of 3-PG to 2-PG is negatively regulated by TP53 (1.4.3), which is in turn regulated by ROS (1.3.3.4). It may then be, that the increase in 3-PG observed in NOMO and THP cells when ROS is reduced (compared with a reduction in other glycolytic metabolites) is reflective of a positive feedback loop which maintains intracellular ROS levels.

3PG is the first step in the synthesis of the amino acid, serine as well as in the synthesis of sphingolipids. Sphingolipid metabolites are reduced in THP and NOMO cells with NOX2 knocked-down and increased in Mv4;11 cells treated with GOX, suggesting that ROS may be associated with increased flux through this pathway, which in turn would generate metabolites for biosynthesis. Interestingly, a recent study reported that the HeLa cell line and the large cell lung cancer cell line H460, both utilised exogenous lactate to synthesise a large percentage of their lipids offering another potential explanation for anomalous ROS related changes in extracellular lactate levels (Chen *et al.*, 2016d). The first step of the SSP involves the conversion of 3-PG to 3-phosphohydroxypyruvate, catalysed by phosphoglycerate dehydrogenase, which has been shown to be upregulated in a variety of cancer cell lines (Possemato *et al.*, 2011, Locasale *et al.*, 2011). Analysis of metabolomic data above shows that serine levels are significantly reduced in THP NOX2-KD cells (though not NOMO NOX2-KD cells) and THP and NOMO cells treated with DPI (Table 6), again suggesting that increased levels of ROS may be associated with increased serine production, thus generating nucleotides for biosynthesis and NADPH (Ye *et al.*, 2014). Additionally, it is noteworthy that ROS inhibition decreased nearly all amino acid metabolite levels in THP cells whilst addition of the lower dose of GOX in Mv4;11 cells resulted in increased amino acid production (Table 6).

One potential implication of an interplay between ROS levels and serine synthesis is that serine activates the tetramer form of PKM2, promoting the PEP to pyruvate reaction and increasing glycolytic flux (reviewed in Mazurek, 2011). However it has also been reported by Anastasiou *et al.*, 2011 that ROS promotes dissociation of the

tetramer PKM2 form to its inactive dimer form, leading to a decrease in PEP to pyruvate reaction and a decrease in glycolytic flux. Given that PEP is also known to inhibit PFK (Blangy *et al.*, 1968), these counteracting mechanisms involving ROS suggest a carefully balanced feedback loop that dynamically alters the metabolic flux of the glycolytic, pentose phosphate and serine synthesis pathways in accordance with cellular ROS levels. These mechanisms may help explain the apparent antithetical ROS induced changes in lactate generation observed between different cell lines (see chapter 6).

4.4.4 Concluding remarks

Data presented in this chapter suggests that not only does mutant RAS and ROS affect glucose uptake and lactate secretion, but it does this by changing the protein expression levels of several key glycolytic enzymes. Further, analysis of metabolomic data in conjunction with western blot analysis suggests that ROS may be involved in a complex network of glycolytic regulation, where increases in ROS, lead to increases in expression of glycolytic enzymes, predominantly in the early part of the glycolytic pathway, which drives this increase in glucose uptake and glycolytic rate. Alongside this, increased ROS levels increase oxidative stress within the cell which are managed via ROS mediated control of glycolytic metabolites in the later part of the glycolytic pathway, controlling flux through the PPP and generating NADPH, an important component in relieving oxidative stress (1.3.2.4). This would suggest that whilst glucose uptake is a useful measure of ROS induced changes in glycolysis, lactate production as a measure of glycolytic changes, maybe confounded by the antioxidant and biosynthetic requirements of the cell.

The predominance of ROS associated changes in PFKFB3 expression in the data presented above strongly suggest a role for ROS in modulating this enzymes expression. The data from chapter 3 suggests that increases in ROS lead to increases in glucose uptake and cellular proliferation. As ROS appears to have additional regulatory functions in controlling glycolytic flux, lactate may not be a good marker as a measure for increased glycolysis. Therefore, the next chapter will focus on examining the implications for cellular glucose uptake and proliferation when PFKFB3 activity is inhibited or knocked-down or overexpressed.

5 Modulation of PFKFB3 activity correlates with glucose uptake and proliferation in AML derived cell lines and this is function of ROS

5.1 Introduction

Chapter 3 demonstrated ROS modulated changes in glucose uptake and proliferation in mutant RAS expressing HPC and AML cell lines. Further, protein expression and metabolomic analysis of these models provided additional evidence that ROS affects cellular glycolytic activity (chapter 4) possibly mediated via changes in PFKFB3 protein expression. PFKFB3 is a key regulator of glycolysis (1.5.1) and has been shown to be overexpressed in numerous solid cancers (Atsumi *et al.*, 2002). Computational modelling has previously led to the identification of a molecular inhibitor of PFKFB3, 3PO, which was shown to decrease glycolytic flux in the Jurkat T-cell leukaemia cell line and result in decreased proliferation in several human cancer cell lines. Furthermore, *in vivo* experiments employing 3PO on three established xenograft models of, Lewis lung carcinomas, MDA-MB231 breast adenocarcinoma cells and HL-60 promyelocytic leukaemia cells in mice, reduced glucose uptake and suppressed tumour growth (Clem *et al.*, 2008). Therefore, this study next sought to examine the role of PFKFB3 in mediating the effects of ROS on glycolysis by chemical inhibition, knock-down or overexpression of this enzyme.

Furthermore, HIF-1α, a master regulator of cellular oxygen homeostasis (1.4.2.1), has been shown to upregulate many glycolytic enzymes, including PFKFB3 (reviewed in Yalcin *et al.*, 2009b). HIF-1α is upregulated as a physiological response to low oxygen levels with concomitant upregulation of a number of glycolytic genes (Greijer *et al.*, 2005). It is also known to be upregulated in a number of solid tumours (reviewed in Lu and Kang, 2010, Semenza, 2010b). Mutant RAS is known to upregulate HIF-1α (Chen *et al.*, 2001, Lim *et al.*, 2004); further, Obach *et al.*, 2004 identified HIF-1α binding sites in the gene promoter region of the *PFKFB3* gene and it has been demonstrated that *PFKFB3* mRNA is induced, both *in vitro* and *in vivo* as part of this hypoxic response (Minchenko *et al.*, 2002). Additionally, ROS is also known to be implicated in HIF-1α upregulation (Niecknig *et al.*, 2012). In the osteosarcoma cell line U2OS, treatment with exogenous H_2O_2 resulted in increased

HIF-1α protein expression after 1 hr, which was reversed after 6 hr. This was linked to direct ROS inhibition of PHD2, which was alleviated by upregulation of *PHD2* after 2-4 hrs (1.4.2.1). However, its exact role is still to be established; though a recent study provided evidence of a ROS driven HIF-1α response to hypoxia in endothelial cells (Paik *et al.*, 2017). Together these reports suggest that a potential mechanism exists, whereby increased ROS, results in increased expression and stabilisation of HIF-1α, which could, in turn leads to increased expression of PFKFB3 and increased glucose uptake. Coupled with the fact that HIF-1α is also upregulated in many cancers (Semenza, 2010b) this chapter additionally examines the potential interplay of ROS, HIF-1α and PFKFB3 to determine a potential mechanism for the ROS modulated changes in cellular glucose uptake, observed in chapter 3.

5.2 Aims and objectives

The main objective of this chapter is to determine the effect of modulating PFKFB3 expression on cellular glucose uptake and proliferation in AML cell lines and in HPC infected with mutant RAS. To achieve this, this chapter has the following aims:-

- To determine the effect of inhibiting PFKFB3 activity in AML cell lines and N-RAS^{G12D} HPC. To achieve this, cells will be treated with either chemical inhibitors of PFKFB3 or PFKFB3 expression will be knocked-down using shRNA and glucose uptake determined;
- To determine the effect of PFKFB3 overexpression on glucose uptake and proliferation in Mv4;11 cells and normal human HPC;
- To determine the effect on proliferation of PFKFB3 inhibition using PFK158 in combination with cytarabine (Ara-C), in AML cell lines;
- To determine the role of HIF-1α in mediating ROS induced changes in PFKFB3 expression. Inhibition of NOX2-derived ROS on protein expression levels of HIF-1α will be determined in THP-1 cells. The impact of HIF-1α knock-down on glucose uptake in this cell line will also be investigated.

5.3 Results

5.3.1 Pharmacological inhibition of PFKFB3 decreases glucose uptake and proliferation in AML cell lines and decreases glucose uptake in HPC

Previously it was shown that addition of exogenous ROS to the AML cell line Mv4;11 generated increased cellular glucose uptake and proliferation (3.3.3) which correlated with increased protein expression of the key glycolytic enzyme PFKFB3 (4.3.3.2). Furthermore, in the ROS producing AML cell line, THP-1, pharmacological inhibition or knock-down of NOX2 using shRNA, decreased protein expression of PFKFB3 (4.3.3.1), which was observed alongside decreased cellular glucose uptake and proliferation (3.3.3). Consequently, it was reasoned that these changes in glucose uptake and proliferation, may be a function of cellular changes in PFKFB3 expression and activity.

5.3.1.1 Pharmacological inhibition of PFKFB3 with 3-PO and PFK158 decreases glucose uptake in the Mv4;11 cell line

Two chemical inhibitors of PFKFB3 (3PO and PFK158) were employed to examine the hypothesis that this protein mediates changes in ROS induced glucose uptake and proliferation. To determine an effective inhibitory dose for 3PO and PFK158, Mv4;11 cells were treated with serial dilutions of the inhibitors over 24h. Using CellTiter-Glo^{TM}, which measures metabolic activity based on ATP generation, (2.8) Figure 5-1A(i) established an EC50 for 3PO (6.25μM) and Figure 5-1A(ii) 625nM for PFK158 in this cell line. To assess the impact of PFKFB3 inhibition on glucose uptake, Mv4;11 cells were treated with either 3PO (5μM), PFK158 (200nM or 625nM) and/or GOX (10mU/mL) (which generates H_2O_2 in the cell culture media) and incubated at 37ºC, 5% CO_2 for 24 h followed by glucose uptake analysis using 2-NBDG. To ensure these chemicals did not affect cell viability, cell death was analysed using flow cytometry (Figure 5-1B). No change in viability in Mv4;11 cells treated with 3PO, GOX or 3PO and GOX combined when compared to vehicle control, was observed. Figure 5-1C shows that these cells tolerated 100nM PFK158 both in the absence and presence of exogenous ROS. Interestingly higher concentrations of PFK158 (625nM) were tolerated by the Mv4;11 cells in the absence of exogenous ROS, but cell death increased when they were treated with GOX (10mU/mL) (see 5.4).

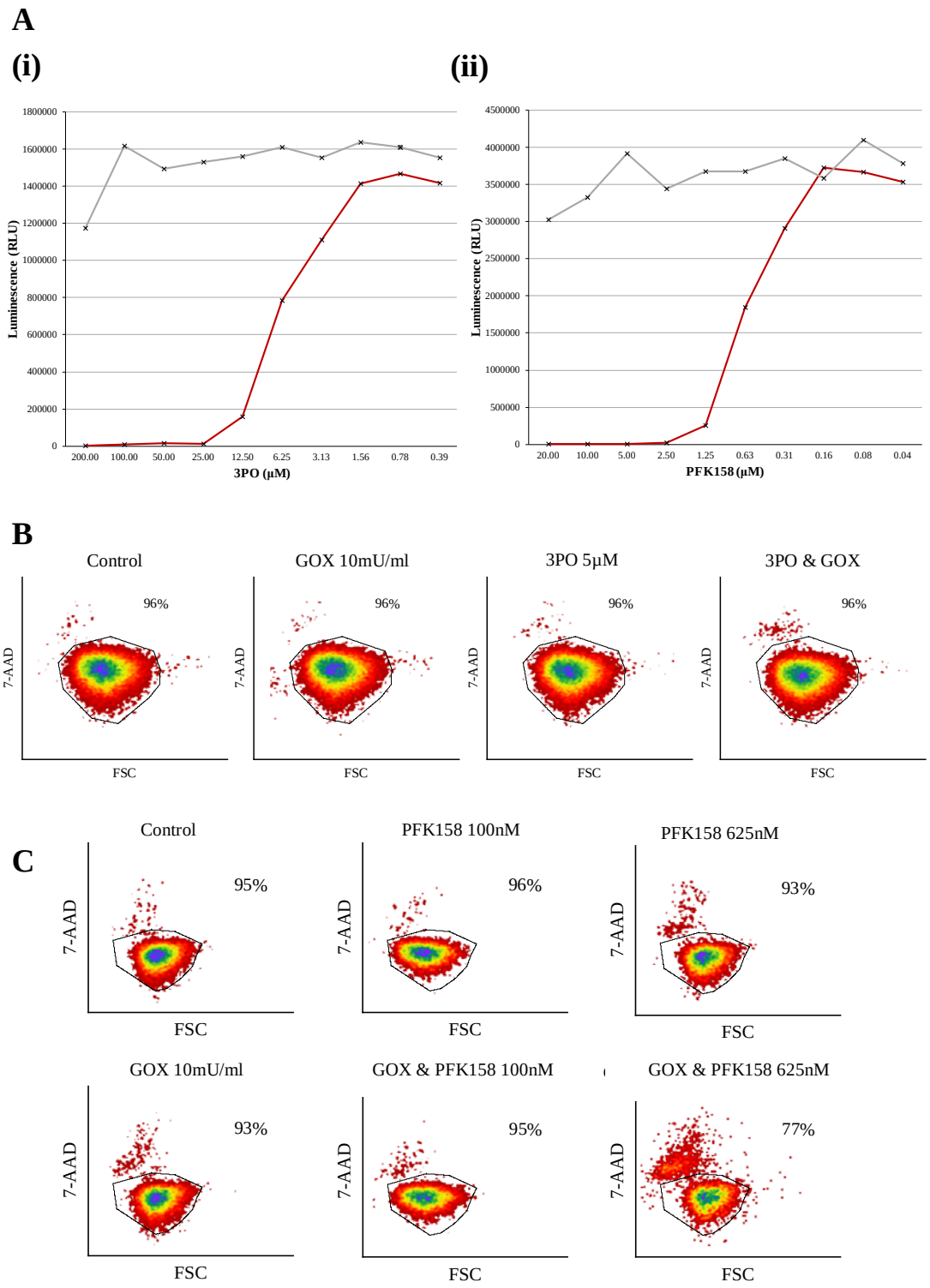

Figure 5-1. Determination of EC50 of 3PO and PFK158 and effect on cell viability on the Mv4;11 cell line. (A) Mv4;11 cells were seeded at 1 x 10^5 and cultured for 24h in the presence of **(i)** 3PO and **(ii)** PFK158 and subsequently assayed using CellTiter-Glo™. Red line represents cells treated with inhibitor, grey line represents cells treated with vehicle control (DMSO **(i)** 0.002-1% **(ii)** 8 x 10^{-5}-0.04%) (n=1). Representative flow cytometric density plots showing percentage of viable Mv4;11 cells, seeded at 2 x 10^5 cells/mL, treated with **(B)** GOX (10mU/mL) and/or 3PO (5µM) **(C)** GOX (10mU/mL) and/or PFK158 (100nM or 625nM) for 72h and compared for vehicle control (**(B)** DMSO 0.025%), **(C)** DMSO 0.0013%)). Data were gated to exclude cell debris based on FSC/SSC. Cells were incubated with 7-AAD, gated area shows proportion of viable cells (n=3).

Treatment of Mv4;11 cells with GOX (10mU/mL) resulted in a 1.2-fold increase in glucose uptake compared with control (as expected), whilst combined treatment with GOX (10mU/mL) and 3PO (5μM) ablated the response to GOX (Figure 5-2A). Treatment with 3PO alone did not alter glucose uptake when compared to control cells. These data indicate that chemical inhibition of PFKFB3 with 3PO counteracts the effect of increased exogenous ROS on glucose uptake in the Mv4;11 cell line.

Figure 5-2B shows treatment of Mv4;11 cells with GOX (10mU/mL) resulted in increased cellular glucose uptake (15% ±5%), however when these cells were additionally treated with either 200nM or 625nM PFK158, this increase in glucose uptake was not observed. No changes were observed in glucose uptake as a consequence of treatment with this compound alone. This suggests that treatment of Mv4;11 cells with the alternative PFKFB3 inhibitor PFK158, also negates ROS induced increases in cellular glucose uptake.

5.3.1.2 Pharmacological inhibition of PFKFB3 with 3-PO and PFK158 decreases glucose uptake and proliferation in the THP-1 cell line

To verify the data above, the ROS generating THP-1 cell line, was also treated with 3-PO and PFK158. To determine an effective inhibitory dose for PFK158 in this cell line, THP-1 cells were treated with serial dilutions of the inhibitor, cultured for a further 24h and assayed using CellTiter-Glo^{TM}. Figure 5-3A established an EC_{50} for this compound of 5μM in this cell line. Figure 5-3B shows that no significant changes in cell viability were observed in THP-1 cells treated with 3PO at a range of concentrations up to 10μM, but at 20μM, a loss in cell viability was observed. Treatment of this cell line with PFK158 was tolerated at 500nM and 1μM doses, whilst treatment with 5μM reduced cell viability (Figure 5-3C). To assess the impact of these compounds on glucose uptake, THP-1 cells were treated with 3PO or PFK158 and incubated for a further 24h prior to analysis with 2-NBDG.

Figure 5-4A shows that treatment with 5μM or 10μM 3PO resulted in a 17% ±13% and significant 19% ± 8% respective reduction in glucose uptake. Treatment with 1μM and 5μM PFK158, resulted in a respective 8% ±14% and 20% ±8% reduction in glucose uptake in these cells compared to control, whilst no change was observed upon treatment with 500nM PFK158 (Figure 5-4B).

To determine whether these changes in glucose uptake were reflected in proliferation, THP-1 cells were treated with 3PO and PFK158 for 72h. Treatment with 3PO resulted in a significant dose dependent decrease in proliferation of THP-1 cells (Figure 5-5A), whilst treatment with PFK158 significantly reduced proliferation by 35% (±5%) and 81% (±13%) at 1μM and 5μM respectively, whilst no change was observed at 500nM (Figure 5-5B). These data show that chemical inhibition of PFKFB3, results in decreased cellular glucose uptake and proliferation and taken together with the ROS dependent changes in PFKFB3 expression observed in chapter 4, suggests a potential ROS dependent mechanism for these changes.

5.3.1.3 Pharmacological inhibition of PFKFB3 with 3PO decreases glucose uptake in HPC expressing mutant RAS

It was previously shown that N-RAS^{G12D} HPC show increased levels of PFKFB3 expression compared to control which is decreased upon treatment with DPI, implicating ROS in mediating this effect (4.3.2.1). Glucose uptake was also increased in N-RAS^{G12D} compared with normal HPC and inhibition of ROS ameliorated this effect (3.3.1.2). To determine whether PFKFB3 inhibition also affected glucose uptake in HPC, N-RAS^{G12D} HPC (co-expressing DsRed) were treated with 3PO (5μM) and incubated for 24h, before glucose uptake was measured using 2-NBDG. As previously (3.3.1.2), N-RAS^{G12D} HPC showed a significant 1.4-fold increase in glucose uptake compared to control, however N-RAS^{G12D} HPC treated with 3PO (5μM) showed only a 1.1-fold increase compared to control, whilst treatment of control HPC with 3PO resulted in a 17% ±3% decrease in glucose uptake (Figure 5-6). These data show that PFKFB3 is important in regulating cellular glucose uptake in N-RAS^{G12D} HPC and that inhibition of this enzyme with 3-PO, results in decreased glucose uptake.

In summary, these data suggest that ROS associated increases in glucose uptake are ameliorated upon PFKFB3 inhibition with 3PO.

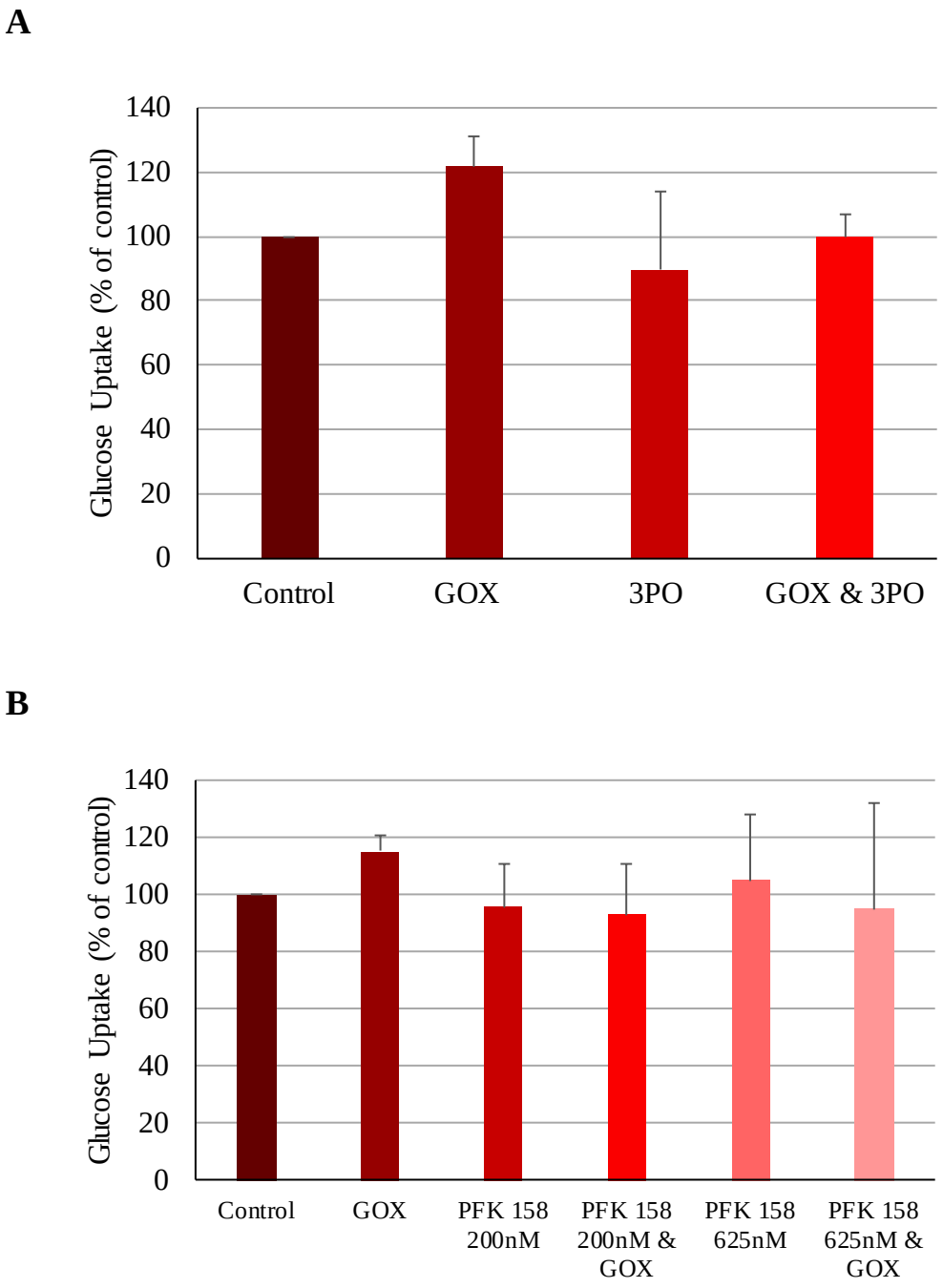

Figure 5-2. Chemical inhibition of PFKFB3 decreases cellular glucose uptake in the Mv4;11 cell line. Glucose uptake (normalised to control) in Mv4;11 cells seeded at 5 x 10^5 and incubated for 24h in the presence/absence of **(A)** 3PO (5µM) and/or GOX (10mU/mL) **(B)** PFK158 (200nM or 625nM) and/or GOX (10mU/mL) (n=3). Vehicle control (**(A)** DMSO 0.025%, **(B)** DMSO 0.0013%)) (dark red), GOX (10mU/mL) treated (deep red), PFK158 (200nM) treated (mid-red), GOX (10mU/mL) and 3PFK158 (200nM) treated (light-red), PFK158 (625nM) treated (dark pink), GOX (10mU/mL) and 3PFK158 (625nM) treated (light pink). Data represents mean ± 1SD.

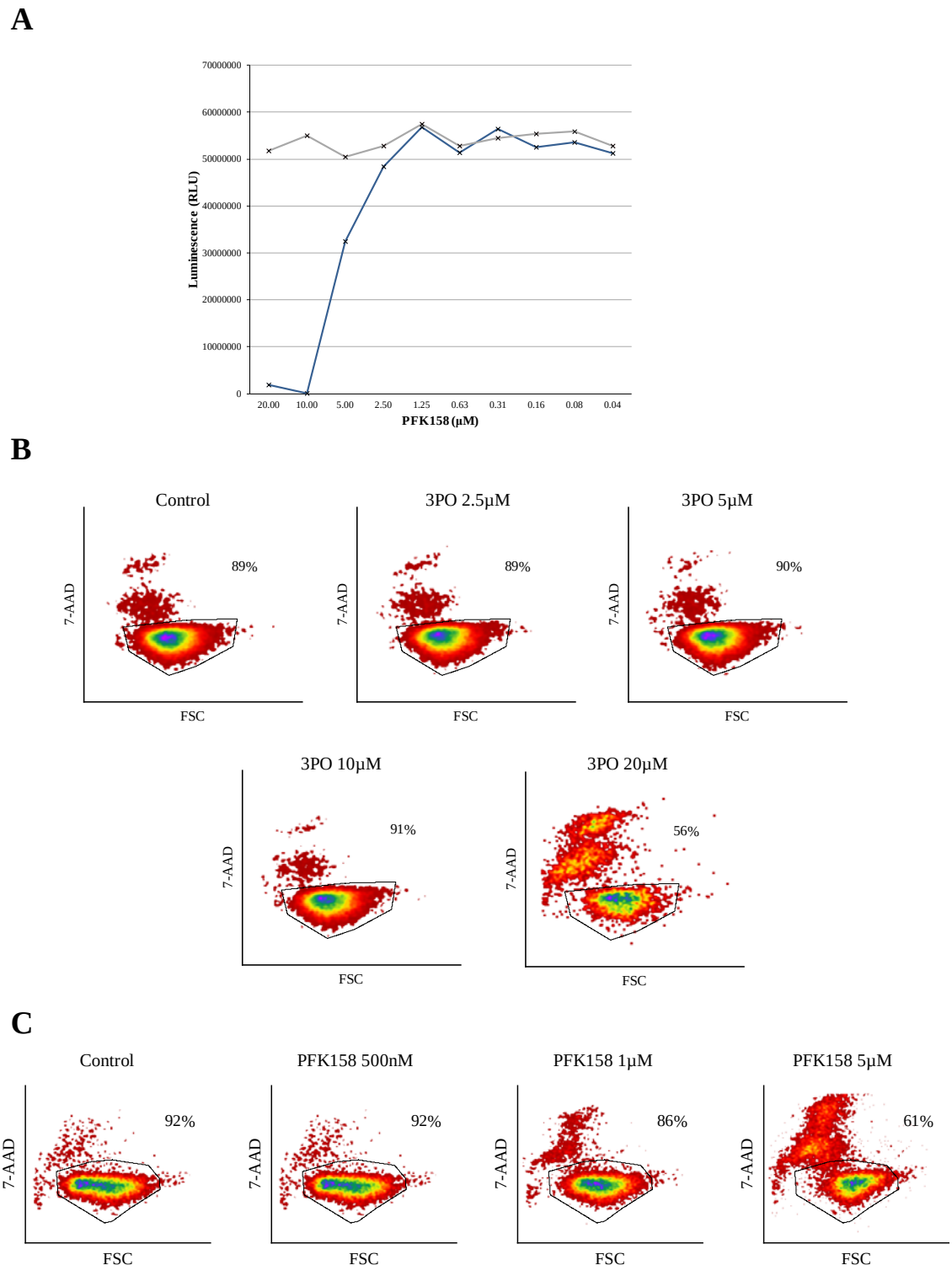

Figure 5-3. Determination of EC50 of PFKFB3 inhibitors and effect on cell viability on the THP-1 cell line. (A) THP-1 cells were seeded at 1 x 10^5 and cultured for 24h in the presence of PFK158. Cells were subsequently assayed using CellTiter-Glo™. Blue line represents cells treated with 3PO, grey line represents cells treated with vehicle control (DMSO 8 x 10^{-5}-0.04%) (n=1). Representative flow cytometric density plots showing percentage of viable THP-1 cells, seeded at 4 x 10^5 cells/mL, treated with **(B)** 3PO or **(C)** PFK158 for 72h and compared for vehicle control (**(B)** DMSO 0.1%, **(C)** DMSO 0.01%)). Data were gated to exclude cell debris based on FSC/SSC. Cells were incubated with 7-AAD, gated area shows proportion of viable cells (n=3).

A

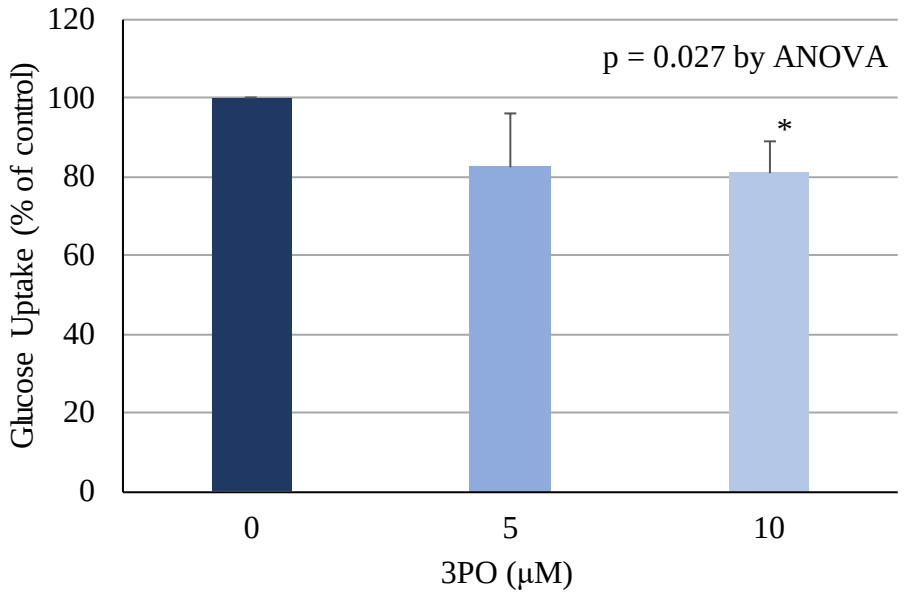

B

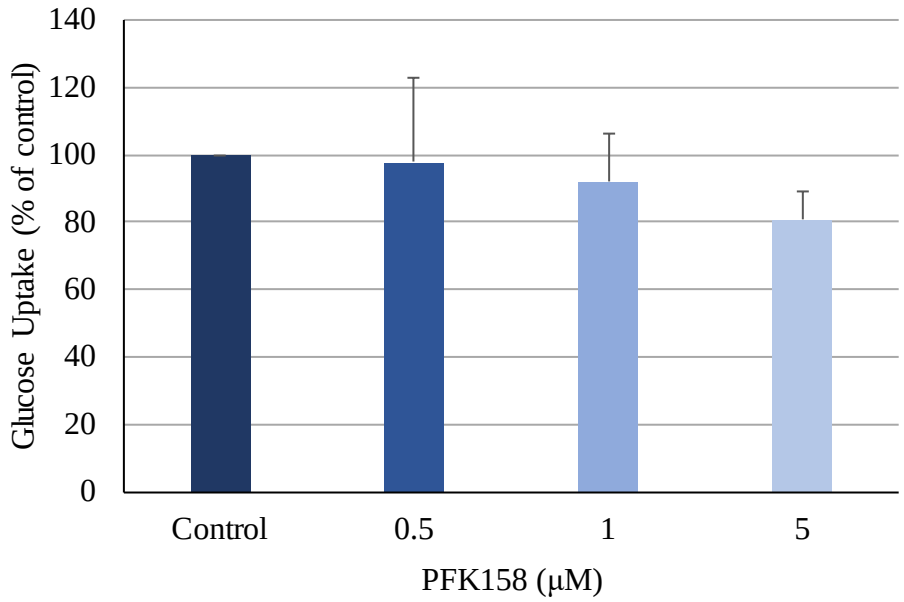

Figure 5-4. Chemical inhibition of PFKFB3 decreases cellular glucose uptake in the THP-1 cell line. Glucose uptake (normalised to control) in THP-1 cells, seeded at 5 x 10^5, treated with **(A)** 3PO, vehicle control (DMSO 0.05%) (dark blue), 3PO (5μM) (light blue), 3PO (10μM) (pale blue); or **(B)** PFK158, vehicle control (DMSO 0.01%) (dark blue), PFK158 (500nM) (blue), PFK158 (1μM) (light blue), PFK158 (5μM) (pale blue); and incubated for a further 24h (n=4). Data represents mean ± 1SD. * denotes $p<0.05$, analysed by ANOVA with Tukey's honestly significance difference.

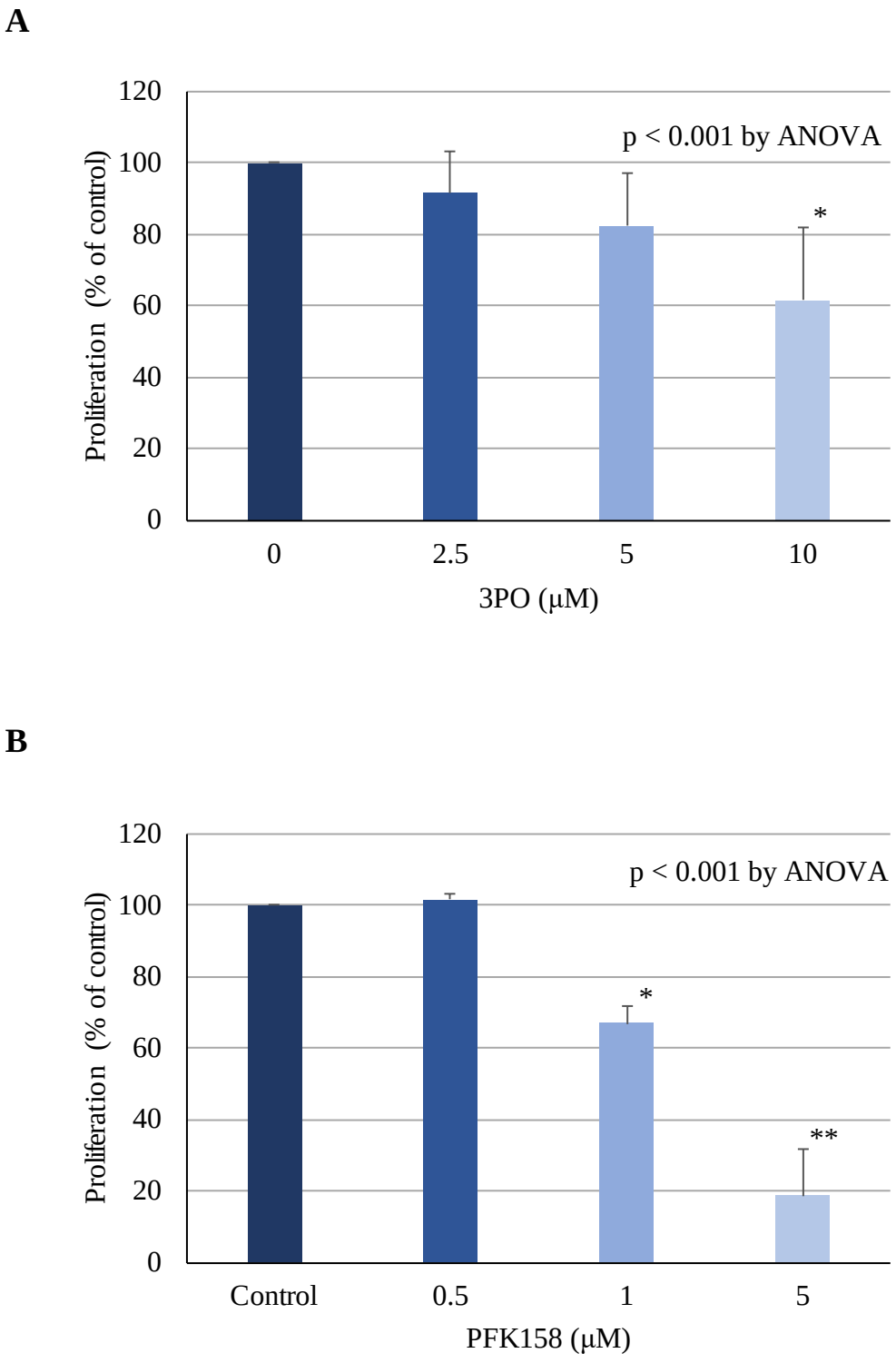

Figure 5-5. Chemical inhibition of PFKFB3 decreases cellular proliferation in the THP-1 cell line. Proliferation (normalised to control) in THP-1 cells, seeded at 4 x 10^5, treated with **(A)** 3PO, vehicle control (DMSO 0.05%) (dark blue), 3PO (5μM) (light blue), 3PO (10μM) (pale blue) (n=6); or **(B)** PFK158, vehicle control (DMSO 0.01%) (dark blue), PFK158 (500nM) (blue), PFK158 (1μM) (light blue), PFK158 (5μM) (pale blue) (n=3); and incubated for a further 72h (n=4). Data represents mean ± 1SD. * and ** denotes $p<0.05$ and represent significantly different groups from control, analysed by ANOVA with Tukey's honestly significance difference.

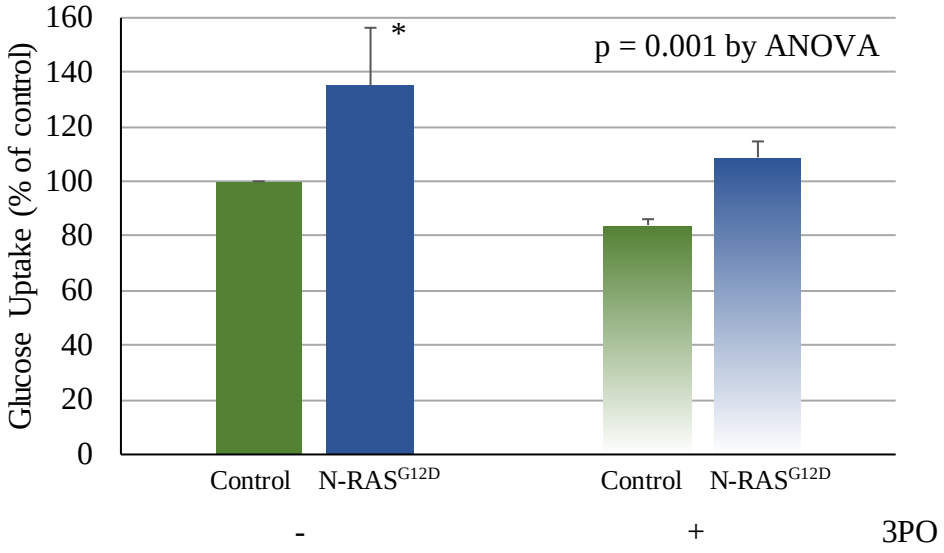

Figure 5-6. Inhibition of PFKFB3 with 3PO decreases cellular glucose uptake in N-RAS^{G12D} expressing HPC. Cellular glucose uptake (normalised to untreated control) in transduced HPC treated with 3PO (5μM). Cells were counted (day5) and cultured for a further 24h in the presence/absence of 3PO, without growth factors at an initial seeding of 6 x 10^5 cells/mL (n=3). Untreated control (solid green), N-RAS^{G12D} HPC (solid blue), control treated with 3PO (gradient green) and N-RAS^{G12D} HPC treated with 3PO (gradient blue). Data represents mean ± 1SD. * denotes $p<0.05$, analysed by ANOVA with Tukey's honestly significance difference.

5.3.2 Knock-down of PFKFB3 expression with shRNA results in decreased proliferation but not glucose uptake in the THP-1 cell line

The data above suggests that inhibition of PFKFB3 results in decreased glucose uptake in AML cell lines and N-RAS^{G12D}. In order to support these data using a more specific targeted approach, five shRNA sequences complementary to PFKFB3 and encoding puromycin resistance were lentivirally infected into Mv4;11 and THP-1 cells. To confirm successful knock-down of PFKFB3, western blots were performed on whole cell lysates. Figure 5-7A shows that knock-down of PFKFB3 in Mv4;11 cells was not successful, as treatment with GOX (20mU/mL maintained an increase in expression of PFKFB3, similar to the observed increase in control cells. However, Figure 5-7B shows that infection of THP-1 cells generated a decrease in PFKFB3 expression in two of the five shRNA clones. Three of the five shRNA clones, failed to proliferate, despite initially surviving puromycin selection (5.4). Of the two surviving clones, Clone 1 showing the largest decrease in PFKFB3 expression was used to analyse glucose uptake and proliferation. Figure 5-8A shows that knock-down of PFKFB3 had no effect on the viability of these cells when compared with control cells lentivirally infected with shRNA coding for a non-mammalian target sequence. Surprisingly, whilst knock-down of PFKFB3 in THP-1 cells resulted in a 1.8-fold reduction in proliferation compared to control (Figure 5-8B), no change in glucose uptake was observed (Figure 5-8C). This suggests that while PFKFB3 expression is important in maintaining the proliferative rate of these cells, it does not do so by modulating glucose uptake (5.4).

A

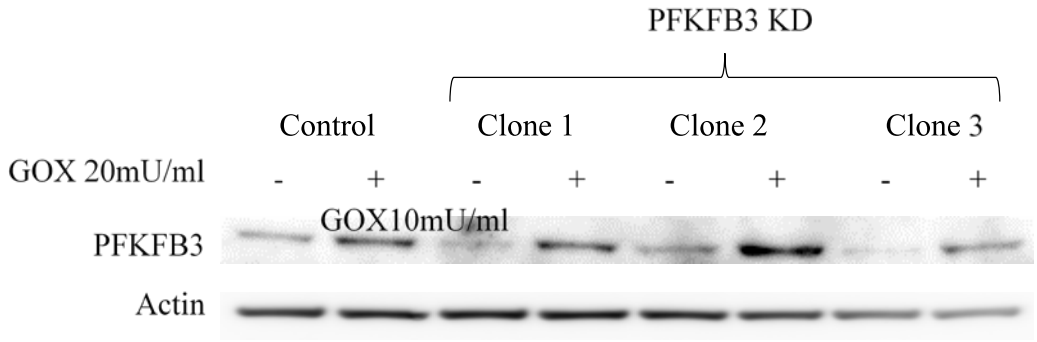

B

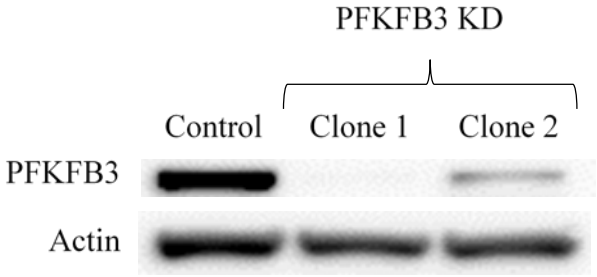

Figure 5-7. Knock-down of PFKFB3 in AML cell lines assayed by western blot. (A) Expression of PFKB3 in Mv4;11 cells with PFKFB3 knocked-down and treated with GOX (20mU/mL) cf. control (3 clones representative of 5). **(B)** Expression of PFKFB3 in THP-1 cells with PFKFB3 knocked-down cf. control. Actin was used as a loading control.

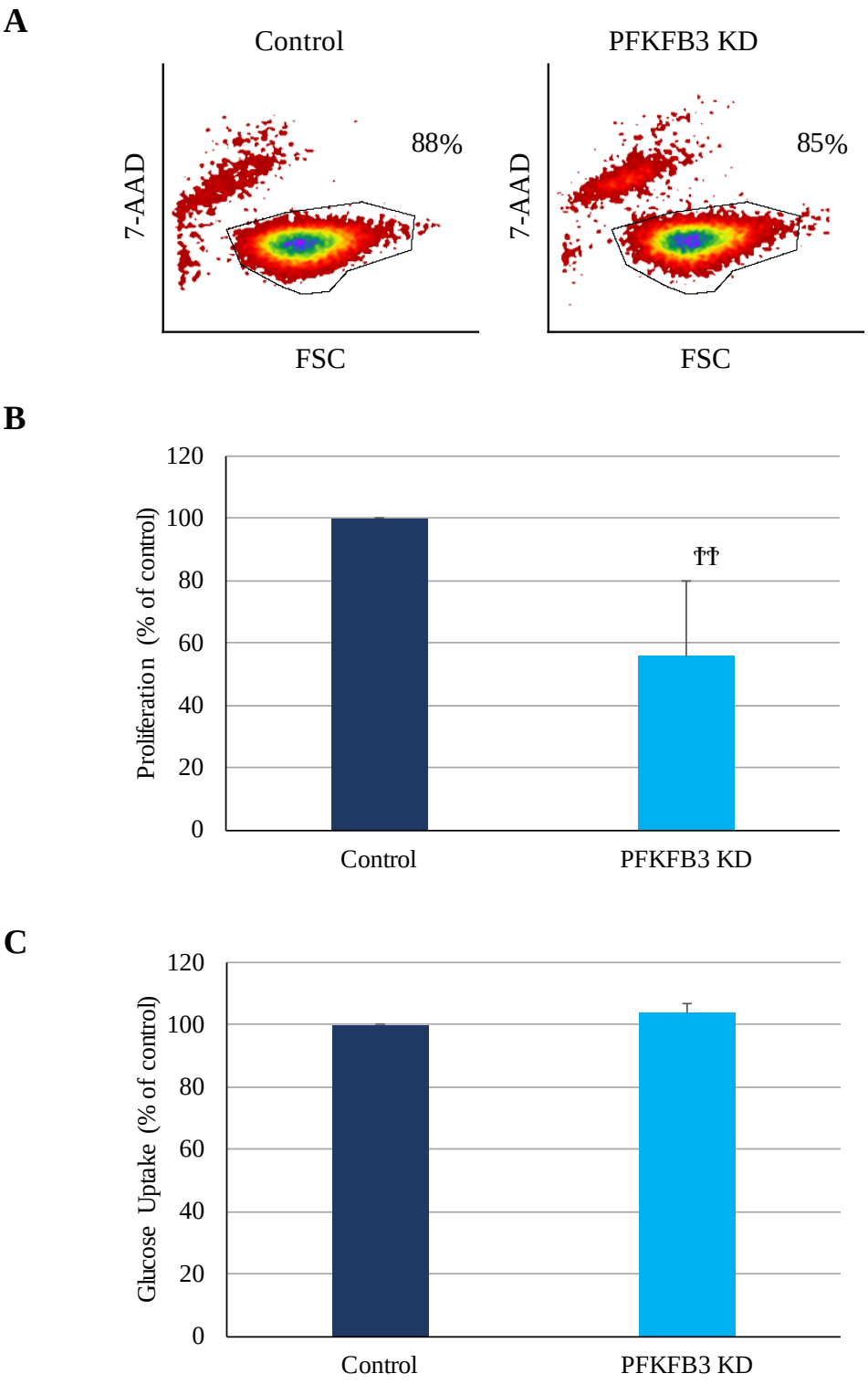

Figure 5-8. Effect of PFKFB3 knock-down on proliferation and glucose uptake in THP-1 cells. **(A)** Representative flow cytometric density plots showing percentage of viable THP PFKFB3-KD cells compared for control. Plots were gated to exclude cell debris based on FSC/SSC. Cells were incubated with 7-AAD, gated area shows proportion of viable cells (n=3). **(B)** Percentage proliferation (normalised to control) of THP PFKFB3-KD cells (bright blue) cf. control (dark blue); cells were seeded at 4 x 10^5 cells/mL and incubated for 72h (n=9). **(C)** Cellular glucose uptake (normalised to control) of THP PFKFB3-KD cells (bright blue) cf. control (dark blue); cells were seeded at 5 x 10^5 and incubated for 24h (n=5). Data represents mean ±1SD. †† denotes $p<0.001$ statistical significance calculated by Student's paired t-test.

5.3.3 Overexpression of PFKFB3 increases glucose uptake and proliferation in an AML cell line but not HPC

The above data demonstrates that pharmacological inhibition of PFKFB3 decreases cellular glucose uptake and proliferation (5.3.1). Furthermore, knock-down of PFKFB3 in THP-1 cells resulted in decreased levels of proliferation, though not glucose uptake. Therefore, it was reasoned that overexpression of this protein may lead to increases in glucose uptake and cellular proliferation. To study this, the DNA sequence of PFKFB3 was directionally subcloned into two different retro/lentiviral vectors (i) PINCO co-expressing DsRed and (ii) pHIV co-expressing GFP (2.2). Mv4;11 cells were infected with the pHIV vector (as these cells resist infection with retrovirus), HPC were infected with the PINCO vector co-expressing DsRed (to allow analysis using the 2-NBDG probe) and changes in proliferation and glucose consumption/uptake compared with controls.

5.3.3.1 Generation of PFKFB3 overexpressing retro- and lenti-viral vectors

The DNA sequence for PFKFB3 was directionally subcloned into the PINCO vector expressing DsRed and the pHIV vector expressing GFP. PFKFB3 cDNA was excised from the expression plasmid, pEX-K4, using *Bam*HI and *Eco*RI, or *XbaI* HF and *HpaI* HF restriction enzymes. As shown in Figure 5-9A, restriction digest results in expected DNA fragments observed around 1.5kb and 2.5kb. As a control, undigested DNA showed a DNA fragment migrating at around 4kb. PFKFB3 DNA was subsequently ligated into the PINCO and pHIV vectors, transformed into competent cells and plasmid DNA extracted using a Qiagen Maxi/Miniprep kit (2.2.2). To verify successful ligation and orientation of the PFKFB3 DNA, a 'test digest' was performed using the restriction enzymes *Sma*I for the pHIV and *Sca*I for PINCO vector (2.2.3.3). Predicted DNA migrating patterns for the digested PINCO vector were 10.7kb and 3.6kb, whilst for the pHIV vector predicted DNA fragment sizes were 7.8kb and 1.5kb. Figure 5-9B shows that ligations into both the PINCO and pHIV vector contained the PFKFB3 DNA sequence in the correct orientation. Integrity of the inserted PFKFB3 DNA was confirmed by Sanger sequencing (courtesy of Eurofins MWG, Ebersberg, Germany).

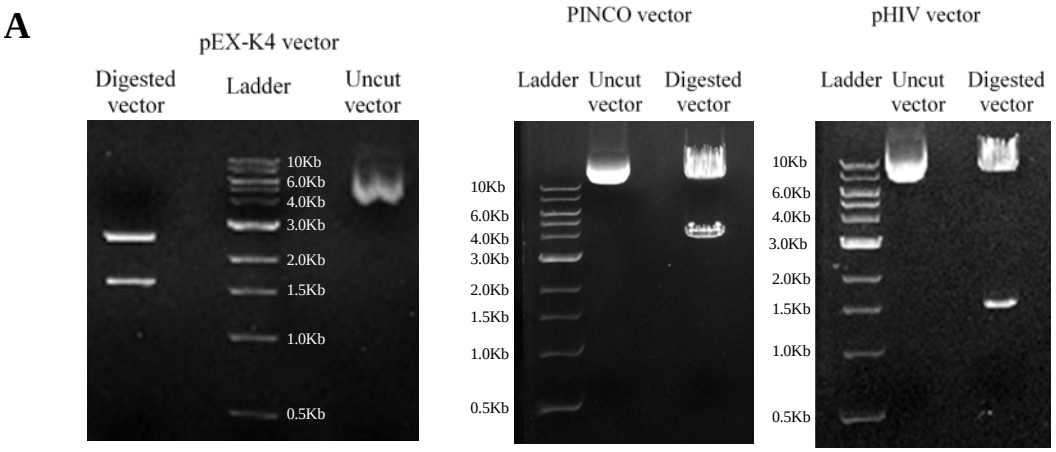

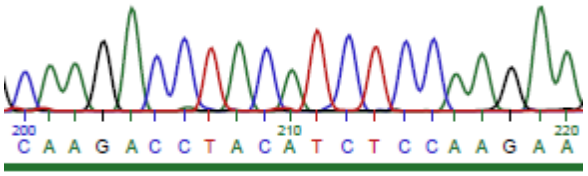


```
P4                  TGTCGCTGATCAAGGTGATTGACGTGGGCCGGAGGTTCCTGGTGAACCGGGTGCAGGACC
PFKFB3(var.2)       tgtcgctgatcaaggtgattgacgtgggccggaggttcctggtgaaccgggtgcaggacc
P3                  TGTCGCTGATCAAGGTGATTGACGTGGGCCGGAGGTTCCTGGTGAACCGGGTGCAGGACC
                    ************************************************************

P4                  ACATCCAGAGCCGCATCGTGTACTACCTGATGAACATCCACGTGCAGCCGCGTACCATCT
PFKFB3(var.2)       acatccagagccgcatcgtgtactacctgatgaacatccacgtgcagccgcgtaccatct
P3                  ACATCCAGAGCCGCATCGTGTACTACCTGATGAACATCCACGTGCAGCCGCGTACCATCT
                    ************************************************************
```

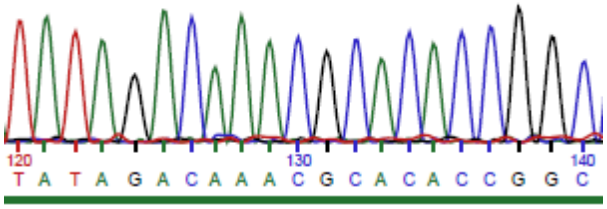


```
PFKFB3(var.2)       tgcccttcaggaaagcctgtgggccaaagctgaccaactccccaccgtcatcgtcatgg
P1                  TGCCCTTCAGGAAAGCCTGTGGGCCAAAGCTGACCAACTCCCCCACCGTCATCGTCATGG
                    ************************************************************

PFKFB3(var.2)       tgggcctccccgcccggggcaagacctacatctccaagaagctgactcgctacctcaact
P1                  TGGGCCTCCCCGCCCGGGGCAAGACCTACATCTCCAAGAAGCTGACTCGCTACCTCAACT
                    ************************************************************
```

Figure 5-9. PFKFB3 DNA sequence "dropped" from pEX-K4 vector and ligated into PINCO and pHIV retro and lentiviral vectors. (A) Agarose gel demonstrating (i) excision of PFKFB3 from pEX-K4 vector using *Hpa*I and *Xba*I restriction enzymes, PFKFB3 fragment 1.57kb; (ii) test digests of PINCO and pHIV vectors containing PFKFB3 DNA (PINCO vector digested using *Sca*I restriction enzyme and pHIV vector digested using *Sma*I restriction enzyme, fragments conform to predicted band sizes (2.2.3.3)). Example partial sequence of reverse 5' to 3' DNA sequence provided by Eurofins MWG (Cytosine (C), Adenine (A), Thymine (T), Guanine (G)), and alignment of forward primer (P1, P3, P4) sequences across subcloning sites compared with published PFKFB3 sequence in **(B)** pHIV and **(C)** PINCO vectors (Figure 2-1). Full sequences are shown in appendices 3 and 4.

5.3.3.2 Overexpression of PFKFB3 results in increased proliferation and increased glucose uptake in Mv4;11 cells

To investigate the effect of PFKFB3 overexpression on glucose uptake and proliferation, Mv4;11 cells were lentivirally infected with PFKFB3, (using pHIV) and compared with control cells lentivirally transduced with shRNA coding for a non-mammalian target sequence. To confirm successful infection and expression of PKFFB3, Mv4;11 cells were analysed by flow cytometry for GFP expression and western blots for PFKFB3 protein expression. Flow cytometric analysis shows that 91% of control cells (Figure 5-10A) and 60% of PFKFB3 overexpression cells (PFKFB3-OE) (Figure 5-10B) expressed GFP, whilst Figure 5-10C demonstrates that PFKFB3-OE cells overexpress PFKFB3 protein compared to control. To assess the impact of PFKFB3 overexpression on cell viability, cells were analysed for 7-AAD fluorescence by flow cytometry. Figure 5-10D shows that overexpression of PFKFB3 did not affect cell viability.

Cells overexpressing PFKFB3 showed a 1.7-fold increase in proliferation over 72h compared to control cells (Figure 5-11A). As the PFKFB3-OE cells co-express GFP, glucose levels in the culture media were assayed, as previously (2.7.1), to determine changes in cellular glucose consumption. Figure 5-11B shows that the concentration of glucose in the culture media of PFKFB3-OE cells after 24h was 15nmol/µL compared with 23nmol/µL in control cells. The initial concentration of glucose in IMDM media is 25nmol/µL. These data suggest that, Mv4;11 cells in which PFKFB3 is overexpressed, show increased levels of proliferation (1.7-fold), alongside increased levels of glucose consumption which are 5-fold higher than that for control cells, and are therefore above that required as a consequence of the increased proliferation.

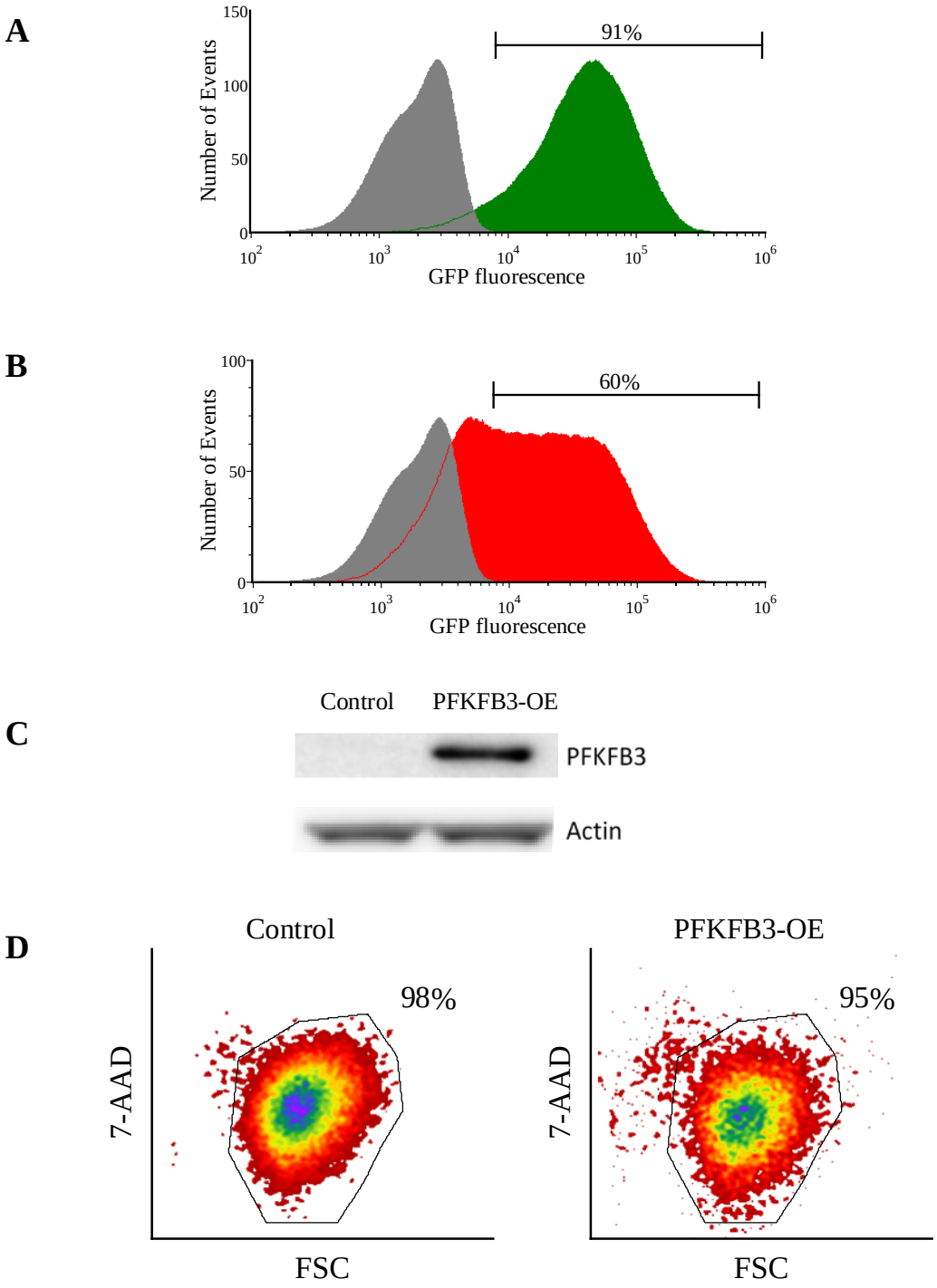

Figure 5-10. Generation of Mv4;11 cells overexpressing PFKFB3. Representative flow cytometric histograms showing percentage of Mv4;11 cells expressing GFP in **(A)** Control (green); **(B)** PFKFB3-OE (red)**.** Histograms were gated to exclude cell debris based on FSC/SSC. Background auto fluorescence was established using Mv4;11 subjected to the equivalent lentiviral infection procedure but in the absence of lentivirus (mock Mv4;11) (grey) infected cells. Percentage within the black marker line represents proportion of cells showing fluorescence greater than background autofluorescence at <0.01%. **(C)** Western blot analysis of PFKFB3 protein comparing control and PFKFB3-overexpression (OE) Mv4;11 cells. Actin was used as a loading control. **(D)** Representative flow cytometric density plots showing percentage of viable Mv4;11 PFKFB3-OE cells compared for control. Plots were gated to exclude cell debris based on FSC/SSC. Cells were incubated with 7-AAD, gated area shows proportion of viable cells (n=3).

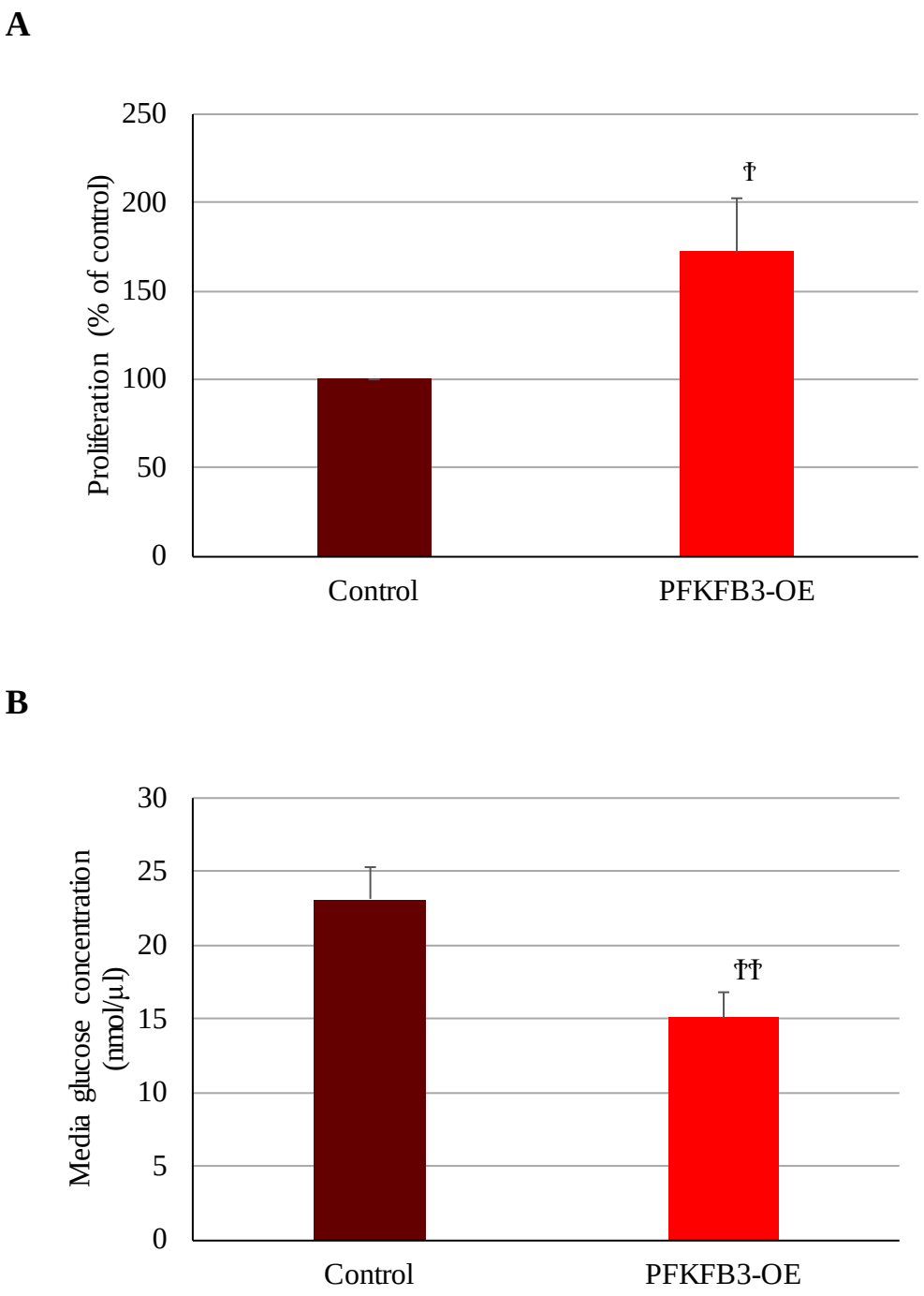

Figure 5-11. Effect of PFKFB3 overexpression on proliferation and glucose uptake in Mv4;11 cells. (A) Percentage proliferation (normalised to control) of Mv4;11 PFKFB3 over-expressed (OE) cells (bright red) cf. control (dark red); cells were seeded at 2 x 10^5 cells/mL and incubated for 72h (n=6). **(C)** Concentration of glucose in the culture media of Mv4;11 PFKFB3-OE cells (bright red) cf. control (dark red) after 24h incubation (n=5). Data represents mean ±1SD. † denotes $p<0.005$ and †† denotes $p<0.001$ statistical significance calculated by Student's paired t-test.

5.3.3.3 Overexpression of PFKFB3 in normal HPC does not affect proliferation or glucose uptake

The data above demonstrates that overexpression of PFKFB3 in Mv4;11 results in increased proliferation and glucose uptake. To examine the effect of PFKFB3 overexpression on normal HPC, $CD34^+$ cells were isolated from neo-natal cord blood and retrovirally infected with PFKFB3 using the PINCO expression vector co-expressing DsRed. To confirm successful gene transduction, HPC were analysed by flow cytometric analysis and western blot. Flow cytometric analysis shows that 25-40% of control cells (Figure 5-12A) and 64-73% of PFKFB3-OE cells (Figure 5-12B) expressed DsRed, whilst Figure 5-12C demonstrates that PFKFB3 overexpressing cells have elevated PFKFB3 protein expression compared to control.

The effects of PFKFB3 overexpression on HPC growth was examined using a haemocytometer. As shown in Figure 5-13A no changes in growth or proliferation were observed because of PFKFB3 overexpression in HPC. Further, using 2-NBDG, no changes in glucose uptake was observed between control HPC and HPC in which PFKFB3 was overexpressed (Figure 5-13B). These data suggest that overexpression of PFKFB3 does not increase glucose uptake or proliferation in normal human HPC (5.4).

5.3.4 Treatment of AML derived cell lines with Ara-C and PFK158 does not augment decreased proliferation compared to Ara-C alone.

The data above demonstrates that chemical inhibition of PFKFB3 with 3PO and PFK158 results in decreased glucose uptake and proliferation in THP-1 cells (5.3.1). Specifically, THP-1 cells showed reduced glucose uptake and proliferation when treated with 1μM PFK158, whilst no changes in glucose uptake or proliferation were observed in cells treated with 500nM PFK158. Conventional chemotherapy which uses Ara-C and daunorubicin to treat AML has reached its therapeutic limit, so the need for adjuncts or alternative treatments targeting specific pathways is clear (Lowenberg *et al.*, 2011). Therefore, to determine whether pharmacological inhibition of PFKFB3 would augment Ara-C treatment, THP-1 cells were treated with a combination of Ara-C and PFK158.

A

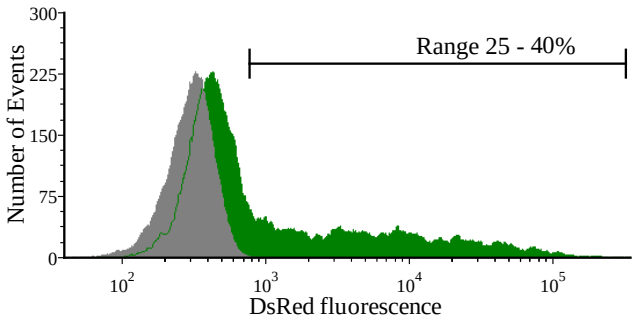

B

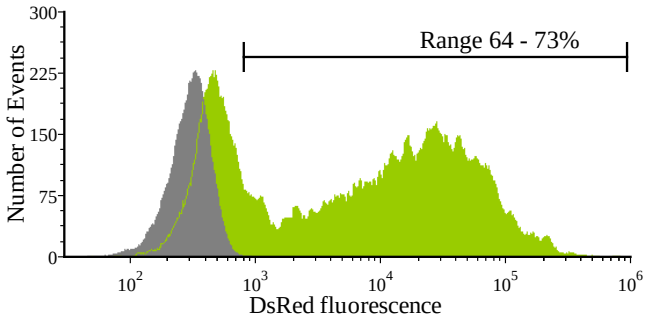

C

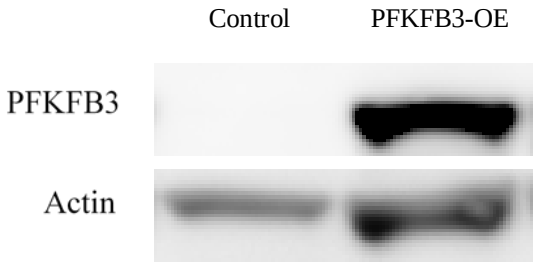

Figure 5-12. Generation of CD34$^+$ HPC overexpressing PFKFB3. Representative flow cytometric histograms showing percentage of HPC expressing DsRed in **(A)** Control (green); **(B)** PFKFB3-OE (lime)**.** Histograms were gated to exclude cell debris based on FSC/SSC. Background auto fluorescence was established using HPC subjected to the equivalent retroviral infection procedure but in the absence of retrovirus (mock HPC) (grey) infected cells. Percentage within the black marker line represents proportion of cells showing fluorescence greater than background autofluorescence at <0.01% (n=3). **(C)** Western blot analysis of PFKFB3 protein comparing control and PFKFB3-OE HPC. Actin was used as a loading control.

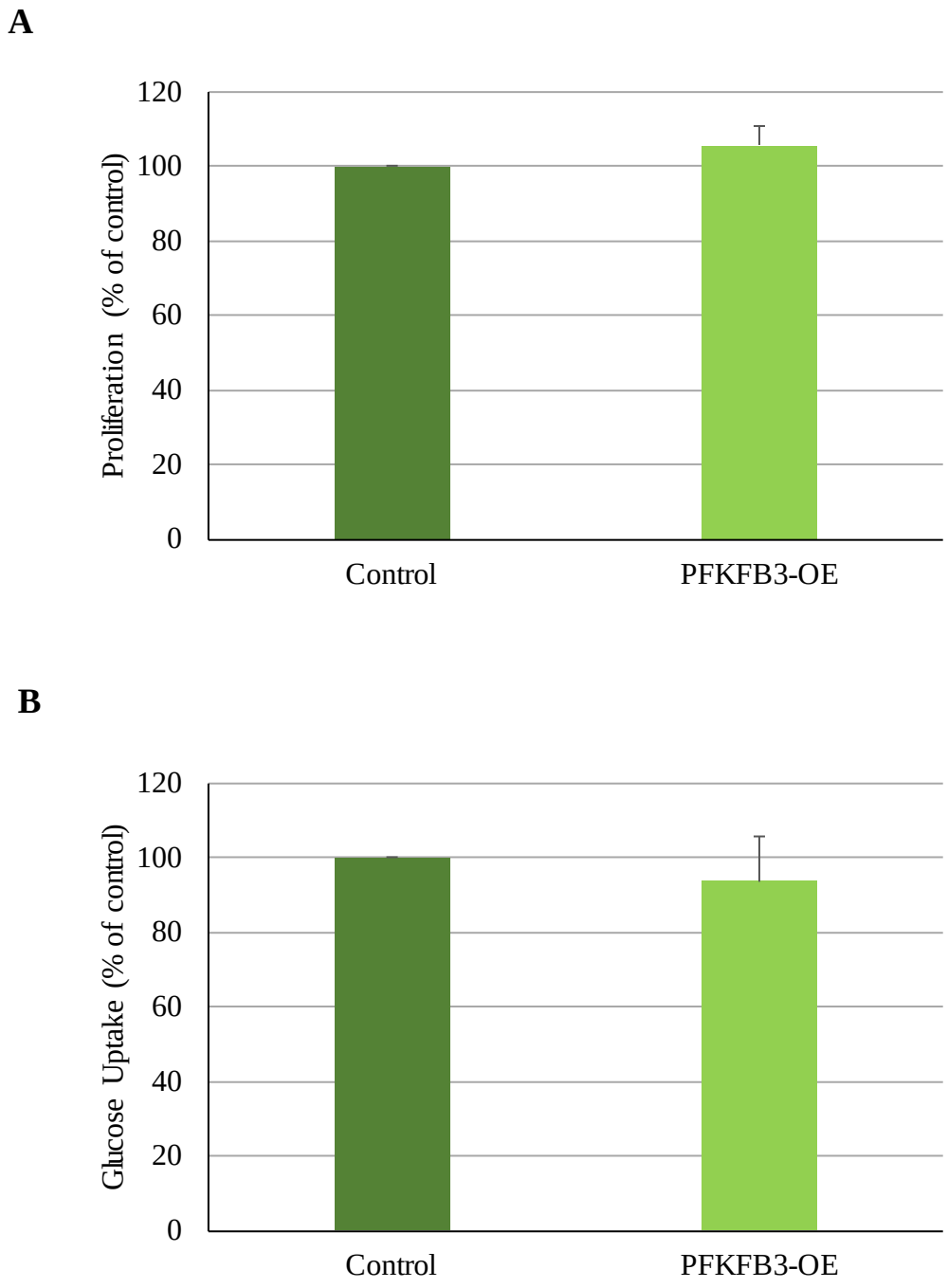

Figure 5-13. Effect of PFKFB3 overexpression on proliferation and glucose uptake in HPC. Cells were counted (day5), and cultured for a further 24h without growth factors at an initial seeding of 6 x 10^5 cells/mL. **(A)** Percentage proliferation and **(B)** Glucose uptake, of transduced HPC (normalised to control); PFKFB3-OE (bright green) control (green) (n=3). Data represents mean ±1SD.

To determine an effective dose for Ara-C in this cell line, cells were assayed as described previously, using CellTiter-Glo™ (2.8). Figure 5-14A shows an EC50 of 660nM for THP-1 cells treated with Ara-C. To determine if additional treatment with PFK158 lowered the EC50 of Ara-C, THP-1 cells were treated with 300nM and 1µM doses of PFK158 and serial dilutions of Ara-C. No changes in the EC50 for Ara-C were observed in cells additionally treated with 300nM PFK158. Treatment of THP-1 cells with 1µM PFK158 however did reduce the EC50 for Ara-C most markedly at a concentration of 330nM (Figure 5-14A).

To determine whether the combined treatment of Ara-C and PFK158 would decrease proliferation in THP cells, THP cells were treated with a combination of the drugs at different doses. Figure 5-14B shows that as expected, treatment with 100nM and 330nM Ara-C resulted in decreased proliferation. Treatment of THP-1 cells with 100nM or 300nM PFK158 did not affect proliferation at either Ara-C dose, whilst treatment of THP-1 cells with 1µM PFK158 and 100nM Ara-C resulted in an additional 7% ± 2% decrease in proliferation compared to Ara-C treatment alone. These data suggest that these compounds demonstrate no apparent synergistic beneficial effect, compared to treatment with each compound alone.

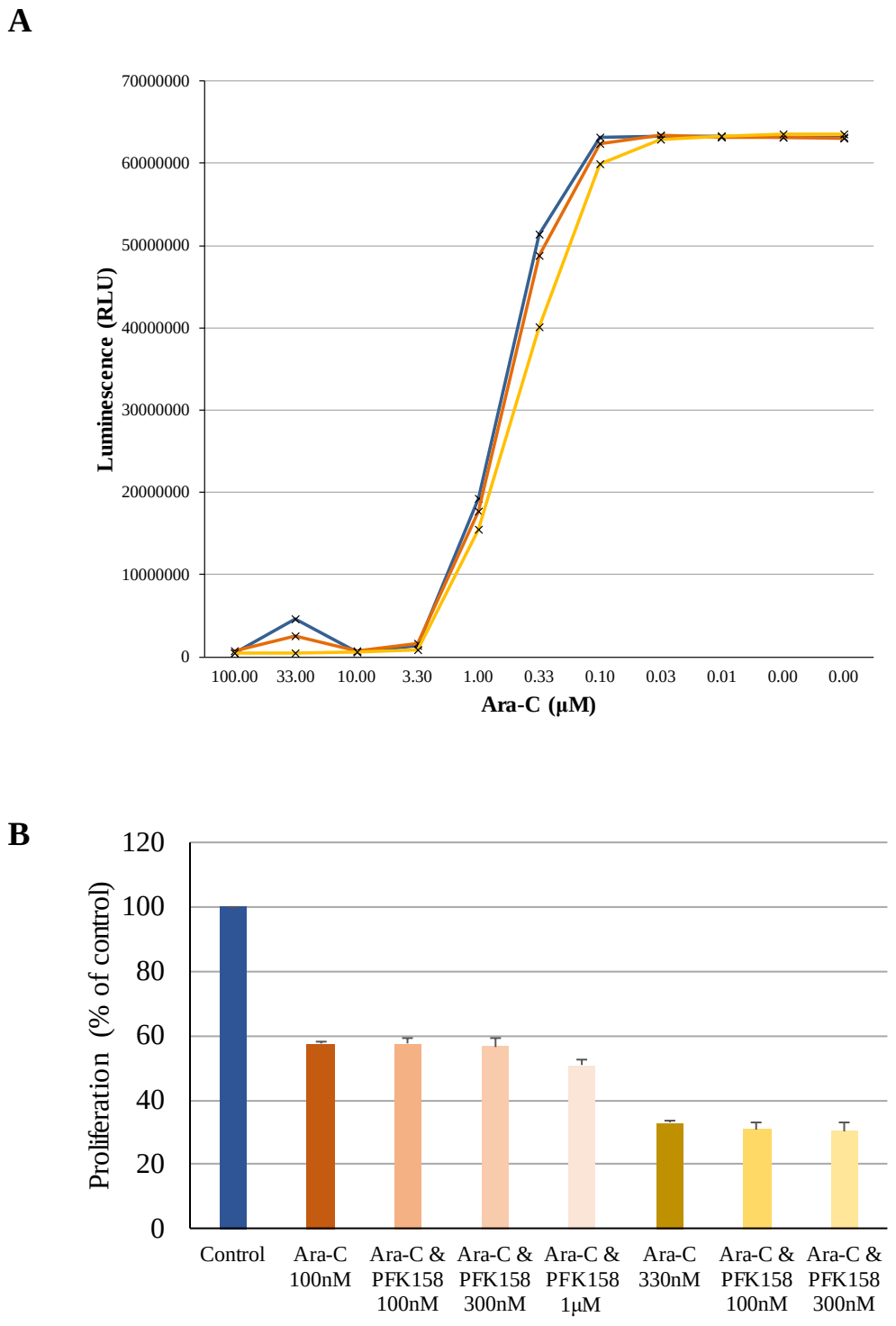

Figure 5-14. Determination of EC50 for Ara-C and Ara-C & PFK158 combined and effect on proliferation. (A) THP-1 cells were seeded at 1 x 10^5 and cultured for 24h in the presence of Ara-C alone or Ara-C and PFK158. Cells were subsequently assayed using CellTiter-Glo™ and luminescence measured using a Chameleon Hidex luminescent plate reader. Blue line represents cells treated with Ara-C alone, orange line represents cells treated with Ara-C and PFK158 (300nM), yellow line represents cells treated with Ara-C and PFK158 (1µM) (n=1). **(B)** Proliferation (normalised to control) in THP-1 cells, seeded at 4 x 10^5, treated with Ara-C alone or Ara-C and PFK158 and incubated for a further 72h (n=4). Data represents mean ±1SD.

5.3.5 ROS does not induce HIF-1α overexpression in the THP-1 cell line

Mutant RAS expressing HPC have been shown to exhibit increased glucose uptake and proliferation, which is mediated by ROS (3.3.2). Modulation of ROS in AML cell lines has additionally been shown to alter cellular glucose uptake and proliferation (3.3.3). Further, both modulation of ROS in N-RAS^{G12D} HPC and in THP-1 and Mv4;11 cell lines has been shown to alter protein expression levels of PFKFB3 (4.3.2.1,4.3.3). In this chapter, chemical inhibition of PFKFB3, knock-down and overexpression of this protein, have all been shown to affect cellular glucose uptake and proliferation in AML cell lines. However, the mechanism governing this effect is not known.

HIF-1α is known to be upregulated in several solid tumours and has been shown to induce increased *PFKFB3* mRNA expression under conditions of hypoxia and ROS is implicated in its regulation (5.1). Therefore, to assess whether ROS may be implicated in the upregulation of HIF-1α in AML, our transcriptome microarray data was analysed (2.10) to identify whether ROS induced changes in mRNA expression of this gene. Figure 5-15A shows that N-RAS^{G12D} HPC show a significant 4.7-fold increase in expression of *HIF-1α* mRNA compared to controls, whilst treatment of these cells with DPI resulted in a 7.8-fold decrease compared with untreated N-RAS^{G12D} HPC. Figure 5-15B shows the relative mRNA expression of *HIF-1α* for each condition. These data suggest that increased mRNA expression of *HIF-1α* in mutant RAS expressing HPC is at least partly dependent on cellular ROS.

As observed previously (Hopkins *et al.*, 2014) mRNA expression levels do not necessarily correlate with changes in protein expression levels. This is potentially pertinent in the case of HIF-1α as under conditions of normoxia, HIF-1α is rapidly degraded by the proteasome within 5 min (D'Angelo *et al.*, 2003). To determine if increased ROS, generated increased HIF-1α protein expression, western blots were performed on THP-1 cells with NOX2 knocked-down or inhibited using DPI. Interestingly, Figure 5-15C demonstrates that under conditions of normoxia, HIF-1α was not expressed at detectable levels in THP cells, regardless of NOX2 status. Treatment of THP-1 cells with cobalt chloride ($CoCl_2$) (which inhibits HIF-1α degradation (Yuan *et al.*, 2003)), acted as positive control and confirmed antibody specificity. These data suggest that ROS does not impact of HIF-1α protein expression in these cells.

Although HIF-1α protein was not detectable in THP-1 cells by western blot, given its rapid degradation in normoxic conditions and its elevated mRNA expression levels in N-RAS^{G12D} HPC, it was reasoned that low levels of this protein may still be affecting glucose uptake and PFKFB3 expression in these cells. Therefore, three shRNA sequences complementary to HIF-1α and encoding puromycin resistance were lentivirally transduced into THP-1 cells. One clone did not survive the puromycin selection process, suggesting that these cells had not been successfully transfected. To confirm knock-down of HIF-1α in the other two shRNA clones, western blots were performed on whole cell lysates treated with $CoCl_2$. Of the two surviving clones, Clone 1 failed to upregulate HIF-1α when treated with $CoCl_2$, suggesting that HIF-1α was successfully knocked down in this clone (Figure 5-16A) (western blot provided courtesy of Dr. Namrata Rastogi). Western blot was performed on the whole cell lysate of Clone 1 to determine PFKFB3 expression. Figure 5-16B shows that knock-down of HIF-1α did not result in any changes in PFKFB3 expression, whilst additionally, no changes in the cellular glucose uptake of these cells were observed (Figure 5-16C). Overall these data are consistent with the idea HIF-1α protein expression does not impact on PFKFB3 expression or cellular glucose uptake in THP-1 cells.

A

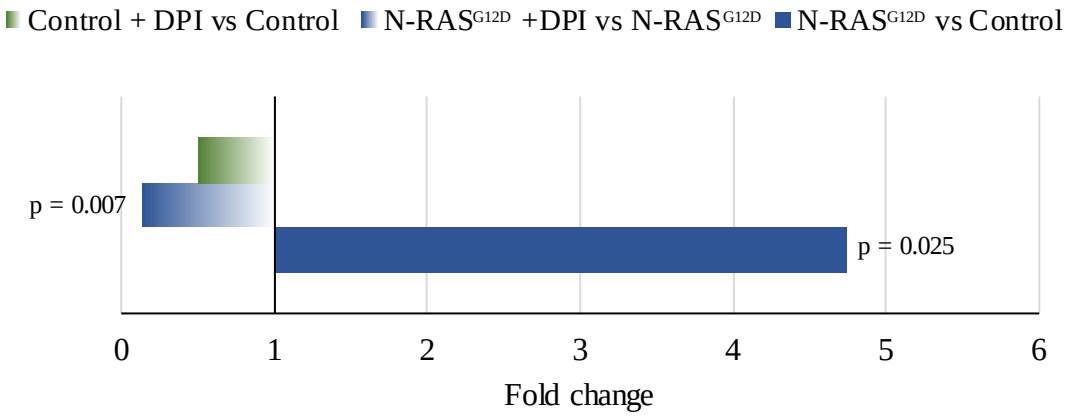

B

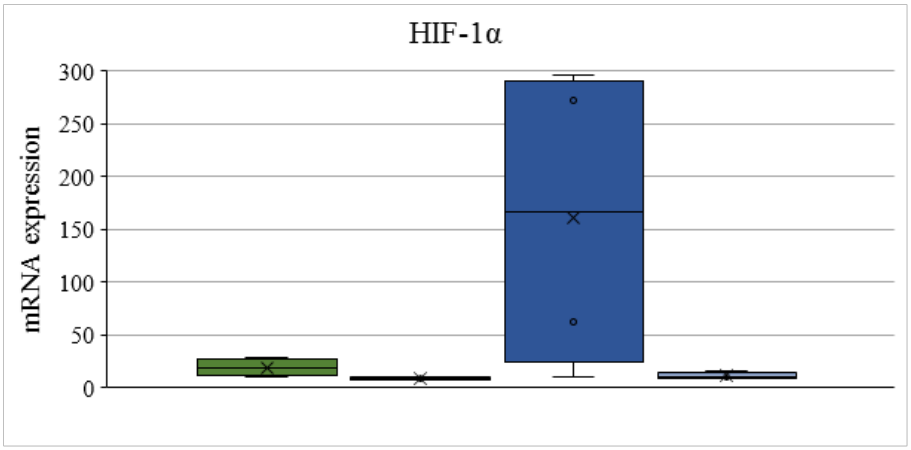

C

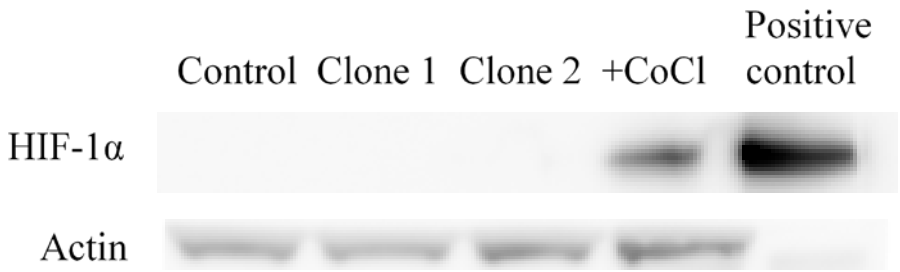

Figure 5-15. ROS dependent changes in mRNA expression of HIF-1α in human HPC. (A) Fold changes in mRNA expression for N-RAS^{G12D} transduced HPC compared to control HPC (blue), N-RAS^{G12D} HPC treated with DPI (100nM) compared to untreated N-RAS^{G12D} (blue gradient) and control HPC treated with DPI (100nM) compared for untreated control HPC (green gradient). DPI treatment occurred for 24 h at 37ºC, 5% CO_2. Data represents mean fold change of n=4; p-value calculated by 2-way ANOVA with Bonferroni multiple testing correction (see methods). **(B)** Normalised log_2 expression of mRNA in control HPC (green), control HPC treated with 100nM DPI (green gradient), N-RAS^{G12D} HPC (blue) and N-RAS^{G12D} HPC treated with DPI (blue gradient). Box plots represent median quartile ranges, x represents mean value (n=4). **(C)** Western blots showing expression of HIF-1α comparing control THP-1, THP NOX2-KD, THP-1 cells treated with DPI (100nM), THP-1 cells treated with $CoCl_2$ (100µM) and HIF-1α recombinant protein (positive control). Cells were seeded at 5 x 10^5 and incubated for a further 24h following treatment. Actin was used as loading control.

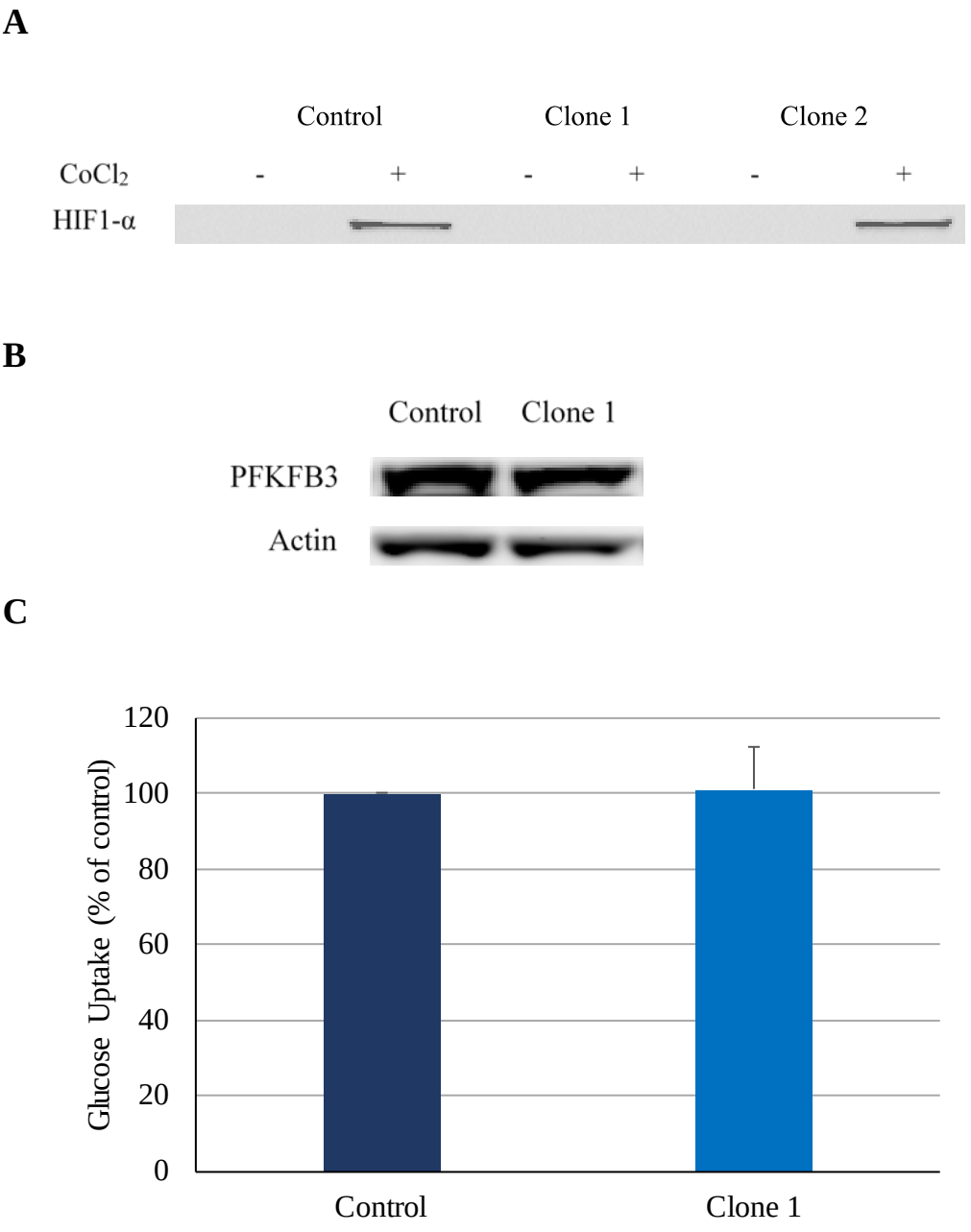

Figure 5-16. HIF-1α dependent changes on PFKFB3 expression and glucose uptake in THP-1 cells. Western blots showing expression of **(A)** HIF-1α, comparing control THP-1 and two THP-1 clones with HIF-1α knocked down untreated and treated with $CoCl_2$ 100µM, for 24h, and **(B)** PFKFB3, comparing control THP-1 and THP-1 with HIF-1α knocked-down. Actin was used as loading control. **(C)** Cellular glucose uptake (normalised to control) of THP HIF-1α KD cells (blue) cf. control (dark blue); cells were seeded at 5 x 10^5 and incubated for 24h (n=3). Data represents mean ±1SD.

5.4 Discussion

The data above shows the effect of loss of PFKFB3 expression or inhibition in AML cell lines and N-RAS^{G12D} HPC on glucose uptake and cellular proliferation. Additionally, the effect of PFKFB3 overexpression on these functions was also determined, both in AML cell lines and normal HPC. Finally, a potential mechanism of ROS induced PFKFB3 expression was investigated. The main findings presented in this chapter are summarised in Table 9

The PFKFB3 inhibitor 3PO has been shown to reduce glucose uptake and tumour burden in xenograft models of several solid tumours (Clem *et al.*, 2008). Alongside its more potent analogues PFK-15 and PFK158 (Clem *et al.*, 2013) its therapeutic potential in cancer as an inhibitor of glycolysis has been investigated and PFK158 is currently undergoing phase I clinical trials (1.5.1.3). In line with studies in solid tumours (O'Neal *et al.*, 2016, Zhu *et al.*, 2016, Imbert-Fernandez *et al.*, 2014), data presented here shows that in the AML cell line THP-1, treatment with either 3PO or PFK158 reduced glucose uptake in a dose dependent manner, whilst proliferation was significantly reduced with the use of either inhibitor (5.3.1.2). The efficacy of 3PO in reducing glucose uptake was also shown in N-RAS^{G12D} expressing HPC, where a significant decrease in glucose uptake was observed in cells treated with the inhibitor (5.3.1.3). Previously in this study it has been established that the addition of exogenous ROS to the AML cell line Mv4;11 results in increased glucose uptake by these cells (3.3.3.2) as well as increased PFKFB3 protein expression (4.3.3.2). To establish whether there is a link between the ROS induced increases in PFKFB3 expression and ROS induced increases in glucose uptake, Mv4;11 cells were treated with exogenous ROS in the presence of 3PO and PFK158. Whilst Mv4;11 cells treated with exogenous ROS showed increases in glucose uptake compared to control, cells treated with exogenous ROS in the presence of either inhibitor showed no equivalent increase (5.3.1.1). Together this data suggests that both 3PO and PFK158 inhibition of PFKFB3 is effective in reducing cellular glucose uptake. Furthermore, the data presented in the Mv4;11 cell line is suggestive of a mechanistic link between increased levels of cellular ROS, increased PFKFB3 expression and increased cellular glucose uptake.

Table 9. Summary of data presented in chapter 5. Table shows a summary of the changes in glucose uptake and proliferation of human haematopoietic progenitor cells (HPC) infected with mutant RAS, human HPC and AML cell lines compared with appropriate control cells, as presented in chapter 5. ↑ indicates an increase compared to control, ↓ represents a decrease compared to control, - represents no observed changes compared to control. * represents data that showed significant changes compared to controls. n/a indicates that this data was not measured. Details of individual test conditions and the statistical analysis can be found in the appropriate results section of the chapter.

Cell	**Pharmaceutical Inhibition of PFKFB3**		**Knock-down of PFKFB3**		**Overexpression of PFKFB3**		**Knock-down of HIF-1α**
	Glucose Uptake	Proliferation	Glucose Uptake	Proliferation	Glucose Uptake	Proliferation	Glucose Uptake
Human HPC N-RAS^{G12D}	↓*	n/a	n/a	n/a	n/a	n/a	n/a
Human HPC	n/a	n/a	n/a	n/a	–	–	n/a
THP-1	↓	↓	–	↓	n/a	n/a	–
Mv4;11	–	n/a	n/a	n/a	↑	↑	n/a
Mv4;11 & GOX	↓	n/a	n/a	n/a	n/a	n/a	n/a

The role of PFKFB3 was explored further in the THP-1 cell line, via the use of shRNA to knock-down expression of this protein in this cell line. Whilst, knock-down of PFKFB3 significantly reduced proliferation (1.8-fold), no changes in glucose uptake were observed (4). Given the link established above between PFKFB3 inhibition and glucose uptake this result was surprising. One potential reason for the discrepancy between these results could arise due to differences in the relative degrees of suppression of PFKFB3. For instance, partial inhibition of PFKFB3 may result in decreased proliferation as cells try to restore energy homeostasis by diverting metabolites away from metabolic pathways important in generating molecules for biosynthesis. A more complete inhibition of PFKFB3 however, may not only compromise a cells ability to proliferate, but additionally to generate energy via glycolysis at all. Alternatively, discrepancies between these results may be the function of the mode of inhibition. The kinase activity of PFKFB3, which generates F-2,6-BP and activates PFK thus increasing glycolytic flux, and its inhibition is a well-known regulatory mechanism in glycolysis (1.5.1). The inhibitory effect of 3PO is a consequence of competitive inhibition of the F-6-P binding site responsible for the kinase activity of this enzyme (Clem *et al.*, 2008), with the phosphatase site remaining active, whilst shRNA knock-down results in a decrease in PFKFB3 protein levels and thus total enzyme activity. However, how this difference would mechanistically explain this anomalous data is not clear, but it may be that in the absence of PFKFB3 protein some regulatory mechanism is instigated, leading to the upregulation of compensatory metabolic pathways that preserve glucose uptake. Finally although no specific off-target effects of 3PO or PFK-158 have been reported in the literature, larger than predicted apoptopic effects compared with metabolic reduction in Jurkat T-cell leukaemia cells treated with PFK15 mean that an impact on mitochondrial mechanism, by this class of inhibitors, cannot be ruled out (Clem *et al.*, 2013).

In order to investigate the link between PFKFB3 expression, glucose uptake and proliferation further, the *PFKFB3* gene was overexpressed in Mv4;11 cells and in normal HPC. Significant increases in glucose consumption and proliferation was observed in the cell cultures of Mv4;11 cells overexpressing this gene (5.3.3.2). These results add further weight to the idea that PFKFB3 is a key enzyme in modulating cellular glucose uptake and proliferation. Interestingly however,

overexpression of PFKFB3 in normal HPC did not result in increased glucose uptake or proliferation (5.3.3.3), suggesting, perhaps, that in the context of non-transformed haematopoietic cells, regulatory mechanisms exist to prevent excessive glycolysis due to increased PFKFB3 expression. For instance, whilst not investigated in this study, PTEN is known to inhibit PFKFB3 activity (1.5.1.1) and is frequently mutated in cancer. It may be that in non-transformed cells, PTEN activity is increased in response to increased glycolysis, whereas in transformed cells this response has become decoupled.

Whilst survival rates of patients with AML has improved greatly over the last thirty years (under 60's 20-75%), in patients over 60, 3-5 year survival rate is still around 10% (Gutierrez and Romero-Oliva, 2013). Consequently, the need for alternative treatments or adjuncts to current treatment programmes is exigent. One effect of chemotherapy is to increase intracellular ROS levels, which can be ameliorated by an increase in cellular antioxidant capacity, of which NADPH production is a crucial component (1.3.2.4). Given that the use of PFKFB3 inhibitors above (5.3.1.1 and 5.3.1.2) and elsewhere (1.5.1.3) results in decreased glucose uptake (which is required for NADPH production via the PPP or SSP (1.4.4)), it was reasoned that use of these inhibitors alongside Ara-C may increase cellular oxidative stress and be of benefit in treating AML. Whilst in THP-1 cells most combined doses showed little improvement on Ara-C treatment alone, a combination dose of 100nM Ara-C and 1μM PFK158 decreased cellular proliferation by a further 7% compared to Ara-C monotherapy. Whilst this suggests that further optimisation of doses and proper drug combination studies may further impact on proliferation of these cells, overall these data do not indicate beneficial synergistic effect. Interestingly, a recent study reported increased PFKFB3 expression in AML cell lines following knock-down of the tumour suppressor protein, tuberous sclerosis 2 (Feng and Wu, 2017). Treatment of these cells with the mTOR inhibitor rapamycin and the PFKFB3 inhibitor PFK-15 resulted in synergistic decreases in cellular proliferation. Given that inhibition of mTOR by rapamycin in ROS high HSC is known to restore quiescence (1.3.3.3) and that mTOR upregulates glycolytic enzymes (1.4.3.1), increases nucleotide and lipid biosynthesis (1.4.2) and is known to upregulate G-6-PD (1.4.4), use of rapamycin alongside the PFKFB3 inhibitors used above, suggests another alternative mechanism that may be explored in future experiments.

The data presented in chapter 3 shows a ROS dependent increase in glucose uptake and proliferation, whilst in chapter 4 a ROS dependent increase in protein expression of PFKFB3 was observed. The data, presented in this chapter suggests that changes in glucose uptake and proliferation are directly linked to these changes in PFKFB3 expression. Therefore, potential mediators of this role were investigated. Analysis of microarray data revealed ROS dependent changes of the master regulator of hypoxia HIF-1α in N-RAS^{G12D} expressing HPC (5.3.5). HIF-1α is stabilised under conditions of hypoxia but degraded under conditions of normoxia. However it has been shown that HIF-1α is also stabilised in many cancers even in the presence of normal oxygen levels (reviewed in Semenza, 2010b) and is responsible for the upregulation of numerous glycolytic genes, including PFKFB3 (Yalcin *et al.*, 2009b). One possible mechanism proposed for the normoxic stabilisation of HIF-1α is ROS induced inhibition of PHD, which in the presence of O_2, normally targets HIF-1α for degradation (Niecknig *et al.*, 2012). Whilst the role of ROS in stabilising HIF-1α remains controversial (reviewed in Hagen, 2012), arguments against its participation in normal cells may not apply in transformed cells (1.4.2.1). Cancer cells generate and tolerate much higher levels of ROS than normal cells (1.3.3.4) suggesting PHD inhibition may still be a factor in these cells. Increased NOX activity in cancer cells (1.3.3.4) provides an alternative source of ROS to the mitochondrial ROS source proposed as a requirement in normal cells. Finally, the proper regulation of HIF-1α in transformed cells may not occur, therefore relief of FIH inhibition from ROS and hence inactivation of HIF-1α may not be a requirement in these cells. Therefore, given the ROS dependent changes observed in HIF-1α mRNA levels in the N-RAS^{G12D} HPC, it was investigated whether ROS dependent changes in HIF-1α protein might also be observed. However, immunoblotting of whole cell lysates of the ROS generating AML cell line THP (3.3.3.1), showed no detectable HIF-1α expression. Furthermore, knock-down of HIF-1α in this cell line revealed no changes in PFKFB3 expression, glucose uptake or proliferation (5.3.5). This suggests that ROS modulation of PFKFB3 expression is not mediated by HIF-1α.

Overall the data presented in this chapter shows that inhibition of PFKFB3 decreases cellular proliferation and inhibits glucose uptake, whilst overexpression in transformed cells increases glucose uptake and proliferation. Furthermore, this mechanism appeared to be a function of ROS. Whilst not analysed rigorously, a

superficial examination of the potential benefits of Ara-C treatment augmented with PFK158 proved disappointing. This may reflect a need for improved dosage optimisation or may reflect regulatory mechanisms of PFKFB3 that protect against increased ROS levels (6). Finally, HIF-1α was identified as a potential mechanistic candidate for the regulation of ROS induced PFKFB3 expression. However, whilst elevated at a transcriptional level by ROS, this elevation was not observed at the translational level.

6 General Discussion

6.1 Summary

AML is a heterogeneous disease, which typically affects older people. Currently, the median age at diagnosis in the U.S.A is 68, with a 1 in 200 chance of being diagnosed with this disease during a person's lifetime. The standard treatment of one or two courses of 3 days of daunorubicin combined with 7 days Ara-C (Burnett, 2012) bring about remission rates in the under 60's and over 60's of 80% and 65% respectively (Newland, 2002); however relapse rates are 50% and 85% in these respective age groups (Burnett *et al.*, 2011). Furthermore, whilst 5-year relative survival rates in the U.S.A have improved from 11.4% in 1980 to 28.1% in 2009 (Estey and Gale, 2017) with a similar picture observed in the UK (1.2.1), this figure falls to <10% in patients over the age of 60. Further, the discovery of revolutionary drugs such as ATRA in the treatment of APL (reviewed in McCulloch *et al.*, 2017) and the development of Imatinib as targeted therapy in CML (reviewed in Deininger *et al.*, 2005), combined with the fact that current treatments appear to have reached their therapeutic limit, mean the need for a similar paradigm shift in the treatment of AML is clear.

Mutations of *RAS* are common in AML (Table 1) leading to its constitutive activation, hyperactivation of signalling pathways such as RAF/MEK/ERK and PI3K/AKT/mTOR, resulting in consequences for cellular proliferation, growth and differentiation which were discussed earlier (1.2.2.3). Previous work in our group linking mutational RAS activation with increased NOX2 derived ROS production and cellular proliferation in HPC (Hole *et al.*, 2010), was supported by studies on AML patient blasts and AML cell lines (Hole *et al.*, 2013). Additionally, FLT3-ITD, another common mutation in AML (Table 1), has been shown to increase levels of ROS. This is associated with increased DNA DSB (Sallmyr *et al.*, 2008) which was subsequently shown to be attributable to NOX4 (Stanicka *et al.*, 2015). The consequence was development of leukaemia-like disease and proliferation in murine models, via inactivation of DEP-1/PTPRTJ, a PTP which regulates FLT3 (Jayavelu *et al.*, 2016b). Clinically, elevated ROS levels have also been observed in ALL and CML patient samples (Devi *et al.*, 2000), whilst a Chinese study of AML patients indicates a causal link between ROS and relapse (Zhou *et al.*, 2010).

ROS also has implications for metabolism, having previously been shown in endothelial cells to increase HIF-1α expression which in turn upregulates numerous glycolytic enzymes (Paik *et al.*, 2017). ROS can also affect other transcription factors involved in metabolic regulation, such as STAT3 and Nf-κB (1.4.2) linked to the promotion of lung cancer metastasis in murine models (Zhao *et al.*, 2014). Building on the work by Hole *et al*, 2010, it was found by our group, that HPC expressing constitutively active RAS not only generated increased levels of NOX2 derived ROS, but that this ROS specifically led to changes in mRNA expression levels of glycolytic enzymes (Hopkins *et al.*, 2014).

This study has shown for the first time that in HPC infected with mutant RAS, both glucose uptake and lactate secretion are increased (3.3.1). Furthermore, inhibition of ROS in this model, results in both a decrease in glucose uptake and proliferation, accompanied, interestingly by an increase in lactate secretion (3.3.2). Support for these findings was provided using AML cell lines, where ROS levels were depleted through chemical inhibition or knock-down of NOX2, or increased (using lines that generate little NOX2 derived ROS) through the addition of exogenous ROS. Inhibition of ROS led to decreased glucose uptake and proliferation, whereas increased glucose uptake and proliferation was associated with exposure to increased ROS levels (3.3.3.2, 3.3.3.4). These data are supportive of an earlier study in the megakaryoblastic cell line M-O7e, which showed decreased ROS, glucose uptake and cell survival in these cells after treatment with DPI or with NOX2 knocked-down. Curiously, whilst depletion of ROS in two AML cell lines led to an increase in lactate secretion, mirroring the results found in mutant RAS expressing HPC treated with DPI, increasing ROS in the Mv4;11 cell line also led to increased lactate secretion (3.3.3.3). Although the reasons for this discrepancy are not clear, they may be context specific or related to relative ROS levels mediating a balance between cellular energy requirements and managing oxidative stress (4.4).

To obtain better insight into the mechanisms of how ROS can lead to changes in carbohydrate metabolism, previously generated microarray data (Hopkins, 2014) was re-evaluated using a supervised approach focussing on glycolytic enzymes. This approach offered a more restrictive analysis by focussing on over 100 genes related to glycolysis and associated genes involved in carbohydrate metabolism; as opposed to analysing the whole genome consisting of over 28,900 genes. Analysis, revealed

several ROS dependent changes in mRNA expression (Figure 4-1), however, at the protein level only the enzyme PFKFB3 showed ROS dependent changes especially in N-RAS^{G12D} expressing HPC (the more clinically relevant mutation in AML) (Figure 4-3). These ROS dependent changes in PFKFB3 were confirmed in the AML cell line THP-1 through the inhibition of ROS using DPI and NOX2 knock-down which led to decreased PFKFB3 protein expression (Figure 4-4), and in the Mv4;11 cell line, through the addition of exogenous ROS, which resulted in increased PFKFB3 protein expression (Figure 4-5).

Subsequently, mass spectrometry was employed to determine ROS modulated changes in metabolites in AML cell lines with a focus on carbohydrate metabolism. Importantly, hierarchical clustering demonstrated that whilst different cell lines provided the largest variation between samples (as expected), ROS modulation within cell lines clearly separated populations. Pleasingly variation in the replicates was minimal (Figure 4-9). Whilst analysis of this data revealed different patterns of metabolite variation dependent on cell line and the nature of ROS modulation, in general, observations were broadly supportive of the functional changes in glycolysis previously observed (4.3.5.3), that decreased ROS levels correlate with decreased levels of glycolytic metabolites and thus decreased glycolysis. Further support for this data was provided by an equivalent experiment using AML patient blast samples, which had been categorised into ROS^{Hi} and ROS^{Lo} producing blasts. Analysis of this data showed ROS^{Hi} blasts had higher intracellular glucose levels than ROS^{Lo} blasts and additionally AML blasts had higher levels of intracellular glucose and lactate than normal haematopoietic (control) cells (4.3.6.1).

Interestingly, ROS modulation in cell lines resulted in changes in intracellular lactate levels that were antithetical to those obtained for extracellular lactate levels. Both NOX2 knock-down, chemical inhibition of ROS and addition of ROS resulted in decreased intracellular lactate levels. Furthermore, in response to ROS modulation, changes in metabolites associated with both the PPP, the SSP and sphingolipid metabolism were observed. These data are suggestive of a reprogramming of metabolic pathways to allow potential recycling of lactate (6.2) the generation of NADPH as a mechanism for managing increased oxidative stress and increases in biosynthetic precursors such as nucleotides for DNA repair and cell growth. In support of this, upregulation of the transcription factor Nrf2, which regulates gene

expression of the peroxiredoxin and glutathione systems, as well as PPP enzymes such as G-6-PD (reviewed in Taguchi and Yamamoto, 2017), has been reported in primary cells collected from AML patients (Rushworth *et al.*, 2012).

Increased PFKFB3 expression has been reported in a variety of solid tumours and is associated with increased glycolysis (1.5.1.3). Here, overexpression of the PFKFB3 gene in the AML cell line Mv4;11 was also shown to lead to increases in glucose uptake, accompanied by increased proliferation (5.3.3.2), though this effect was not observed in HPC (5.3.3.3). Conversely, chemical inhibition of PFKFB3 led to decreased glucose uptake in AML cell lines and importantly this was shown to be an effect of changes in ROS levels (5.3.1). Several post-translational modifications of PFKFB3 have been reported in the literature as a result of changes in ROS levels (1.5.1.2). Therefore, ROS induced phosphorylation of PFKFB3 at Ser-461 was investigated as part of this study, however results were equivocal and may represent non-specific binding of the antibody, rather than any actual ROS effect (4.3.4.1). To try to mechanistically understand how exposure to ROS leads to changes in PFKFB3 expression, this study analysed our microarray data for HIF-1α expression. The data showed increased expression of HIF-1α mRNA correlated with increased ROS levels and given that *PFKFB3* is known to be a target of HIF-1α (1.5.1) it was reasoned that changes in HIF-1α expression may be driving PFKFB3 expression. However, immunoblotting showed that HIF-1α was not expressed at detectable levels in the AML cell line THP-1 and furthermore knock-down of the mRNA for this protein did not result in any changes in glucose uptake (5.3.5).

The role of ROS as a signalling molecule is now well documented (1.3.3.2). The antioxidant enzyme Prx1 has been shown to transduce a H_2O_2 signal through oxidation of the apoptosis signal-regulating kinase 1 protein, resulting in activation of the $p38^{MAPK}$ pathway, in the AML cell line U937 (Jarvis *et al.*, 2012). Activation of $p38^{MAPK}$ by ROS was shown to occur in this study in both AML cell lines (Figure 3-12) and HPC expressing mutant RAS (Figure 3-6), whilst the promoter region of the *PFKFB3* gene contains a serum response element which has been shown to be activated by the $p38^{MAPK}$ pathway (Novellasdemunt *et al.*, 2013). This then represents an alternative mechanism by which ROS may modulate PFKFB3 expression.

ROS is also known to activate both AKT and AMPK which upregulates catabolic metabolic processes, increases glycolytic flux and mediates against ROS accumulation (reviewed in Zhao *et al.*, 2017). Whilst outside the scope of this study, metabolomic data generated as part of this study indicated increased levels of ROS correlated with an increase in fatty acid metabolites and sphingomyelins (data not shown). Fatty acid metabolism generates NADPH and is activated by AMPK (reviewed in Carracedo *et al.*, 2013), whilst sphingomyelinase activity has been shown to increase NOX2 derived ROS (Loehr *et al.*, 2015), suggesting that ROS maybe important in these pathways. This activation of fatty acid metabolism by AMPK is interesting given that ROS activation of AMPK has also been shown to potentially mediate HSC differentiation (Liu *et al.*, 2015), whilst increased PFKFB3 expression and increased glycolysis via phosphorylation of PFKFB3 at Ser-461 have also been shown to be a consequence of AMPK activation (Mendoza *et al.*, 2012). AMPK therefore represents another potential candidate by which ROS modulation of PFKFB3 could be enacted.

GAPDH has also been shown to operate as a ROS sensor through oxidation of cys-152 and renders GAPDH inactive until NADPH levels are restored and this offers a further mechanism by which ROS may modulate glycolytic flux (Peralta *et al.*, 2015).

6.2 Comparisons to current knowledge and future directions

Whilst this study clearly establishes a link between ROS, PFKFB3 expression cellular glucose uptake and proliferation, several areas warrant further investigation. Firstly, it is often stated as a key tenet of the Warburg effect, that transformed cells show an increase in aerobic glycolysis, accompanied by increased cellular glucose uptake and lactate secretion. In this study, whilst increases in ROS were shown to increase cellular glucose uptake, corresponding changes in lactate secretion were not observed and the reasons for this have not been delineated. Indeed, data presented here suggests that typically, increased ROS led to decreased lactate secretion, although curiously intracellular lactate levels were increased. One plausible explanation is that ROS effects changes in MCT or LDH expression, resulting in decreased lactate excretion, or increased lactate uptake and increased conversion of lactate into pyruvate. The conversion of pyruvate to lactate is catalysed by LDHA

and whilst in this study no changes in expression of LDHA were observed, expression of LDHB was not investigated. Alternatively, the main transporter of lactate out of the cell is the monocarboxylic transporter, MCT4. However, there are fourteen isoforms of MCT and again while MCT4 showed no ROS dependent changes in expression, expression of MCT1 the main transporter of lactate into the cell was not examined. Overexpression of MCT1 has been observed in several cancers and imported lactate can be used for both energy production and biosynthesis (reviewed in San-Millan and Brooks, 2017). In support of this, a recent study showed that both HeLa cells and the lung cancer cell line H460 use lactate to synthesise lipids during proliferation and as an alternative to pyruvate as a point of entry into the mitochondria and the generation of energy through the citric acid cycle (Chen *et al.*, 2016d). Furthermore, the process of converting pyruvate into lactate additionally generates NAD^+, which can then be used to support an increased glycolytic rate. This then suggests a model whereby lactate, rather than being secreted by the cell is instead retained for internal energy production and lipid synthesis.

The increased excretion of lactate in many cancers means inhibition of the isoform LDH5 (comprising of four LDHA subunits (1.4.3)), represents an attractive target for inhibition in the treatment of cancer. Whilst numerous inhibitors have been identified, problems with selectivity, pharmokinetic properties or cellular entry mean that none, as of yet, have entered clinical trials (reviewed in Rani and Kumar, 2016). The lactate transporters MCT also represent an attractive target. Recently, a MCT1 inhibitor based on the alpha-cyano-4-hydoxycinnamic acid has been shown to inhibit tumour growth in colorectal adenocarcinoma xenograft models (Gurrapu *et al.*, 2015), whilst another compound, AZD3965 was shown to be effective in tissue samples of small cell lung cancer patients expressing high levels of MCT1 (Polanski *et al.*, 2014). The application of these inhibitors within the models used in this study, may then provide useful insights into discerning better the effect of ROS on metabolic mechanisms and their potential for therapeutic benefit in these cells.

Alternatively, lactate is known to inhibit PFK activity (Leite *et al.*, 2007) and thus glycolytic flux. Increased cellular ROS generates oxidative stress, and the removal of this ROS is facilitated by the generation of NADPH. Inhibition of glycolytic flux, may result in the diversion of glycolytic metabolites into the PPP, which is a major

metabolic pathway in the production of NADPH. Recently it was reported that PPP genes were upregulated in >60% of AML patients, whilst inhibition of G-6-PD using the inhibitor 6-aminonictoinamide inhibited growth and migration of AML *in vitro* (Chen *et al.*, 2016c). More recently, inhibition of 6-PGD with Physicon in combination with dihydroartemisinin (an antimalarial drug) decreased tumour growth of the K562 cell line in xenograft models (Elf *et al.*, 2017). Further support for the idea that ROS may decrease glycolytic flux can be found from the observations that ROS can potentially decrease PFKFB3 kinase activity by S-glutathionylation of Cys-206 (Seo and Lee, 2014) or by mediating phosphorylation of the enzyme at Ser-269 (Reid *et al.*, 2016). Analysis of metabolomic data presented in this study is consistent with the idea that increased ROS results in increased flux through the PPP (4.4.2) and further examination of both changes in expression of PPP enzymes and post-translational modifications of PFKFB3, alongside the use of PPP inhibitors, may lend further support to this hypothesis.

It is perhaps worth reiterating that data in this study clearly show a link between increased ROS levels and increased PFKFB3 expression, which is known to increase glycolytic flux. What is proposed above is that these increased levels of total PFKFB3 protein, are subject to further regulation by ROS in order to manage oxidative stress and cellular energy requirements (Figure 6-1).

Linked to this potential regulatory mechanism is another glycolytic enzyme that in this context is worthy of further study, PKM2. PKM2 is upregulated in many cancers and exists both as an active tetramer and inactive dimer (1.4.3). Whilst in this study ROS was not shown to modulate total PKM2 expression, the effect of ROS on the PKM2 tetramer/dimer ratio was not investigated.

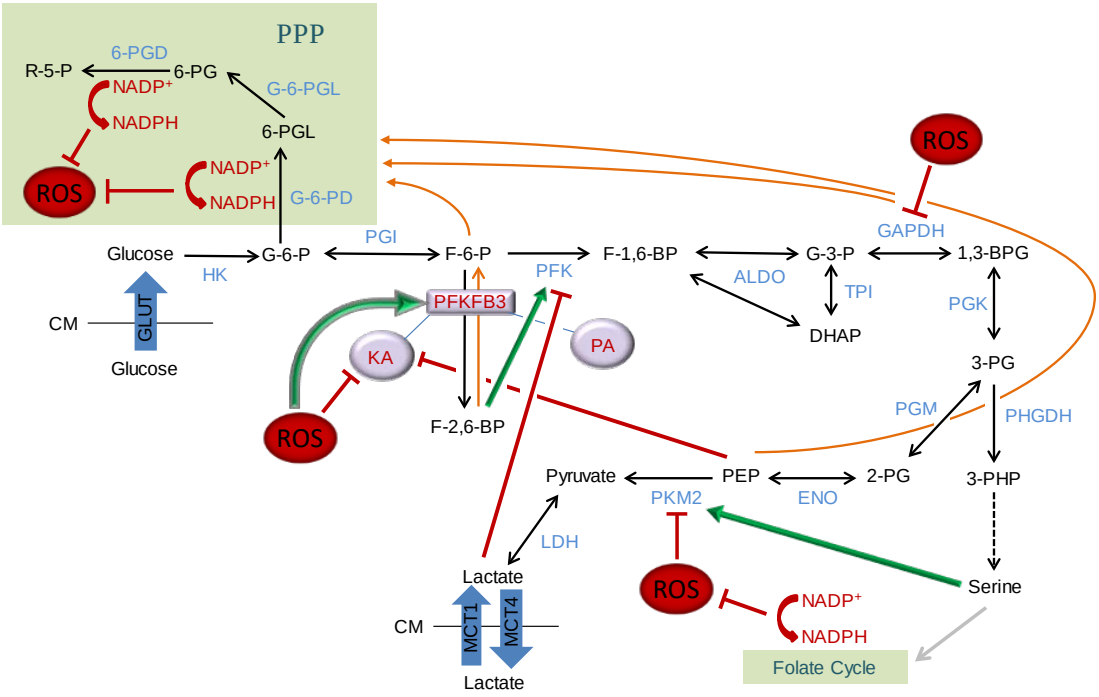

Figure 6-1. Regulation of glycolysis by reactive oxygen species (ROS) based on published literature and observations of this study. Schematic illustration of the regulation of 6-phosphofructo-2-kinase/fructoste-2,6-bisphosphatase (PFKFB3) and other key glycolytic enzymes. ROS upregulates the bifunctional enzyme PFKFB3, which promotes glycolysis. The kinase activity (KA) of PFKFB3 generates fructose-2,6-bisphosphate (F-2,6-BP) which activates phosphofructokinase (PFK) and is inhibited by ROS and by phosphoenolpyruvate (PEP). Inhibition of PFKFB3 KA results in increased fructose-6-phosphate (F-6-P) an accumulation of glycolytic intermediates and potential diversion (orange arrows) of glucose-6-phosphate (G-6-P) into the pentose phosphate pathway (PPP). ROS is also known to inhibit glyceraldehyde phosphate dehydrogenase (GAPDH) and also promote the dimerisation (and hence inhibition) of pyruvate kinase muscle 2 (PKM2), with a corresponding accumulation of glycolytic intermediates. The production of nicotinamide adenine dinucleotide phosphate (NADPH) either via the PPP or serine synthesis helps maintain redox homeostasis. Serine promotes PKM2 tetramer formation and the production of pyruvate.

Key:

Blue arrows represent transport across the cell membrane (CM), green arrows represent activation, red ‘T’ represent inhibition. Ribulose-5-phosphate (R-5-P), 6-phosphogluconate dehydrogenase (6-PGD), 6-phosphogluconate (6-PG), gluconolactonase (G-6-PGL), 6-phosphogluconolactone (6-PGL), glucose-6-phosphate dehydrogenase (G-6-PD), hexokinase (HK), phosphoglucose isomerase (PGI), fructose-1,6-bisphosphate (F-1,6-BP), glyceraldehyde-3-phosphate (G-3-P), dihydroxyacetone phosphate (DHAP), aldolase (ALDO), triosephosphate isomerase (TPI), 1,3-bisphosphoglycerate (1,3-BPG), phosphoglycerate kinase (PGK), 3-phosphoglycerate (3-PG), 2-phosphoglycerate (2-PG), phosphoglycerate mutase (PGM), enolase (ENO), phosphoglycerate dehydrogenase (PHGDH), 3-phosphohydroxypyruvate (3-PHP), lactate dehydrogenase (LDH), glucose transporter (GLUT), monocarboxylic transporter (MCT), phosphatase activity (PA).

However high levels of ROS have been shown to induce PKM2 dimerisation, which correlates with decreased lactate production and increased PEP levels (Anastasiou *et al.*, 2011) and furthermore PEP is an inhibitor of PFKFB3 kinase activity (Manes and El-Maghrabi, 2005, Kim *et al.*, 2007). Increased PKM2 dimer formation would then inhibit glycolytic flux and potentially divert intermediates into the PPP, and whilst this would not explain the ROS related changes in lactate secretion observed in this study, it would correlate with the observed increases in intracellular lactate levels.

Serine synthesis through the SSP is another avenue worthy of exploration. The SSP and folate cycle are another source of NADPH generation, and the metabolomic data here showed reduced ROS levels correlated with decreased serine levels. Interestingly, serine promotes PKM2 tetramer formation (Chaneton *et al.*, 2012) and increased utilisation of this pathway would both increase glycolysis and help manage cellular ROS levels. Analogues of the compound piperazine-1-carbothioamide have been shown to inhibit the SSP enzyme PHGDH and to inhibit growth of breast cancer cells *in vivo* and *in vitro* (Pacold *et al.*, 2016).

Finally, the mechanistic pathways for ROS modulation of PFKFB3 outlined above (4), whilst yet to be investigated, all represent potential targets in the treatment of AML, should a link be established. 5-aminoimidazole-4-carboxamide is an inhibitor of AMPK and was recently shown to have efficacy in combination with the anti-obesity drug, Orlistat, in prostate cancer cell lines (Wright *et al.*, 2017), whilst the activity of GAPDH was shown to be inhibited in hepatoma cell lines (Ganapathy-Kanniappan *et al.*, 2009). Numerous inhibitors of the $p38^{MAPK}$ pathway have been developed and whilst this pathway has been shown to be important in tumour suppression, its role in metastasis and chemotherapy resistance make it a potential target in cancer treatment (Igea and Nebreda, 2015).

6.3 Concluding remarks

Data presented in this study establishes for the first time a link between increased ROS production, glycolysis and increased expression of the key glycolytic regulatory enzyme PFKFB3 in AML. Increased ROS in human HPC expressing mutant RAS (a common mutation in AML) resulted in increased cellular glucose uptake, as measured by the glucose bioprobe 2-NBDG, and increased proliferation.

Modulation of ROS in AML cell lines was supportive of these findings. Gene expression profiling of HPC expressing mutant RAS showed ROS related changes in several glycolytic enzymes, whilst immunoblotting revealed translational changes in the regulatory glycolytic enzyme PFKFB3. As before, these ROS dependent changes in PFKFB3 expression were verified in AML cell lines. Metabolomic analysis of the AML cell lines in which ROS was modulated compared to controls, revealed significant changes in key glycolytic metabolites and further, suggested metabolic changes consistent with increased PPP and SSP flux, which generate the key antioxidant NADPH. Overexpression of PFKFB3 in Mv4;11 cells resulted in increased glucose uptake and cellular proliferation, whilst chemical inhibition of PFKFB3 decreased glucose uptake and cellular proliferation in THP-1 cells and HPC expressing mutant RAS. Furthermore, treatment of the Mv4;11 cell line with exogenous ROS increased glucose uptake in these cells, which was ablated upon treatment with PFKFB3 inhibitors, establishing a causal link between ROS levels, cellular glucose uptake and PFKFB3 activity. Upregulation of HIF-1α was investigated as a potential mechanism, but no ROS induced changes in protein expression were observed. Further studies will aim to elucidate this mechanism, which may, in combination with PFKFB3 inhibitors, offer new therapeutic windows for treatment of AML.

References

Adachi, T., Pimentel, D. R., Heibeck, T., Hou, X. Y., Lee, Y. J.*, et al.* 2004. S-glutathiolation of Ras mediates redox-sensitive signaling by angiotensin II in vascular smooth muscle cells. *Journal of Biological Chemistry,* 279, 29857-29862.

Ahmad, A., Aboukameel, A., Kong, D. J., Wang, Z. W., Sethi, S.*, et al.* 2011. Phosphoglucose Isomerase/Autocrine Motility Factor Mediates Epithelial-Mesenchymal Transition Regulated by miR-200 in Breast Cancer Cells. *Cancer Research,* 71, 3400-3409.

Ahmad, S. S., Glatzle, J., Bajaeifer, K., Buhler, S., Lehmann, T.*, et al.* 2013. Phosphoglycerate kinase 1 as a promoter of metastasis in colon cancer. *International Journal of Oncology,* 43, 586-590.

Ahmed, Z., Timsah, Z., Suen, K. M., Cook, N. P., Lee, G. R.*, et al.* 2015. Grb2 monomer-dimer equilibrium determines normal versus oncogenic function. *Nature Communications,* 6, DOI 10.1038/ncomms8354, e7354.

Akashi, K., Traver, D., Miyamoto, T. & Weissman, I. L. 2000. A clonogenic common myeloid progenitor that gives rise to all myeloid lineages. *Nature,* 404, 193-197.

Akers, L. J., Fang, W., Levy, A. G., Franklin, A. R., Huang, P.*, et al.* 2011. Targeting glycolysis in leukemia: A novel inhibitor 3-BrOP in combination with rapamycin. *Leukemia Research,* 35, 814-820.

Al Hasawi, N., Alkandari, M. F. & Luqmani, Y. A. 2014. Phosphofructokinase: A mediator of glycolytic flux in cancer progression. *Critical Reviews in Oncology Hematology,* 92, 312-321.

Aldieri, E., Riganti, C., Polimeni, M., Gazzano, E., Lussiana, C.*, et al.* 2008. Classical Inhibitors of NOX NAD(P) H Oxidases Are Not Specific. *Current Drug Metabolism,* 9, 686-696.

Alemdehy, M. F. & Erkeland, S. J. 2012. MicroRNAs: key players of normal and malignant myelopoiesis. *Current Opinion in Hematology,* 19, 261-267.

Altenhofer, S., Kleikers, P. W. M., Radermacher, K. A., Scheurer, P., Hermans, J. J. R.*, et al.* 2012. The NOX toolbox: validating the role of NADPH oxidases in physiology and disease. *Cellular and Molecular Life Sciences,* 69, 2327-2343.

Altomare, D. A. & Testa, J. R. 2005. Perturbations of the AKT signaling pathway in human cancer. *Oncogene,* 24, 7455-7464.

Alvarez-Errico, D., Vento-Tormo, R., Sieweke, M. & Ballestar, E. 2015. Epigenetic control of myeloid cell differentiation, identity and function. *Nature Reviews Immunology,* 15, 7-17.

Anastasiou, D., Poulogiannis, G., Asara, J. M., Boxer, M. B., Jiang, J.-K.*, et al.* 2011. Inhibition of Pyruvate Kinase M2 by Reactive Oxygen Species Contributes to Cellular Antioxidant Responses. *Science,* 334, 1278-1283.

Anderson, M., Marayati, R., Moffitt, R. & Yeh, J. J. 2017. Hexokinase 2 promotes tumor growth and metastasis by regulating lactate production in pancreatic cancer. *Oncotarget,* 8, 56081-56094.

Angelova, P. R. & Abramov, A. Y. 2016. Functional role of mitochondrial reactive oxygen species in physiology. *Free Radical Biology and Medicine,* 100, 81-85.

Arai, F., Hirao, A., Ohmura, M., Sato, H., Matsuoka, S.*, et al.* 2004. Tie2/angiopoietin-1 signaling regulates hematopoietic stem cell quiescence in the bone marrow niche. *Cell,* 118, 149-161.

Arber, D. A., Orazi, A., Hasserjian, R., Thiele, J., Borowitz, M. J.*, et al.* 2016. The 2016 revision to the World Health Organization classification of myeloid neoplasms and acute leukemia. *Blood,* 127, 2391-2405.

Atsumi, T., Chesney, J., Metz, C., Leng, L., Donnelly, S*., et al.* 2002. High expression of inducible 6-phosphofructo-2-kinase/fructose-2,6-bisphosphatase (iPFK-2; PFKFB3) in human cancers. *Cancer Research,* 62, 5881-5887.

Babior, B. M., Kipnes, R. S. & Curnutte, J. T. 1973. Biological Defense Mechanisms. The production by leukocytes of superoxide, a potential bactericidal agent. *Journal of Clinical Investigation,* 52, 741-744.

Bae, Y. S., Kang, S. W., Seo, M. S., Baines, I. C., Tekle, E*., et al.* 1997. Epidermal growth factor (EGF)-induced generation of hydrogen peroxide - Role in EGF receptor-mediated tyrosine phosphorylation. *Journal of Biological Chemistry,* 272, 217-221.

Baggstrom, M. Q., Qi, Y. W., Koczywas, M., Argiris, A., Johnson, E. A*., et al.* 2011. A Phase II Study of AT-101 (Gossypol) in Chemotherapy-Sensitive Recurrent Extensive-Stage Small Cell Lung Cancer. *Journal of Thoracic Oncology,* 6, 1757-1760.

Baltazar, F., Pinheiro, C., Morais-Santos, F., Azevedo-Silva, J., Queiros, O*., et al.* 2014. Monocarboxylate transporters as targets and mediators in cancer therapy response. *Histology and Histopathology,* 29, 1511-1524.

Bando, H., Atsumi, T., Nishio, T., Niwa, H., Mishima, S*., et al.* 2005. Phosphorylation of the 6-phosphofructo-2-kinase/fructose 2,6-bisphosphatase/PFKFB3 family of glycolytic regulators in human cancer. *Clinical Cancer Research,* 11, 5784-5792.

Barker, J. E. 1994. Sl/sl(d) hematopoietic progenitors are deficient in-situ. *Experimental Hematology,* 22, 174-177.

Barron, C. C., Bilan, P. J., Tsakiridis, T. & Tsiani, E. 2016. Facilitative glucose transporters: Implications for cancer detection, prognosis and treatment. *Metabolism-Clinical and Experimental,* 65, 124-139.

Bauer, D. E., Harris, M. H., Plas, D. R., Lum, J. J., Hammerman, P. S*., et al.* 2004. Cytokine stimulation of aerobic glycolysis in hematopoietic cells exceeds proliferative demand. *Faseb Journal,* 18, 1303-1323.

Baum, C. M., Weissman, I. L., Tsukamoto, A. S., Buckle, A. M. & Peault, B. 1992. Isolation of a candidate human hematopoietic stem-cell population. *Proceedings of the National Academy of Sciences of the United States of America,* 89, 2804-2808.

Bedard, K. & Krause, K. H. 2007. The NOX family of ROS-generating NADPH oxidases: physiology and pathophysiology. *Physiological Reviews,* 87, 245-313.

Bennett, J. M., Catovsky, D., Daniel, M. T., Flandrin, G., Galton, D. A*., et al.* 1976. Proposals for the classification of the acute leukaemias. French-American-British (FAB) co-operative group. . *British Journal of Haematology,* 33, 451-458.

Bensaad, K., Tsuruta, A., Selak, M. A., Vidal, M. N. C., Nakano, K*., et al.* 2006. TIGAR, a p53-inducible regulator of glycolysis and apoptosis. *Cell,* 126, 107-120.

Benveniste, P., Frelin, C., Janmohamed, S., Barbara, M., Herrington, R*., et al.* 2010. Intermediate-Term Hematopoietic Stem Cells with Extended but Time-Limited Reconstitution Potential. *Cell Stem Cell,* 6, 48-58.

Berkholz, D. S., Faber, H. R., Savvides, S. N. & Karplus, P. A. 2008. Catcalytic cycle of human glutathione reductase near 1 angstrom resolution. *Journal of Molecular Biology,* 382, 371-384.

Bertolotti, M., Bestetti, S., Garcia-Manteiga, J. M., Medrano-Fernandez, I., Dal Mas, A*., et al.* 2013. Tyrosine Kinase Signal Modulation: A Matter of H2O2 Membrane Permeability? *Antioxidants & Redox Signaling,* 19, 1447-1451.

Bhanot, H., Reddy, M. M., Nonami, A., Weisberg, E. L., Bonal, D*., et al.* 2015. Pathological glycogenesis through glycogen synthase 1 and suppression of excessive AMP kinase activity in myeloid leukemia cells. *Leukemia,* 29, 1555-1563.

Bhayat, F., Das-Gupta, E., Smith, C., Mckeever, T. & Hubbard, R. 2009. The incidence of and mortality from leukaemias in the UK: a general population-based study. *Bmc Cancer,* 9, DOI 10.1186/1471-2407-1189-1252, e1252.
Bienert, G. P. & Chaumont, F. 2014. Aquaporin-facilitated transmembrane diffusion of hydrogen peroxide. *Biochimica Et Biophysica Acta-General Subjects,* 1840, 1596-1604.
Bienert, G. P., Schjoerring, J. K. & Jahn, T. P. 2006. Membrane transport of hydrogen peroxide. *Biochimica Et Biophysica Acta-Biomembranes,* 1758, 994-1003.
Blangy, D., Buc, H. & Monod, J. 1968. Kinetics of allosteric interactions of phosphofructokinase from escherichia coli. *Journal of Molecular Biology,* 31, 13-&.
Blank, U. & Karlsson, S. 2015. TGF-beta signaling in the control of hematopoietic stem cells. *Blood,* 125, 3542-3550.
Bobarykina, A. Y., Minchenko, D. O., Opentanova, I. L., Moenner, M., Caro, J.*, et al.* 2006. Hypoxic regulation of PFYFB-3 and PFKFB-4 gene expression in gastric and pancreatic cancer cell lines and expression of PFYFB genes in gastric cancers. *Acta Biochimica Polonica,* 53, 789-799.
Bonello, S., Zahringer, C., Belaiba, R. S., Djordjevic, T., Hess, J.*, et al.* 2007. Reactive oxygen species activate the HIF-1 alpha promoter via a functional NF kappa B site. *Arteriosclerosis Thrombosis and Vascular Biology,* 27, 755-761.
Boriack-Sjodin, P. A., Margarit, S. M., Bar-Sagi, D. & Kuriyan, J. 1998. The structural basis of the activation of Ras by Sos. *Nature,* 394, 337-343.
Borrego, S., Vazquez, A., Dasi, F., Cerda, C., Iradi, A.*, et al.* 2013. Oxidative Stress and DNA Damage in Human Gastric Carcinoma: 8-Oxo-7 ' 8-dihydro-2 '-deoxyguanosine (8-oxo-dG) as a Possible Tumor Marker. *International Journal of Molecular Sciences,* 14, 3467-3486.
Bos, J. L., Rehmann, H. & Wittinghofer, A. 2007. GEFs and GAPs: Critical elements in the control of small G proteins. *Cell,* 129, 865-877.
Bower, H., Andersson, T. M. L., Bjorkholm, M., Dickman, P. W., Lambert, P. C.*, et al.* 2016. Continued improvement in survival of acute myeloid leukemia patients: an application of the loss in expectation of life. *Blood Cancer Journal,* 6, DOI 10.1038/bcj.2016.1033, e1390.
Bowler, M. W. 2013. Conformational dynamics in phosphoglycerate kinase, an open and shut case? *Febs Letters,* 587, 1878-1883.
Brar, S. S., Corbin, Z., Kennedy, T. P., Hemendinger, R., Thornton, L.*, et al.* 2003. NOX5 NAD(P)H oxidase regulates growth and apoptosis in DU 145 prostate cancer cells. *American Journal of Physiology-Cell Physiology,* 285, C353-C369.
Brito, P. M. & Antunes, F. 2014. Estimation of kinetic parameters related to biochemical interactions between hydrogen peroxide and signal transduction proteins. *Frontiers in Chemistry,* 2, DOI 10.3389/fchem.2014.00082, e00082.
Brunet, A., Bonni, A., Zigmond, M. J., Lin, M. Z., Juo, P.*, et al.* 1999. Akt promotes cell survival by phosphorylating and inhibiting a forkhead transcription factor. *Cell,* 96, 857-868.
Buday, L. & Downward, J. 2008. Many faces of Ras activation. *Biochimica Et Biophysica Acta-Reviews on Cancer,* 1786, 178-187.
Bullinger, L., Dohner, K. & Dohner, H. 2017. Genomics of Acute Myeloid Leukemia Diagnosis and Pathways. *Journal of Clinical Oncology,* 35, 934-946.
Bulua, A. C., Simon, A., Maddipati, R., Pelletier, M., Park, H.*, et al.* 2011. Mitochondrial reactive oxygen species promote production of proinflammatory cytokines and are elevated in TNFR1-associated periodic syndrome (TRAPS). *Journal of Experimental Medicine,* 208, 519-533.

Burnett, A., Wetzler, M. & Lowenberg, B. 2011. Therapeutic Advances in Acute Myeloid Leukemia. *Journal of Clinical Oncology,* 29, 487-494.
Burnett, A. K. 2012. Treatment of acute myeloid leukemia: are we making progress? *Hematology-American Society Hematology Education Program*, 1-6.
Calvi, L. M., Adams, G. B., Weibrecht, K. W., Weber, J. M., Olson, D. P.*, et al.* 2003. Osteoblastic cells regulate the haematopoietic stem cell niche. *Nature,* 425, 841-846.
Campa, V. M. & Kypta, R. M. 2011. Issues associated with the use of phosphospecific antibodies to localise active and inactive pools of GSK-3 in cells. *Biology Direct,* 6, DOI 10.1186/1745-6150-1186-1184, e1184.
Cao, J. X., Schulte, J., Knight, A., Leslie, N. R., Zagozdzon, A.*, et al.* 2009. Prdx1 inhibits tumorigenesis via regulating PTEN/AKT activity. *Embo Journal,* 28, 1505-1517.
Cao, W. G., Yacoub, S., Shiverick, K. T., Namiki, K., Sakai, Y.*, et al.* 2008. Dichloroacetate (DCA) sensitizes both wild-type and over expressing Bcl-2 prostate cancer cells in vitro to radiation. *Prostate,* 68, 1223-1231.
Carlsson, L. M., Jonsson, J., Edlund, T. & Marklund, S. L. 1995. Mice lacking extracellular-superoxide dismutase are more sensitive to hyperoxia. *Proceedings of the National Academy of Sciences of the United States of America,* 92, 6264-6268.
Carracedo, A., Cantley, L. C. & Pandolfi, P. P. 2013. Cancer metabolism: fatty acid oxidation in the limelight. *Nature Reviews Cancer,* 13, 227-232.
Casey, P. J., Solski, P. A., Der, C. J. & Buss, J. E. 1989. P21RAS is modified by a farnesyl isoprenoid. *Proceedings of the National Academy of Sciences of the United States of America,* 86, 8323-8327.
Caspi, M., Perry, G., Skalka, N., Meisel, S., Firsow, A.*, et al.* 2014. Aldolase positively regulates of the canonical Wnt signaling pathway. *Molecular Cancer,* 13, DOI 10.1186/1476-4598-1113-1164, e1164.
Cavalier, M. C., Kim, S.-G., Neau, D. & Lee, Y.-H. 2012. Molecular basis of the fructose-2,6-bisphosphatase reaction of PFKFB3: Transition state and the C-terminal function. *Proteins-Structure Function and Bioinformatics,* 80, 1143-1153.
Cervantes-Madrid, D., Romero, Y. & Duenas-Gonzalez, A. 2015. Reviving Lonidamine and 6-Diazo-5-oxo-L-norleucine to Be Used in Combination for Metabolic Cancer Therapy. *Biomedical Research International*, DOI 10.1155/2015/690492, e690492.
Chaneton, B., Hillmann, P., Zheng, L., Martin, A. C. L., Maddocks, O. D. K.*, et al.* 2012. Serine is a natural ligand and allosteric activator of pyruvate kinase M2. *Nature,* 491, 458-462.
Chang, H. H., Hemberg, M., Barahona, M., Ingber, D. E. & Huang, S. 2008. Transcriptome-wide noise controls lineage choice in mammalian progenitor cells. *Nature,* 453, 544-U510.
Chang, Y. C., Chan, Y. C., Chang, W. M., Lin, Y. F., Yang, C. J.*, et al.* 2017. Feedback regulation of ALDOA activates the HIF-1 alpha/MMP9 axis to promote lung cancer progression. *Cancer Letters,* 403, 28-36.
Chelikani, P., Fita, I. & Loewen, P. C. 2004. Diversity of structures and properties among catalases. *Cellular and Molecular Life Sciences,* 61, 192-208.
Chen, C. H., Pore, N., Behrooz, A., Ismail-Beigi, F. & Maity, A. 2001. Regulation of glut1 mRNA by hypoxia-inducible factor-1 - Interaction between H-ras and hypoxia. *Journal of Biological Chemistry,* 276, 9519-9525.
Chen, L. L., Zhao, J. J., Tang, Q. M., Li, H. G., Zhang, C. G.*, et al.* 2016a. PFKFB3 Control of Cancer Growth by Responding to Circadian Clock Outputs. *Scientific Reports,* 6, DOI DOI 10.3389/fonc.2017.00117, e00117.

Chen, W.-L., Wang, J.-H., Zhao, A.-H., Xu, X., Wang, Y.-H*., et al.* 2014. A distinct glucose metabolism signature of acute myeloid leukemia with prognostic value. *Blood,* 124, 1645-1654.
Chen, W. L., Wang, Y. Y., Zhao, A. H., Xia, L., Xie, G. X*., et al.* 2016b. Enhanced Fructose Utilization Mediated by SLC2A5 Is a Unique Metabolic Feature of Acute Myeloid Leukemia with Therapeutic Potential. *Cancer Cell,* 30, 779-791.
Chen, Y., Xu, Q., Ji, D. X., Wei, Y. L., Chen, H. M*., et al.* 2016c. Inhibition of pentose phosphate pathway suppresses acute myelogenous leukemia. *Tumor Biology,* 37, 6027-6034.
Chen, Y. J., Mahieu, N. G., Huang, X. J., Singh, M., Crawford, P. A*., et al.* 2016d. Lactate metabolism is associated with mammalian mitochondria. *Nature Chemical Biology,* 12, 937-943.
Cherfils, J. & Zeghouf, M. 2013. REGULATION OF SMALL GTPases BY GEFs, GAPs, AND GDIs. *Physiological Reviews,* 93, 269-309.
Chesney, J. & Telang, S. 2013. Regulation of Glycolytic and Mitochondrial Metabolism by Ras. *Current Pharmaceutical Biotechnology,* 14, 251-260.
Christofk, H. R., Vander Heiden, M. G., Harris, M. H., Ramanathan, A., Gerszten, R. E*., et al.* 2008. The M2 splice isoform of pyruvate kinase is important for cancer metabolism and tumour growth. *Nature,* 452, 230-U274.
Ciccarese, F. & Ciminale, V. 2017. Escaping Death: Mitochondrial Redox Homeostasis in Cancer Cells. *Frontiers in Oncology,* 7, DOI 10.3389/fonc.2017.00117, e00117.
Civin, C. I., Strauss, L. C., Brovall, C., Fackler, M. J., Schwartz, J. F*., et al.* 1984. Antigenic analysis of hematopoiesis .3. A hematopoietic progenitor-cell surface-antigen defined by a monoclonal-antibody raised against kg-1a cells. *Journal of Immunology,* 133, 157-165.
Clem, B., Telang, S., Clem, A., Yalcin, A., Meier, J*., et al.* 2008. Small-molecule inhibition of 6-phosphofructo-2-kinase activity suppresses glycolytic flux and tumor growth. *Molecular Cancer Therapeutics,* 7, 110-120.
Clem, B. F., O'neal, J., Tapolsky, G., Clem, A. L., Imbert-Fernandez, Y*., et al.* 2013. Targeting 6-Phosphofructo-2-Kinase (PFKFB3) as a Therapeutic Strategy against Cancer. *Molecular Cancer Therapeutics,* 12, 1461-1470.
Contractor, T. & Harris, C. R. 2012. p53 Negatively Regulates Transcription of the Pyruvate Dehydrogenase Kinase Pdk2. *Cancer Research,* 72, 560-567.
Cooke, M. S., Evans, M. D., Dizdaroglu, M. & Lunec, J. 2003. Oxidative DNA damage: mechanisms, mutation, and disease. *Faseb Journal,* 17, 1195-1214.
Corcoran, A. & Cotter, T. G. 2013. Redox regulation of protein kinases. *Febs Journal,* 280, 1944-1965.
Cordero-Espinoza, L. & Hagen, T. 2013. Increased Concentrations of Fructose 2,6-Bisphosphate Contribute to the Warburg Effect in Phosphatase and Tensin Homolog (PTEN)-deficient Cells. *Journal of Biological Chemistry,* 288, 36020-36028.
Cortes, J. E., Faderl, S., Pagel, J., Jung, C. W., Yoon, S. S*., et al.* 2015. Phase 1 study of CWP232291 in relapsed/refractory acute myeloid leukemia (AML) and myelodysplastic syndrome (MDS). *Journal of Clinical Oncology,* 33, 7044-7044.
Cosentino, C., Grieco, D. & Costanzo, V. 2011. ATM activates the pentose phosphate pathway promoting anti-oxidant defence and DNA repair. *Embo Journal,* 30, 546-555.
Crane, G. M., Jeffery, E. & Morrison, S. J. 2017. Adult haematopoietic stem cell niches. *Nature Reviews Immunology,* 17, 573-590.
Crochet, R. B., Kim, J. D., Lee, H., Yim, Y. S., Kim, S. G*., et al.* 2017. Crystal structure of heart 6-phosphofructo-2-kinase/fructose-2,6-bisphosphatase (PFKFB2) and the

inhibitory influence of citrate on substrate binding. *Proteins-Structure Function and Bioinformatics,* 85, 117-124.
Cvejic, A. 2016. Mechanisms of fate decision and lineage commitment during haematopoiesis. *Immunology and Cell Biology,* 94, 230-235.
Cyert, M. S. 2001. Regulation of nuclear localization during signaling. *Journal of Biological Chemistry,* 276, 20805-20808.
D'angelo, G., Duplan, E., Boyer, N., Vigne, P. & Frelin, C. 2003. Hypoxia up-regulates prolyl hydroxylase activity - A feedback mechansim that limits HIF-1 responses during reoxygenation. *Journal of Biological Chemistry,* 278, 38183-38187.
Dalla Sega, F. V., Zambonin, L., Fiorentini, D., Rizzo, B., Caliceti, C*., et al.* 2014. Specific aquaporins facilitate Nox-produced hydrogen peroxide transport through plasma membrane in leukaemia cells. *Biochimica Et Biophysica Acta-Molecular Cell Research,* 1843, 806-814.
Dang, L. N., Jin, S. F. & Su, S. S. M. 2010. IDH mutations in glioma and acute myeloid leukemia. *Trends in Molecular Medicine,* 16, 387-397.
Darley, R. L., Pearn, L., Omidvar, N., Sweeney, M., Fisher, J*., et al.* 2002. Protein kinase C mediates mutant N-Ras-induced developmental abnormalities in normal human erythroid cells. *Blood,* 100, 4185-4192.
David, C. J., Chen, M., Assanah, M., Canoll, P. & Manley, J. L. 2010. HnRNP proteins controlled by c-Myc deregulate pyruvate kinase mRNA splicing in cancer. *Nature,* 463, 364-U114.
De Carvalho, D. D., Sadolk, A., Bourgarel-Rey, V., Gattacceca, F., Penel, C*., et al.* 2008. Nox1 downstream of 12-lipoxygenase controls cell proliferation but not cell spreading of colon cancer cells. *International Journal of Cancer,* 122, 1757-1764.
Deberardinis, R. J. & Chandel, N. S. 2016. Fundamentals of cancer metabolism. *Science Advances,* 2, DOI 10.1126/sciadv.1600200, UNSP e1600200.
Decoursey, T. E. & Ligeti, E. 2005. Regulation and termination of NADPH oxidase activity. *Cellular and Molecular Life Sciences,* 62, 2173-2193.
Deininger, M., Buchdunger, E. & Druker, B. J. 2005. The development of imatinib as a therapeutic agent for chronic myeloid leukemia. *Blood,* 105, 2640-2653.
Del Prete, A., Zaccagnino, P., Di Paola, M., Saltarella, M., Celis, C. O*., et al.* 2008. Role of mitochondria and reactive oxygen species in dendritic cell differentiation and functions. *Free Radical Biology and Medicine,* 44, 1443-1451.
Delaunay, A., Pflieger, D., Barrault, M. B., Vinh, J. & Toledano, M. B. 2002. A thiol peroxidase is an H2O2 receptor and redox-transducer in gene activation. *Cell,* 111, 471-481.
Denu, J. M. & Tanner, K. G. 1998. Specific and reversible inactivation of protein tyrosine phosphatases by hydrogen peroxide: Evidence for a sulfenic acid intermediate and implications for redox regulation. *Biochemistry,* 37, 5633-5642.
Desai, S., Ding, M. M., Wang, B., Lu, Z. M., Zhao, Q*., et al.* 2014. Tissue-specific isoform switch and DNA hypomethylation of the pyruvate kinase PKM gene in human cancers. *Oncotarget,* 5, 8202-8210.
Desideri, E., Vegliante, R., Cardaci, S., Nepravishta, R., Paci, M*., et al.* 2014. MAPK14/p38 alpha-dependent modulation of glucose metabolism affects ROS levels and autophagy during starvation. *Autophagy,* 10, 1652-1665.
Devi, G. S., Prasad, M. H., Saraswathi, I., Raghu, D., Rao, D. N*., et al.* 2000. Free radicals antioxidant enzymes and lipid peroxidation in different types of leukemias. *Clinica Chimica Acta,* 293, 53-62.
Deynoux, M., Sunter, N., Herault, O. & Mazurier, F. 2016. Hypoxia and Hypoxia-inducible Factors in Leukemias. *Frontiers in Oncology,* 6, DOI 10.3389/fonc.2016.00041, e00041.

Diaz-Ramos, A., Roig-Borrellas, A., Garcia-Melero, A. & Lopez-Alemany, R. 2012. alpha-Enolase, a Multifunctional Protein: Its Role on Pathophysiological Situations. *Journal of Biomedicine and Biotechnology*.

Diehn, M., Cho, R. W., Lobo, N. A., Kalisky, T., Dorie, M. J*., et al.* 2009. Association of reactive oxygen species levels and radioresistance in cancer stem cells. *Nature,* 458, 780-U123.

Ding, L. & Morrison, S. J. 2013. Haematopoietic stem cells and early lymphoid progenitors occupy distinct bone marrow niches. *Nature,* 495, 231-235.

Ding, L., Saunders, T. L., Enikolopov, G. & Morrison, S. J. 2012. Endothelial and perivascular cells maintain haematopoietic stem cells. *Nature,* 481, 457-U465.

Djinovic, K., Gatti, G., Coda, A., Antolini, L., Pelosi, G*., et al.* 1991. Structure solution and molecular-dynamics refinement of the yeast cu,zn enzyme superoxide-dismutase. *Acta Crystallographica Section B-Structural Science,* 47, 918-927.

Doherty, J. R. & Cleveland, J. L. 2013. Targeting lactate metabolism for cancer therapeutics. *Journal of Clinical Investigation,* 123, 3685-3692.

Dolado, I., Swat, A., Ajenjo, N., De Vita, G., Cuadrado, A*., et al.* 2007. p38 alpha MAP kinase as a sensor of reactive oxygen species in tumorigenesis. *Cancer Cell,* 11, 191-205.

Domenech, E., Maestre, C., An-Martinez, L. E., Partidal, D., Pascual, R*., et al.* 2015. AMPK and PFKFB3 mediate glycolysis and survival in response to mitophagy during mitotic arrest. *Nature Cell Biology,* 17, 1304-1316.

Dong, G. C., Mao, Q. X., Xia, W. J., Xu, Y. T., Wang, J*., et al.* 2016. PKM2 and cancer: The function of PKM2 beyond glycolysis. *Oncology Letters,* 11, 1980-1986.

Dorritie, K. A., Mccubrey, J. A. & Johnson, D. E. 2014. STAT transcription factors in hematopoiesis and leukemogenesis: opportunities for therapeutic intervention. *Leukemia,* 28, 248-257.

Doulatov, S., Notta, F., Laurenti, E. & Dick, J. E. 2012. Hematopoiesis: A Human Perspective. *Cell Stem Cell,* 10, 120-136.

Drose, S. & Brandt, U. 2008. The mechanism of mitochondrial superoxide production by the cytochrome bc(1) complex. *Journal of Biological Chemistry,* 283, 21649-21654.

Duffy, M. J., Synnott, N. C. & Crown, J. 2017. Mutant p53 as a target for cancer treatment. *European Journal of Cancer,* 83, 258-265.

Dunbar, E. M., Coats, B. S., Shroads, A. L., Langaee, T., Lew, A*., et al.* 2014. Phase 1 trial of dichloroacetate (DCA) in adults with recurrent malignant brain tumors. *Investigational New Drugs,* 32, 452-464.

Efeyan, A., Zoncu, R. & Sabatini, D. M. 2012. Amino acids and mTORC1: from lysosomes to disease. *Trends in Molecular Medicine,* 18, 524-533.

Eigenbrodt, E., Basenau, D., Holthusen, S., Mazurek, S. & Fischer, G. 1997. Quantification of tumor type M2 pyruvate kinase (Tu M2-PK) in human carcinomas. *Anticancer Research,* 17, 3153-3156.

Elchuri, S., Oberley, T. D., Qi, W. B., Eisenstein, R. S., Roberts, L. J*., et al.* 2005. CuZnSOD deficiency leads to persistent and widespread oxidative damage and hepatocarcinogenesis later in life. *Oncogene,* 24, 367-380.

Elf, S., Lin, R., Xia, S., Pan, Y., Shan, C*., et al.* 2017. Targeting 6-phosphogluconate dehydrogenase in the oxidative PPP sensitizes leukemia cells to antimalarial agent dihydroartemisinin. *Oncogene,* 36, 254-262.

Ema, H., Morita, Y. & Suda, T. 2014. Heterogeneity and hierarchy of hematopoietic stem cells. *Experimental Hematology,* 42, 74-82.

Emadi, A., Sadowska, M., Carter-Cooper, B., Bhatnagar, V., Van Der Merwe, I*., et al.* 2015. Perturbation of cellular oxidative state induced by dichloroacetate and

arsenic trioxide for treatment of acute myeloid leukemia. *Leukemia Research,* 39, 719-729.
Endele, M., Etzrodt, M. & Schroeder, T. 2014. Instruction of hematopoietic lineage choice by cytokine signaling. *Experimental Cell Research,* 329, 207-213.
Enver, T., Heyworth, C. M. & Dexter, T. M. 1998. Do stem cells play dice? *Blood,* 92, 348-351.
Epsztejn, S., Kakhlon, O., Glickstein, H., Breuer, W. & Cabantchik, Z. I. 1997. Fluorescence analysis of the labile iron pool of mammalian cells. *Analytical Biochemistry,* 248, 31-40.
Essers, M. a. G., Weijzen, S., De Vries-Smits, A. M. M., Saarloos, I., De Ruiter, N. D*., et al.* 2004. FOXO transcription factor activation by oxidative stress mediated by the small GTPase Ral and JNK. *Embo Journal,* 23, 4802-4812.
Esteban-Martinez, L., Domenech, E., Boya, P., Salazar-Roa, M. & Malumbres, M. 2015. Mitophagy in mitosis: More than a myth. *Autophagy,* 11, 2379-2380.
Estey, E. & Dohner, H. 2006. Acute myeloid leukaemia. *Lancet,* 368, 1894-1907.
Estey, E. & Gale, R. P. 2017. Acute myeloid leukemia therapy and the chosen people. *Leukemia,* 31, 269-271.
Fairbairn, L. J., Cowling, G. J., Reipert, B. M. & Dexter, T. M. 1993. Suppression of apoptosis allows differentiation and development of a multipotent hematopoietic-cell line in the absence of added growth-factors. *Cell,* 74, 823-832.
Feng, Y. H. & Wu, L. S. 2017. mTOR up-regulation of PFKFB3 is essential for acute myeloid leukemia cell survival. *Biochemical and Biophysical Research Communications,* 483, 897-903.
Franken, S. M., Scheidig, A. J., Krengel, U., Rensland, H., Lautwein, A*., et al.* 1993. 3-dimensional structures and properties of a transforming and a nontransforming glycine-12 mutant of p21(H-RAS). *Biochemistry,* 32, 8411-8420.
Gackowski, D., Kowalewski, J., Siomek, A. & Olinski, R. 2005. Oxidative DNA damage and antioxidant vitamin level: Comparison among lung cancer patients, healthy smokers and nonsmokers. *International Journal of Cancer,* 114, 153-156.
Gaglio, D., Metallo, C. M., Gameiro, P. A., Hiller, K., Danna, L. S*., et al.* 2011. Oncogenic K-Ras decouples glucose and glutamine metabolism to support cancer cell growth. *Molecular Systems Biology,* 7, DOI 10.1038/msb.2011.1056, e1523.
Galadari, S., Rahman, A., Pallichankandy, S. & Thayyullathil, F. 2017. Reactive oxygen species and cancer paradox: To promote or to suppress? *Free Radical Biology and Medicine,* 104, 144-164.
Ganapathy-Kanniappan, S., Geschwind, J.-F. H., Kunjithapatham, R., Buijs, M., Vossen, J. A*., et al.* 2009. Glyceraldehyde-3-phosphate Dehydrogenase (GAPDH) Is Pyruvylated during 3-Bromopyruvate Mediated Cancer Cell Death. *Anticancer Research,* 29, 4909-4918.
Gandhi, U. H., Kaushal, N., Hegde, S., Finch, E. R., Kudva, A. K*., et al.* 2014. Selenium Suppresses Leukemia through the Action of Endogenous Eicosanoids. *Cancer Research,* 74, 3890-3901.
Gao, X. & Schottker, B. 2017. Reduction-oxidation pathways involved in cancer development: a systematic review of literature reviews. *Oncotarget,* 8, 51888-51906.
Gao, X. N., Yan, F., Lin, J., Gao, L., Lu, X. L*., et al.* 2015. AML1/ETO cooperates with HIF1 alpha to promote leukemogenesis through DNMT3 alpha transactivation. *Leukemia,* 29, 1730-1740.
Ge, X., Lyu, P. W., Cao, Z., Li, J. R., Guo, G. C*., et al.* 2015a. Overexpression of miR-206 suppresses glycolysis, proliferation and migration in breast cancer cells via PFKFB3 targeting. *Biochemical and Biophysical Research Communications,* 463, 1115-1121.

Ge, X., Lyu, P. W., Gu, Y. T., Li, L., Li, J. R., *et al.* 2015b. Sonic hedgehog stimulates glycolysis and proliferation of breast cancer cells: Modulation of PFKFB3 activation. *Biochemical and Biophysical Research Communications,* 464, 862-868.
Gorrini, C., Harris, I. S. & Mak, T. W. 2013. Modulation of oxidative stress as an anticancer strategy. *Nature Reviews Drug Discovery,* 12, 931-947.
Graham, K. A., Kulawiec, M., Owens, K. M., Li, X. R., Desouki, M. M., *et al.* 2010. NADPH oxidase 4 is an oncoprotein localized to mitochondria. *Cancer Biology & Therapy,* 10, e12207.
Granchi, C., Fancelli, D. & Minutolo, F. 2014. An update on therapeutic opportunities offered by cancer glycolytic metabolism. *Bioorganic & Medicinal Chemistry Letters,* 24, 4915-4925.
Granchi, C., Fortunato, S. & Minutolo, F. 2016. Anticancer agents interacting with membrane glucose transporters. *Medchemcomm,* 7, 1716-1729.
Greer, S. N., Metcalf, J. L., Wang, Y. & Ohh, M. 2012. The updated biology of hypoxia-inducible factor. *Embo Journal,* 31, 2448-2460.
Greijer, A. E., Van Der Groep, P., Kemming, D., Shvarts, A., Semenza, G. L., *et al.* 2005. Up-regulation of gene expression by hypoxia is mediated predominantly by hypoxia-inducible factor 1 (HIF-1). *Journal of Pathology,* 206, 291-304.
Gremer, L., Gilsbach, B., Ahmadian, M. R. & Wittinghofer, A. 2008. Fluoride complexes of oncogenic Ras mutants to study the Ras-RasGAP interaction. *Biological Chemistry,* 389, 1163-1171.
Grignani, F., Kinsella, T., Mencarelli, A., Valtieri, M., Riganelli, D., *et al.* 1998. High-efficiency gene transfer and selection of human hematopoietic progenitor cells with a hybrid EBV/retroviral vector expressing the green fluorescence protein. *Cancer Research,* 58, 14-19.
Groemping, Y. & Rittinger, K. 2005. Activation and assembly of the NADPH oxidase: a structural perspective. *Biochemical Journal,* 386, 401-416.
Gruning, N. M., Du, D. J., Keller, M. A., Luisi, B. F. & Ralser, M. 2014. Inhibition of triosephosphate isomerase by phosphoenolpyruvate in the feedback-regulation of glycolysis. *Open Biology,* 4, DOI 10.1098/rsob.130232, e130232.
Gu, J. K., Wu, M., Guo, R. Y., Yan, K. G., Lei, J. L., *et al.* 2016. The architecture of the mammalian respirasome. *Nature,* 537, 639-643.
Guitart, A. V., Panagopoulou, T. I., Villacreces, A., Vukovic, M., Sepulveda, C., *et al.* 2017. Fumarate hydratase is a critical metabolic regulator of hematopoietic stem cell functions. *Journal of Experimental Medicine,* 214, 719-735.
Guo, C. M., Liu, S. Q. & Sun, M. Z. 2013. Novel insight into the role of GAPDH playing in tumor. *Clinical & Translational Oncology,* 15, 167-172.
Guo, W. J., Qiu, Z. P., Wang, Z. C., Wang, Q. F., Tan, N., *et al.* 2015. MiR-199a-5p is negatively associated with malignancies and regulates glycolysis and lactate production by targeting hexokinase 2 in liver cancer. *Hepatology,* 62, 1132-1144.
Gurrapu, S., Jonnalagadda, S. K., Alam, M. A., Nelson, G. L., Sneve, M. G., *et al.* 2015. Monocarboxylate Transporter 1 Inhibitors as Potential Anticancer Agents. *Acs Medicinal Chemistry Letters,* 6, 558-561.
Gutierrez, S. E. & Romero-Oliva, F. A. 2013. Epigenetic changes: a common theme in acute myelogenous leukemogenesis. *Journal of Hematology & Oncology,* 6, DOI 10.1186/1756-8722-1186-1157, e1157.
Gutsche, M., Sobotta, M. C., Wabnitz, G. H., Ballikaya, S., Meyer, A. J., *et al.* 2009. Proximity-based Protein Thiol Oxidation by H2O2-scavenging Peroxidases. *Journal of Biological Chemistry,* 284, 31532-31540.

Guzy, R. D., Hoyos, B., Robin, E., Chen, H., Liu, L. P., *et al.* 2005. Mitochondrial complex III is required for hypoxia-induced ROS production and cellular oxygen sensing. *Cell Metabolism,* 1, 401-408.
Hagen, T. 2012. Oxygen versus Reactive Oxygen in the Regulation of HIF-1alpha: The Balance Tips. *Biochemistry research international,* 2012, 436981-436981.
Han, T. Y., Kang, D., Ji, D. K., Wang, X. Y., Zhan, W. H., *et al.* 2013. How does cancer cell metabolism affect tumor migration and invasion? *Cell Adhesion & Migration,* 7, 395-403.
Hancock, J. F., Paterson, H. & Marshall, C. J. 1990. A polybasic domain or palmitoylation is required in addition to the caax motif to localize p21ras to the plasma-membrane. *Cell,* 63, 133-139.
Hara, M. R., Agrawal, N., Kim, S. F., Cascio, M. B., Fujimuro, M., *et al.* 2005. S-nitrosylated GAPDH initiates apoptotic cell death by nuclear translocation following Siah1 binding. *Nature Cell Biology,* 7, 665-U640.
Hasemann, C. A., Istvan, E. S., Uyeda, K. & Deisenhofer, J. 1996. The crystal structure of the bifunctional enzyme 6-phosphofructo-2-kinase/fructose-2,6-bisphosphatase reveals distinct domain homologies. *Structure,* 4, 1017-1029.
Heffetz, D. & Zick, Y. 1989. H2o2 potentiates phosphorylation of novel putative substrates for the insulin-receptor kinase in intact fao cells. *Journal of Biological Chemistry,* 264, 10126-10132.
Herst, P. M., Howman, R. A., Neeson, P. J., Berridge, M. V. & Ritchie, D. S. 2011. The level of glycolytic metabolism in acute myeloid leukemia blasts at diagnosis is prognostic for clinical outcome. *J Leukoc Biol,* 89, 51-55.
Heyworth, C., Pearson, S., May, G. & Enver, T. 2002. Transcription factor-mediated lineage switching reveals plasticity in primary committed progenitor cells. *Embo Journal,* 21, 3770-3781.
Hirota, K., Murata, M., Sachi, Y., Nakamura, H., Takeuchi, J., *et al.* 1999. Distinct roles of thioredoxin in the cytoplasm and in the nucleus - A two-step mechanism of redox regulation of transcription factor NF-kappa B. *Journal of Biological Chemistry,* 274, 27891-27897.
Hitosugi, T., Kang, S., Heiden, M. G. V., Chung, T.-W., Elf, S., *et al.* 2009. Tyrosine Phosphorylation Inhibits PKM2 to Promote the Warburg Effect and Tumor Growth. *Science Signaling,* 2, DOI 10.1126/scisignal.2000431, ra2000473.
Hitosugi, T., Zhou, L., Arellano, M., Khoury, H., Boggon, T., *et al.* 2013. Phosphoglycerate mutase 1 coordinates glycolysis and biosynthesis to promote tumor growth. *Cancer Research,* 73, DOI 10.1158/1538-7445.am2013-4612.
Hitosugi, T., Zhou, L., Elf, S., Fan, J., Kang, H. B., *et al.* 2012. Phosphoglycerate Mutase 1 Coordinates Glycolysis and Biosynthesis to Promote Tumor Growth. *Cancer Cell,* 22, 585-600.
Ho, M. S. H., Medcalf, R. L., Livesey, S. A. & Traianedes, K. 2015. The dynamics of adult haematopoiesis in the bone and bone marrow environment. *British Journal of Haematology,* 170, 472-486.
Hole, P. S. 2010. Role of reactive oxygen species in RAS-mediated leukaemogenesis. *PhD Thesis, Cardiff University*.
Hole, P. S., Darley, R. L. & Tonks, A. 2011. Do reactive oxygen species play a role in myeloid leukemias? *Blood,* 117, 5816-5826.
Hole, P. S., Pearn, L., Tonks, A. J., James, P. E., Burnett, A. K., *et al.* 2010. Ras-induced reactive oxygen species promote growth factor-independent proliferation in human CD34(+) hematopoietic progenitor cells. *Blood,* 115, 1238-1246.

Hole, P. S., Zabkiewicz, J., Munje, C., Newton, Z., Pearn, L.*, et al.* 2013. Overproduction of NOX-derived ROS in AML promotes proliferation and is associated with defective oxidative stress signaling. *Blood,* 122, 3322-3330.
Hong, M., Xia, Y., Zhu, Y., Zhao, H. H., Zhu, H.*, et al.* 2016. TP53-induced glycolysis and apoptosis regulator protects from spontaneous apoptosis and predicts poor prognosis in chronic lymphocytic leukemia. *Leukemia Research,* 50, 72-77.
Hopkins, G. L. 2014. Identification of therapeutic targets in acute myeloid leukaemia expressing the mutant RAS oncogene. *PhD Thesis, Cardiff University*.
Hopkins, G. L., Robinson, A. J., Hole, P. S., Darley, R. L. & Tonks, A. 2014. Analysis of ROS-Responsive Genes in Mutant RAS Expressing Hematopoietic Progenitors Identifies the Glycolytic Pathway As a Major Target Promoting Both Proliferation and Survival. *Blood,* 124, 2210.
Hsieh, A. L., Walton, Z. E., Altman, B. J., Stine, Z. E. & Dang, C. V. 2015. MYC and metabolism on the path to cancer. *Seminars in Cell & Developmental Biology,* 43, 11-21.
Hu, W. Q., Wang, X. X. & Yang, R. R. 2016. Evaluation of D-dimer and lactate dehydrogenase plasma levels in patients with relapsed acute leukemia. *Oncology Letters,* 12, 591-596.
Hu, Z.-Y., Xiao, L., Bode, A. M., Dong, Z. & Cao, Y. 2014. Glycolytic genes in cancer cells are more than glucose metabolic regulators. *Journal of Molecular Medicine-Jmm,* 92, 837-845.
Huang, H., Kim, H. J., Chang, E. J., Lee, Z. H., Hwang, S. J.*, et al.* 2009. IL-17 stimulates the proliferation and differentiation of human mesenchymal stem cells: implications for bone remodeling. *Cell Death and Differentiation,* 16, 1332-1343.
Huang, W. C., Chio, C. C., Chi, K. H., Wu, H. M. & Lin, W. W. 2002. Superoxide anion-dependent Raf/MEK/ERK activation by peroxisome proliferator activated receptor gamma agonists 15-deoxy-Delta(12,14)-prostaglandin J(2), ciglitazone, and GW1929. *Experimental Cell Research,* 277, 192-200.
Hunter, J. C., Manandhar, A., Carrasco, M. A., Gurbani, D., Gondi, S.*, et al.* 2015. Biochemical and Structural Analysis of Common Cancer-Associated KRAS Mutations. *Molecular Cancer Research,* 13, 1325-1335.
Ichikawa, M., Asai, T., Saito, T., Yamamoto, G., Seo, S.*, et al.* 2004. AML-1 is required for megakaryocytic maturation and lymphocytic differentiation, but not for maintenance of hematopoietic stem cells in adult hematopoiesis. *Nature Medicine,* 10, 299-304.
Igea, A. & Nebreda, A. R. 2015. The Stress Kinase p38 alpha as a Target for Cancer Therapy. *Cancer Research,* 75, 3997-4002.
Imbert-Fernandez, Y., Clem, B. F., O'neal, J., Kerr, D. A., Spaulding, R.*, et al.* 2014. Estradiol Stimulates Glucose Metabolism via 6-Phosphofructo-2-kinase (PFKFB3). *Journal of Biological Chemistry,* 289, 9440-9448.
Imperato, M. R., Cauchy, P., Obier, N. & Bonifer, C. 2015. The RUNX1-PU.1 axis in the control of hematopoiesis. *International Journal of Hematology,* 101, 319-329.
Ito, K., Hirao, A., Arai, F., Matsuoka, S., Takubo, K.*, et al.* 2004. Regulation of oxidative stress by ATM is required for self-renewal of haematopoietic stem cells. *Nature,* 431, 997-1002.
Iwasaki, H., Somoza, C., Shigematsu, H., Duprez, E. A., Iwasaki-Arai, J.*, et al.* 2005. Distinctive and indispensable roles of PU.1 in maintenance of hematopoietic stem cells and their differentiation. *Blood,* 106, 1590-1600.
Iyer, G. Y., Islam, M. F. & Quastel, J. H. 1961. Biochemical aspects of phagocytosis. *Nature,* 192, 535-&.

Jackson, M. D. & Denu, J. M. 2001. Molecular reactions of protein phosphatases - Insights from structure and chemistry. *Chemical Reviews,* 101, 2313-2340.
Jan, M., Snyder, T. M., Corces-Zimmerman, M. R., Vyas, P., Weissman, I. L.*, et al.* 2012. Clonal Evolution of Preleukemic Hematopoietic Stem Cells Precedes Human Acute Myeloid Leukemia. *Science Translational Medicine,* 4, DOI 10.1126/scitranslmed.3004315, e3004149ra3004118.
Jang, Y. Y. & Sharkis, S. J. 2007. A low level of reactive oxygen species selects for primitive hematopoietic stem cells that may reside in the low-oxygenic niche. *Blood,* 110, 3056-3063.
Jarvis, R. M., Hughes, S. M. & Ledgerwood, E. C. 2012. Peroxiredoxin 1 functions as a signal peroxidase to receive, transduce, and transmit peroxide signals in mammalian cells. *Free Radical Biology and Medicine,* 53, 1522-1530.
Jayavelu, A. K., Moloney, J. N., Bohmer, F. D. & Cotter, T. G. 2016a. NOX-driven ROS formation in cell transformation of FLT3-ITD-positive AML. *Experimental Hematology,* 44, 1113-1122.
Jayavelu, A. K., Muller, J. P., Bauer, R., Bohmer, S. A., Lassig, J.*, et al.* 2016b. NOX4-driven ROS formation mediates PTP inactivation and cell transformation in FLT3ITD-positive AML cells. *Leukemia,* 30, 473-483.
Jeffery, C. J., Bahnson, B. J., Chien, W., Ringe, D. & Petsko, A. 2000. Crystal structure of rabbit phosphoglucose isomerase, a glycolytic enzyme that moonlights as neuroleukin, autocrine motility factor, and differentiation mediator. *Biochemistry,* 39, 955-964.
Jen, K. Y. & Cheung, V. G. 2005. Identification of novel p53 target genes in ionizing radiation response. *Cancer Research,* 65, 7666-7673.
Ji, S. R., Zhang, B., Liu, J., Qin, Y., Liang, C.*, et al.* 2016. ALDOA functions as an oncogene in the highly metastatic pancreatic cancer. *Cancer Letters,* 374, 127-135.
Jiang, X. L., Sun, Q., Li, H., Li, K. & Ren, X. B. 2014. The role of phosphoglycerate mutase 1 in tumor aerobic glycolysis and its potential therapeutic implications. *International Journal of Cancer,* 135, 1991-1996.
Katagiri, M., Karasawa, H., Takagi, K., Nakayama, S., Yabuuchi, S.*, et al.* 2017. Hexokinase 2 in colorectal cancer: a potent prognostic factor associated with glycolysis, proliferation and migration. *Histology and Histopathology,* 32, 351-360.
Kawamoto, H., Ikawa, T., Masuda, K., Wada, H. & Katsura, Y. 2010. A map for lineage restriction of progenitors during hematopoiesis: the essence of the myeloid-based model. *Immunological Reviews,* 238, 23-36.
Kawamoto, H. & Katsura, Y. 2009. A new paradigm for hematopoietic cell lineages: revision of the classical concept of the myeloid-lymphoid dichotomy. *Trends in Immunology,* 30, 193-200.
Kawauchi, K., Araki, K., Tobiume, K. & Tanaka, N. 2008. P53 regulates glucose metabolism through an IKK-NF-kappa B pathway and inhibits cell transformation. *Nature Cell Biology,* 10, 611-618.
Kessler, R., Bleichert, F., Warnke, J. P. & Eschrich, K. 2008. 6-phosphofructo-2-kinase/fructose-2,6-bisphosphatase (PFKFB3) is up-regulated in high-grade astrocytomas. *Journal of Neuro-Oncology,* 86, 257-264.
Khatri, S., Yepiskoposyan, H., Gallo, C. A., Tandon, P. & Plas, D. R. 2010. FOXO3a Regulates Glycolysis via Transcriptional Control of Tumor Suppressor TSC1. *Journal of Biological Chemistry,* 285, 15960-15965.
Kim, A. D., Stachura, D. L. & Traver, D. 2014. Cell signaling pathways involved in hematopoietic stem cell specification. *Experimental Cell Research,* 329, 227-233.
Kim, H. M., Haraguchi, N., Ishii, H., Ohkuma, M., Okano, M.*, et al.* 2012. Increased CD13 Expression Reduces Reactive Oxygen Species, Promoting Survival of Liver

Cancer Stem Cells via an Epithelial-Mesenchymal Transition-like Phenomenon. *Annals of Surgical Oncology,* 19, S539-S548.
Kim, J. W., Tchernyshyov, I., Semenza, G. L. & Dang, C. V. 2006a. HIF-1-mediated expression of pyruvate dehydrogenase kinase: A metabolic switch required for cellular adaptation to hypoxia. *Cell Metabolism,* 3, 177-185.
Kim, S. G., Cavalier, M., El-Maghrabi, M. R. & Lee, Y. H. 2007. A direct substrate-substrate interaction found in the kinase domain of the bifunctional enzyme, 6-phosphofructo-2-kinase/fructose-2,6-bisphosphatase. *Journal of Molecular Biology,* 370, 14-26.
Kim, S. G., Manes, N. P., El-Maghrabi, M. R. & Lee, Y. H. 2006b. Crystal structure of the hypoxia-inducible form of 6-phosphofructo-2-kinase/fructose-2,6-bisphosphatase (PFKFB3) - A possible new target for cancer therapy. *Journal of Biological Chemistry,* 281, 2939-2944.
Kitagishi, Y. & Matsuda, S. 2013. Redox regulation of tumor suppressor PTEN in cancer and aging (Review). *International Journal of Molecular Medicine,* 31, 511-515.
Kizilkaya, H. & Reckzeh, K. 2016. Pharmaceutical targeting of pyruvate dehydrogenase kinases in t(8;21) acute myeloid leukemia. *Haematologica,* 101, 220-220.
Klarer, A. C., O'neal, J., Imbert-Fernandez, Y., Clem, A., Ellis, S. R*., et al.* 2014. Inhibition of 6-phosphofructo-2-kinase (PFKFB3) induces autophagy as a survival mechanism. *Cancer & metabolism,* 2, 2-2.
Kocabas, F., Xie, L., Xie, J. J., Yu, Z., Deberardinis, R. J*., et al.* 2015. Hypoxic metabolism in human hematopoietic stem cells. *Cell and Bioscience,* 5, DOI 10.1186/s13578-13015-10020-13573, e13539.
Kode, A., Mosialou, I., Manavalan, S. J., Rathinam, C. V., Friedman, R. A*., et al.* 2016. FoxO1-dependent induction of acute myeloid leukemia by osteoblasts in mice. *Leukemia,* 30, 1-13.
Kogan, S. C., Lagasse, E., Atwater, S., Bae, S. C., Weissman, I*., et al.* 1998. The PEBP2 beta MYH11 fusion created by Inv(16)(p13;q22) in myeloid leukemia impairs neutrophil maturation and contributes to granulocytic dysplasia. *Proceedings of the National Academy of Sciences of the United States of America,* 95, 11863-11868.
Kondo, M., Scherer, D. C., Miyamoto, T., King, A. G., Akashi, K*., et al.* 2000. Cell-fate conversion of lymphoid-committed progenitors by instructive actions of cytokines. *Nature,* 407, 383-386.
Kondo, M., Weissman, I. L. & Akashi, K. 1997. Identification of clonogenic common lymphoid progenitors in mouse bone marrow. *Cell,* 91, 661-672.
Kops, G., Dansen, T. B., Polderman, P. E., Saarloos, I., Wirtz, K. W. A*., et al.* 2002. Forkhead transcription factor FOXO3a protects quiescent cells from oxidative stress. *Nature,* 419, 316-321.
Koukourakis, M. I., Giatromanolaki, A., Simopoulos, C., Polychronidis, A. & Sivridis, E. 2005. Lactate dehydrogenase 5 (LDH5) relates to up-regulated hypoxia inducible factor pathway and metastasis in colorectal cancer. *Clinical & Experimental Metastasis,* 22, 25-30.
Koukourakis, M. I., Giatromanolaki, A., Sivridis, E., Bougioukas, G., Didilis, V*., et al.* 2003. Lactate dehydrogenase-5 (LDH-5) overexpression in non-small-cell lung cancer tissues is linked to tumour hypoxia, angiogenic factor production and poor prognosis. *British Journal of Cancer,* 89, 877-885.
Koukourakis, M. I., Giatromanolaki, A., Winter, S., Leek, R., Sivridis, E*., et al.* 2009. Lactate Dehydrogenase 5 Expression in Squamous Cell Head and Neck Cancer

Relates to Prognosis following Radical or Postoperative Radiotherapy. *Oncology,* 77, 285-292.
Kuiper, J. W. P., Sun, C. X., Magalhaes, M. a. O. & Glogauer, M. 2011. Rac regulates PtdInsP(3) signaling and the chemotactic compass through a redox-mediated feedback loop. *Blood,* 118, 6164-6171.
Kulisz, A., Chen, N. F., Chandel, N. S., Shao, Z. H. & Schumacker, P. T. 2002. Mitochondrial ROS initiate phosphorylation of p38 MAP kinase during hypoxia in cardiomyocytes. *American Journal of Physiology-Lung Cellular and Molecular Physiology,* 282, L1324-L1329.
Kumar, R., And Evans, Todd 2015. Haematopoiesis. *eLS. 1-11, doi: 10.1002/9780470015902.a0000518.pub4*.
Kwon, J., Lee, S. R., Yang, K. S., Ahn, Y., Kim, Y. J.*, et al.* 2004. Reversible oxidation and inactivation of the tumor suppressor PTEN in cells stimulated with peptide growth factors. *Proceedings of the National Academy of Sciences of the United States of America,* 101, 16419-16424.
Lagadinou, E. D., Sach, A., Callahan, K., Rossi, R. M., Neering, S. J.*, et al.* 2013. BCL-2 Inhibition Targets Oxidative Phosphorylation and Selectively Eradicates Quiescent Human Leukemia Stem Cells. *Cell Stem Cell,* 12, 329-341.
Landry, J. R., Kinston, S., Knezevic, K., De Bruijn, M., Wilson, N.*, et al.* 2008. Runx genes are direct targets of Scl/Tal1 in the yolk sac and fetal liver. *Blood,* 111, 3005-3014.
Lane, S. W. & Gilliland, D. G. 2010. Leukemia stem cells. *Seminars in Cancer Biology,* 20, 71-76.
Lapidot, T., Sirard, C., Vormoor, J., Murdoch, B., Hoang, T.*, et al.* 1994. A cell initiating human acute myeloid-leukemia after transplantation into scid mice. *Nature,* 367, 645-648.
Laslo, P., Spooner, C. J., Warmflash, A., Lancki, D. W., Lee, H. J.*, et al.* 2006. Multilineage transcriptional priming and determination of alternate hematopoietic cell fates. *Cell,* 126, 755-766.
Lee, M. N., Ha, S. H., Kim, J., Koh, A., Lee, C. S.*, et al.* 2009. Glycolytic Flux Signals to mTOR through Glyceraldehyde-3-Phosphate Dehydrogenase-Mediated Regulation of Rheb. *Molecular and Cellular Biology,* 29, 3991-4001.
Lee, Y. H., Li, Y., Uyeda, K. & Hasemann, C. A. 2003. Tissue-specific structure/function differentiation of the liver isoform of 6-phosphofructo-2-kinase/fructose-2,6-bisphosphatase. *Journal of Biological Chemistry,* 278, 523-530.
Leite, T. C., Da Silva, D., Coelho, R. G., Zancan, P. & Sola-Penna, M. 2007. Lactate favours the dissociation of skeletal muscle 6-phosphofructo-1-kinase tetramers down-regulating the enzyme and muscle glycolysis. *Biochemical Journal,* 408, 123-130.
Leslie, N. R., Bennett, D., Lindsay, Y. E., Stewart, H., Gray, A.*, et al.* 2003. Redox regulation of PI 3-kinase signalling via inactivation of PTEN. *Embo Journal,* 22, 5501-5510.
Li, C., Xiao, Z. Q., Chen, Z. C., Zhang, X. P., Li, J. L.*, et al.* 2006. Proteome analysis of human lung squamous carcinoma. *Proteomics,* 6, 547-558.
Li, H. & Jogl, G. 2009. Structural and Biochemical Studies of TIGAR (TP53-induced Glycolysis and Apoptosis Regulator). *Journal of Biological Chemistry,* 284, 1748-1754.
Li, H. M., Yang, J. G., Liu, Z. J., Wang, W. M., Yu, Z. L.*, et al.* 2017a. Blockage of glycolysis by targeting PFKFB3 suppresses tumor growth and metastasis in head and neck squamous cell carcinoma. *Journal of Experimental & Clinical Cancer Research,* 36, DOI 10.1186/s13046-13016-10481-13041, e13047.

Li, M., Jin, R., Wang, W. H., Zhang, T. Y., Sang, J.*, et al.* 2017b. STAT3 regulates glycolysis via targeting hexokinase 2 in hepatocellular carcinoma cells. *Oncotarget,* 8, 24777-24784.
Li, Q. G., Li, Y. Q., Xu, J. Y., Wang, S., Xu, Y.*, et al.* 2017c. Aldolase B Overexpression is Associated with Poor Prognosis and Promotes Tumor Progression by Epithelial-Mesenchymal Transition in Colorectal Adenocarcinoma. *Cellular Physiology and Biochemistry,* 42, 397-406.
Liaw, K. Y., Lee, P. H., Wu, F. C., Tsai, J. S. & Linshiau, S. Y. 1997. Zinc, copper, and superoxide dismutase in hepatocellular carcinoma. *American Journal of Gastroenterology,* 92, 2260-2263.
Liberti, M. V. & Locasale, J. W. 2016. The Warburg Effect: How Does it Benefit Cancer Cells? *Trends in Biochemical Sciences,* 41, 211-218.
Lim, J. H., Lee, E. S., You, H. J., Lee, J. W., Park, J. W.*, et al.* 2004. Ras-dependent induction of HIF-1a(785) via the Raf/MEK/ERK pathway: a novel mechanism of Ras-mediated tumor promotion. *Oncogene,* 23, 9427-9431.
Liu, C. C., Wang, H., Wang, J. H., Wang, L., Geng, Q. R.*, et al.* 2016. Serum neuron-specific enolase levels are upregulated in patients with acute lymphoblastic leukemia and are predictive of prognosis. *Oncotarget,* 7, 55181-55190.
Liu, G., Kelly, W. K., Wilding, G., Leopold, L., Brill, K.*, et al.* 2009. An Open-Label, Multicenter, Phase I/II Study of Single-Agent AT-101 in Men with Castrate-Resistant Prostate Cancer. *Clinical Cancer Research,* 15, 3172-3176.
Liu, T. & Yin, H. L. 2017. PDK1 promotes tumor cell proliferation and migration by enhancing the Warburg effect in non-small cell lung cancer. *Oncology Reports,* 37, 193-200.
Liu, X., Zheng, H., Yu, W. M., Cooper, T. M., Bunting, K. D.*, et al.* 2015. Maintenance of mouse hematopoietic stem cells ex vivo by reprogramming cellular metabolism. *Blood,* 125, 1562-1565.
Liu, Y., Cao, Y., Zhang, W., Bergmeier, S., Qian, Y.*, et al.* 2012. A Small-Molecule Inhibitor of Glucose Transporter 1 Downregulates Glycolysis, Induces Cell-Cycle Arrest, and Inhibits Cancer Cell Growth In Vitro and In Vivo. *Molecular Cancer Therapeutics,* 11, 1672-1682.
Lo, Y. Y. C. & Cruz, T. F. 1995. Involvement of reactive oxygen species in cytokine and growth-factor induction of c-fos expression in chondrocytes. *Journal of Biological Chemistry,* 270, 11727-11730.
Locasale, J. W., Grassian, A. R., Melman, T., Lyssiotis, C. A., Mattaini, K. R.*, et al.* 2011. Phosphoglycerate dehydrogenase diverts glycolytic flux and contributes to oncogenesis. *Nature Genetics,* 43, 869-U879.
Lochter, A., Galosy, S., Muschler, J., Freedman, N., Werb, Z.*, et al.* 1997. Matrix metalloproteinase stromelysin-1 triggers a cascade of molecular alterations that leads to stable epithelial-to-mesenchymal conversion and a premalignant phenotype in mammary epithelial cells. *Journal of Cell Biology,* 139, 1861-1872.
Loehr, J. A., Abo-Zahrah, R., Pal, R. & Rodney, G. G. 2015. Sphingomyelinase promotes oxidant production and skeletal muscle contractile dysfunction through activation of NADPH oxidase. *Frontiers in physiology,* 5, DOI 10.3389/fphys.2014.00530, e00530.
Lowenberg, B., Pabst, T., Vellenga, E., Van Putten, W., Schouten, H. C.*, et al.* 2011. Cytarabine Dose for Acute Myeloid Leukemia. *New England Journal of Medicine,* 364, 1027-1036.
Lu, C. W., Lin, S. C., Chien, C. W., Lee, C. T., Lin, B. W.*, et al.* 2011. Overexpression of Pyruvate Dehydrogenase Kinase 3 Increases Drug Resistance and Early Recurrence in Colon Cancer. *American Journal of Pathology,* 179, 1405-1414.

Lu, M., Ammar, D., Ives, H., Albrecht, F. & Gluck, S. L. 2007. Physical interaction between aldolase and vacuolar H+-ATPase is essential for the assembly and activity of the proton pump. *Journal of Biological Chemistry,* 282, 24495-24503.
Lu, X. & Kang, Y. 2010. Hypoxia and Hypoxia-Inducible Factors: Master Regulators of Metastasis. *Clinical Cancer Research,* 16, 5928-5935.
Ludin, A., Gur-Cohen, S., Golan, K., Kaufmann, K. B., Itkin, T.*, et al.* 2014. Reactive Oxygen Species Regulate Hematopoietic Stem Cell Self-Renewal, Migration and Development, As Well As Their Bone Marrow Microenvironment. *Antioxidants & Redox Signaling,* 21, 1605-1619.
Luis, T. C., Killmann, N. M. B. & Staal, F. J. T. 2012. Signal transduction pathways regulating hematopoietic stem cell biology: Introduction to a series of Spotlight Reviews. *Leukemia,* 26, 86-90.
Luo, W., Hu, H., Chang, R., Zhong, J., Knabel, M.*, et al.* 2011. Pyruvate Kinase M2 Is a PHD3-Stimulated Coactivator for Hypoxia-Inducible Factor 1. *Cell,* 145, 732-744.
Lyng, H., Brovig, R. S., Svendsrud, D. H., Holm, R., Kaalhus, O.*, et al.* 2006. Gene expressions and copy numbers associated with metastatic phenotypes of uterine cervical cancer. *Bmc Genomics,* 7, DOI 10.1186/1471-2164-1187-1268, e1268.
Ma, Y., Liu, Z., Hider, R. & Petrat, F. 2007. Determination of the Labile Iron Pool of Human Lymphocytes using the Fluorescent Probe, CP655. *Analytical Chemistry Insights,* 2, 61-67.
Magnani, F., Nenci, S., Fananas, E. M., Ceccon, M., Romero, E.*, et al.* 2017. Crystal structures and atomic model of NADPH oxidase. *Proceedings of the National Academy of Sciences of the United States of America,* 114, 6764-6769.
Manes, N. P. & El-Maghrabi, M. R. 2005. The kinase activity of human brain 6-phosphofructo-2-kinase/fructose-2,6-bisphosphatase is regulated via inhibition by phosphoenolpyruvate. *Archives of Biochemistry and Biophysics,* 438, 125-136.
Manevich, Y., Feinstein, S. I. & Fisher, A. B. 2004. Activation of the antioxidant enzyme 1-CYS peroxiredoxin requires glutathionylation mediated by heterodimerization with pi GST. *Proceedings of the National Academy of Sciences of the United States of America,* 101, 3780-3785.
Mansfield, K. D., Guzy, R. D., Pan, Y., Young, R. M., Cash, T. P.*, et al.* 2005. Mitochondrial dysfunction resulting from loss of cytochrome c impairs cellular oxygen sensing and hypoxic HIF-alpha activation. *Cell Metabolism,* 1, 393-399.
Marinho, H. S., Real, C., Cyrne, L., Soares, H. & Antunes, F. 2014. Hydrogen peroxide sensing, signaling and regulation of transcription factors. *Redox Biology,* 2, 535-562.
Marshall, C. J. 1995. Specificity of receptor tyrosine kinase signaling - transient versus sustained extracellular signal-regulated kinase activation. *Cell,* 80, 179-185.
Marsin, A. S., Bouzin, C., Bertrand, L. & Hue, L. 2002. The stimulation of glycolysis by hypoxia in activated monocytes is mediated by AMP-activated protein kinase and inducible 6-phosphofructo-2-kinase. *Journal of Biological Chemistry,* 277, 30778-30783.
Martelli, A. M., Evangelisti, C., Chiarini, F., Grimaldi, C., Cappellini, A.*, et al.* 2010. The emerging role of the phosphatidylinositol 3-kinase/Akt/mammalian target of rapamycin signaling network in normal myelopoiesis and leukemogenesis. *Biochimica Et Biophysica Acta-Molecular Cell Research,* 1803, 991-1002.
Masella, R., Di Benedetto, R., Vari, R., Filesi, C. & Giovannini, C. 2005. Novel mechanisms of natural antioxidant compounds in biological systems: Involvement of glutathione and glutathione-related enzymes. *Journal of Nutritional Biochemistry,* 16, 577-586.

Masson, N., Singleton, R. S., Sekirnik, R., Trudgian, D. C., Ambrose, L. J., *et al.* 2012. The FIH hydroxylase is a cellular peroxide sensor that modulates HIF transcriptional activity. *Embo Reports,* 13, 251-257.
Matoba, S., Kang, J. G., Patino, W. D., Wragg, A., Boehm, M., *et al.* 2006. p53 regulates mitochondrial respiration. *Science,* 312, 1650-1653.
Matsui, A., Ikeda, T., Enomoto, K., Hosoda, K., Nakashima, H., *et al.* 2000. Increased formation of oxidative DNA damage, 8-hydroxy-2 '-deoxyguanosine, in human breast cancer tissue and its relationship to GSTP1 and COMT genotypes. *Cancer Letters,* 151, 87-95.
Mattiucci, D., Maurizi, G., Izzi, V., Cenci, L., Ciarlantini, M., *et al.* 2018. Bone marrow adipocytes support hematopoietic stem cell survival. *Journal of Cellular Physiology,* 233, 1500-1511.
Mayers, J. R. & Vander Heiden, M. G. 2015. Famine versus feast: understanding the metabolism of tumors in vivo. *Trends in Biochemical Sciences,* 40, 130-140.
Mazurek, S. 2011. Pyruvate kinase type M2: A key regulator of the metabolic budget system in tumor cells. *International Journal of Biochemistry & Cell Biology,* 43, 969-980.
Mazurek, S., Zwerschke, W., Jansen-Durr, P. & Eigenbrodt, E. 2001. Metabolic cooperation between different oncogenes during cell transformation: interaction between activated ras and HPV-16 E7. *Oncogene,* 20, 6891-6898.
Mccleland, M. L., Adler, A. S., Deming, L., Cosino, E., Lee, L., *et al.* 2013. Lactate Dehydrogenase B Is Required for the Growth of KRAS-Dependent Lung Adenocarcinomas. *Clinical Cancer Research,* 19, 773-784.
Mccord, J. M. & Fridovic.I 1969. Superoxide dismutase an enzymic function for erythrocuprein (hemocuprein). *Journal of Biological Chemistry,* 244, 6049-&.
Mccrann, D. J., Eliades, A., Makitalo, M., Matsuno, K. & Ravid, K. 2009. Differential expression of NADPH oxidases in megakaryocytes and their role in polyploidy. *Blood,* 114, 1243-1249.
Mccubrey, J. A., Steelman, L. S., Bertrand, F. E., Davis, N. M., Abrams, S. L., *et al.* 2014. Multifaceted roles of GSK-3 and Wnt/beta-catenin in hematopoiesis and leukemogenesis: opportunities for therapeutic intervention. *Leukemia,* 28, 15-33.
Mccubrey, J. A., Steelman, L. S., Chappell, W. H., Abrams, S. L., Wong, E. W. T., *et al.* 2007. Roles of the Raf/MEK/ERK pathway in cell growth, malignant transformation and drug resistance. *Biochimica Et Biophysica Acta-Molecular Cell Research,* 1773, 1263-1284.
Mcculloch, D., Brown, C. & Iland, H. 2017. Retinoic acid and arsenic trioxide in the treatment of acute promyelocytic leukemia: current perspectives. *Oncotargets and Therapy,* 10, 1585-1601.
Medeiros, B. C., Lancet, J. E., Cortes, J. E., Newell, L. F., Lin, T. L., *et al.* 2016. Analysis of Efficacy By Age for Patients Aged 60-75 with Untreated Secondary Acute Myeloid Leukemia (AML) Treated with CPX-351 Liposome Injection Versus Conventional Cytarabine and Daunorubicin in a Phase III Trial. *Blood,* 128, e902.
Meister, A. & Anderson, M. E. 1983. Glutathione. *Annual Review of Biochemistry,* 52, 711-760.
Mendelson, A. & Frenette, P. S. 2014. Hematopoietic stem cell niche maintenance during homeostasis and regeneration. *Nature Medicine,* 20, 833-846.
Mendoza, E. E., Pocceschi, M. G., Kong, X. G., Leeper, D. B., Caro, J., *et al.* 2012. Control of Glycolytic Flux by AMP-Activated Protein Kinase in Tumor Cells Adapted to Low pH. *Translational Oncology,* 5, 208-216.
Metcalf, D. 2008. Hematopoietic cytokines. *Blood,* 111, 485-491.

Metcalf, D. & Burgess, A. W. 1982. Clonal analysis of progenitor-cell commitment to granulocyte or macrophage production. *Journal of Cellular Physiology,* 111, 275-283.
Miao, P., Sheng, S., Sun, X., Liu, J. & Huang, G. 2013. Lactate Dehydrogenase A in Cancer: A Promising Target for Diagnosis and Therapy. *Iubmb Life,* 65, 904-910.
Mikawa, T., Lleonart, M. E., Takaori-Kondo, A., Inagaki, N., Yokode, M.*, et al.* 2015. Dysregulated glycolysis as an oncogenic event. *Cellular and Molecular Life Sciences,* 72, 1881-1892.
Mikkola, H. K. A., Klintman, J., Yang, H. D., Hock, H., Schlaeger, T. M.*, et al.* 2003. Haematopoietic stem cells retain long-term repopulating activity and multipotency in the absence of stem-cell leukaemia SCL/tal-1 gene. *Nature,* 421, 547-551.
Miller, E. W., Dickinson, B. C. & Chang, C. J. 2010. Aquaporin-3 mediates hydrogen peroxide uptake to regulate downstream intracellular signaling. *Proceedings of the National Academy of Sciences of the United States of America,* 107, 15681-15686.
Minchenko, A., Leshchinsky, I., Opentanova, I., Sang, N. L., Srinivas, V.*, et al.* 2002. Hypoxia-inducible factor-1-mediated expression of the 6-phosphofructo-2-kinase/fructose-2,6-bisphosphatase-3 (PFKFB3) gene - Its possible role in the Warburg effect. *Journal of Biological Chemistry,* 277, 6183-6187.
Mitsuishi, Y., Taguchi, K., Kawatani, Y., Shibata, T., Nukiwa, T.*, et al.* 2012. Nrf2 Redirects Glucose and Glutamine into Anabolic Pathways in Metabolic Reprogramming. *Cancer Cell,* 22, 66-79.
Miyamoto, K., Araki, K. Y., Naka, K., Arai, F., Takubo, K.*, et al.* 2007. Foxo3a is essential for maintenance of the hematopoietic stem cell pool. *Cell Stem Cell,* 1, 101-112.
Mondal, S., Roy, D., Kalogera, E., Khurana, A., Tapolsky, G. H.*, et al.* 2015. Inhibition of PFKFB3/glycolysis overcomes chemoresistance in ovarian cancers. *Cancer Research,* 75, DOI 10.1158/1538-7445.am2015-2706.
Monteiro, G., Horta, B. B., Pimenta, D. C., Augusto, O. & Netto, L. E. S. 2007. Reduction of 1-Cys peroxiredoxins by ascorbate changes the thiol-specific antioxidant paradigm, revealing another function of vitamin C. *Proceedings of the National Academy of Sciences of the United States of America,* 104, 4886-4891.
Motohashi, H., Kimura, M., Fujita, R., Inoue, A., Pan, X. Q.*, et al.* 2010. NF-E2 domination over Nrf2 promotes ROS accumulation and megakaryocytic maturation. *Blood,* 115, 677-686.
Muller-Sieburg, C. E., Cho, R. H., Thoman, M., Adkins, B. & Sieburg, H. B. 2002. Deterministic regulation of hematopoietic stem cell self-renewal and differentiation. *Blood,* 100, 1302-1309.
Murphy, M. P. 2009. How mitochondria produce reactive oxygen species. *Biochemical Journal,* 417, 1-13.
Murrell, G. a. C., Francis, M. J. O. & Bromley, L. 1990. Modulation of fibroblast proliferation by oxygen free-radicals. *Biochemical Journal,* 265, 659-665.
Nacken, W., Manitz, M. P. & Sorg, C. 1996. Molecular characterisation of the genomic locus of the mouse MRP8 gene. *Biochimica Et Biophysica Acta-Molecular Basis of Disease,* 1315, 1-5.
Nakamura, H., Nakamura, K. & Yodoi, J. 1997. Redox regulation of cellular activation. *Annual Review of Immunology,* 15, 351-369.
Nanduri, J., Vaddi, D. R., Khan, S. A., Wang, N., Makarenko, V.*, et al.* 2015. HIF-1 alpha Activation by Intermittent Hypoxia Requires NADPH Oxidase Stimulation by Xanthine Oxidase. *Plos One,* 10.

Nanduri, J., Vaddi, D. R., Khan, S. A., Wang, N., Makerenko, V.*, et al.* 2013. Xanthine Oxidase Mediates Hypoxia-Inducible Factor-2 alpha Degradation by Intermittent Hypoxia. *Plos One,* 8, DOI 10.1371/journal.pone.0075838, e0075838.
Naoe, T. & Kiyoi, H. 2013. Gene mutations of acute myeloid leukemia in the genome era. *International Journal of Hematology,* 97, 165-174.
Navarro-Sabate, A., Manzano, A., Riera, L., Rosa, J. L., Ventura, F.*, et al.* 2001. The human ubiquitous 6-phosphofructo-2-kinase/fructose-2,6-bisphosphatase gene (PFKFB3): promoter characterization and genomic structure. *Gene,* 264, 131-138.
Nerlov, C. & Graf, T. 1998. PU.1 induces myeloid lineage commitment in multipotent hematopoietic progenitors. *Genes Dev,* 12, 2403-2412.
Newbold, R. F. & Overell, R. W. 1983. Fibroblast immortality is a prerequisite for transformation by ej c-ha-ras oncogene. *Nature,* 304, 648-651.
Newland, A. 2002. Progress in the treatment of acute myeloid leukaemia in adults. *International Journal of Hematology,* 76, 253-258.
Nie, Y. C., Han, Y. C. & Zou, Y. R. 2008. CXCR4 is required for the quiescence of primitive hematopoietic cells. *Journal of Experimental Medicine,* 205, 777-783.
Niecknig, H., Tug, S., Delos Reyes, B., Kirsch, M., Fandrey, J.*, et al.* 2012. Role of reactive oxygen species in the regulation of HIF-1 by prolyl hydroxylase 2 under mild hypoxia. *Free Radical Research,* 46, 705-717.
Nordberg, J. & Arner, E. S. J. 2001. Reactive oxygen species, antioxidants, and the mammalian thioredoxin system. *Free Radical Biology and Medicine,* 31, 1287-1312.
Notta, F., Doulatov, S., Laurenti, E., Poeppl, A., Jurisica, I.*, et al.* 2011. Isolation of Single Human Hematopoietic Stem Cells Capable of Long-Term Multilineage Engraftment. *Science,* 333, 218-221.
Novellasdemunt, L., Bultot, L., Manzano, A., Ventura, F., Rosa, J. L.*, et al.* 2013. PFKFB3 activation in cancer cells by the p38/MK2 pathway in response to stress stimuli. *Biochemical Journal,* 452, 531-543.
Novellasdemunt, L., Obach, M., Millan-Arino, L., Manzano, A., Ventura, F.*, et al.* 2012. Progestins activate 6-phosphofructo-2-kinase/fructose-2,6-bisphosphatase 3 (PFKFB3) in breast cancer cells. *Biochemical Journal,* 442, 345-356.
O'brien, J. J., Spinelli, S. L., Tober, J., Blumberg, N., Francis, C. W.*, et al.* 2008. 15-deoxy-Delta(12,14)-PGJ(2) enhances platelet production from megakaryocytes. *Blood,* 112, 4051-4060.
O'neal, J., Clem, A., Reynolds, L., Dougherty, S., Imbert-Fernandez, Y.*, et al.* 2016. Inhibition of 6-phosphofructo-2-kinase (PFKFB3) suppresses glucose metabolism and the growth of HER2+ breast cancer. *Breast Cancer Research and Treatment,* 160, 29-40.
Obach, M., Navarro-Sabate, A., Caro, J., Kong, X. G., Duran, J.*, et al.* 2004. 6-phosphofructo-2-kinase (pfkfb3) gene promoter contains hypoxia-inducible factor-1 binding sites necessary for transactivation in response to hypoxia. *Journal of Biological Chemistry,* 279, 53562-53570.
Obtulowicz, T., Swoboda, M., Speina, E., Gackowski, D., Rozalski, R.*, et al.* 2010. Oxidative stress and 8-oxoguanine repair are enhanced in colon adenoma and carcinoma patients. *Mutagenesis,* 25, 463-471.
Oburoglu, L., Romano, M., Taylor, N. & Kinet, S. 2016. Metabolic regulation of hematopoietic stem cell commitment and erythroid differentiation. *Current Opinion in Hematology,* 23, 198-205.
Omidvar, N., Kogan, S., Beurlet, S., Pogam, C. I., Janin, A.*, et al.* 2007. BCL-2 and mutant NRAS interact physically and functionally in a mouse model of progressive myelodysplasia. *Cancer Research,* 67, 11657-11667.

Oshikawa, J., Kim, S. J., Furuta, E., Caliceti, C., Chen, G. F.*, et al.* 2012. Novel role of p66Shc in ROS-dependent VEGF signaling and angiogenesis in endothelial cells. *American Journal of Physiology-Heart and Circulatory Physiology,* 302, H724-H732.
Pacold, M. E., Brimacombe, K. R., Chan, S. H., Rohde, J. M., Lewis, C. A.*, et al.* 2016. A PHGDH inhibitor reveals coordination of serine synthesis and one-carbon unit fate. *Nature Chemical Biology,* 12, 452-U118.
Pai, E. F., Kabsch, W., Krengel, U., Holmes, K. C., John, J.*, et al.* 1989. Structure of the guanine-nucleotide-binding domain of the ha-ras oncogene product p21 in the triphosphate conformation. *Nature,* 341, 209-214.
Paik, J. Y., Jung, K. H., Lee, J. H., Park, J. W. & Lee, K. H. 2017. Reactive oxygen species-driven HIFI alpha triggers accelerated glycolysis in endothelial cells exposed to low oxygen tension. *Nuclear Medicine and Biology,* 45, 8-14.
Pan, Y., Mansfield, K. D., Bertozzi, C. C., Rudenko, V., Chan, D. A.*, et al.* 2007. Multiple factors affecting cellular redox status and energy metabolism modulate hypoxia-inducible factor prolyl hydroxylase activity in vivo and in vitro. *Molecular and Cellular Biology,* 27, 912-925.
Panday, A., Sahoo, M. K., Osorio, D. & Batra, S. 2015. NADPH oxidases: an overview from structure to innate immunity-associated pathologies. *Cellular & Molecular Immunology,* 12, DOI 10.1038/cmi.2014.1089.
Parmar, K., Mauch, P., Vergilio, J. A., Sackstein, R. & Down, J. D. 2007. Distribution of hematopoietic stem cells in the bone marrow according to regional hypoxia. *Proceedings of the National Academy of Sciences of the United States of America,* 104, 5431-5436.
Patra, K. C. & Hay, N. 2014. The pentose phosphate pathway and cancer. *Trends in Biochemical Sciences,* 39, 347-354.
Pearn, L., Fisher, J., Burnett, A. K. & Darley, R. L. 2007. The role of PKC and PDK1 in monocyte lineage specification by Ras. *Blood,* 109, 4461-4469.
Peralta, D., Bronowska, A. K., Morgan, B., Doka, E., Van Laer, K.*, et al.* 2015. A proton relay enhances H2O2 sensitivity of GAPDH to facilitate metabolic adaptation. *Nature Chemical Biology,* 11, 156-U105.
Pilkis, S. J., Elmaghrabi, M. R., Pilkis, J., Claus, T. H. & Cumming, D. A. 1981. Fructose 2,6-bisphosphate - a new activator of phosphofructokinase. *Journal of Biological Chemistry,* 256, 3171-3174.
Polanski, R., Hodgkinson, C. L., Fusi, A., Nonaka, D., Priest, L.*, et al.* 2014. Activity of the Monocarboxylate Transporter 1 Inhibitor AZD3965 in Small Cell Lung Cancer. *Clinical Cancer Research,* 20, 926-937.
Polet, F., Corbet, C., Pinto, A., Rubio, L. I., Martherus, R.*, et al.* 2016. Reducing the serine availability complements the inhibition of the glutamine metabolism to block leukemia cell growth. *Oncotarget,* 7, 1765-1776.
Polyak, K., Xia, Y., Zweier, J. L., Kinzler, K. W. & Vogelstein, B. 1997. A model for p53-induced apoptosis. *Nature,* 389, 300-305.
Ponka, P. 1999. Cellular iron metabolism. *Kidney International,* 55, S2-S11.
Ponomaryov, T., Peled, A., Petit, I., Taichman, R. S., Habler, L.*, et al.* 2000. Induction of the chemokine stromal-derived factor-1 following DNA damage improves human stem cell function. *Journal of Clinical Investigation,* 106, 1331-1339.
Poprac, P., Jomova, K., Simunkova, M., Kollar, V., Rhodes, C. J.*, et al.* 2017. Targeting Free Radicals in Oxidative Stress-Related Human Diseases. *Trends in Pharmacological Sciences,* 38, 592-607.
Possemato, R., Marks, K. M., Shaul, Y. D., Pacold, M. E., Kim, D.*, et al.* 2011. Functional genomics reveal that the serine synthesis pathway is essential in breast cancer. *Nature,* 476, 346-U119.

Prata, C., Maraldi, T., Fiorentini, D., Zambonin, L., Hakim, G.*, et al.* 2008. Nox-generated ROS modulate glucose uptake in a leukaemic cell line. *Free Radical Research,* 42, 405-414.
Prior, I. A., Lewis, P. D. & Mattos, C. 2012. A Comprehensive Survey of Ras Mutations in Cancer. *Cancer Research,* 72, 2457-2467.
Protopopova, M., Bandi, M., Bardenhagen, J., Bristow, C., Carroll, C.*, et al.* 2015. IACS-10759: A novel OXPHOS inhibitor which selectively kill tumors with metabolic vulnerabilities. *Cancer Research,* 75, DOI 10.1158/1538-7445.am2015-4380.
Putker, M., Madl, T., Vos, H. R., De Ruiter, H., Visscher, M.*, et al.* 2013. Redox-Dependent Control of FOXO/DAF-16 by Transportin-1. *Molecular Cell,* 49, 730-742.
Pyo, C. W., Choi, J. H., Oh, S. M. & Choi, S. Y. 2013. Oxidative stress-induced cyclin D1 depletion and its role in cell cycle processing. *Biochimica Et Biophysica Acta-General Subjects,* 1830, 5316-5325.
Qian, S. X., Li, J. Y., Hong, M., Zhu, Y., Zhao, H. H.*, et al.* 2016. TIGAR cooperated with glycolysis to inhibit the apoptosis of leukemia cells and associated with poor prognosis in patients with cytogenetically normal acute myeloid leukemia. *Journal of Hematology & Oncology,* 9, DOI 10.1186/s13045-13016-10360-13044, e13128.
Racker, E., Resnick, R. J. & Feldman, R. 1985. Glycolysis and methylaminoisobutyrate uptake in rat-1 cells transfected with RAS or MYC oncongenes. *Proceedings of the National Academy of Sciences of the United States of America,* 82, 3535-3538.
Radisky, D. C., Levy, D. D., Littlepage, L. E., Liu, H., Nelson, C. M.*, et al.* 2005. Rac1b and reactive oxygen species mediate MMP-3-induced EMT and genomic instability. *Nature,* 436, 123-127.
Rae, T. D., Schmidt, P. J., Pufahl, R. A., Culotta, V. C. & O'halloran, T. V. 1999. Undetectable intracellular free copper: The requirement of a copper chaperone for superoxide dismutase. *Science,* 284, 805-808.
Rani, R. & Kumar, V. 2016. Recent Update on Human Lactate Dehydrogenase Enzyme 5 (hLDH5) Inhibitors: A Promising Approach for Cancer Chemotherapy. *Journal of Medicinal Chemistry,* 59, 487-496.
Reagan, M. R. & Rosen, C. J. 2016. Navigating the bone marrow niche: translational insights and cancer-driven dysfunction. *Nature Reviews Rheumatology,* 12, 154-168.
Reid, M. A., Lowman, X. H., Pan, M., Tran, T. Q., Warmoes, M. O.*, et al.* 2016. IKK beta promotes metabolic adaptation to glutamine deprivation via phosphorylation and inhibition of PFKFB3. *Genes Dev,* 30, 1837-1851.
Renneville, A., Roumier, C., Biggio, V., Nibourel, O., Boissel, N.*, et al.* 2008. Cooperating gene mutations in acute myeloid leukemia: a review of the literature. *Leukemia,* 22, 915-931.
Rhee, S. G., Chae, H. Z. & Kim, K. 2005. Peroxiredoxins: A historical overview and speculative preview of novel mechanisms and emerging concepts in cell signaling. *Free Radical Biology and Medicine,* 38, 1543-1552.
Rhyu, D. Y., Yang, Y. Q., Ha, H. J., Lee, G. T., Song, J. S.*, et al.* 2005. Role of reactive oxygen species in TGF-beta 1-induced mitogen-activated protein kinase activation and epithelial-mesenchymal transition in renal tubular epithelial cells. *Journal of the American Society of Nephrology,* 16, 667-675.
Rieger, M. A., Hoppe, P. S., Smejkal, B. M., Eitelhuber, A. C. & Schroeder, T. 2009. Hematopoietic Cytokines Can Instruct Lineage Choice. *Science,* 325, 217-218.
Rieger, M. A. & Schroeder, T. 2012. Hematopoiesis. *Cold Spring Harbor Perspectives in Biology,* 4, DOI 10.1101/cshperspect.a008250, a008250.

Riganti, C., Gazzano, E., Polimeni, M., Costamagna, C., Bosia, A*., et al.* 2004. Diphenyleneiodonium inhibits the cell redox metabolism and induces oxidative stress. *Journal of Biological Chemistry,* 279, 47726-47731.
Robb, L. 2007. Cytokine receptors and hematopoietic differentiation. *Oncogene,* 26, 6715-6723.
Ros, S. & Schulze, A. 2013. Balancing glycolytic flux: the role of 6-phosphofructo-2-kinase/fructose 2,6-bisphosphatases in cancer metabolism. *Cancer & metabolism,* 1, 8-8.
Rosenbauer, F. & Tenen, D. G. 2007. Transcription factors in myeloid development: balancing differentiation with transformation. *Nat Rev Immunol,* 7, 105-117.
Rouault-Pierre, K., Lopez-Onieva, L., Foster, K., Anjos-Afonso, F., Lamrissi-Garcia, I*., et al.* 2013. HIF-2 alpha Protects Human Hematopoietic Stem/Progenitors and Acute Myeloid Leukemic Cells from Apoptosis Induced by Endoplasmic Reticulum Stress. *Cell Stem Cell,* 13, 549-563.
Roy, K., Wu, Y., Meitzler, J. L., Juhasz, A., Liu, H*., et al.* 2015. NADPH oxidases and cancer. *Clinical Science,* 128, 863-875.
Rushworth, S. A., Bowles, K. M., Raninga, P. & Macewan, D. J. 2010. NF-kB-Inhibited Acute Myeloid Leukemia Cells Are Rescued from Apoptosis by Heme Oxygenase-1 Induction. *Cancer Research,* 70, 2973-2983.
Rushworth, S. A., Macewan, D. J. & O'connell, M. A. 2008. Lipopolysaccharide-Induced Expression of NAD(P)H:Quinone Oxidoreductase 1 and Heme Oxygenase-1 Protects against Excessive Inflammatory Responses in Human Monocytes. *Journal of Immunology,* 181, 6730-6737.
Rushworth, S. A., Zaitseva, L., Murray, M. Y., Shah, N. M., Bowles, K. M*., et al.* 2012. The high Nrf2 expression in human acute myeloid leukemia is driven by NF-kappa B and underlies its chemo-resistance. *Blood,* 120, 5188-5198.
Ryland, L. K., Doshi, U. A., Shanmugavelandy, S. S., Fox, T. E., Aliaga, C*., et al.* 2013. C6-Ceramide Nanoliposomes Target the Warburg Effect in Chronic Lymphocytic Leukemia. *Plos One,* 8, DOI 10.1371/journal.pone.0084648, e0084648.
Sabharwal, S. S. & Schumacker, P. T. 2014. Mitochondrial ROS in cancer: initiators, amplifiers or an Achilles' heel? *Nature Reviews Cancer,* 14, 709-721.
Sablina, A. A., Budanov, A. V., Ilyinskaya, G. V., Agapova, L. S., Kravchenko, J. E*., et al.* 2005. The antioxidant function of the p53 tumor suppressor. *Nature Medicine,* 11, 1306-1313.
Sallmyr, A., Fan, J., Datta, K., Kim, K. T., Grosu, D*., et al.* 2008. Internal tandem duplication of FLT3 (FLT3/ITD) induces increased ROS production, DNA damage, and misrepair: implications for poor prognosis in AML. *Blood,* 111, 3173-3182.
Samland, A. K. & Sprenger, G. A. 2009. Transaldolase: From biochemistry to human disease. *International Journal of Biochemistry & Cell Biology,* 41, 1482-1494.
San-Millan, I. & Brooks, G. A. 2017. Reexamining cancer metabolism: lactate production for carcinogenesis could be the purpose and explanation of the Warburg Effect. *Carcinogenesis,* 38, 119-133.
Sanjuan-Pla, A., Macaulay, I. C., Jensen, C. T., Woll, P. S., Luis, T. C*., et al.* 2013. Platelet-biased stem cells reside at the apex of the haematopoietic stem-cell hierarchy. *Nature,* 502, 232-236.
Sardina, J. L., Lopez-Ruano, G., Sanchez-Abarca, L. I., Perez-Simon, J. A., Gaztelumendi, A*., et al.* 2010. p22(phox)-dependent NADPH oxidase activity is required for megakaryocytic differentiation. *Cell Death and Differentiation,* 17, 1842-1854.

Sardina, J. L., Lopez-Ruano, G., Sanchez-Sanchez, B., Llanillo, M. & Hernandez-Hernandez, A. 2012. Reactive oxygen species: Are they important for haematopoiesis? *Critical Reviews in Oncology Hematology,* 81, 257-274.
Sattler, M., Winkler, T., Verma, S., Byrne, C. H., Shrikhande, G.*, et al.* 1999. Hematopoietic growth factors signal through the formation of reactive oxygen species. *Blood,* 93, 2928-2935.
Savitsky, P. A. & Finkel, T. 2002. Redox regulation of Cdc25C. *Journal of Biological Chemistry,* 277, 20535-20540.
Saygin, C. & Carraway, H. E. 2017. Emerging therapies for acute myeloid leukemia. *Journal of Hematology & Oncology,* 10, DOI 10.1186/s13045-13017-10463-13046, e13093.
Schneider, J., Neu, K., Grimm, H., Velcovsky, H. G., Weisse, G.*, et al.* 2002. Tumor M2-pyruvate kinase in lung cancer patients: Immunohistochemical detection and disease monitoring. *Anticancer Research,* 22, 311-318.
Schofield, R. 1978. Relationship between spleen colony-forming cell and hematopoietic stem-cell - hypothesis. *Blood Cells,* 4, 7-25.
Schutte, J., Viallet, J., Nau, M., Segal, S., Fedorko, J.*, et al.* 1989. Jun-b inhibits and c-fos stimulates the transforming and trans-activating activities of c-jun. *Cell,* 59, 987-997.
Scialo, F., Fernandez-Ayala, D. J. & Sanz, A. 2017. Role of Mitochondrial Reverse Electron Transport in ROS Signaling: Potential Roles in Health and Disease. *Frontiers in physiology,* 8, DOI 10.3389/fphys.2017.00428, e00428.
Segal, A. W., Webster, D., Jones, O. T. G. & Allison, A. C. 1978. Absence of a newly described cytochrome-b from neutrophils of patients with chronic granulomatous disease. *Lancet,* 2, 446-449.
Semenza, G. L. 2010a. Defining the role of hypoxia-inducible factor 1 in cancer biology and therapeutics. *Oncogene,* 29, 625-634.
Semenza, G. L. 2010b. HIF-1: upstream and downstream of cancer metabolism. *Curr Opin Genet Dev,* 20, 51-56.
Semenza, G. L. 2012. Hypoxia-Inducible Factors in Physiology and Medicine. *Cell,* 148, 399-408.
Sengsuk, C., Tangvarasittichai, O., Chantanaskulwong, P., Pimanprom, A., Wantaneeyawong, S.*, et al.* 2014. Association of Iron Overload with Oxidative Stress, Hepatic Damage and Dyslipidemia in Transfusion-Dependent β-Thalassemia/HbE Patients. *Indian Journal of Clinical Biochemistry,* 29, 298-305.
Seo, M. & Lee, Y.-H. 2014. PFKFB3 Regulates Oxidative Stress Homeostasis via Its S-Glutathionylation in Cancer. *Journal of Molecular Biology,* 426, 830-842.
Serrano, M., Lin, A. W., Mccurrach, M. E., Beach, D. & Lowe, S. W. 1997. Oncogenic ras provokes premature cell senescence associated with accumulation of p53 and p16(INK4a). *Cell,* 88, 593-602.
Shaulian, E. & Karin, M. 2002. AP-1 as a regulator of cell life and death. *Nature Cell Biology,* 4, E131-E136.
Shi, Q. H., Gao, S., Song, L. N., Zhao, Y. M., Li, X. O.*, et al.* 2015. Comparative proteomics analysis of differential proteins in respond to doxorubicin resistance in myelogenous leukemia cell lines. *Proteome Science,* 13, DOI 10.1186/s12953-12014-10057-y, e12951.
Shinohara, A., Imai, Y., Nakagawa, M., Takahashi, T., Ichikawa, M.*, et al.* 2014. Intracellular Reactive Oxygen Species Mark and Influence the Megakaryocyte-Erythrocyte Progenitor Fate of Common Myeloid Progenitors. *Stem Cells,* 32, 548-557.

Shlush, L. I., Zandi, S., Mitchell, A., Chen, W. C., Brandwein, J. M*., et al.* 2014. Identification of pre-leukaemic haematopoietic stem cells in acute leukaemia. *Nature,* 506, 328-333.
Siegel, R. L., Miller, K. D. & Jemal, A. 2016. Cancer Statistics, 2016. *Ca-a Cancer Journal for Clinicians,* 66, 7-30.
Sies, H. 1993. Strategies of antioxidant defense. *European Journal of Biochemistry,* 215, 213-219.
Simanshu, D. K., Nissley, D. V. & Mccormick, F. 2017. RAS Proteins and Their Regulators in Human Disease. *Cell,* 170, 17-33.
Simon-Molas, H., Calvo-Vidal, M. N., Castano, E., Rodriguez-Garcia, A., Navarro-Sabate, A*., et al.* 2016. Akt mediates TIGAR induction in HeLa cells following PFKFB3 inhibition. *Febs Letters,* 590, 2915-2926.
Simsek, T., Kocabas, F., Zheng, J., Deberardinis, R. J., Mahmoud, A. I*., et al.* 2010. The Distinct Metabolic Profile of Hematopoietic Stem Cells Reflects Their Location in a Hypoxic Niche. *Cell Stem Cell,* 7, 380-390.
Sohn, J. & Rudolph, J. 2003. Catalytic and chemical competence of regulation of Cdc25 phosphatase by oxidation/reduction. *Biochemistry,* 42, 10060-10070.
Song, C., Hu, C. D., Masago, M., Kariya, K., Yamawaki-Kataoka, Y*., et al.* 2001. Regulation of a novel human phospholipase C, PLC epsilon, through membrane targeting by Ras. *Journal of Biological Chemistry,* 276, 2752-2757.
Song, K., Li, M., Xu, X. J., Xuan, L., Huang, G. N*., et al.* 2016. Resistance to chemotherapy is associated with altered glucose metabolism in acute myeloid leukemia. *Oncology Letters,* 12, 334-342.
Song, K., Li, M., Xu, X. J., Xuan, L., Huang, G. N*., et al.* 2014. HIF-1 alpha and GLUT1 Gene Expression is Associated with Chemoresistance of Acute Myeloid Leukemia. *Asian Pacific Journal of Cancer Prevention,* 15, 1823-1829.
Sosa, V., Moline, T., Somoza, R., Paciucci, R., Kondoh, H*., et al.* 2013. Oxidative stress and cancer: An overview. *Ageing Research Reviews,* 12, 376-390.
Spencer, J. A., Ferraro, F., Roussakis, E., Klein, A., Wu, J*., et al.* 2014. Direct measurement of local oxygen concentration in the bone marrow of live animals. *Nature,* 508, 269-+.
Stanicka, J., Russell, E. G., Woolley, J. F. & Cotter, T. G. 2015. NADPH Oxidase-generated Hydrogen Peroxide Induces DNA Damage in Mutant FLT3-expressing Leukemia Cells. *Journal of Biological Chemistry,* 290, 9348-9361.
Sturgill, E. M. & Guzman, M. L. 2014. The M2 isoform of pyruvate kinase (PKM2) contributes to leukemia stem cell persistence by maintaining oxidative homeostasis and promoting glycolysis. *Cancer Research,* 74, DOI 10.1158/1538-7445.am2014-4793.
Sugiyama, T., Kohara, H., Noda, M. & Nagasawa, T. 2006. Maintenance of the hematopoietic stem cell pool by CXCL12-CXCR4 chemokine signaling in bone marrow stromal cell niches. *Immunity,* 25, 977-988.
Suh, Y. A., Arnold, R. S., Lassegue, B., Shi, J., Xu, X. X*., et al.* 1999. Cell transformation by the superoxide-generating oxidase Mox1. *Nature,* 401, 79-82.
Sun, R. C., Fadia, M., Dahlstrom, J. E., Parish, C. R., Board, P. G*., et al.* 2010. Reversal of the glycolytic phenotype by dichloroacetate inhibits metastatic breast cancer cell growth in vitro and in vivo. *Breast Cancer Research and Treatment,* 120, 253-260.
Sun, S., Liang, X., Zhang, X., Liu, T., Shi, Q*., et al.* 2015. Phosphoglycerate kinase-1 is a predictor of poor survival and a novel prognostic biomarker of chemoresistance to paclitaxel treatment in breast cancer. *British Journal of Cancer,* 112, 1332-1339.

Sundaresan, M., Yu, Z. X., Ferrans, V. J., Irani, K. & Finkel, T. 1995. Requirement for generation of h2o2 for platelet-derived growth-factor signal-transduction. *Science,* 270, 296-299.

Suresh, S. & Irvine, A. E. 2015. The NOTCH signaling pathway in normal and malignant blood cell production. *Journal of Cell Communication and Signaling,* 9, 5-13.

Swerdlow, S. H., Campo, E., Pileri, S. A., Harris, N. L., Stein, H.*, et al.* 2016. The 2016 revision of the World Health Organization classification of lymphoid neoplasms. *Blood,* 127, 2375-2390.

Sykes, S. M., Lane, S. W., Bullinger, L., Kalaitzidis, D., Yusuf, R.*, et al.* 2011. AKT/FOXO Signaling Enforces Reversible Differentiation Blockade in Myeloid Leukemias. *Cell,* 146, 697-708.

Szatrowski, T. P. & Nathan, C. F. 1991. Production of large amounts of hydrogen-peroxide by human tumor-cells. *Cancer Research,* 51, 794-798.

Taguchi, K. & Yamamoto, M. 2017. The KeAP1-NRF2 System in Cancer. *Frontiers in Oncology,* 7, DOI 10.3389/fonc.2017.00085, e00085.

Tak, T., Tesselaar, K., Pillay, J., Borghans, J. a. M. & Koenderman, L. 2013. What's your age again? Determination of human neutrophil half-lives revisited. *J Leukoc Biol,* 94, 595-601.

Takashima, A. & Faller, D. V. 2013. Targeting the RAS oncogene. *Expert Opinion on Therapeutic Targets,* 17, 507-531.

Takubo, K., Goda, N., Yamada, W., Iriuchishima, H., Ikeda, E.*, et al.* 2010. Regulation of the HIF-1 alpha Level Is Essential for Hematopoietic Stem Cells. *Cell Stem Cell,* 7, 391-402.

Tamada, M., Suematsu, M. & Saya, H. 2012. Pyruvate Kinase M2: Multiple Faces for Conferring Benefits on Cancer Cells. *Clinical Cancer Research,* 18, 5554-5561.

Tamamyan, G., Kadia, T., Ravandi, F., Borthakur, G., Cortes, J.*, et al.* 2017. Frontline treatment of acute myeloid leukemia in adults. *Critical Reviews in Oncology Hematology,* 110, 20-34.

Tamura, T., Nagamura-Inoue, T., Shmeltzer, Z., Kuwata, T. & Ozato, K. 2000. ICSBP directs bipotential myeloid progenitor cells to differentiate into mature macrophages. *Immunity,* 13, 155-165.

Tang, Y., Zhang, G. J., Baird, M., Racke, F. & Zhao, W. Q. 2014. A Novel Role of CYP2E1 in Human Megakaryocyte Development. *In Vivo,* 28, 1077-1084.

Tao, X. X., Chen, B. & Yan, Y. F. 2017. Correlation between aldolase c (ALDOC) expression and the prognosis of esophageal cancer. *International Journal of Clinical and Experimental Pathology,* 10, 2036-2041.

Tarasova, A., Haylock, D. & Winkler, D. 2011. Principal signalling complexes in haematopoiesis: Structural aspects and mimetic discovery. *Cytokine & Growth Factor Reviews,* 22, 231-253.

Telang, S., O'neal, J., Imbert-Fernandez, Y., Clem, B., Lypova, N.*, et al.* 2015. 6-Phosphofructo-2-Kinase (PFKFB3): At the crossroads of resistance to targeted cancer therapies. *Cancer Research,* 75, DOI 10.1158/1538-7445.am2015-4478.

Telang, S., Yalcin, A., Clem, A. L., Bucala, R., Lane, A. N.*, et al.* 2006. Ras transformation requires metabolic control by 6-phosphofructo-2-kinase. *Oncogene,* 25, 7225-7234.

Tothova, Z. & Gilliland, D. G. 2007. FoxO transcription factors and stem cell homeostasis: Insights from the hematopoietic system. *Cell Stem Cell,* 1, 140-152.

Tothova, Z., Kollipara, R., Huntly, B. J., Lee, B. H., Castrillon, D. H.*, et al.* 2007. FoxOs are critical mediators of hematopoietic stem cell resistance to physiologic oxidative stress. *Cell,* 128, 325-339.

Tsouko, E., Khan, A. S., White, M. A., Han, J. J., Shi, Y., *et al.* 2014. Regulation of the pentose phosphate pathway by an androgen receptor-mTOR-mediated mechanism and its role in prostate cancer cell growth. *Oncogenesis,* 3, DOI 10.1038/oncsis.2014.1018, e1103.

Tsutsumi, S., Fukasawa, T., Yamauchi, H., Kato, T., Kigure, W., *et al.* 2009. Phosphoglucose isomerase enhances colorectal cancer metastasis. *International Journal of Oncology,* 35, 1117-1121.

Undi, R. B., Gutti, U., Sahu, I., Sarvothaman, S., Pasupuleti, S. R., *et al.* 2016. Wnt Signaling: Role in Regulation of Haematopoiesis. *Indian Journal of Hematology and Blood Transfusion,* 32, 123-134.

Ushio-Fukai, M., Alexander, R. W., Akers, M., Yin, Q. Q., Fujio, Y., *et al.* 1999. Reactive oxygen species mediate the activation of Akt/protein kinase B by angiotensin II in vascular smooth muscle cells. *Journal of Biological Chemistry,* 274, 22699-22704.

Valgimigli, M., Valgimigli, L., Trere, D., Gaiani, S., Pedulli, G. F., *et al.* 2002. Oxidative stress EPR measurement in human liver by radical-probe technique. Correlation with etiology, histology and cell proliferation. *Free Radical Research,* 36, 939-948.

Valko, M., Leibfritz, D., Moncol, J., Cronin, M. T. D., Mazur, M., *et al.* 2007. Free radicals and antioxidants in normal physiological functions and human disease. *International Journal of Biochemistry & Cell Biology,* 39, 44-84.

Valko, M., Rhodes, C. J., Moncol, J., Izakovic, M. & Mazur, M. 2006. Free radicals, metals and antioxidants in oxidative stress-induced cancer. *Chemico-Biological Interactions,* 160, 1-40.

Van Remmen, H., Ikeno, Y., Hamilton, M., Pahlavani, M., Wolf, N., *et al.* 2003. Life-long reduction in MnSOD activity results in increased DNA damage and higher incidence of cancer but does not accelerate aging. *Physiological Genomics,* 16, 29-37.

Vardiman, J. W., Thiele, J., Arber, D. A., Brunning, R. D., Borowitz, M. J., *et al.* 2009. The 2008 revision of the World Health Organization (WHO) classification of myeloid neoplasms and acute leukemia: rationale and important changes. *Blood,* 114, 937-951.

Velasco-Hernandez, T., Hyrenius-Wittsten, A., Rehn, M., Bryder, D. & Cammenga, J. 2014. HIF-1 alpha can act as a tumor suppressor gene in murine acute myeloid leukemia. *Blood,* 124, 3597-3607.

Velten, L., Haas, S. F., Raffel, S., Blaszkiewicz, S., Islam, S., *et al.* 2017. Human haematopoietic stem cell lineage commitment is a continuous process. *Nature Cell Biology,* 19, 271-281.

Vivanco, I. & Sawyers, C. L. 2002. The phosphatidylinositol 3-kinase-AKT pathway in human cancer. *Nature Reviews Cancer,* 2, 489-501.

Vogel, C. & Marcotte, E. M. 2012. Insights into the regulation of protein abundance from proteomic and transcriptomic analyses. *Nature Reviews Genetics,* 13, 227-232.

Vrhovac, I., Breljak, D. & Sabolic, I. 2014. Glucose transporters in the mammalian blood cells. *Periodicum Biologorum,* 116, 131-138.

Vukovic, M., Guitart, A. V., Sepulveda, C., Villacreces, A., O'duibhir, E., *et al.* 2015. Hif-1 alpha and Hif-2 alpha synergize to suppress AML development but are dispensable for disease maintenance. *Journal of Experimental Medicine,* 212, 2223-2234.

Vurusaner, B., Poli, G. & Basaga, H. 2012. Tumor suppressor genes and ROS: complex networks of interactions. *Free Radical Biology and Medicine,* 52, 7-18.

Wagner, E. F. & Nebreda, A. R. 2009. Signal integration by JNK and p38 MAPK pathways in cancer development. *Nature Reviews Cancer,* 9, 537-549.
Wallace, D. C. 2012. Mitochondria and cancer. *Nature Reviews Cancer,* 12, 685-698.
Wang, J. H., Chen, W. L., Li, J. M., Wu, S. F., Chen, T. L.*, et al.* 2013. Prognostic significance of 2-hydroxyglutarate levels in acute myeloid leukemia in China. *Proceedings of the National Academy of Sciences of the United States of America,* 110, 17017-17022.
Wang, L. D. & Wagers, A. J. 2011. Dynamic niches in the origination and differentiation of haematopoietic stem cells. *Nature Reviews Molecular Cell Biology,* 12, 643-655.
Wang, P., Sun, C., Zhu, T. T. & Xu, Y. H. 2015. Structural insight into mechanisms for dynamic regulation of PKM2. *Protein & Cell,* 6, 275-287.
Wang, X. F., Huang, S. L. & Chen, J. L. 2017. Understanding of leukemic stem cells and their clinical implications. *Molecular Cancer,* 16, DOI 10.1186/s12943-12016-10574-12947, e12942.
Wang, Y., Liu, Y., Malek, S. N. & Zheng, P. 2011. Targeting HIF1 alpha Eliminates Cancer Stem Cells in Hematological Malignancies. *Cell Stem Cell,* 8, 399-411.
Wang, Y., Liu, Y., Tang, F., Bernot, K. M., Schore, R.*, et al.* 2014. Echinomycin protects mice against relapsed acute myeloid leukemia without adverse effect on hematopoietic stem cells. *Blood,* 124, 1127-1135.
Wanka, C., Steinbach, J. P. & Rieger, J. 2012. Tp53-induced Glycolysis and Apoptosis Regulator (TIGAR) Protects Glioma Cells from Starvation-induced Cell Death by Up-regulating Respiration and Improving Cellular Redox Homeostasis. *Journal of Biological Chemistry,* 287, 33436-33446.
Warburg, O. 1956. Origin of cancer cells. *Science,* 123, 309-314.
Weinberg, F., Hamanaka, R., Wheaton, W. W., Weinberg, S., Joseph, J.*, et al.* 2010. Mitochondrial metabolism and ROS generation are essential for Kras-mediated tumorigenicity. *Proceedings of the National Academy of Sciences of the United States of America,* 107, 8788-8793.
Weitzman, S. A., Weitberg, A. B., Clark, E. P. & Stossel, T. P. 1985. Phagocytes as carcinogens - malignant transformation produced by human-neutrophils. *Science,* 227, 1231-1233.
Welch, J. S., Ley, T. J., Link, D. C., Miller, C. A., Larson, D. E.*, et al.* 2012. The Origin and Evolution of Mutations in Acute Myeloid Leukemia. *Cell,* 150, 264-278.
Wennerberg, K., Rossman, K. L. & Der, C. J. 2005. The Ras superfamily at a glance. *Journal of Cell Science,* 118, 843-846.
Wientjes, F. B., Hsuan, J. J., Totty, N. F. & Segal, A. W. 1993. P40(phox), a 3rd cytosolic component of the activation complex of the nadph oxidase to contain src homology 3 domains. *Biochemical Journal,* 296, 557-561.
Wilson, J. E. 2003. Isozymes of mammalian hexokinase: structure, subcellular localization and metabolic function. *Journal of Experimental Biology,* 206, 2049-2057.
Winkler, I. G., Barbier, V., Wadley, R., Zannettino, A. C. W., Williams, S.*, et al.* 2010. Positioning of bone marrow hematopoietic and stromal cells relative to blood flow in vivo: serially reconstituting hematopoietic stem cells reside in distinct nonperfused niches. *Blood,* 116, 375-385.
Wojcik, I., Szybka, M., Golanska, E., Rieske, P., Blonski, J. Z.*, et al.* 2005. Abnormalities of the P53, MDM2, BCL2 and BAX genes in acute leukemias. *Neoplasma,* 52, 318-324.

Wolf, A., Agnihotri, S., Micallef, J., Mukherjee, J., Sabha, N., *et al.* 2011. Hexokinase 2 is a key mediator of aerobic glycolysis and promotes tumor growth in human glioblastoma multiforme. *Journal of Experimental Medicine,* 208, 313-326.
Wolff, L. & Humeniuk, R. 2013. Concise Review: Erythroid Versus Myeloid Lineage Commitment: Regulating the Master Regulators. *Stem Cells,* 31, 1237-1244.
Won, K. Y., Lim, S. J., Kim, G. Y., Kim, Y. W., Han, S. A., *et al.* 2012. Regulatory role of p53 in cancer metabolism via SCO2 and TIGAR in human breast cancer. *Human Pathology,* 43, 221-228.
Wong, J. Y. Y., Huggins, G. S., Debidda, M., Munshi, N. C. & De Vivo, I. 2008. Dichloroacetate induces apoptosis in endometrial cancer cells. *Gynecologic Oncology,* 109, 394-402.
Wong, N., De Melo, J. & Tang, D. 2013. PKM2, a Central Point of Regulation in Cancer Metabolism. *International journal of cell biology,* 2013, 242513-242513.
Woo, H. A., Yim, S. H., Shin, D. H., Kang, D., Yu, D. Y., *et al.* 2010. Inactivation of Peroxiredoxin I by Phosphorylation Allows Localized H2O2 Accumulation for Cell Signaling. *Cell,* 140, 517-528.
Woolthuis, C. M. & Park, C. Y. 2016. Hematopoietic stem/progenitor cell commitment to the megakaryocyte lineage. *Blood,* 127, 1242-1248.
Wright, C., Iyer, A. K. V., Kaushik, V. & Azad, N. 2017. Anti-Tumorigenic Potential of a Novel Orlistat-AICAR Combination in Prostate Cancer Cells. *Journal of Cellular Biochemistry,* 118, 3834-3845.
Wu, J. Y., Hu, L. R., Wu, F. P., Zou, L. & He, T. P. 2017. Poor prognosis of hexokinase 2 overexpression in solid tumors of digestive system: a meta-analysis. *Oncotarget,* 8, 32332-32344.
Xie, J. S., Dai, C. Y. & Hu, X. 2016. Evidence That Does Not Support Pyruvate Kinase M2 (PKM2)-catalyzed Reaction as a Rate-limiting Step in Cancer Cell Glycolysis. *Journal of Biological Chemistry,* 291, 8987-8999.
Xie, T. & Spradling, A. C. 1998. decapentaplegic is essential for the maintenance and division of germline stem cells in the Drosophila ovary. *Cell,* 94, 251-260.
Xu, Q., Simpson, S. E., Scialla, T. J., Bagg, A. & Carroll, M. 2003. Survival of acute myeloid leukemia cells requires PI3 kinase activation. *Blood,* 102, 972-980.
Yalcin, A., Clem, B. F., Imbert-Fernandez, Y., Ozcan, S. C., Peker, S., *et al.* 2014. 6-Phosphofructo-2-kinase (PFKFB3) promotes cell cycle progression and suppresses apoptosis via Cdk1-mediated phosphorylation of p27. *Cell Death & Disease,* 5.
Yalcin, A., Clem, B. F., Simmons, A., Lane, A., Nelson, K., *et al.* 2009a. Nuclear Targeting of 6-Phosphofructo-2-kinase (PFKFB3) Increases Proliferation via Cyclin-dependent Kinases. *Journal of Biological Chemistry,* 284, 24223-24232.
Yalcin, A., Simmons, A., Clem, A., Telang, S., Wattenberg, B., *et al.* 2006. Nuclear compartmentalization of a key regulator of glycolysis, 6-phosphofructo-2-kinase (PFKFB3). *Faseb Journal,* 20, A1295-A1296.
Yalcin, A., Telang, S., Clem, B. & Chesney, J. 2009b. Regulation of glucose metabolism by 6-phosphofructo-2-kinase/fructose-2,6-bisphosphatases in cancer. *Experimental and Molecular Pathology,* 86, 174-179.
Yalcin, S., Zhang, X., Luciano, J. P., Mungamuri, S. K., Marinkovic, D., *et al.* 2008. Foxo3 is essential for the regulation of ataxia telangiectasia mutated and oxidative stress-mediated homeostasis of hematopoietic stem cells. *Journal of Biological Chemistry,* 283, 25692-25705.
Yamamoto, N. & Ashida, H. 2012. Evaluation Methods for Facilitative Glucose Transport in Cells and Their Applications. *Food Science and Technology Research,* 18, 493-503.

Yamamoto, T., Sakaguchi, N., Hachiya, M., Nakayama, F., Yamakawa, M.*, et al.* 2009. Role of catalase in monocytic differentiation of U937 cells by TPA: hydrogen peroxide as a second messenger. *Leukemia,* 23, 761-769.
Yamamoto, T., Takano, N., Ishiwata, K., Ohmura, M., Nagahata, Y.*, et al.* 2014. Reduced methylation of PFKFB3 in cancer cells shunts glucose towards the pentose phosphate pathway. *Nature Communications,* 5, DOI 10.1038/ncomms4480, e3480.
Yan, J. S., Li, Y. D., Liu, S. H., Yin, Q. Q., Liu, X. Y.*, et al.* 2017. The t(8;21) fusion protein RUNX1-ETO downregulates PKM2 in acute myeloid leukemia cells. *Leukemia & Lymphoma,* 58, 1985-1988.
Yang, J., Li, J. Q., Le, Y. P., Zhou, C. W., Zhang, S.*, et al.* 2016. PFKL/miR-128 axis regulates glycolysis by inhibiting AKT phosphorylation and predicts poor survival in lung cancer. *American Journal of Cancer Research,* 6, 473-485.
Yang, M. & Vousden, K. H. 2016. Serine and one-carbon metabolism in cancer. *Nature Reviews Cancer,* 16, 650-662.
Yang, W. & Lu, Z. 2013. Regulation and function of pyruvate kinase M2 in cancer. *Cancer Letters,* 339, 153-158.
Yang, Z., Fujii, H., Mohan, S. V., Goronzy, J. J. & Weyand, C. M. 2013. Phosphofructokinase deficiency impairs ATP generation, autophagy, and redox balance in rheumatoid arthritis T cells. *Journal of Experimental Medicine,* 210, 2119-2134.
Yasueda, A., Urushima, H. & Ito, T. 2016. Efficacy and Interaction of Antioxidant Supplements as Adjuvant Therapy in Cancer Treatment: A Systematic Review. *Integrative Cancer Therapies,* 15, 17-39.
Ye, F., Huang, W. T. & Guo, G. J. 2017. Studying hematopoiesis using single-cell technologies. *Journal of Hematology & Oncology,* 10, DOI 10.1186/s13045-13017-10401-13047, e13027.
Ye, J. B., Fan, J., Venneti, S., Wan, Y. W., Pawel, B. R.*, et al.* 2014. Serine Catabolism Regulates Mitochondrial Redox Control during Hypoxia. *Cancer discovery,* 4, 1406-1417.
Yen, K., Travins, J., Wang, F., David, M. D., Artin, E.*, et al.* 2017. AG-221, a First-in-Class Therapy Targeting Acute Myeloid Leukemia Harboring Oncogenic IDH2 Mutations. *Cancer discovery,* 7, 478-493.
Ying, H., Kimmelman, A. C., Lyssiotis, C. A., Hua, S., Chu, G. C.*, et al.* 2012. Oncogenic Kras Maintains Pancreatic Tumors through Regulation of Anabolic Glucose Metabolism. *Cell,* 149, 656-670.
Yoo, S. K., Starnes, T. W., Deng, Q. & Huttenlocher, A. 2011. Lyn is a redox sensor that mediates leukocyte wound attraction in vivo. *Nature,* 480, 109-U278.
Yoshioka, K., Saito, M., Oh, K. B., Nemoto, Y., Matsuoka, H.*, et al.* 1996. Intracellular fate of 2-NBDG, a fluorescent probe for glucose uptake activity, in Escherichia coli cells. *Bioscience Biotechnology and Biochemistry,* 60, 1899-1901.
You, Z. M., Zhao, L., Xia, J., Wei, Q., Liu, Y. M.*, et al.* 2014. Down-regulation of Phosphoglucose Isomerase/Autocrine Motility Factor Enhances Gensenoside Rh2 Pharmacological Action on Leukemia KG1 alpha Cells. *Asian Pacific Journal of Cancer Prevention,* 15, 1099-1104.
Yu, H., Zhang, H. Q., Dong, M. J., Wu, Z., Shen, Z. L.*, et al.* 2017a. Metabolic reprogramming and AMPK alpha 1 pathway activation by caulerpin in colorectal cancer cells. *International Journal of Oncology,* 50, 161-172.
Yu, M., Han, Y. Z., Chen, S., Luo, X., Lin, Y.*, et al.* 2017b. The prognostic value of GLUT1 in cancers: a systematic review and meta-analysis. *Oncotarget,* 8, 43356-43367.

Yuan, Y., Hilliard, G., Ferguson, T. & Millhorn, D. E. 2003. Cobalt inhibits the interaction between hypoxia-inducible factor-alpha and von Hippel-Lindau protein by direct binding to hypoxia-inducible factor-alpha. *Journal of Biological Chemistry,* 278, 15911-15916.

Zancan, P., Sola-Penna, M., Furtado, C. M. & Da Silva, D. 2010. Differential expression of phosphofructokinase-1 isoforms correlates with the glycolytic efficiency of breast cancer cells. *Molecular Genetics and Metabolism,* 100, 372-378.

Zeng, C., Wu, Q. P., Wang, J., Yao, B., Ma, L.*, et al.* 2016. NOX4 supports glycolysis and promotes glutamine metabolism in non-small cell lung cancer cells. *Free Radical Biology and Medicine,* 101, 236-248.

Zhang, J. W., Niu, C., Ye, L., Huang, H. Y., He, X.*, et al.* 2003. Identification of the haematopoietic stem cell niche and control of the niche size. *Nature,* 425, 836-841.

Zhao, J. D., Du, F., Luo, Y., Shen, G. S., Zheng, F. C.*, et al.* 2015. The emerging role of hypoxia-inducible factor-2 involved in chemo/radioresistance in solid tumors. *Cancer Treatment Reviews,* 41, 623-633.

Zhao, L. Q., Mao, Y. T., Zhao, Y. L., Cao, Y. & Chen, X. 2016a. Role of multifaceted regulators in cancer glucose metabolism and their clinical significance. *Oncotarget,* 7, 31572-31585.

Zhao, M., Fan, J., Liu, Y., Yu, Y. X., Xu, J. H.*, et al.* 2016b. Oncogenic role of the TP53-induced glycolysis and apoptosis regulator in nasopharyngeal carcinoma through NF-kappa B pathway modulation. *International Journal of Oncology,* 48, 756-764.

Zhao, S. M., Lin, Y., Xu, W., Jiang, W. Q., Zha, Z. Y.*, et al.* 2009. Glioma-Derived Mutations in IDH1 Dominantly Inhibit IDH1 Catalytic Activity and Induce HIF-1 alpha. *Science,* 324, 261-265.

Zhao, T., Zhu, Y., Morinibu, A., Kobayashi, M., Shinomiya, K.*, et al.* 2014. HIF-1-mediated metabolic reprogramming reduces ROS levels and facilitates the metastatic colonization of cancers in lungs. *Scientific Reports,* 4, DOI 10.1038/srep03793, e03793.

Zhao, X. X., Xu, B., Bhattacharjee, A., Oldfield, C. M., Wientjes, F. B.*, et al.* 2005. Protein kinase C delta regulates p67phox phosphorylation in human monocytes. *J Leukoc Biol,* 77, 414-420.

Zhao, Y., Butler, E. B. & Tan, M. 2013. Targeting cellular metabolism to improve cancer therapeutics. *Cell Death & Disease,* 4, DOI 10.1038/cddis.2013.1060, e1532.

Zhao, Y., Hu, X. B., Liu, Y. J., Dong, S. M., Wen, Z. W.*, et al.* 2017. ROS signaling under metabolic stress: cross-talk between AMPK and AKT pathway. *Molecular Cancer,* 16, DOI 10.1186/s12943-12017-10648-12941, e-12979.

Zheng, W., Tayyari, F., Gowda, G. a. N., Raftery, D., Mclamore, E. S.*, et al.* 2015. Altered Glucose Metabolism in Harvey-ras Transformed MCF10A Cells. *Molecular Carcinogenesis,* 54, 111-120.

Zhou, F. L., Zhang, W. G., Wei, Y. C., Meng, S., Bai, G. G.*, et al.* 2010. Involvement of Oxidative Stress in the Relapse of Acute Myeloid Leukemia. *Journal of Biological Chemistry,* 285, 15010-15015.

Zhu, W., Ye, L., Zhang, J. Z., Yu, P. F., Wang, H. B.*, et al.* 2016. PFK15, a Small Molecule Inhibitor of PFKFB3, Induces Cell Cycle Arrest, Apoptosis and Inhibits Invasion in Gastric Cancer. *Plos One,* 11, DOI 10.1371/journal.pone.0163768, e0163768.

Zon, L. I. 2008. Intrinsic and extrinsic control of haematopoietic stem-cell self-renewal. *Nature,* 453, 306-313.

Appendices

Appendix 1. shRNA sequences complementary to PFKFB3. (i) TRC2 N0000314690, (ii) TRC2 N0000314746, (iii) N0000314747, (iv) N0000314748, (v) TRC2 N0000381874**.**

(i) **Sequence:**
CCGGACCCGCTCATGAGACGCAATACTCGAGTATTGCGTCTCATGAGCGGGTTTTTTG

(ii) **Sequence:**
CCGGCGTGTCGGTTCCATTCCATTTCTCGAGAAATGGAATGGAACCGACACGTTTTTG

(iii) **Sequence:**
CCGGCGTGACTGTTTGGTGCATCTTCTCGAGAAGATGCACCAAACAGTCACGTTTTTG

(iv) **Sequence:**
CCGGTGTCGCTGATCAAGGTGATTGCTCGAGCAATCACCTTGATCAGCGACATTTTTG

(v) Sequence:
GTACCGGTCTCCAGCCCGGATTACAAAGCTCGAGCTTTGTAATCCGGGCTGGAGATTTTT
TG

Appendix 2. shRNA sequences complementary to HIF-1*α*. (i) TRC N0000003808, (ii) N0000003809, (iii) N0000003810, (iv) N0000003811, (v) TRC N0000010819

(i) Sequence:
CCGGCCGCTGGAGACACAATCATATCTCGAGATATGATTGTGTCTCCAGCGGTTTTT

(ii) **Sequence:**
CCGGCCAGTTATGATTGTGAAGTTACTCGAGTAACTTCACAATCATAACTGGTTTTT

(iii) **Sequence:**
CCGGGTGATGAAAGAATTACCGAATCTCGAGATTCGGTAATTCTTTCATCACTTTTT

(iv) **Sequence:**
CCGGCGGCGAAGTAAAGAATCTGAACTCGAGTTCAGATTCTTTACTTCGCCGTTTTT

(v) Sequence:
CCGGTGCTCTTTGTGGTTGGATCTACTCGAGTAGATCCAACCACAAAGAGCATTTTT

Appendix 3. PFKFB3 DNA sequence "dropped" from pEX-K4 vector and ligated into PINCO retroviral vector. Sequence of reverse 5' to 3' DNA sequence provided by Eurofins MWG (Cytosine (C), Adenine (A), Thymine (T), Guanine (G)), and alignment of forward primer (P1) and reverse primer (P2) sequences across subcloning sites compared with published PFKFB3 sequence.

```
P2              ------------------------------------------------------------
PFKFB3(var.2)   ------------------------------------------------------------a
P1              CGGGGGTGGACCATCCTCTAGACTGCCGGATCCTAGATAACTGATCAAGATCTGCCACCA

P2              ------------------------------------------------------------
PFKFB3(var.2)   tgcccttcaggaaagcctgtgggccaaagctgaccaactcccccaccgtcatcgtcatgg
P1              TGCCCTTCAGGAAAGCCTGTGGGCCAAAGCTGACCAACTCCCCCACCGTCATCGTCATGG

P2              ------------------------------------------------------------
PFKFB3(var.2)   tgggcctccccgcccggggcaagacctacatctccaagaagctgactcgctacctcaact
P1              TGGGCCTCCCCGCCCGGGGCAAGACCTACATCTCCAAGAAGCTGACTCGCTACCTCAACT

P2              ------------------------------------------------------------
PFKFB3(var.2)   ggattggcgtccccacaaaagtgttcaacgtcggggagtatcgccgggaggctgtgaagc
P1              GGATTGGCGTCCCCACAAAAGTGTTCAACGTCGGGGAGTATCGCCGGGAGGCTGTGAAGC

P2              ------------------------------------------------------------
PFKFB3(var.2)   agtacagctcctacaacttcttccgccccgacaatgaggaagccatgaaagtccggaagc
P1              AGTACAGCTCCTACAACTTCTTCCGCCCCGACAATGAGGAAGCCATGAAAGTCCGGAAGC

P2              ------------------------------------------------------------
PFKFB3(var.2)   aatgtgccttagctgccttgagagatgtcaaaagctacctggcgaaagaaggggacaaa
P1              AATGTGCCTTAGCTGCCTTGAGAGATGTCAAAAGCTACCTGGCGAAAGAAGGGGGACAAA

P2              ------------------------------------------------------------
PFKFB3(var.2)   ttgcggttttcgatgccaccaatactactagagagaggagacacatgatccttcattttg
P1              TTGCGGTTTTCGATGCCACCAATACTACTAGAGAGAGGAGACACATGATCCTTCATTTTG

P2              ------------------------------------------------------------
PFKFB3(var.2)   ccaaagaaaatgactttaaggcgtttttcatcgagtcggtgtgcgacgaccctacagttg
P1              CCAAAGAAAATGACTTTAAGGCGTTTTTCATCGAGTCGGTGTGCGACGACCCTACAGTTG

P2              ------------------------------------------------------------
PFKFB3(var.2)   tggcctccaatatcatggaagttaaaatctccagcccggattacaaagactgcaactcgg
P1              TGGCCTCCAATATCATGGAAGTTAAAATCTCCAGCCCGGATTACAAAGACTGCAACTCGG

P2              ------------------------------------------------------------
PFKFB3(var.2)   cagaagccatggacgacttcatgaagaggatcagttgctatgaagccagctaccagcccc
P1              CAGAAGCCATGGACGACTTCATGAAGAGGATCAGTTGCTATGAAGCCAGCTACCAGCCCC

P2              ------------------------------------------------------------
PFKFB3(var.2)   tcgaccccgacaaatgcgacagggacttgtcgctgatcaaggtgattgacgtgggccgga
P1              TCGACCCCGACAAATGCGACAGGGACTTGTCGCTGATCAAGGTGATTGACGTGGGCCGGA

P2              ------------------------------------------------------------
PFKFB3(var.2)   ggttcctggtgaaccgggtgcaggaccacatccagagccgcatcgtgtactacctgatga
P1              GGTTCCTGGTGAACCGGGTGCAGGACCACATCCAGAGCCGCATCGTGTACTACCTGATGA

P2              ------------------------------------------------------------
PFKFB3(var.2)   acatccacgtgcagccgcgtaccatctacctgtgccggcacggcgagaacgagcacaacc
P1              ACATCCACGTGCAGCCGCGTACCATCTACCTGTGCCGGCACGGC---------------

P2              ------------------------------------------------------------
PFKFB3(var.2)   tccagggccgcatcgggggcgactcaggcctgtccagccggggcaagaagtttgccagtg
P1              ------------------------------------------------------------


P2              CTCTGAGCAAGTTCGTGGAGGAGCAGAACCTGAAGGACCTGCGCGTGTGGACCAGCCAGC
PFKFB3(var.2)   ctctgagcaagttcgtggaggagcagaacctgaaggacctgcgcgtgtggaccagccagc
P1              ------------------------------------------------------------
```

```
P2              TGAAGAGCACCATCCAGACGGCCGAGGCGCTGCGGCTGCCCTACGAGCAGTGGAAGGCGC
PFKFB3(var.2)   tgaagagcaccatccagacggccgaggcgctgcggctgccctacgagcagtggaaggcgc
P1              ------------------------------------------------------------

P2              TCAATGAGATCGACGCGGGCGTCTGTGAGGAGCTGACCTACGAGGAGATCAGGGACACCT
PFKFB3(var.2)   tcaatgagatcgacgcgggcgtctgtgaggagctgacctacgaggagatcagggacacct
P1              ------------------------------------------------------------

P2              ACCCTGAGGAGTATGCGCTGCGGGAGCAGGACAAGTACTATTACCGCTACCCCACCGGGG
PFKFB3(var.2)   accctgaggagtatgcgctgcgggagcaggacaagtactattaccgctaccccaccgggg
P1              ------------------------------------------------------------

P2              AGTCCTACCAGGACCTGGTCCAGCGCTTGGAGCCAGTGATCATGGAGCTGGAGCGGCAGG
PFKFB3(var.2)   agtcctaccaggacctggtccagcgcttggagccagtgatcatggagctggagcggcagg
P1              ------------------------------------------------------------

P2              AGAATGTGCTGGTCATCTGCCACCAGGCCGTCCTGCGCTGCCTGCTTGCCTACTTCCTGG
PFKFB3(var.2)   agaatgtgctggtcatctgccaccaggccgtcctgcgctgcctgcttgcctacttcctgg
P1              ------------------------------------------------------------

P2              ATAAGAGTGCAGAGGAGATGCCCTACCTGAAATGCCCTCTTCACACCGTCCTGAAACTGA
PFKFB3(var.2)   ataagagtgcagaggagatgccctacctgaaatgccctcttcacaccgtcctgaaactga
P1              ------------------------------------------------------------

P2              CGCCTGTCGCTTATGGCTGCCGTGTGGAATCCATCTACCTGAACGTGGAGTCCGTCTGCA
PFKFB3(var.2)   cgcctgtcgcttatggctgccgtgtggaatccatctacctgaacgtggagtccgtctgca
P1              ------------------------------------------------------------

P2              CACACCGGGAGAGGTCAGAGGATGCAAAGAAGGGACCTAACCCGCTCATGAGACGCAATA
PFKFB3(var.2)   cacaccgggagaggtcagaggatgcaaagaagggacctaacccgctcatgagacgcaata
P1              ------------------------------------------------------------

P2              GTGTCACCCCGCTAGCCAGCCCCGAACCCACCAAAAAGCCTCGCATCAACAGCTTTGAGG
PFKFB3(var.2)   gtgtcaccccgctagccagccccgaacccaccaaaaagcctcgcatcaacagctttgagg
P1              ------------------------------------------------------------

P2              AGCATGTGGCCTCCACCTCGGCCGCCCTGCCCAGCTGCCTGCCCCCGGAGGTGCCCACGC
PFKFB3(var.2)   agcatgtggcctccacctcggccgccctgcccagctgcctgcccccggaggtgcccacgc
P1              ------------------------------------------------------------

P2              AGCTGCCTGGACAAAACATGAAAGGCTCCCGGAGCAGCGCTGACTCCTCCAGGAAACACT
PFKFB3(var.2)   agctgcctggacaaaacatgaaaggctcccggagcagcgctgactcctccaggaaacact
P1              ------------------------------------------------------------

P2              GAGAATTCGATCGATGTACGGGCCAGATATACGCGTTGACATTGATTATTGACTAGTTAT
PFKFB3(var.2)   ga--------------------------------------------------------
P1              ------------------------------------------------------------
```

Appendix 4. PFKFB3 DNA sequence "dropped" from pEX-K4 vector and ligated into pHIV lentiviral vector. Sequence of reverse 5' to 3' DNA sequence provided by Eurofins MWG (Cytosine (C), Adenine (A), Thymine (T), Guanine (G)), and alignment of forward primer (P3 and P4) and reverse primer (P5) sequences across subcloning sites compared with published PFKFB3 sequence.

```
P5              ------------------------------------------------------------
P4              ------------------------------------------------------------
PFKFB3(var.2)   ------------------------------atgcccttcaggaaagcctgtgggccaa
P3              GGATCCTAGATAACTGATCAAGATCTGCCACCATGCCCTTCAGGAAAGCCTGTGGGCCAA

P5              ------------------------------------------------------------
P4              ------------------------------------------------------------
PFKFB3(var.2)   agctgaccaactccccccaccgtcatcgtcatggtgggcctccccgcccggggcaagacct
P3              AGCTGACCAACTCCCCCACCGTCATCGTCATGGTGGGCCTCCCCGCCCGGGGCAAGACCT

P5              ------------------------------------------------------------
P4              ------------------------------------------------------------
PFKFB3(var.2)   acatctccaagaagctgactcgctacctcaactggattggcgtccccacaaaagtgttca
P3              ACATCTCCAAGAAGCTGACTCGCTACCTCAACTGGATTGGCGTCCCCACAAAAGTGTTCA

P5              ------------------------------------------------------------
P4              ------------------------------------------------------------
PFKFB3(var.2)   acgtcggggagtatcgccgggaggctgtgaagcagtacagctcctacaacttcttccgcc
P3              ACGTCGGGGAGTATCGCCGGGAGGCTGTGAAGCAGTACAGCTCCTACAACTTCTTCCGCC

P5              ------------------------------------------------------------
P4              ------------------------------------------------------------
PFKFB3(var.2)   ccgacaatgaggaagccatgaaagtccggaagcaatgtgccttagctgccttgagagatg
P3              CCGACAATGAGGAAGCCATGAAAGTCCGGAAGCAATGTGCCTTAGCTGCCTTGAGAGATG

P5              ------------------------------------------------------------
P4              ------------------------------------------------------------
PFKFB3(var.2)   tcaaaagctacctggcgaaagaaggggacaaattgcggttttcgatgccaccaatacta
P3              TCAAAAGCTACCTGGCGAAAGAAGGGGGACAAATTGCGGTTTTCGATGCCACCAATACTA

P5              ------------------------------------------------------------
P4              ------------------------------------------------------------
PFKFB3(var.2)   ctagagagaggagacacatgatccttcattttgccaaagaaaatgactttaaggcgtttt
P3              CTAGAGAGAGGAGACACATGATCCTTCATTTTGCCAAAGAAAATGACTTTAAGGCGTTTT

P5              ------------------------------------------------------------
P4              ------------------------------------------------------------
PFKFB3(var.2)   tcatcgagtcggtgtgcgacgaccctacagttgtggcctccaatatcatggaagttaaaa
P3              TCATCGAGTCGGTGTGCGACGACCCTACAGTTGTGGCCTCCAATATCATGGAAGTTAAAA

P5              ------------------------------------------------------------
P4              ------------------------------------------------------------
PFKFB3(var.2)   tctccagcccggattacaaagactgcaactcggcagaagccatggacgacttcatgaaga
P3              TCTCCAGCCCGGATTACAAAGACTGCAACTCGGCAGAAGCCATGGACGACTTCATGAAGA

P5              ------------------------------------------------------------
P4              -----------------AGCGCTACCAGCCCCTCGACCCCGACAAATGCGACAGGGACT
PFKFB3(var.2)   ggatcagttgctatgaagccagctaccagcccctcgaccccgacaaatgcgacagggact
P3              GGATCAGTTGCTATGAAGCCAGCTACCAGCCCCTCGACCCCGACAAATGCGACAGGGACT

P5              ------------------------------------------------------------
P4              TGTCGCTGATCAAGGTGATTGACGTGGGCCGGAGGTTCCTGGTGAACCGGGTGCAGGACC
PFKFB3(var.2)   tgtcgctgatcaaggtgattgacgtgggccggaggttcctggtgaaccgggtgcaggacc
P3              TGTCGCTGATCAAGGTGATTGACGTGGGCCGGAGGTTCCTGGTGAACCGGGTGCAGGACC

P5              ------------------------------------------------------------
P4              ACATCCAGAGCCGCATCGTGTACTACCTGATGAACATCCACGTGCAGCCGCGTACCATCT
PFKFB3(var.2)   acatccagagccgcatcgtgtactacctgatgaacatccacgtgcagccgcgtaccatct
P3              ACATCCAGAGCCGCATCGTGTACTACCTGATGAACATCCACGTGCAGCCGCGTACCATCT
```

```
P5              ------------------------------------------------------------
P4              ACCTGTGCCGGCACGGCGAGAACGAGCACAACCTCCAGGGCCGCATCGGGGGCGACTCAG
PFKFB3(var.2)   acctgtgccggcacggcgagaacgagcacaacctccagggccgcatcgggggcgactcag
P3              ACCTGTGCCGGCACGGCGAGAACGAGCACAACCTCCAGGGCCGCATCGGGGGCGACTCAG

P5              ------------------------------------------------------------
P4              GCCTGTCCAGCCGGGGCAAGAAGTTTGCCAGTGCTCTGAGCAAGTTCGTGGAGGAGCAGA
PFKFB3(var.2)   gcctgtccagccggggcaagaagtttgccagtgctctgagcaagttcgtggaggagcaga
P3              GCCTGTCCAGCCGGGGCAAGAAGTTTGCCAGTGCTCTGAGCAAGTTCGTGG---------

P5              ------------------------------------------------------------
P4              ACCTGAAGGACCTGCGCGTGTGGACCAGCCAGCTGAAGAGCACCATCCAGACGGCCGAGG
PFKFB3(var.2)   acctgaaggacctgcgcgtgtggaccagccagctgaagagcaccatccagacggccgagg
P3              ------------------------------------------------------------

P5              ------------------------------------------------------------
P4              CGCTGCGGCTGCCCTACGAGCAGTGGAAGGCGCTCAATGAGATCGACGCGGGCGTCTGTG
PFKFB3(var.2)   cgctgcggctgccctacgagcagtggaaggcgctcaatgagatcgacgcgggcgtctgtg
P3              ------------------------------------------------------------

P5              ----GGTGACCTACGAGGAGATCAGGGACACCTACCCTGAGGAGTATGCGCTGCGGGAGC
P4              AGGAGCTGACCTACGAGGAGATCAGGGACACCTACCCTGAGGAGTATGCGCTGCGGGAGC
PFKFB3(var.2)   aggagctgacctacgaggagatcagggacacctaccctgaggagtatgcgctgcgggagc
P3              ------------------------------------------------------------

P5              AGGACAAGTACTATTACCGCTACCCCACCGGGGAGTCCTACCAGGACCTGGTCCAGCGCT
P4              AGGACAAGTACTATTACCGCTACCCCACCGGGGAGTCCTACCAGGACCTGGTCCAGCGCT
PFKFB3(var.2)   aggacaagtactattaccgctaccccaccggggagtcctaccaggacctggtccagcgct
P3              ------------------------------------------------------------

P5              TGGAGCCAGTGATCATGGAGCTGGAGCGGCAGGAGAATGTGCTGGTCATCTGCCACCAGG
P4              TGGAGCCAGTGATCATGGAGCTGGAGCGGCAGGAGAATGTGCTGGTCATCTGCCACCAGG
PFKFB3(var.2)   tggagccagtgatcatggagctggagcggcaggagaatgtgctggtcatctgccaccagg
P3              ------------------------------------------------------------

P5              CCGTCCTGCGCTGCCTGCTTGCCTACTTCCTGGATAAGAGTGCAGAGGAGATGCCCTACC
P4              CCGTCCTGCGCTGCCTGCTTGCCTACTTCCTGGATAAGAGTGCAGAGGAGATGCCCTACC
PFKFB3(var.2)   ccgtcctgcgctgcctgcttgcctacttcctggataagagtgcagaggagatgccctacc
P3              ------------------------------------------------------------

P5              TGAAATGCCCTCTTCACACCGTCCTGAAACTGACGCCTGTCGCTTATGGCTGCCGTGTGG
P4              TGAAATGCCCTCTTCACACCGTCCTGAAACTGACGCCTGTCGCTTATGGCTGCCGTGTGG
PFKFB3(var.2)   tgaaatgccctcttcacaccgtcctgaaactgacgcctgtcgcttatggctgccgtgtgg
P3              ------------------------------------------------------------

P5              AATCCATCTACCTGAACGTGGAGTCCGTCTGCACACACCGGGAGAGGTCAGAGGATGCAA
P4              AATCCATCTACCTGAACGTGGAGTCCGTCTGCACACACCGGGAGAGGTCAGAGGATGCAA
PFKFB3(var.2)   aatccatctacctgaacgtggagtccgtctgcacacaccgggagaggtcagaggatgcaa
P3              ------------------------------------------------------------

P5              AGAAGGGACCTAACCCGCTCATGAGACGCAATAGTGTCACCCCGCTAGCCAGCCCCGAAC
P4              AGAAGGGACCTAACCCGCTCATGAGACGCAATAGTGTCACCCCGCTAGCCAGCCCCGAAC
PFKFB3(var.2)   agaagggacctaacccgctcatgagacgcaatagtgtcaccccgctagccagccccgaac
P3              ------------------------------------------------------------

P5              CCACCAAAAAGCCTCGCATCAACAGCTTTGAGGAGCATGTGGCCTCCACCTCGGCCGCCC
P4              CCACCAAAAAGCCTCGCATCAACAGCTTTGAGGAGCATGTGGCCTCCACCTCGGCCGCCC
PFKFB3(var.2)   ccaccaaaaagcctcgcatcaacagctttgaggagcatgtggcctccacctcggccgccc
P3              ------------------------------------------------------------

P5              TGCCCAGCTGCCTGCCCCCGGAGGTGCCCACGCAGCTGCCTGGACAAAACATGAAAGGCT
P4              TGCCCAGCTGCCTGCCCCCGGAGGTGCCCACGCAGCTGCCTGGACAAAACATGAAAGGCT
PFKFB3(var.2)   tgcccagctgcctgcccccggaggtgcccacgcagctgcctggacaaaacatgaaaggct
P3              ------------------------------------------------------------

P5              CCCGGAGCAGCGCTGACTCCTCCAGGAAACACTGAGAATTCCCCGGGAGATCCTCTAGAG
P4              CCCGGAGCAGCGCTGACTCCTC-----------------------------------
PFKFB3(var.2)   cccggagcagcgctgactcctccaggaaacactga-----------------------
```